(handwritten notations in top margin)

UAH Propulsion Research Center

Determination Of Uncertainties For The New SSME Model

Final Technical Report

NASA/Marshall Space Flight Center
NASA Contract Number NAS8-38609 D.O. 140

Prepared by

(signature)

Kendall K. Brown

Submitted to:

John P. Butas, EP-14
Marshall Space Flight Center, AL 35812

Dr. Hugh W. Coleman
Principal Investigator

Dr. Clark W. Hawk
Center Director

Propulsion Research Center
The University of Alabama in Huntsville

May 16, 1996

Final Technical Report

1 May 1995 to 16 May 1996

Determination of Uncertainties for the New SSME Model

National Aeronautics and Space Administration
Marshall Space Flight Center
Contract Number NAS8-38609
Delivery Order #140

by
Kendall K. Brown and Hugh W. Coleman
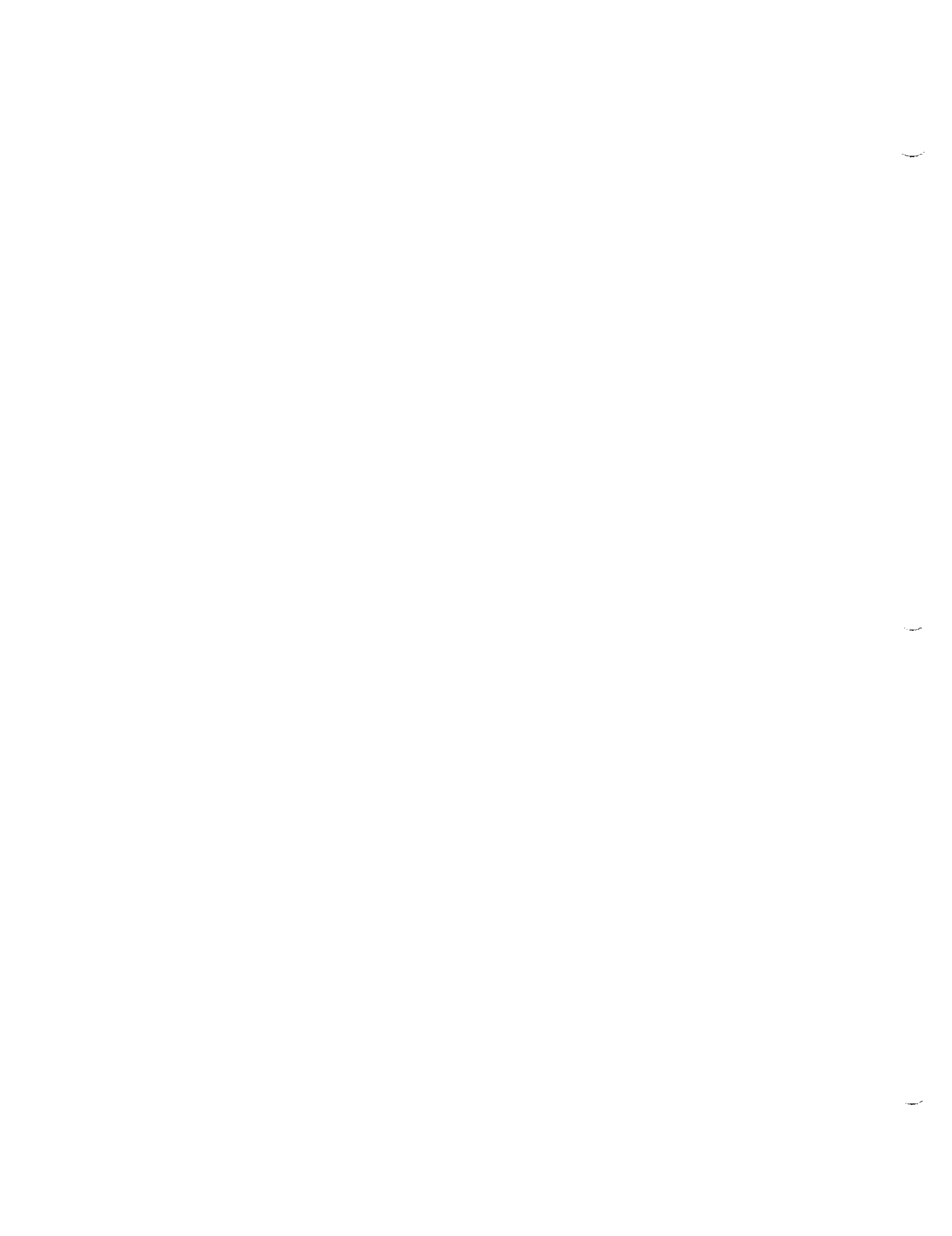Propulsion Research Center
University of Alabama in Huntsville

Table of Contents

1.0   Introduction

This report will discuss the methodology used and the development of uncertainties for use with the New SSME Model. The New SSME Model was developed by Dr. L. Michael Santi of Christian Brothers University through a separate contract effort. The new model requires information about the experimental uncertainties from the Technology Test Bed (TTB) test measurements and about the uncertainties within the component models of the new model.

This effort was a follow-on and continuation of an engineering and research effort begun under delivery order 106, which terminated 30 April 1995[1]. The primary products of that effort were an assessment of the experimental uncertainty in the determination of the venturi flowrates and the initial development of a methodology to assess the uncertainty in linear regressions.

The primary products of this effort include information about the experimental uncertainty in additional TTB measurements (i.e. temperatures, pressures, turbopump rotational speeds, and valve positions), additional assessment of conceptual bias uncertainties, development of methodology to assess the uncertainty in linear regressions, and assessment of the uncertainty in the model hardware characteristics.

A three month period at the beginning of this effort, June, July, and August was excluded from the contract performance period. This was done to allow Mr. Kendall Brown, Graduate Research Assistant working on this contract, to participate in the Air Force Office of Scientific Research Graduate Summer Research Program at the U. S. Air Force's Arnold Engineering Development Center (AEDC). The purpose of his participation was to work with engineers at AEDC who were also interested in developing methods to incorporate uncertainties in the modeling and testing programs of advanced aerospace systems. While at AEDC, Mr. Brown made substantial progress in developing a new methodology to assess the uncertainty in linear regressions (curvefits)[2]. The products of the AFOSR Summer Research Program were immediately applicable to this effort and was a great leveraging of resources.

---

[1] Coleman, Hugh W., and Brown, Kendall K., "Impact of Uncertainty on Modeling and Testing," Propulsion Research Center Report # 95-001, Final Report on NASA-Marshall Space Flight Center Contract NAS8-38609 D.O. #106, 10 January 1994 to 30 April 1995.

[2] Brown, Kendall K., "A Methodology for Assessing Experimental Uncertainties in Curvefits with Application to Compressor Map Characteristics," Air Force Office of Scientific Research graduate summer Research Program Final Report, Arnold Engineering Development Center, Arnold AFB, TN, Aug 1995.

1.1   Statement of Work

The Statement of Work for this contractual effort is provided. The 31 March 1996 delivery order termination date was extended to 16 May 1996 under a 45 day, no-cost extension

The work identified under this statement of work is a continuation of work performed under UAH Contract NAS8-38609, Delivery Order No. 106. The primary focus of the work performed under Delivery Order No. 106 was to establish methods for generating uncertainty estimates for selected Technology Test Bed (TTB) experimental flowrate measurements and to assess the impact of these uncertainties on developing a new test integration strategy. The goal of this new effort is to generate or finalize uncertainty estimates for TTB pressure and temperature measurements and to evaluate these estimates within the new Space Shuttle Main Engine (SSME) steady-state performance model. The incorporation of these uncertainty estimates will enhance the capability to better support current performance analysis requirements such as, assessing vehicle/engine feed system interface flow characteristics, engine hardware design changes, evaluating engine hardware performance, predicting engine hardware operation, and supporting failure investigations.

Rocket engine performance models consist of mathematical relationships which model physical processes within the engine. Experimental data is use to anchor these physical relationships. Performance models are used to derive engine component hardware characteristics from experimental data. Both experimental data and the physical relationships within a model contain various sources of errors. These sources of errors include calibration errors, signal processing and localized effects, uncertainties in both physical approximations and fluid property data. These sources of errors are neglected within the current SSME steady-state performance model. Experimental data is treated as absolute and computational predictions are forced to agree with the data at instrumented locations, often at the expense of physical consistency. This situation impacts the integration of experimental data within the model, thus reducing the accuracy of the computed hardware characteristics.

A new SSME steady-state performance prediction program is currently being developed to evaluate and utilize experimental data derived from recent TTB tests. A modified test data integration scheme has been developed which reconciles uncertain experimental data with uncertain physical relationships. This strategy systematically transforms uncertain experimental data into a physically self consistent set of data. This is accomplished by forcing the minimum adjustment required in engine fluid measurements to satisfy prescribed uncertainty constraints. This reconciliation scheme was reformulated during this last year based on the method developed in estimating the experimental uncertainties of the few TTB measurements. The overall success of the reconciliation strategy is a function of determining a reliable method to both generate and incorporate these required uncertainty estimates. Thus, the incorporation of these uncertainty estimates will enhance the use of experimental data to anchor the physical relationships which in turn, will improve the overall accuracy of the performance predictions.

4

The research required to implement these uncertainty analysis concepts will be conducted within the SSME engine 3001 test program which is currently being conducted on the TTB test facility. Engine 3001 provides a significantly larger number of experimental measurements as compared to standard SSME flight engines. This test program provides a unique opportunity to assess how accurate we can predict SSME hardware performance based on selected instrumentation.

A two phase research effort will be established to support the modified test data reconciliation strategy, and ultimately will improve the use of experimental data in generating performance predictions. Phase I involves generating or finalizing uncertainty estimates for TTB pressure and temperature measurements that were not generated under UAH Contract NAS8-38609, Delivery Order No. 106. Phase II involves estimating the uncertainties associated with incorporating previous experimental data and fluid property data within the model. A detail description of the specific tasks to support these phases are described below:

Phase I - Estimate uncertainties for TTB pressure and temperature measurement.
Task 1)   Perform statistical analysis on existing pressure and temperature TTB test data.
Task 2)   Identify all significant sources of errors within instrumentation system for these measurements
Task 3)   Estimate both precision and bias uncertainties for the TTB pressure and temperature measurements
Task 4)   Estimate uncertainties associated with localized effects due to measurement locations.

Phase II - Estimate uncertainties for incorporating previous experimental data and fluid property data within the new SSME model.
Task 1)   Identify the sub-models within the new SSME model which incorporate previous experimental data and fluid property data.
Task 2)   Estimate uncertainties associated with the use of previous experimental data (duct and valve characteristics, for example).
Task 3)   Estimate uncertainties associated with fluid property data.

The following represent the deliverable products expected for each of the two phases:

Phase I - Estimate uncertainties for TTB pressure and temperature measurement.
1) Interim report documenting uncertainty estimates as completed for each of the TTB measurements selected.
Phase II - Estimate uncertainties for incorporating previous experimental data and fluid property data within the new SSME model.
1)   Final report documenting research conducted in developing the methods for estimating uncertainties in test measurements and in the model.

1.2   Relationship of this contract to overall effort

A technical paper for the 32nd AIAA/SAE/ASME/ASEE Joint Propulsion Conference was jointly authored by the researchers on this contract, Dr. L. Michael Santi, and the COTR, Mr. John P. Butas[3]. This technical paper presented the overall effort to the propulsion community and was well received. A copy of this technical paper is provided as Appendix 4.

As described in the technical paper, the overall goal of this effort is to develop a new model of the Space Shuttle Main Engine which incorporates the uncertainties in the experimental test program and some of the uncertainties in the modeling process. A key feature of the new model is that it is a physical model, it satisfies the conservation of mass and energy, whereas the existing model does not. As the developer of the new model, Dr. Santi, of Christian Brothers University, Memphis, TN, was responsible for developing the numerical solution strategy and how to incorporate the experimental and modeling uncertainties. As these parallel research efforts proceeded, this effort of assessing of the various uncertainties evolved into supporting Dr. Santi's modeling effort. Extensive communication with the COTR and Dr. Santi ensured proper information.

1.3   Organization of this report

This report is broken into two main sections, first a discussion of uncertainties in the experimental data, and secondly a discussion of the modeling uncertainties.

In order to support the new model, the assessment of experimental uncertainties in almost all types of TTB SSME measurements was required, the notable exceptions were strain gage and accelerometer measurements. An initial assessment of temperature, pressure, and flowrate uncertainties was conducted under the previous contract. Further investigation into the experimental uncertainty in these measurements, as well as investigation of the turbopump speeds and the valve positions sensors, was conducted under this effort. Conceptual bias uncertainties are often significant components of the experimental uncertainty, and discussion of efforts to assess these uncertainties is included.

The primary model uncertainty sources being included in this effort are the uncertainty in the physical property data, the uncertainty in the hardware characteristics, and the propagation of these uncertainties into the

---

[3] Brown, Kendall K., Coleman, Hugh W., Santi, L. Michael, and Butas, John P., "Enhancing Rocket Engine Test Analysis and Performance with the Incorporation of Uncertainties," 31st AIAA/ASME/SAE/ASEE Joint Propulsion Conference, AIAA paper 95-3073, San Diego, CA, July 1995.
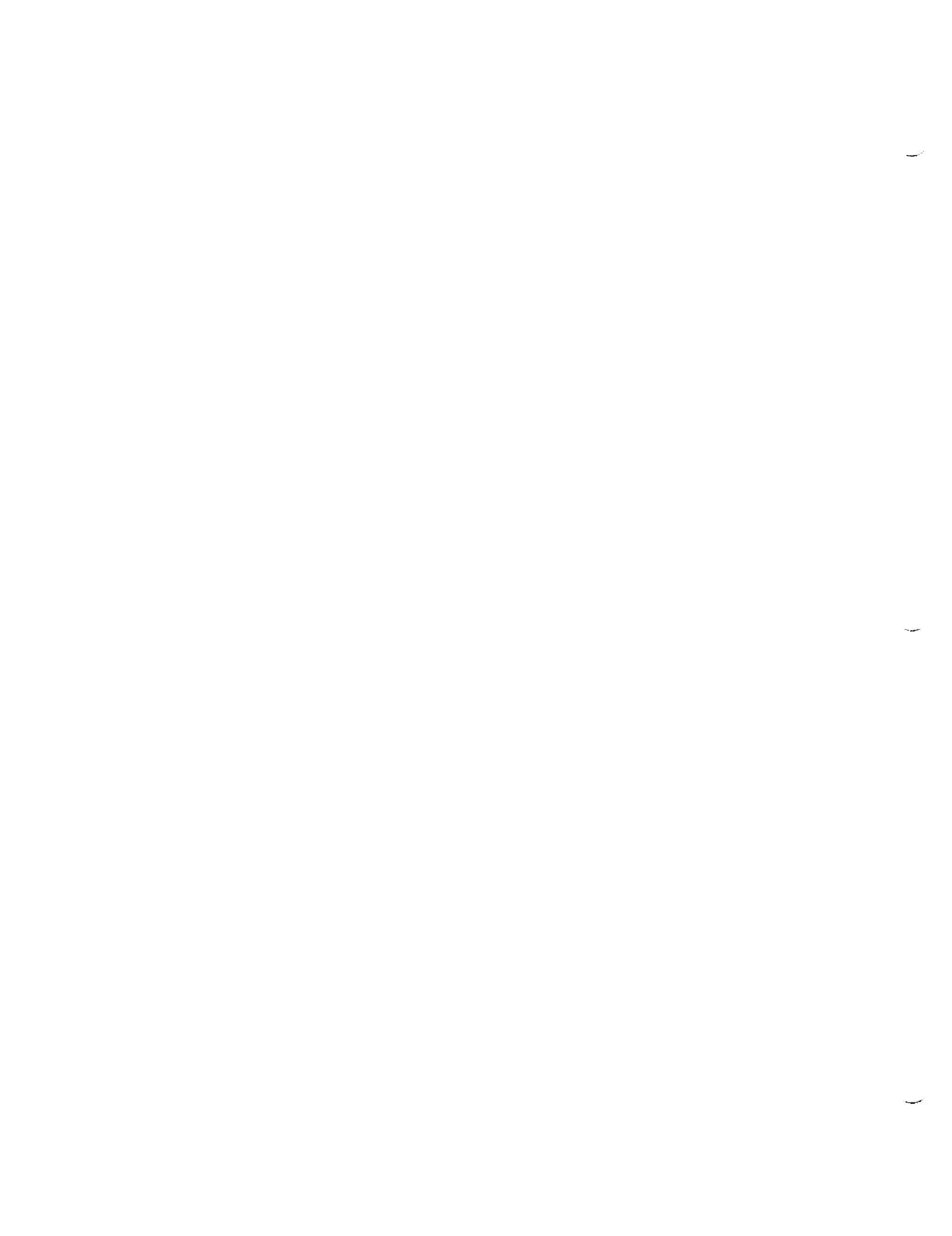
uncertainty associated with the balance relations within the model. The assessment of the uncertainty in the hardware characteristics and their propagation is a new topic and methods to assess these parameters had to be developed. Many of the SSME components, particularly the turbopumps utilize maps, or curvefits to represent their performance. These maps are generated using other information, and usually by conducting a sub-component test program and scaling the results to the engine operating conditions. The available documentation of how each specific hardware characteristic was generated is very poor, and thus the information presented in this report represents the best information that could be obtained.

In some cases the information needed to make a more accurate uncertainty estimate was not available, so this report will present the methodology used to assess the uncertainties, so that when the appropriate information becomes available the uncertainties can then be estimated and included in the model.
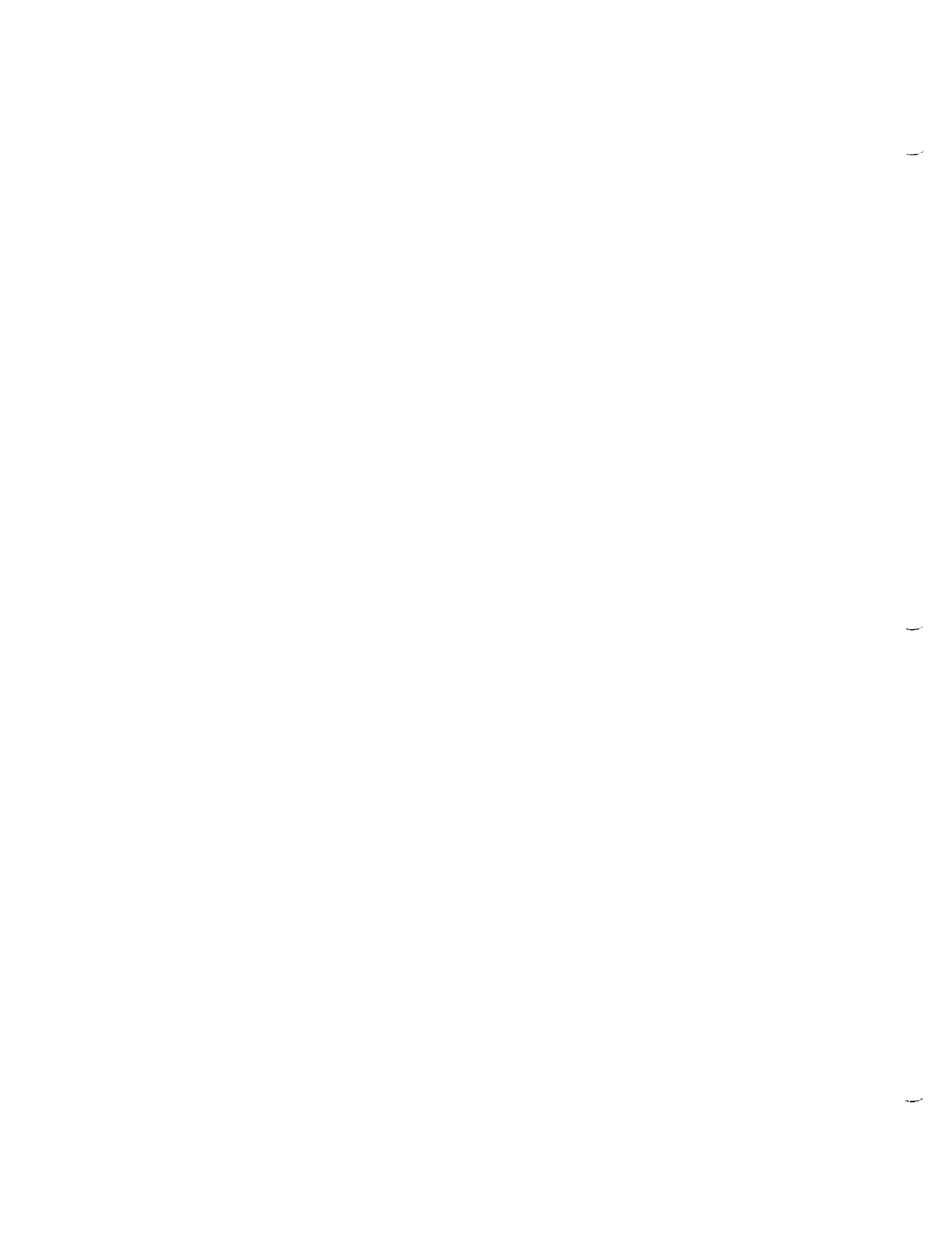
2.0 Test Data Uncertainty Considerations

The assessment of the experimental uncertainties of the data obtained from the Technology Test Bed (TTB) SSME Engine 3001 test program was conducted using the methodology described in Appendix 1. As described in Appendix 1, the determination of uncertainty is comprised of two main components, bias (systematic) uncertainties and precision (random) uncertainties. The manner in which the uncertainty value is used dictates how the uncertainty is estimated, and conversely, the way in which the uncertainty is estimated dictates how it may be used. Thus, a proper understanding of how the uncertainties would be used in the new model was necessary in order to make appropriate uncertainty estimates. This section describes how the uncertainty estimates were determined for use with the new model.

2.1 Development of the Baseline Data Set (BDS)

A baseline data set (BDS) was developed in order to specifically identify the measurements to be used to validate the new model and solution methodology. This data needed to represent the best information available about the operation of the engine, and the associated uncertainty. The new model contained hardware characteristics representing a Phase II engine, thus the data used to build the BDS must be taken from TTB tests with Engine 3001 configurations similar to a Phase II engine. This limited the available tests to TTB021-TTB038 and TTB052-TTB065. This group of tests was further limited because of a series of tests with the Pratt and Whitney ATD HPFTP. Since the performance of the Pratt and Whitney turbopump is different than the Rocketdyne turbopump, and since the new model is using HPFTP maps representing the performance of the Rocketdyne turbopump, this data had to be excluded from the BDS. The test profiles from the remaining tests were examined to find tests which were conducted at the same engine operating conditions. The primary engine control conditions used in the test program are the power level, the fuel/oxidizer mixture ratio, the propellant inlet pressures, and the propellant repressurization flowrates. It was desired to get sets from four different power level settings, 100% rpl, 104% rpl, and 109% rpl, and a low power level (90% rpl or lower). There was insufficient data available at a low power level to create a data set for use in the model.

After the four tests were identified, specific 5-second time slices within each power level of each test were selected. These 5-second time slices were chosen in regions of the test profile where the engine was operating in essentially a steady-state, regions sufficiently far from the engine start transient or power level changes where those effects would not be included in
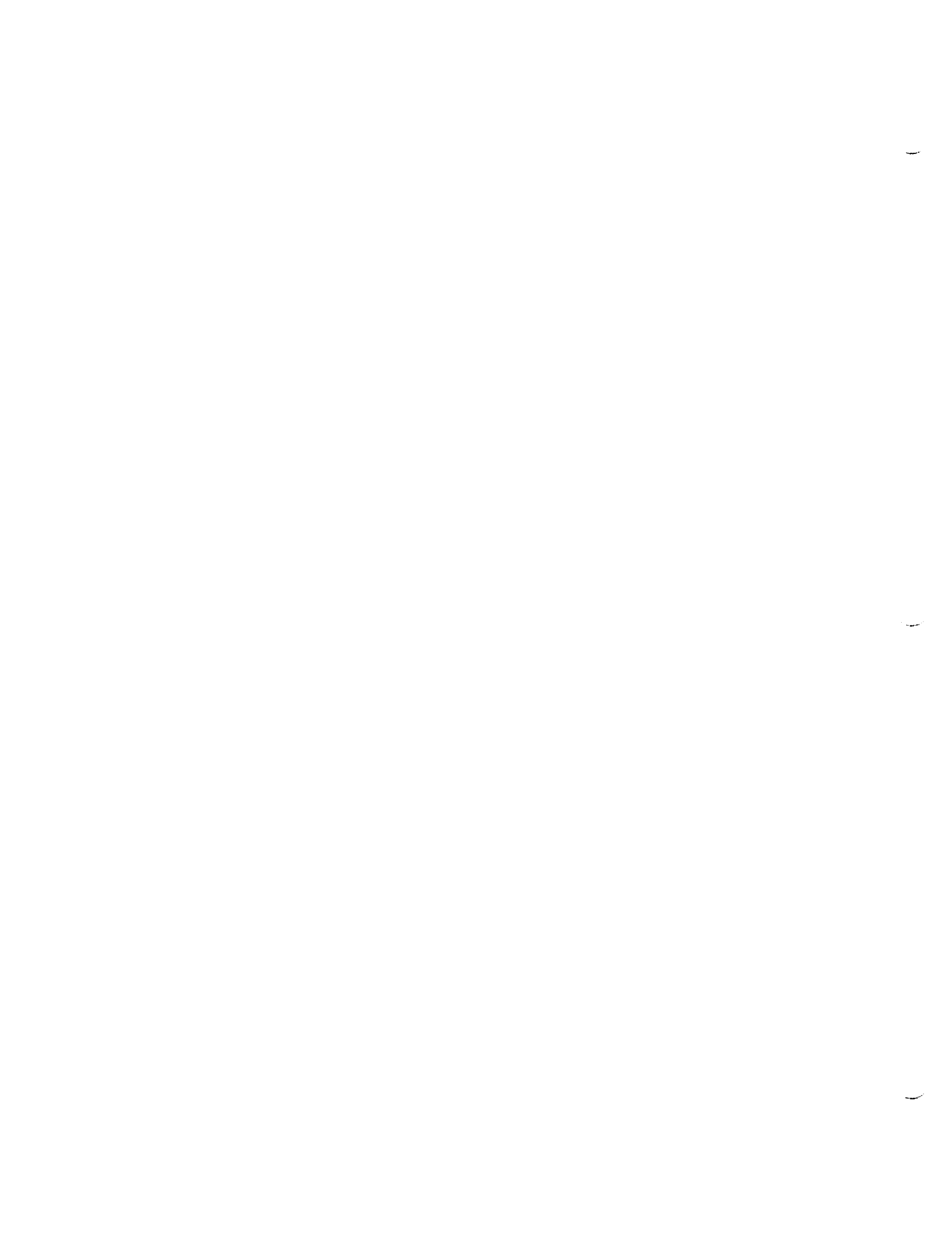
the data. The data from within these 5-second time slices were averaged to obtain a single test point representing the operation of the engine during that test and at that power level. The data point from each of the four tests were then averaged to obtain the data point for the baseline data set. The data in the BDS is the best representation of the operation of the SSME at the given operating conditions.

The TTB measurements included in the BDS were chosen based upon a sensitivity study performed by Dr. Santi and the personal experience of the COTR in performing SSME analyses. The precision uncertainty estimates to associate with the values in the BDS must reflect the test-to-test variation.

2.2   Data Reduction Data Set

One of the main purposes of the New SSME Model is test data reduction, incorporating the test data into the model to find anomalous readings. As such, a second set of data needed to be generated to use in the validation of the new model. The same base set of measurements were used and additional measurements were included, these additional measurements could be used to increase the number of data points used in data reduction or for comparison with output from the new model. The precision estimates to associate with the values in this data set must include the test-to-test variation and the variation of the data within tests.

2.3   Precision Uncertainty Estimates

The appropriate precision limit to use with a given set of data must reflect how that data was generated, the usage of the data, and the usage of the uncertainty estimates. Since the baseline data set is a single point which represents the average of data points from four separate tests, the appropriate precision limit is based upon the standard deviation of the four points. This precision limit represents the test-to-test variation of the engine operation. As discussed in Appendix 1, when using less than approximately ten points in a standard deviation calculation the large-sample approximation should not be used. The sample standard deviation calculated with the BDS is shown in Table 1 in Appendix 2.

The precision uncertainty to use when using the new model for test data reduction is slightly different. While it still must include the test-to-test precision variation it must also include the within test variation for the 1-second averaged data. Hence the sample standard deviation is determined based upon five data points in the four tests, for a total of twenty data points. Since twenty data points are being used in the sample standard deviation the

9

large-sample approximation can be used. Table 2, in Appendix 2, shows the measurements included in the data reduction data set, the average value, and the uncertainties at 104% rated power level (rpl). It shows that the precision uncertainty is approximately equal to that determined for the BDS, indicating that the test-to-test variation dominates the within-test variation.

A pooled sample standard deviation for the data reduction data set was also calculated and verified that the test-to-test variation is much greater than the within-test variation. Using the pooled standard deviation is not appropriate since it does not include the test-to-test variation.

2.4   General Discussion of Conceptual Bias Uncertainties

Potentially significant bias uncertainty sources to consider in the TTB SSME measurements are conceptual bias uncertainties. The conceptual bias uncertainties in the temperature and pressure measurements are particularly important in this effort because of the interest in comparing the experimental results with the analytical predictions. In many of the SSME measurements, the flowfield is highly complex due to the sharp turns and bends, valves, pump and turbine inlets and discharges, and other complicating factors. These factors accentuate the difference between the physical quantity at the sensor and the quantity for which the measurement is desired, typically an average value at a cross-section. These assessments require extensive review of the measurement, the sensor and its installation, the thermodynamic and fluid dynamic flowfield, and their interaction.

The conceptual bias uncertainties can be estimated by reviewing the results of other analyses and reviewing the test data or computational model results. For example, data from the cold-flow testing of the HPFTP turbine shows a temperature profile at the turbine exit and this information can be used to estimate the temperature profile which might exist downstream at the sensor position.

For the conceptual bias uncertainty associated with RTD temperature measurements a simple 1-D heat transfer analysis can be done to get a rough estimate of the temperature profile caused by the heat transfer through the duct walls. This analysis provides an order-of-magnitude estimate and helps determine if the conceptual bias uncertainty is significant or not.

2.5   Discussion of Temperature Uncertainties

The fluid temperature measurements used in this effort were obtained using RTD temperature probes. RTD probes typically provide very accurate
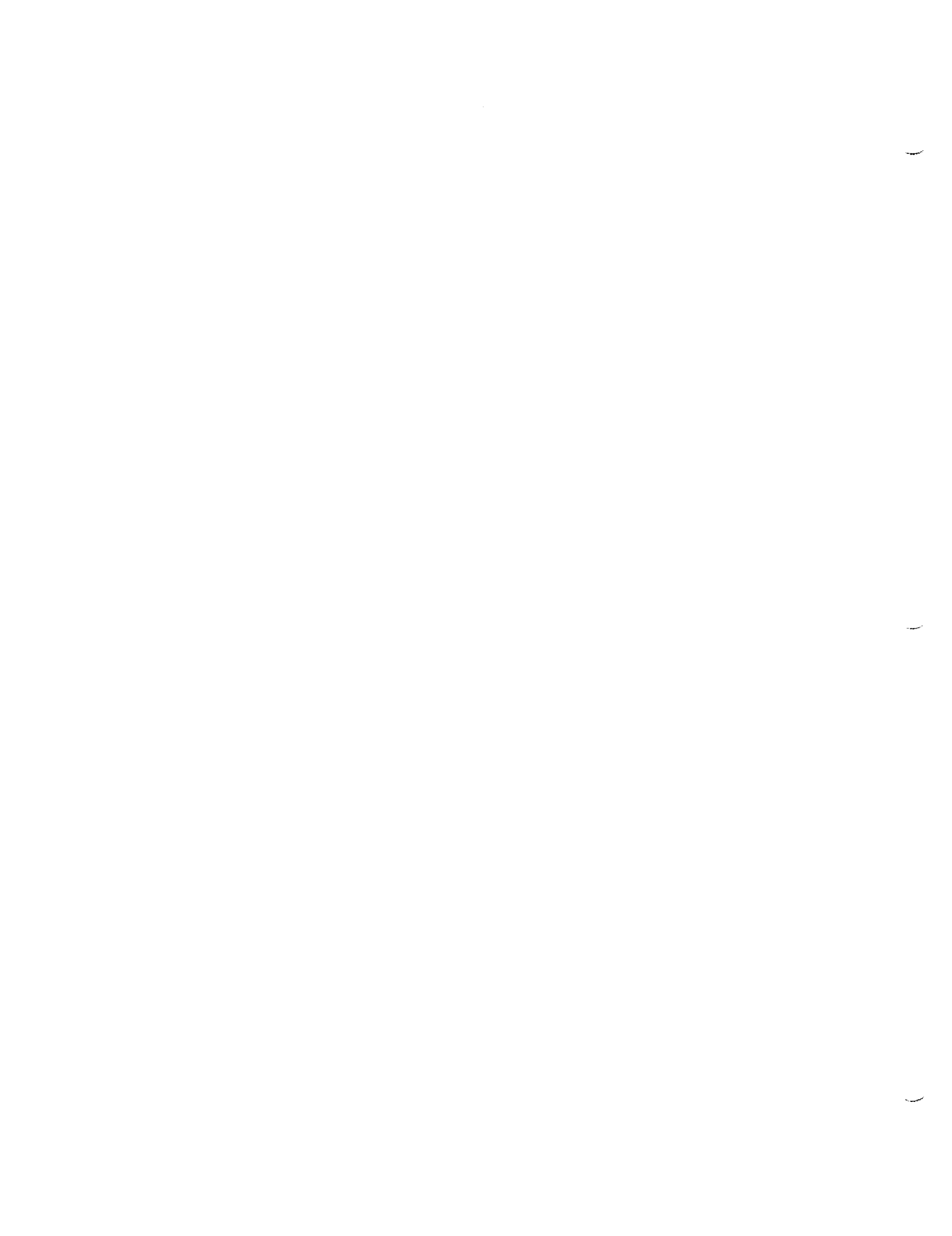
measurements and the primary systematic uncertainty sources are calibration, data acquisition, and conceptual biases. The precision uncertainty estimates were obtained as previously discussed and represent the within-test and test-to-test precision variation.

The systematic uncertainty estimates for the calibration and data acquisition system were based upon the information in the TTB pre-test Data Review Documents (DRD). The temperature calibration and data acquisition system systematic uncertainties in the DRD were based upon a Sverdrup Technology study by Mr. James Fish[4]. The conceptual bias uncertainty added to the DRD listed uncertainty was based upon engineering judgment, since little information was available to make a more precise estimate. The RTDs typically used in the TTB instrumentation extend into the flowfield, up to approximately 2 inches, and are designed so that some of the spatial variation of the flow will essentially average out. Thus, the conceptual bias represents an estimate of the difference between the measured temperature and the one-dimensional average temperature at that location. Thus, a total systematic uncertainty of 2% of the measured value is used for the majority of the temperature measurements. This value is probably conservative and when experimental or computational results are obtained which provide additional information about the temperature profiles at the instrumented locations, the conceptual bias estimate can be updated.

2.6   Discussion of Pressure Uncertainties

The pressure measurements used in this effort were obtained using various pressure transducers, however usually strain-gage type transducers were used. The primary systematic uncertainty sources are calibration, data acquisition, and conceptual biases. The precision uncertainty estimates were obtained as previously discussed and represent the within-test and test-to-test precision variation.

The systematic uncertainty estimates for the calibration and data acquisition system were based upon the information in the TTB pre-test Data Review Documents (DRD). The pressure calibration and data acquisition system systematic uncertainties in the DRD were based upon the Fish study[4]. The conceptual bias uncertainty added to the DRD listed uncertainty was based upon engineering judgment, since little information was available to make a more precise estimate. The pressure transducers are typically mounted along a duct wall. The location of the pressure measurements and the geometry of the engine components and ducts provides the potential for

---

[4] Fish, James, E., "NASA/MSFC Test Area Measurement System Uncertainty Study," Sverdrup Technology, Inc., MSFC Group, Report no. 335-002-92, October 1992.
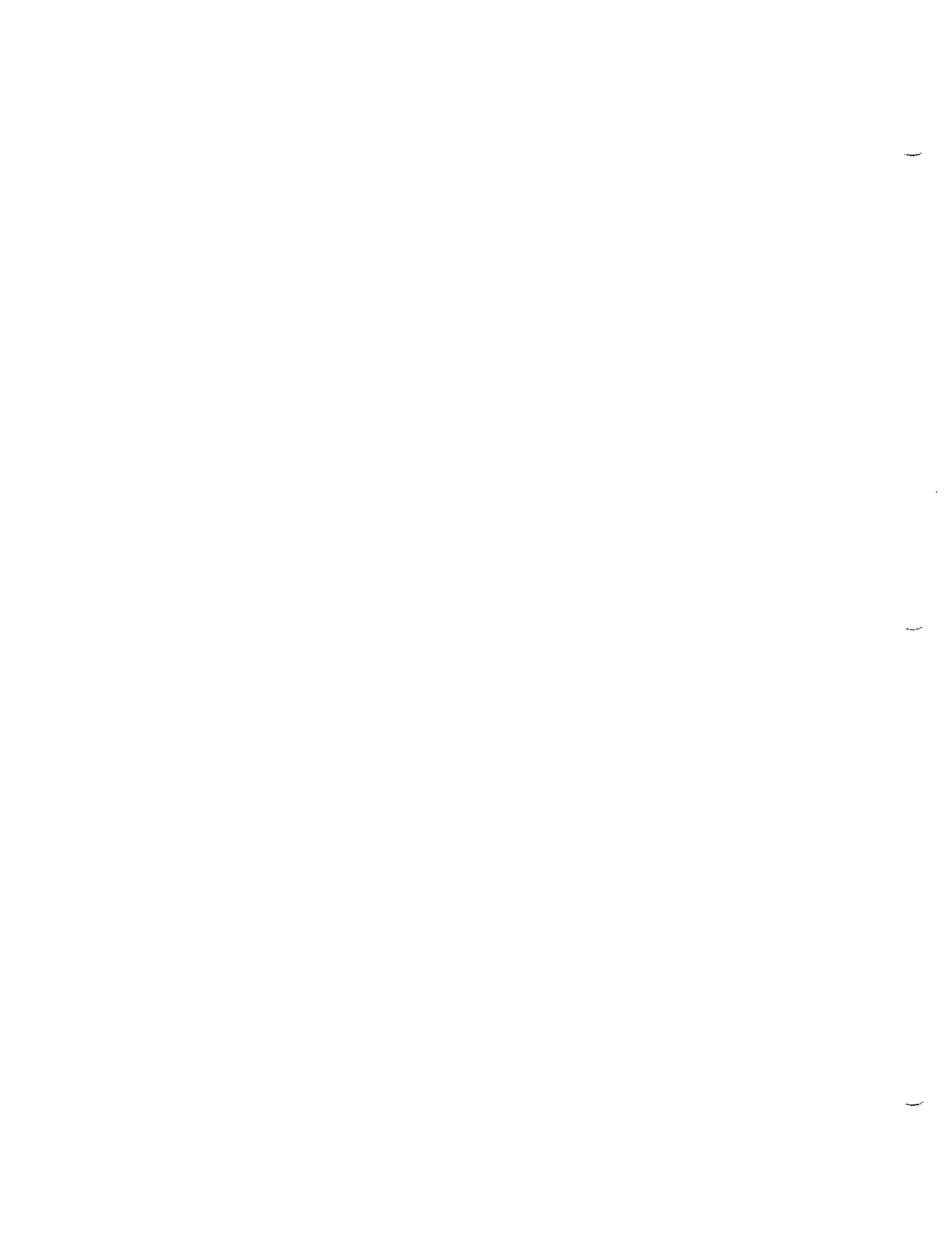
substantial pressure variations in the flowfield. Connected directly to the discharge of the High Pressure Oxidizer Pump (HPOP) is a venturi to determine the flowrate. The pressure is measured at the entrance of the venturi and another pressure transducer is located on the side of the duct in the middle of the duct turn. A pressure profile will exist at both of the pressure measurement locations. Thus, the conceptual bias represents an estimate of the difference between the measured pressure and the one-dimensional average pressure at that location. Thus, total systematic uncertainties between 1.5% and 2% of the measured value are used for the majority of the pressure measurements. These values are probably appropriate, however when experimental or computational results are obtained which provide additional information about the pressure profiles at the instrumented locations is obtained, the conceptual bias estimate can be updated.

2.7 Discussion of Venturi Systematic Uncertainties

The previous contract report[1] discussed in detail the estimation of the venturi flowrate uncertainties. The systematic uncertainties associated with the venturi flowrate determinations are between 2% and 3%. The primary uncertainty source was found to be the uncertainty associated with the venturi discharge coefficients. The venturis were calibrated with water at room temperature at maximum Reynolds numbers less than 10% of the Reynolds number during engine operation[5]. The difference between using water to simulate cryogenic propellants and the Reynolds number extrapolation for discharge coefficient are sources of systematic uncertainty.

It was also observed during the previous effort that the precision uncertainty of the flowrate measurements is a function of how the engine balances during the specific test. Meaning the precision uncertainty of a flowrate measurement represents the variation in the engine operation and not a measurement related variation.

2.8 Discussion of Valve Position Uncertainties

The systematic uncertainty estimate for the valve position measurements was used directly from the pre-test data review documents, 0.5%. The RVDT's were manufactured by Moxon, Inc., however attempts to contact Moxon for uncertainty information were unsuccessful. The precision uncertainty estimates based upon the baseline data set and the data

---

[5] Lepore, Frank A., Rocketdyne Division, Space Shuttle Main Engine No. 3001, Technology Test Bed, Differential Flowmeters Calibration Final Report, Contract No. NAS8-27980, March 1980.

reduction data sets indicates that the valve position test-to-test variation is the dominant uncertainty characteristic.

2.9   Discussion of Speed Measurement Uncertainties

Little information was obtained upon which to base turbopump speed measurement uncertainty estimates. A nominal 1% systematic uncertainty was estimated based upon engineering judgment. This is probably a very conservative value and should be updated when more information is obtained to support a better estimate.

3.0 Modeling Uncertainty Considerations

The numerical optimization and numerical solution strategy developed by Dr. Santi for the New SSME Model requires the uncertainty associated with each balance relation. The balance relations are used in the numerical solution algorithm to ensure that the conservation of mass and energy are within a certain preset tolerance at each node of the system. The numerical solution strategy in the new model uses uncertainty estimates to replace the numerical tolerances used in the basic ROCETS model. This section discusses how uncertainty estimates for the engine subcomponent models were obtained. A total of 92 balance relations are used in the current version of the model, the balance relations and the uncertainty estimates for each balance relation are shown in Appendix 5.

No accepted methodology currently exists for the assessment of uncertainties from analytical models. Within this research effort considerable progress has been made towards addressing this issue.

When comparing output of a model with experimental data, the uncertainties that should be associated with the model predictions must be considered for proper conclusions to be drawn. In the past, most of the work reported in this area has simply considered the sensitivity of the model output to uncertainties in the input data. This obviously does not include any uncertainties in the model itself and thus is not a satisfactory approach. In this research effort, we have divided the sources that cause uncertainty in the model output into three categories: (1) uncertainties due to assumptions and approximations in the model, (2) uncertainties due to the incorporation of previous experimental data into the model, and (3) uncertainties due to the numerical solution algorithm. Uncertainties due to the numerical solution algorithm are not considered in this effort because the magnitude of those uncertainties are much, much less than the uncertainties in the test data and the uncertainties in the subcomponent models.

3.01 Modeling Assumptions and Approximations

When a model of a physical system is developed, assumptions and approximations about the system are made to simplify the system to one which mathematical expressions can describe. By making these simplifications an error is introduced and the model cannot exactly describe the physical system. Some of the primary assumptions and approximations made within the subcomponent flow models include: 1-dimensional, fully developed, steady-state, adiabatic, ideal gas, inviscid, etc.

If the uncertainty to associate with a particular assumption or approximation can be estimated, then sometimes the model should be improved to include this estimate instead of trying to estimate the

14

uncertainty. For example, Dr. Santi determined that a turbine exit temperature was being predicted using an ideal gas, constant specific heat approximation, which for the specific temperature range of interest was a poor approximation. Instead of trying to estimate an uncertainty to associate with that approximation, the model was altered to include a better thermodynamic description of the process.

The first category, uncertainties due to assumptions and approximations in the model, does not include the installation and/or conceptual bias sources since those uncertainties are associated with the measured value. Consider the temperature at a particular position in the flow. The uncertainty associated with the measured value of the temperature includes the effect of making a point measurement but desiring a cross-sectional averaged value. The inability of the model to calculate a correct average temperature at a particular location because the one-dimensional flow approximation has been made results in an uncertainty in the predicted temperature. (Stated another way, if the model predicts the correct average temperature at a particular location, then the one-dimensional flow approximation has caused no uncertainty in the model output.)

If the individual engine subcomponent models are developed based upon the soundest assumptions and approximations available, assessing the uncertainty due to these assumptions and approximations would require an effort beyond the scope of the current research program.

3.02   Uncertainties from Previous Information

Uncertainties due to the incorporation of previous experimental data in the model arise when physical property data is used, when valve resistance characteristics are used, when turbopump performance maps are used, etc. These are all instances in which previous experimental data has been used by replacing the data with curvefits. The original data contained uncertainties, but the curvefit equations used in the predictive models have been treated as the "truth" in most previous considerations of uncertainty in model outputs. Adding further complication, there is no accepted way of estimating the influence of systematic uncertainties on the uncertainty associated with a regression. The methodology developed as a part of this program to assess regression uncertainties is discussed later.

In all of the sub-component modules, information from previous testing is used. For example, the model of the liquid oxygen flow through a duct or through a valve is based upon its component testing, which provides an equation for the resistance through the duct as function of the flowrate. This test information is often reduced to the form of a line or curve. The values of the polynomial constants in the thermodynamic property routines
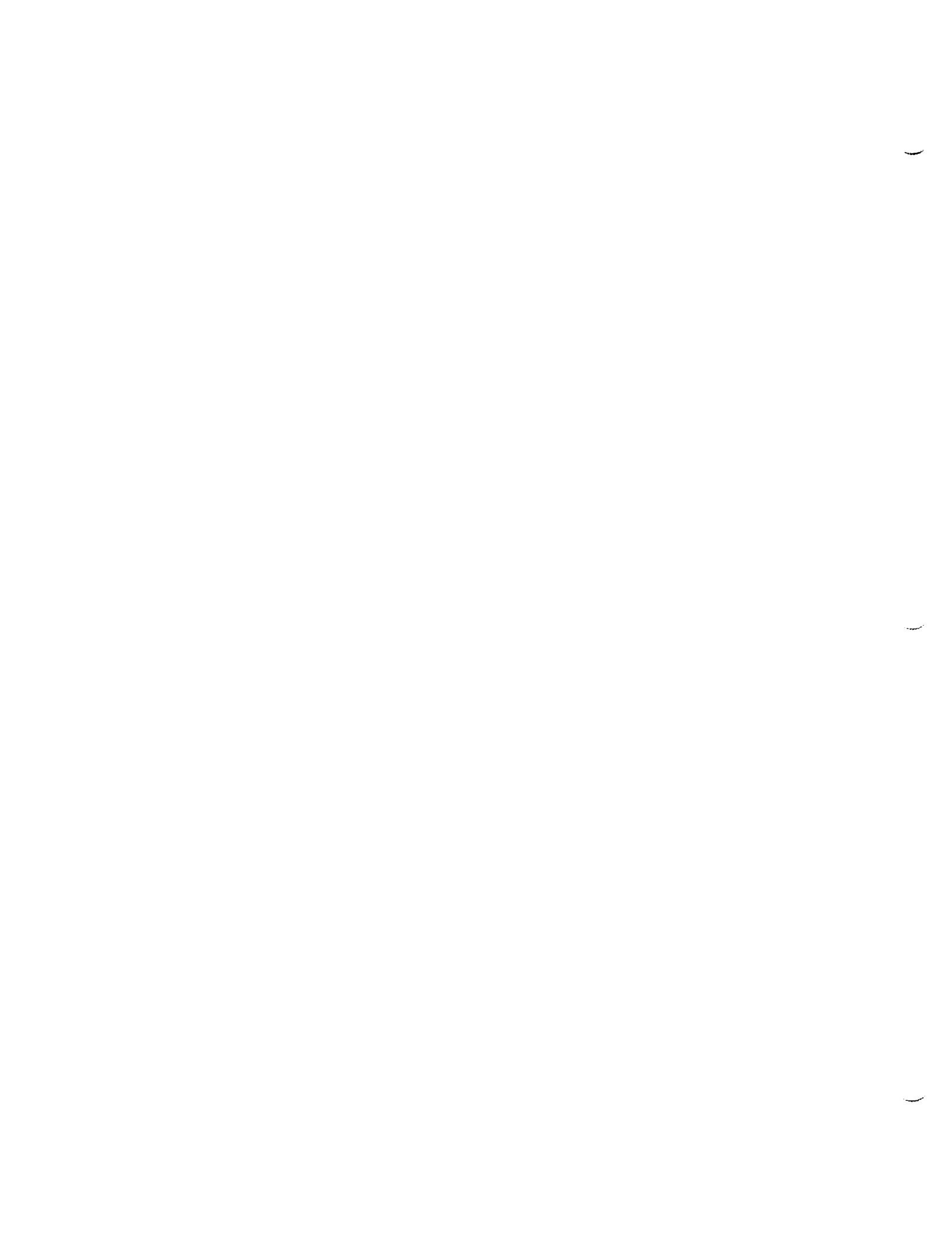
are also examples of using previously obtained uncertain test information in a model.

The methodology to assess the uncertainty in the coefficients of a linear regression were developed as part of this effort. The uncertainty analysis methodology presented in Appendix 1 was applied to the expressions for the regression coefficients to develop the technique. The details of this methodology were presented at the 1995 AIAA Aerospace Sciences conference[6]. The work presented in that paper demonstrated this technique provides the uncertainty in linear regression coefficients, and properly incorporates the effects of correlated systematic uncertainties. The research conducted during the AFOSR research program extended the methodology to provide the appropriate uncertainty interval for the predicted value using the regression model equation. The application of the regression uncertainty methodology to the types of models and previous experimental information found in the SSME program is shown in Appendices 3 and 4.

This chapter will discuss specific aspects of the assessment of the balance relation uncertainties. The only uncertainty sources being considered in the balance relation uncertainties are those due to the uncertain physical property data and the uncertainty due to the hardware characteristics, no uncertainties due to modeling assumptions and approximations were considered. The only exception to that statement is that an overall uncertainty for the heat flux correlation model is being estimated instead of propagating uncertainties for the individual constants.

3.1 Discussion of Physical Property Data Routine Uncertainties

When the model calls the physical property data subroutine to obtain the value of a state variable, density, enthalpy, entropy, etc., an uncertainty is introduced because the property data model is not the truth. The property data subroutines use data generated using curvefit equations to model experimental data. The thermophysical property package used in ROCETS is a property routine developed by Pratt & Whitney called PROP05.[7] PROP05 contains thermophysical property subroutines for Para-Hydrogen(H2), Oxygen (O2), steam (ST), Nitrogen (N2), and Methane (ME). The P&W letter introducing the availability of PROP05 states that the O2

---

[6] Brown, Kendall K., Coleman, Hugh W., and Steele, W. Glenn, "Estimating Uncertainty Intervals for Linear Regression," AIAA Paper 95-0796, 33rd Aerospace Sciences Meeting and Exhibit, Reno, NV, January 9-12, 1995.

[7] Long, R.A., and Perry, Michael, J., Internal Correspondence: Introduction of Property Package PROP05, August 16, 1988.

and ST tables are based on NASA Lewis database, which is provided in the programs GASP[8] and WASP[9], respectively. It also states that the "H2 tables are based on NBS database up to about 600 degree R and GASP database from 600 degree R to 5400 degree R."

The GASP documentation shows the uncertainty in density for Oxygen to be within ±0.2% outside the critical region and within approximately ±2.0% near the critical region. The WASP documentation shows the uncertainty in density for Steam to be within ±0.25% for the conditions of interest. The GASP documentation shows the uncertainty for Hydrogen outside of the critical region to be within ±0.2%. The NBS data[10] for low temperature hydrogen shows the uncertainty for density to be within ±0.1% outside the critical region and within approximately ±6.0% near the critical region. However, it is interesting to note that the GASP documentation shows that the uncertainty for the H2 property data near the critical region to be within ±2.5%. McCarty indicates the GASP routine uses a modified Benedict Webb Rubin (MBWR) equation of state and "the main disadvantage of the MBWR is that it is functionally incorrect in the critical region,   i.e. $\rho = \rho_c \pm 20\% \ \rho_c$.

3.2   Discussion of Combustion Routines

Related to the property routine uncertainty is the uncertainty in the combustion routines. Combustion occurs in the fuel and oxidizer preburners and the main combustion chamber. The combustion occurs at very high pressures, over 5200 psia in the preburners and 3126 psia in the main combustion chamber. Much of the combustion process is fuel-rich. The documentation available on the combustion routines in ROCETS is limited, the following comments are in the computer code:

1. THESE COMBUSTION CURVES WERE GENERATED FROM BRINKLY PERFECT GAS COMBUSTION DECK.

2. AN UNCOMBUSTED H2/O2 MIXED TEMPERATURE IS CALCULATED USING CONSTANT VALUES OF CP'S. THESE CP'S ARE CONSISTENT WITH THE VALUES OF CP'S USED TO GENERATE THE COMBUSTION PROPERTIES.

---

[8] Hendricks, Robert C., Baron, Anne K., and Peller, Ildiko C., *GASP - A Computer Code for Calculating the Thermodynamic and Transport Properties for Ten Fluids: Parahydrogen Helium, Neon, Methane, Nitrogen, Carbon Monoxide, Oxygen, Fluorine, Argon, and Carbon Dioxide*, NASA TN D-7808, February 1975.

[9] Hendricks, Robert C., Peller, Ildiko C, and Baron, Anne K., :*WASP - A Flexible Fortran IV Computer Code for Calculating Water and Steam Properties*, NASA TN D-7391, November 1973.

[10] McCarty, Robert D., *Hydrogen Technological Survey - Thermophysical Properties*, NASA SP-3089, Washington, DC, 1975.

3. NEXT THE H2/O2 COMBUSTION PROPERTIES ARE LOOKED UP AS A FUNCTION OF OFR AND MIXED TEMPERATURE. THESE COMBUSTION PROPERTIES WERE GENERATED AT 2500 PSI, AND WERE GENERATED FOR 5 MIXED H2/O2 TEMPERATURES OVER AN O/F RANGE OF .25 TO 100. A PRESSURE CORRECTION IS THEN APPLIED TO THE COMBUSTION TEMP. THE MAP INPUTS AND RESPECTIVE RANGES ARE:

    P   - 100. TO 5000. PSI
    TMIX - 200 TO 1000. DEG R (FOR BURN OPTION)
    TC   - 200 TO 6998. DEG R (FOR UNBURN OPTION)
    OFR - 0. TO 1.0

4. THE COMBUSTION PROPERTIES ARE THEN DILUTED FOR HELIUM.

An uncertainty for the combustion properties will exist based upon the assumptions and approximations and the property data used to build the combustion routine. One of the primary assumptions upon which the combustion routines are based is Dalton's partial pressure model, at high pressures and temperatures the Dalton model is not very accurate because of real gas effects. The constant specific heat assumption is also questionable at high temperatures and pressures. The injector characteristics, such as atomization, and heat transfer effects also introduce difficulties in the combustion modeling. From the information available, it could not be determined how well the other aspects of the combustion routine account for the real-gas and other real effects in high pressure, high temperature, fuel rich combustion processes. Thus, it is difficult to provide uncertainty estimates for the combustion properties, with the likely uncertainty in the 10% to 20% range.

3.3 Discussion of Hardware Characteristics Uncertainties

In general, the hardware characteristics used in the New SSME Model were taken from the Rocketdyne SSME Power Balance Model, version PBM 91a. The hardware characteristics are specific to each component and in most cases are based upon sub-component level testing. For example, the turbines were cold-flow tested to determine their non-dimensional performance and this information, after adjusting to engine operating conditions, is used in the model. Since this information was experimentally obtained it contains experimental uncertainties and obtaining or independently assessing the uncertainties was necessary for this effort. The following sections discuss the information obtained and the assessment of hardware characteristic uncertainties.

18
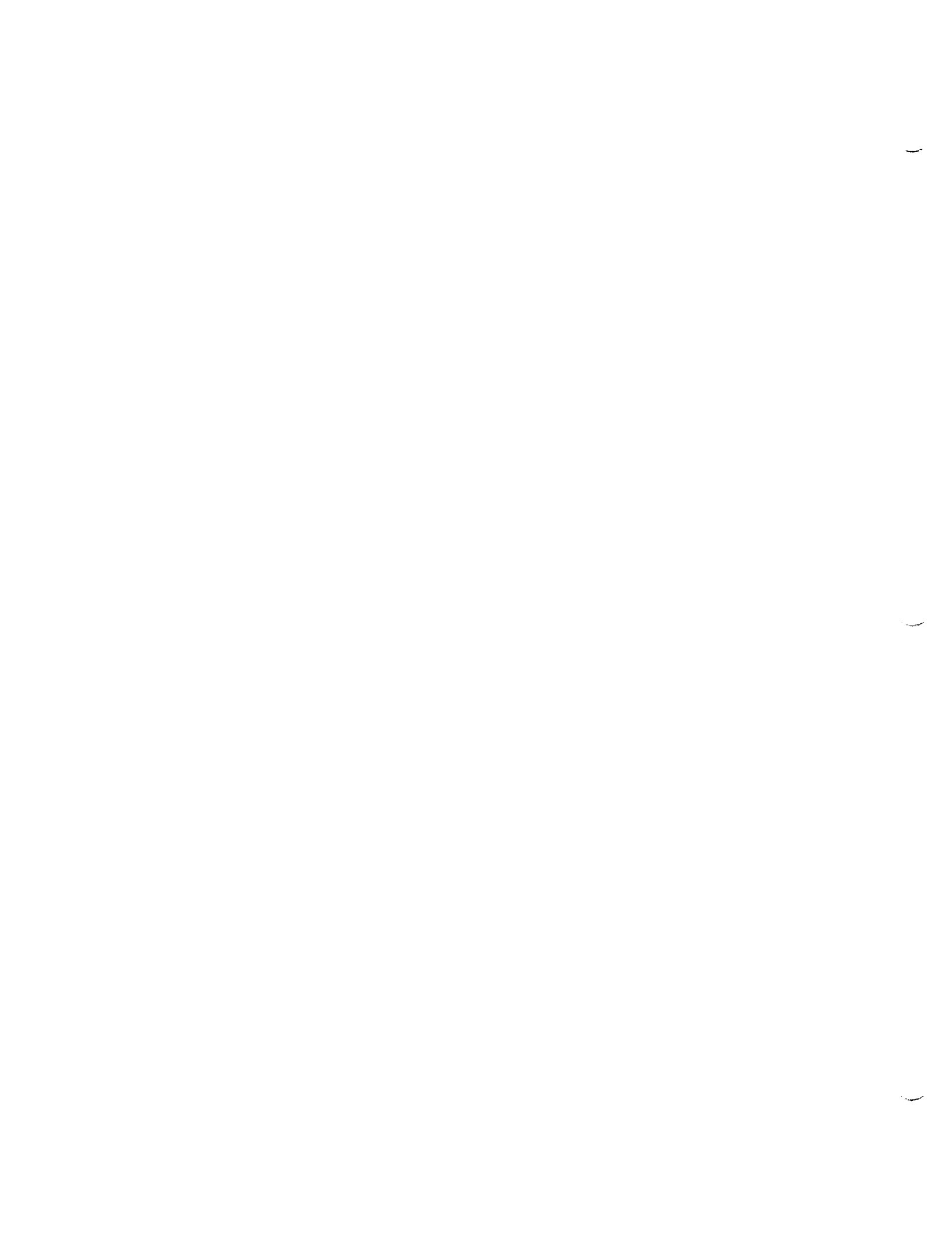
3.3.1   Discussion of Turbine Map Uncertainties

The performance of the turbines are represented in the models by using performance maps. These maps are based upon the available subcomponent test data or other analyses, and as such they are not perfect representations of the turbine performance. The uncertainty associated with each map must be estimated based upon how that particular map was generated.

3.3.1.1   HPFT Map Uncertainty

The HPFTP turbine efficiency map used in the ROCETS SSME model was obtained from the Digital Transient Model (DTM) and the SSME Power Balance Model, PBM 91a. Where the portion of the turbine efficiency parameter versus speed parameter map for the nominal operating points of the SSME (i.e. 100%, 104%, 109%) was taken from the Power Balance Model, version 91a The remaining portion of the map was taken from the DTM and is only used during transient simulations, engine starts and shutdowns. As discussed more thoroughly in Appendix 4, the high pressure fuel turbine was tested in the Turbine Test Equipment facility at MSFC in 1991.[11] The results of the cold-flow testing were analyzed by Rocketdyne engineers and the cold-flow turbine efficiency map was decreased by 3.2% to adjust to engine operating conditions[12]. The conversion of the air test results for SSME engine operation were made to account for thermal effects, Reynolds number effects, disk cooling, and platform seal leakage effects. Since each of these corrections is based upon a number of assumptions and approximation they introduce additional uncertainties, so an uncertainty source to account for the uncertainty in the correction terms must be included.

When the results from this testing, after applying the corrections, are plotted in the same form as the HPFT map in ROCETS, turbine efficiency divided by speed parameter versus speed parameter, Figure 1 is obtained. Since the map obtained from the cold-flow testing of the HPFT model provides essentially the same results at the mainstay operating conditions, it is proposed that the uncertainty associated with this map be used as the uncertainty in the HPFT balance relation. Details of how the uncertainty associated with a value from the air-test HPFT map are given in Appendix 3.

---

[11] Hudson, Susan T., Gaddis, Stephen W., Johnson, P., Dean, and Boynton, James, L., "Cold Flow Testing of the Space Shuttle Main Engine High Pressure Fuel Turbine Model," AIAA Technical Paper 91-2503, AIAA/SAE/ASME/ASEE 27th Joint Propulsion Conference, June 24-26, 1991, Sacramento, CA.

[12] Boynton, J., and Daumann, A., "Revision of SSME HPFTP Turbine Performance Based on NASA/MSFC Baseline Air Test Results," July 23, 1991.
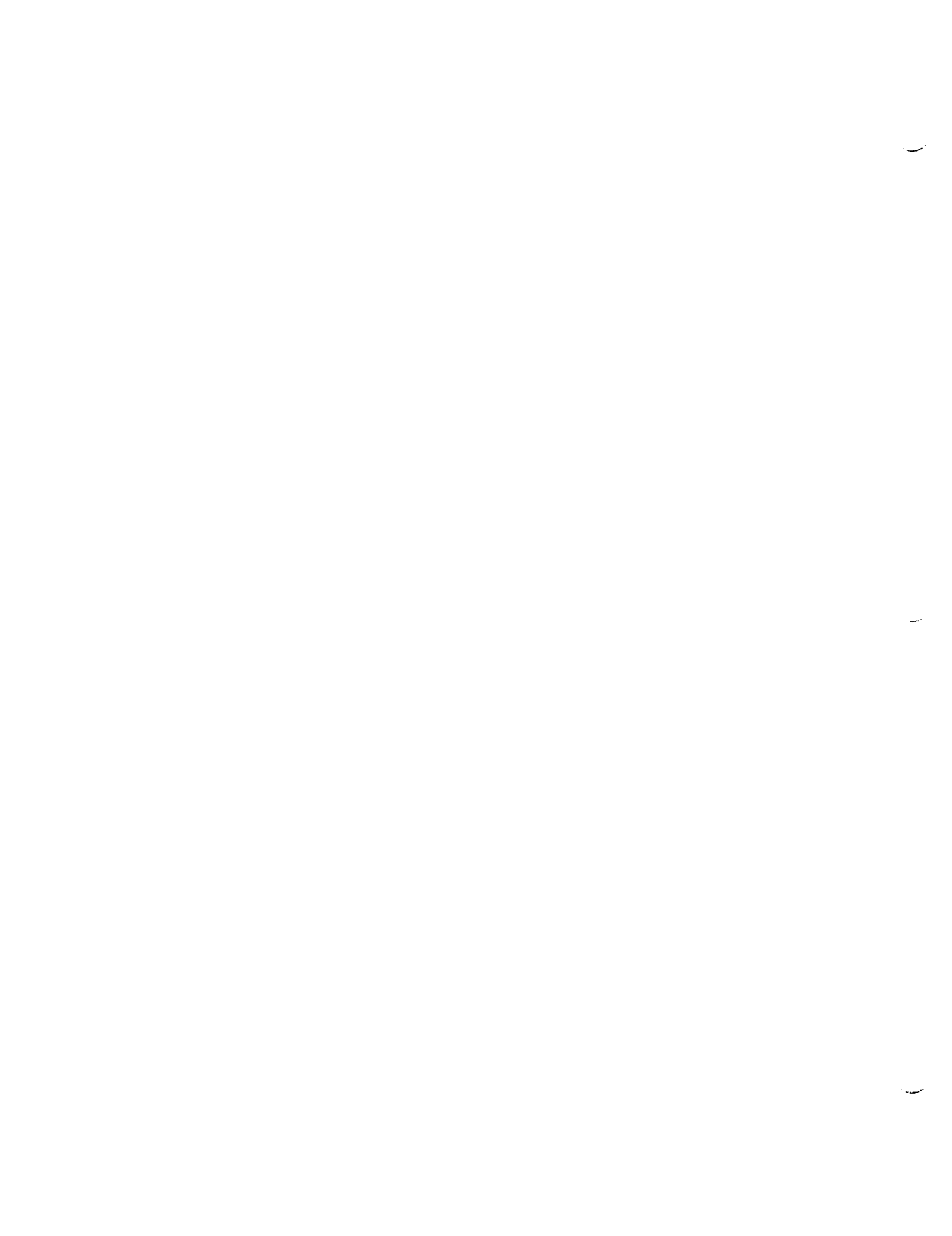
The total uncertainty associated with the HPFT map is the combination of the uncertainty from the cold-flow testing and the uncertainty in the corrections to engine conditions. This data reduction equation is

$$ETA_{map} = ETA_{test} + X_{cor} \times ETA_{test}$$
$$= ETA_{test} \times (1 + X_{cor})$$

(1)

The uncertainty expression for this equation is

$$U_{ETA_{map}} = \left\{ \left(\frac{\partial ETA_{map}}{\partial ETA_{test}} \right)^2 U^2_{ETA_{test}} + \left(\frac{\partial ETA_{map}}{\partial X_{cor}} \right)^2 U^2_{X_{cor}} \right\}^{\frac{1}{2}}$$

(2)

and after determining the partial derivatives and algebraically reducing the above equation the uncertainty expression can be written as

$$\frac{U_{ETA_{map}}}{ETA_{map}} = \left\{ \frac{U^2_{ETA_{test}}}{ETA^2_{test}} + \frac{U^2_{X_{cor}}}{(1 + X_{cor})^2} \right\}^{\frac{1}{2}}$$

(3)

Using the uncertainty in the cold-flow efficiency map determined in Appendix 3 of 0.75% and making a conservative estimation that the corrections applied to adjust to engine conditions is within 25%, the uncertainty in the map efficiency is 1.1%.
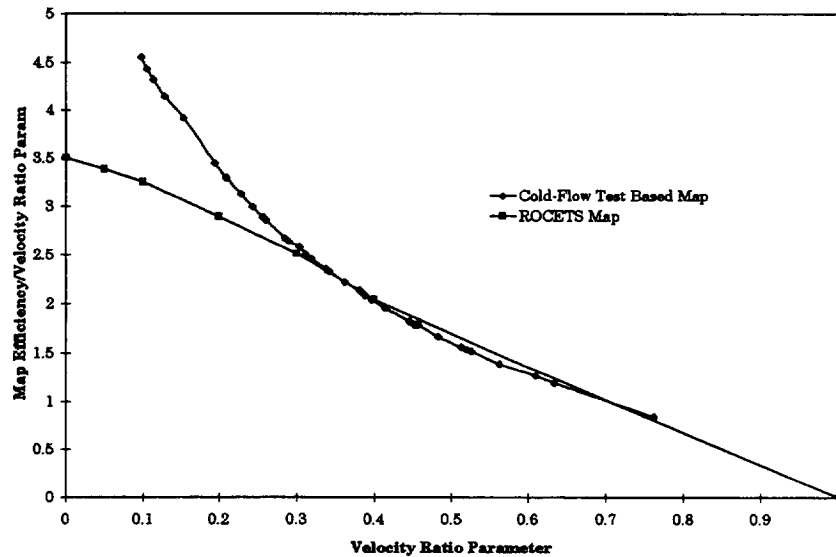
Figure 1 Comparison of HPFT Maps, map existing in ROCETS and map based upon cold-flow testing of the HPFT.

This uncertainty estimate represents the uncertainty in the performance on a high pressure turbine with the same characteristics as the model used in the cold-flow tests. This uncertainty does not include any

20

uncertainty due to manufacturing variations or any uncertainty due to wear-related performance degradations. By comparing this uncertainty estimate with the uncertainty estimates from the turbopump pump maps, which include these additional uncertainty sources, the uncertainty for the HPFT performance maps is increased to 4.0%.

3.3.1.2 Other Turbine Performance Map Uncertainties

Similar information was obtained for the high pressure oxidizer turbine; however, the HPOT test program was conducted in 1974 and while the cold-flow tests were conducted similarly to the HPFT tests, the experimental uncertainty would be expected to be greater.[13] Uncertainty estimates for the HPOT performance maps using this information and including additional uncertainty to account for manufacturing variability provides performance map uncertainties of 5%.

No information was obtained upon which to base uncertainty estimates for the low pressure fuel and oxidizer turbines., LPOT, and LPFT. Thus, uncertainty estimates of 5% were used for the turbine performance maps.

3.3.2 Discussion of Turbopump Pump Map Uncertainties

Information concerning the SSME turbopump pump maps was requested from the Turbomachinery Branch, Rocketdyne Division. Pump performance maps with $\pm 2\sigma$ bands representing the performance variation caused by manufacturing variability were provided, however the nomenclature and scale of the maps were not the same as the performance maps in the ROCETS model. The maps for the HPFP and the LPFP provided by Rocketdyne show "Normalized Head" versus "Normalized Flow," and the maps used in ROCETS show "Head Coefficient" versus "Flow Coefficient." The Rocketdyne provided maps for the LPOP and the HPOP use the same nomenclature of "Head Coefficient" versus "Flow Coefficient," but the scales and units are different. The relationship between the Rocketdyne provided performance maps and the ROCETS maps could not be determined prior to the end of this contract.

In order to make uncertainty estimates for the pump hardware characteristics, it is being assumed that the relationships between the two sets of maps are linear transformations that account for unit conversions and design point normalizations. Making this assumption allows the percent uncertainty from the Rocketdyne maps to be directly transferred to the ROCETS maps, and that uncertainty estimate will be used to determine the

---

[13] Boynton, J., Rocketdyne Division, Personal Communication, 27 March 1996.
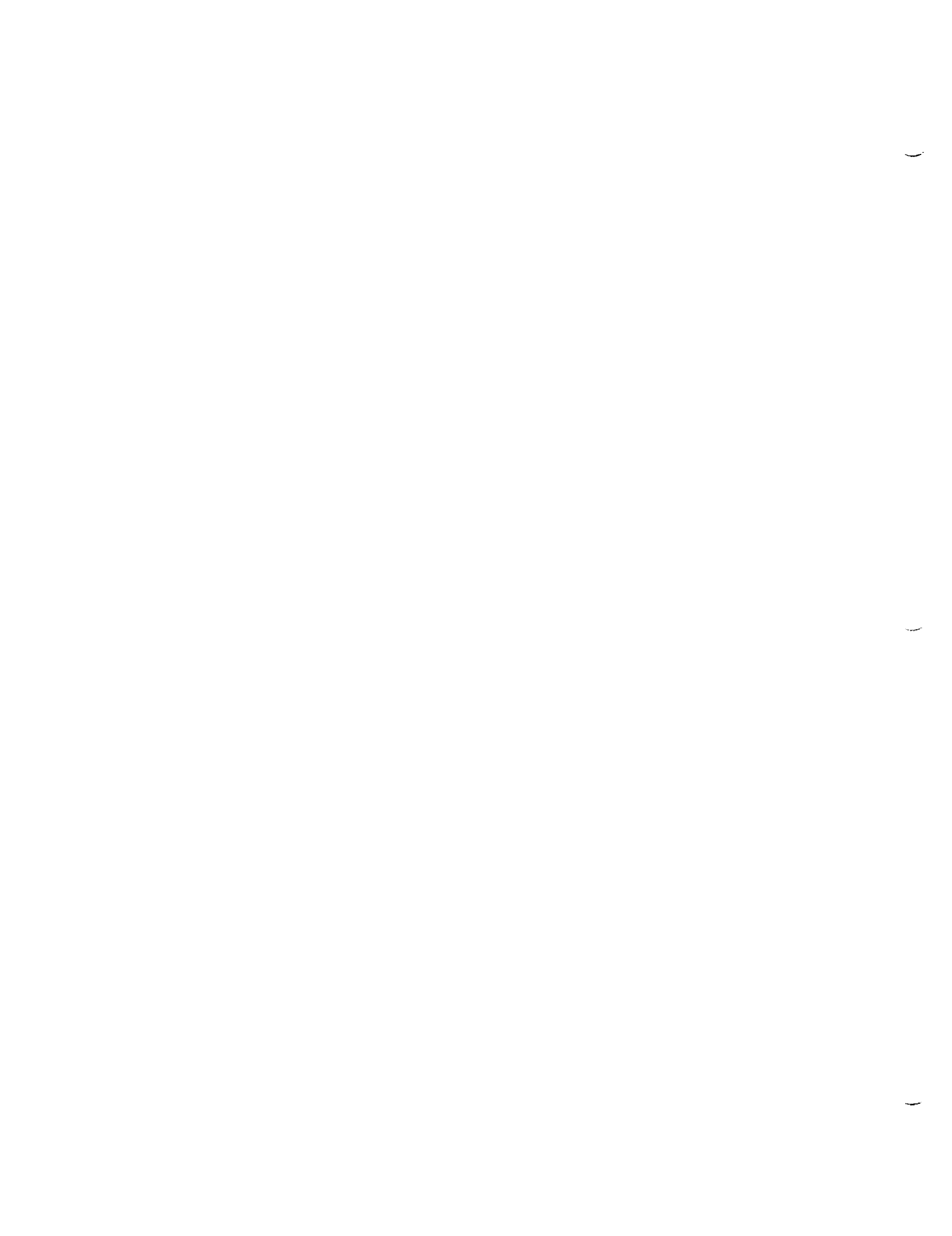
balance relation uncertainty. It is felt that this is a good assumption, with the information available If future information shows the relationship is non-linear then the hardware characteristic uncertainty for the pump performance maps will have to be estimated using the uncertainty propagation methodology provided in Appendix 1.

3.3.3   Discussion of Duct, and Valve Resistances

The duct and valve resistance values used in the ROCETS model originated from a variety of sources, and for most cases the exact origin of the resistance or flow coefficient values are not known. The uncertainties to associate with the values of the flow resistance hardware characteristics in the model must be estimated. Very little information is currently available to base these estimates. The ideal way to assess these uncertainties is to independently test the particular duct section at engine operating conditions and determine the flow resistance. This however is impractical, so the resistance values and their uncertainties must be otherwise estimated.

The resistance values for the ducts which contain the venturi flowmeters were taken from the venturi calibration report.[5] The venturi flowmeters were calibrated within the duct as installed in the TTB engine as an assembly. The resistance for the duct assemblies, with the venturi flowmeter, are provided in the venturi calibration report, however the uncertainties associated with the experimental determination of the resistance values are not provided. The origin of the resistance values of the other ducts and for the valves is unclear. The resistance values in the Rocketdyne Power Balance Model were obtained by analyzing engine hot-fire data and from separate analytical estimates. While some of the ROCETS resistance values could be obtained from the PBM, the PBM resistances cannot be used directly in the ROCETS model because the model flow circuits are significantly different

A review of how uncertainty estimates for the resistance would be estimated would be helpful. The flow resistance is defined by the expression

$$R = \frac{\Delta P \times RHO}{W^2} \tag{4}$$

where W is the total mass flowrate, ΔP is the pressure difference across the duct section, and RHO is the density of the fluid. The uncertainty expression is then

$$U_R = \left\{ \left(\frac{\partial R}{\partial \Delta P}\right)^2 U_{\Delta P}^2 + \left(\frac{\partial R}{\partial RHO}\right)^2 U_{RHO}^W + \left(\frac{\partial R}{\partial W}\right)^2 U_W^2 \right\}^{\frac{1}{2}} \tag{5}$$

22
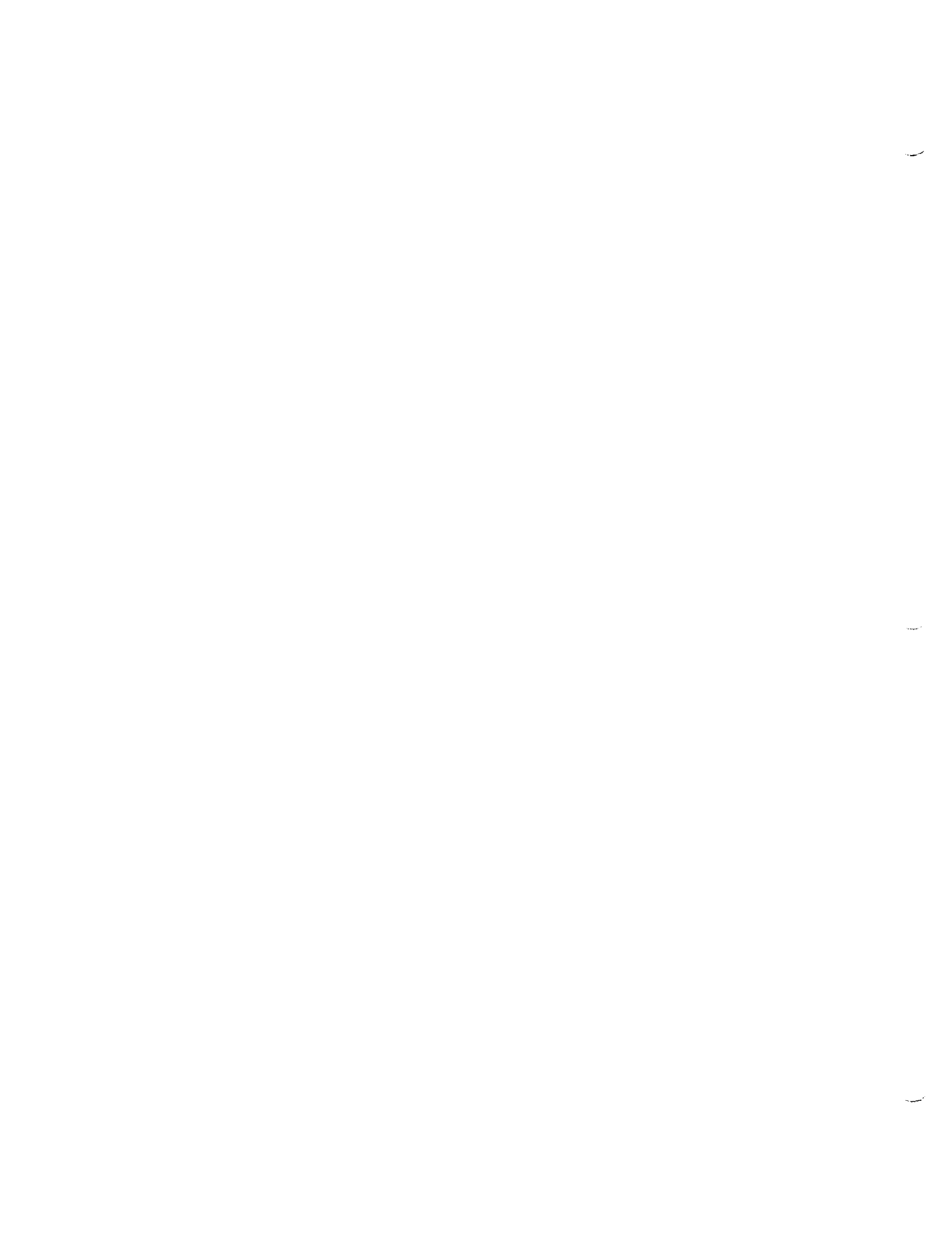
and the expression can be written in terms of percentage uncertainty as

$$\frac{U_R}{R} = \left\{ \left(\frac{U_{\Delta P}}{\Delta P}\right)^2 + \left(\frac{U_{RHO}}{RHO}\right)^2 + \left(-2 \times \frac{U_W}{W}\right)^2 \right\}^{\frac{1}{2}} \tag{6}$$

Now the resistance uncertainty can be examined by considering the uncertainties in the possible test rigs or test data. As Eq. (6) shows, the mass flowrate uncertainty has twice as much influence as the pressure difference or the density. As with the venturi calibration testing, the tests would be conducted with water at ambient conditions and the data would be extrapolated to engine operating Reynolds numbers. As was extensively discussed in the previous contract report, additional uncertainties may be introduced by not performing the tests with the actual cryogenic fluid.

3.3.4 Heat Transfer Calculations

The subroutines QH2 and QO2 calculate the convective heat flux to, or from, the fluid in a duct. This flux is multiplied by an effective area to obtain the total energy added to or removed from that volume. For example, the nozzle coolant heat transfer is calculated by using QH2 to determine the heat flux between the hot wall of the nozzle and the liquid Hydrogen coolant. This value is then multiplied by an effective heat transfer area to obtain the total energy added to the nozzle coolant volume. The heat flux calculation in QH2 is

$$Q' = \frac{0.0303}{D^{1.8}} \frac{W}{W^{0.2}} \left(\frac{TF}{TM}\right)^{.55} \left(\frac{C_P}{\mu}\right)^{.4} k^{.6}(TM - TF) \tag{7}$$

where W is the weight flowrate, D is the hydraulic diameter, TF is the fluid temperature, TM is the metal temperature, and C_P, μ, and k are fluid specific heat, viscosity, and thermal resistance, respectively. A different heat flux equation is in QH2 if coolant boiling occurs. The total heat transfer Q is then found with

$$Q = Q' \bullet A_{eff} \tag{8}$$

The origin of the heat flux correlation is not known, there is no documentation in the QH2 subroutine. The uncertainty for the heat flux equation can be estimated in two ways. First, uncertainties could be estimated for each of the parameters and constants in Eq. (6) and then propagated to obtain an uncertainty in Q'. But, probably the most appropriate way is to estimate the uncertainty for the overall heat transfer correlation by examining how the heat flux equation was developed. Since no information is available for these heat flux correlations, uncertainty estimates must be estimated based upon engineering judgment and knowledge of the accuracy of other heat transfer correlations. It is obvious that the uncertainty will be rather large by noting that the uncertainty in C_P,

23

μ, and k would be large for super-critical Hydrogen. Thus, heat flux uncertainties of 20% will be used.

The value of the effective area is also subject to uncertainty. Again looking at the nozzle coolant heat transfer, since the nozzle is made up of over a thousand individual tubes an accurate estimation of the actual heat transfer area would be difficult. The uncertainty to associate with the effective area must be estimated based upon how detailed the area calculation was.

3.4   Module Calculations and Uncertainty Expressions

The uncertainties from the physical property data and the hardware characteristics are propagated to obtain the uncertainties for the result of each module using the methodology presented in Appendix 1. This section will briefly present the equations used in each of the major subcomponent modules and how the hardware characteristics are propagated to obtain the uncertainty for the module results. The uncertainty expressions and calculations for each subcomponent are shown in Appendix 4.

3.4.1   Duct and Valve Flow Modules

The equation used in the FLOW00 module for the flowrate, W, through a duct is

$$W = \sqrt{\frac{\Delta P \times RHO}{R}} \tag{9}$$

where ΔP is the pressure difference across that section of duct, RHO is the density of the fluid in the duct, and R is the hardware characteristic for the flow resistance of the duct.

The expression for the uncertainty in the flowrate due to uncertainties in density from the property routine and uncertainty in the flow resistance value.

$$U_w = \left\{ \left(\frac{\partial W}{\partial R}\right)^2 U_R^2 + \left(\frac{\partial W}{\partial RHO}\right)^2 U_{RHO}^2 \right\}^{\frac{1}{2}} \tag{10}$$

and the expression can be written in terms of percentage uncertainty as

$$\frac{U_w}{W} = \left\{ \left(\frac{-1}{2}\frac{U_R}{R}\right)^2 + \left(\frac{1}{2}\frac{U_{RHO}}{RHO}\right)^2 \right\}^{\frac{1}{2}} \tag{11}$$

The calculations and the uncertainty calculations for the fuel and oxidizer valves are performed in the same manner as for the ducts and lines. The primary difference is that the resistance for the valve is a function of the
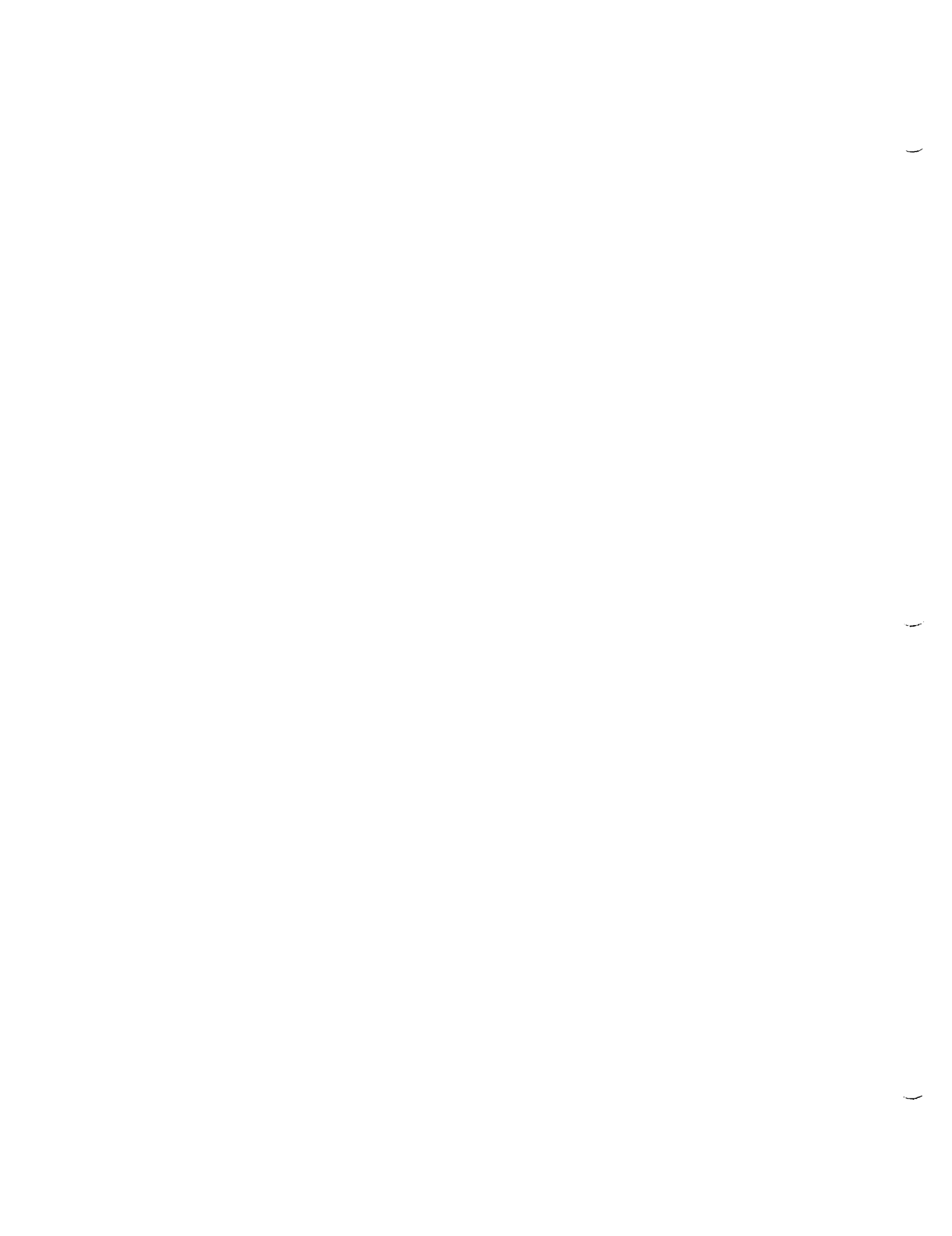
valve position and the resistance of the valve is added to the resistance value for the duct in which the valve is located.

Some of the ducts and valves use a slightly different model, they use a flow coefficient, CF, instead of a resistance. The equations for these ducts and valves have the form

$$W = \sqrt{\Delta P \times RHO \times CF^2 \times FLOCON} \qquad (12)$$

where FLOCON is defined as the flow constant, and considering uncertainties in density and the flow coefficient the uncertainty propagation for this is

$$\frac{U_W}{W} = \left\{ \left(\frac{U_{CF}}{CF}\right)^2 + \left(\frac{1}{2}\frac{U_{RHO}}{RHO}\right)^2 \right\}^{\frac{1}{2}} \qquad (13)$$

Comparing Eq. (13) to Eq. (11) shows that the uncertainty in flow coefficient has a direct relationship on the flow uncertainty, while only half of the uncertainty in resistance is propagated into the flow uncertainty.

3.4.2 Turbine Modules

The mass flowrate from the turbine is obtained directly from a map and thus the uncertainty is that of the map.

The energy from the exit of the turbine is found from the expression

$$HTOUT = HTIN - DH \qquad (14)$$

where *DH* is the predicted enthalpy drop across the turbine and obtained from the turbine maps for ETA_{map} and $DHIDL_{map}$ and the expression

$$DH = \left(ETA_{map}\right)\left(DHIDL_{map}\right) \qquad (15)$$

where

$$\begin{aligned} DHIDL_{map} &= HTIN - HTOUTI \\ &= HTIN - f(SIN, PTOUT) \end{aligned} \qquad (16)$$

and HTOUTI is the ideal exit enthalpy and is determined as an isentropic turbine process as a function of the exit pressure, inlet entropy, and the thermophysical property routine. Thus the energy balance relation uncertainty is a function of the uncertainty in the efficiency map and the physical property routine uncertainties. The uncertainty expression in percentage form is
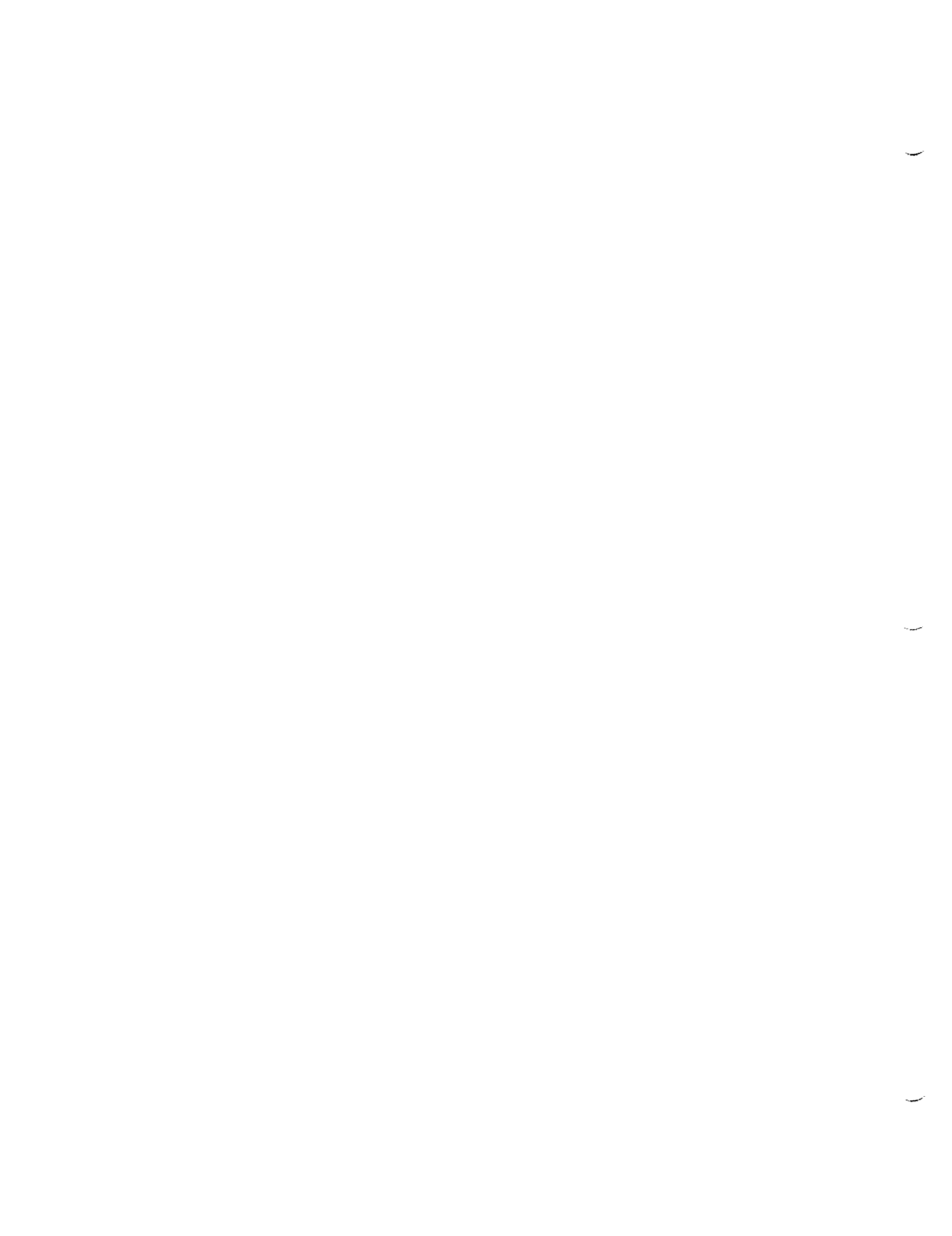
$$\frac{U_{DH}}{DH} = \left\{ \left(\frac{U_{ETA_{map}}}{ETA_{map}} \right)^2 + \left(\frac{U_{Prop}}{Prop} \right)^2 \right\}^{\frac{1}{2}} \tag{17}$$

Using the efficiency map uncertainty of 1.1% and an uncertainty of 0.5% from the thermophysical property package, the total uncertainty in DH is 1.2%.

3.4.3   Pump Modules

The equation for the exit pressure from a pump is

$$PT_{OUT} = PT_{IN} + PSI \times RHO \times SNRAD^2 \tag{18}$$

where PSI is the value from the head coefficient map at the flow coefficient, PHI, determined from the expression

$$PHI = \frac{W_{IN}}{RHO \times SNRAD} \tag{19}$$

and where W_{IN}, is the flowrate into the pump, and SNRAD is the pump speed in radians per second. The power required by the pump, QDOT, is calculated with

$$QDOT = -TORQ \times \frac{SNRAD}{RJ} \tag{20}$$

where TORQ is the pump torque. The pump torque is determined in the model with the equation

$$TORQ = -TAU \times RHO \times SNRAD^2 \tag{21}$$

where TAU is from the torque map parameter versus flow coefficient performance map.

The flows through the pumps are iteration variables, so the pump discharge pressure and the power required by the pump are the results used in the balance relations.

3.5   Balance Relation Uncertainties

The ROCETS model uses conservation of mass and conservation of energy at each flow circuit node to balance the system in the numerical solution algorithm. The 92 balance relations are shown in Appendix 4, as provided by Dr. Santi. In the data reconciliation optimization strategy developed by Dr. Santi the balance relation numerical tolerances are replaced by balance relation uncertainties based upon the hardware characteristic uncertainties and the physical property data uncertainties.

26
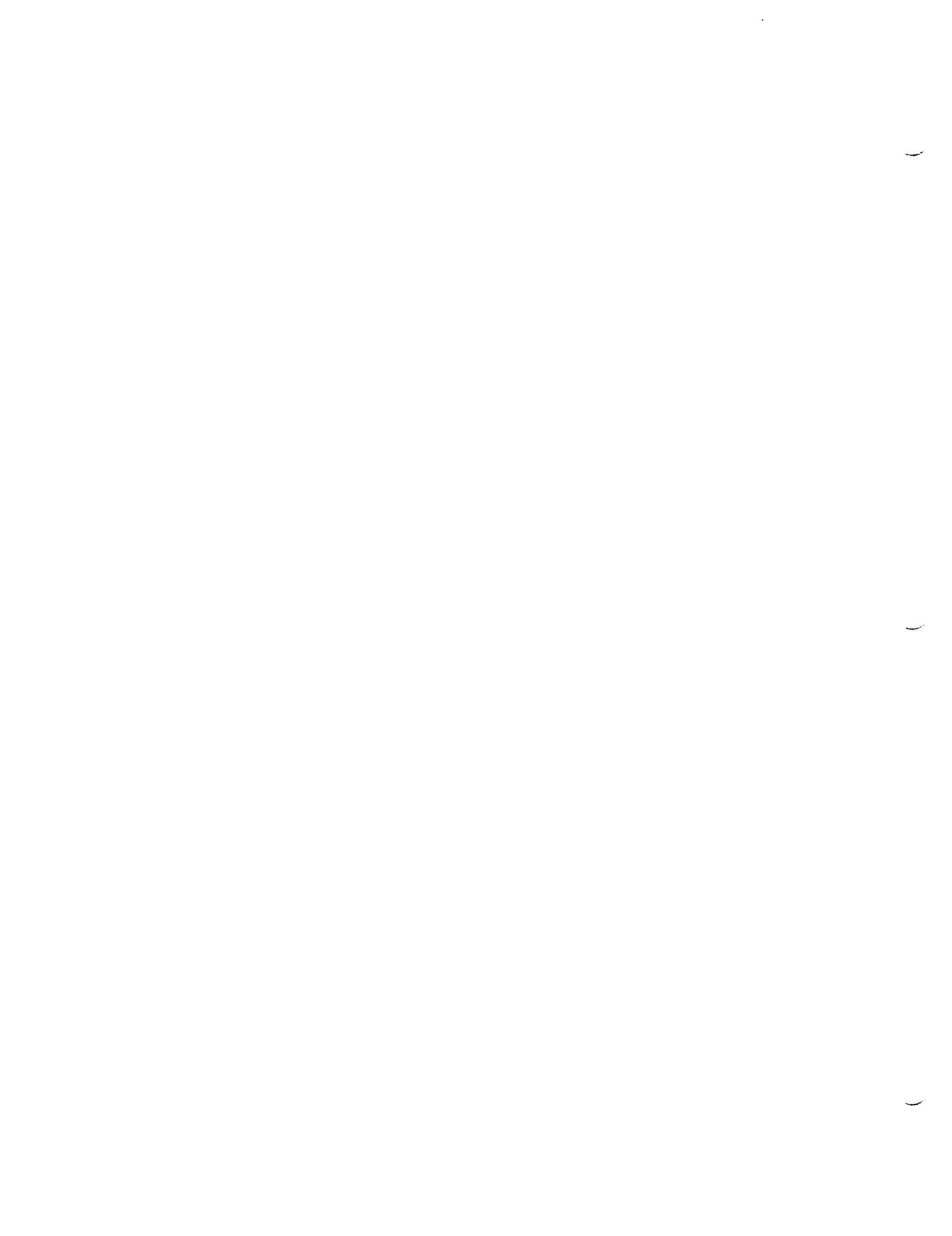
The balance relation can be rewritten by subtracting the left-hand side from the right-hand side, for the continuity and energy balance relations can be rewritten as

$$BAL\# = \sum W_{OUT} - \sum W_{IN} \qquad (22)$$

and

$$BAL\# = \sum Energy_{OUT} - \sum Energy_{IN} \qquad (23)$$

The balance relation uncertainty is determined by using the balance relations in this form and applying the uncertainty propagation methodology as presented in Appendix 1. In the solution algorithm certain parameters, pump flowrates, pressures, and enthalpies are iteration variables. No uncertainties are being considered for iteration variables.

Appendix 4 is the output from a MathCAD v.6.0+ file which contains the equations and calculations for the module parameters and uncertainties and the balance relation uncertainties. The balance relation equations and the balance relation uncertainties are summarized in Table 1 in Appendix 4.

4.0 Summary

This report has discussed the primary areas of uncertainty in the testing and modeling of a new Space Shuttle Main Engine model and performance analysis tool. The uncertainty estimates in this report will support the development of the new data integration and reconciliation model. The overall uncertainty estimates for the test data indicate systematic uncertainties are very important, and are often the dominate uncertainty characteristic. The development of the data reduction data sets indicated precision uncertainty estimates must be performed carefully to ensure proper comparisons. The work conducted to assess the uncertainties in the ROCETS subcomponent models was a unique extension of the uncertainty analysis methodology. It is now apparent that significant uncertainties exist in the hardware characteristics due to the uncertainty in the information used in the development of the characteristics. A methodology for assessing the uncertainty in linear regressions was developed and used to assess the uncertainty in the HPOT efficiency map.

4.1 Uncertainty Estimate Improvements

The uncertainty estimates provided in this report represent the best information available at the time of this report. They should not be considered final uncertainty estimates, they should be updated as more and better information becomes available. The uncertainty analysis methodologies presented in the appendices should be used to improve these estimates.

The following items are areas that need further investigation, or are areas where information was obtained too late in the performance period to allow proper analysis and inclusion in this report.

1. The balance relation uncertainty estimates for balance relations 50-69 and 79-93 need to be completed. These balance relations involve the combustion routines and involve the hot gas ducts and engine components. The complexity of many of these relations and time did not allow detailed investigation of these balance relations.

2. The pump maps provided by Rocketdyne do not correlate with the maps in the ROCETS model. The exact correlation of these maps and the map uncertainties must be obtained and the performance map uncertainty estimates updated, if necessary. The information provided by Rocketdyne is included in Appendix 7.

3. No uncertainty information was obtained for the LPOTP turbine and the LPFTP turbine. This information should be obtained and the balance relation uncertainty calculations updated.

4. The only uncertainty information obtained for HPOTP and HPFTp turbine performance maps was from cold flow testing of a single turbine model. Information describing the turbine performance variation based upon manufacturing variability is needed to update the estimates used in the balance relation uncertainty calculations.

5. The conceptual bias estimates for the static pressure measurements a the inlet and exits of the high pressure fuel and high pressure oxidizer pumps need to be re-examined. Information was provided by the MSFC Aerophysics Branch, Experimental Division, Structures and Dynamics Laboratory upon which better estimates of the conceptual bias uncertainties can be made. However, this information was obtained too late for inclusion in this report.
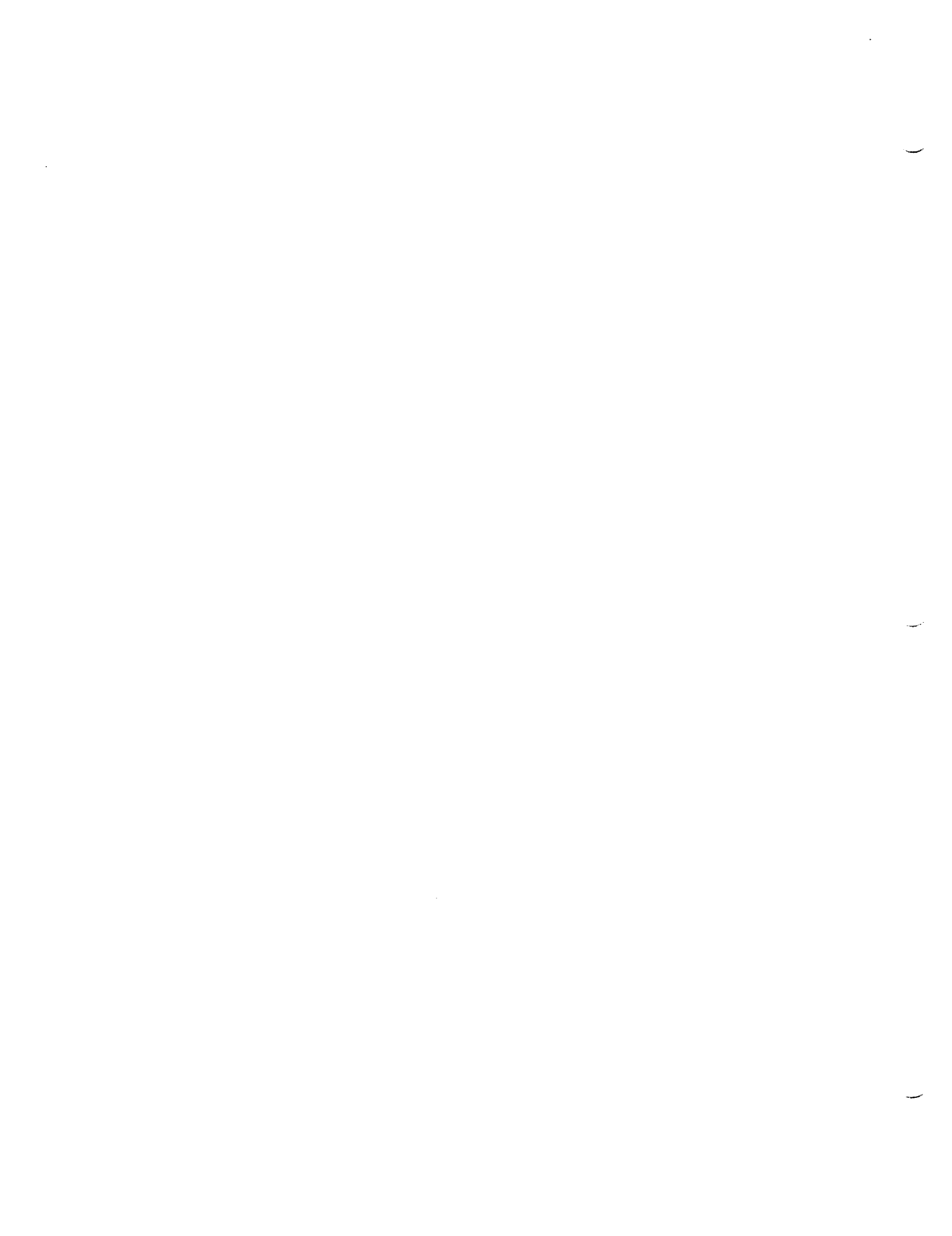
Appendix 1

Uncertainty Analysis

The use and application of uncertainty analysis in engineering has evolved considerably since Kline and McClintock's classic paper[1] in 1953. Developments in the field have been especially rapid and significant over the past decade, with the methods formulated by Abernethy and co-workers[2] that were incorporated into ANSI/ASME Standards in 1984[3] and 1986[4] being superseded by a more rigorous approach[5]. Publication in late 1993 by the International Organization for Standardization (ISO) of the *Guide to the Expression of Uncertainty in Measurement*[5] in the name of ISO and six other international organizations has, in everything but name only, established a new international experimental uncertainty standard.

The approach in the ISO Guide deals with "Type A" and "Type B" categories of uncertainties, not the more traditional engineering categories of bias and precision uncertainties, and is of sufficient complexity that its application in normal engineering practice is unlikely. This issue has been addressed by AGARD Working Group 15 on Quality Assessment for Wind Tunnel Testing and by the Standards Subcommittee of the AIAA Ground Test Technical Committee. The documents[6,7] produced by these groups present and discuss the additional assumptions necessary to achieve a less complex "large sample" methodology that is consistent with the ISO Guide, that is applicable to the vast majority of engineering testing (including most single-sample tests), and that retains the use of the traditional engineering concepts of bias and precision uncertainties. (The chapters on uncertainty methodology in the AGARD[6] and AIAA[7] documents were authored by the Principal Investigator of this research program.)

---

[1] Kline, S. J., and McClintock, F. A., "Describing Uncertainties in Single-Sample Experiments," *Mechanical Engineering*, Vol. 75, 1953.

[2] Abernethy, R. B., Benedict, R. P., and Dowdell, R. B., "ASME Measurement Uncertainty," *J. Fluids Engineering*, Vol. 107, 1985.

[3] American National Standards Institute/American Society of Mechanical Engineers, *Measurement Uncertainty for Fluid Flow in Closed Conduits*, MFC-2M-1983, ASME, 1984

[4] American National Standards Institute/American Society of Mechanical Engineers, *Measurement Uncertainty*, PTC 19.1-1985 Part 1, ASME, 1986.

[5] International Organization for Standardization, *Guide to the Expression of Uncertainty in Measurement*, ISO, ISBN 92-67-10188-9, 1993

[6] *Quality Assessment for Wind Tunnel Testing*, AGARD-AR-304, 1994.

[7] American Institute of Aeronautics and Astronautics, *Assessment of Wind Tunnel Data Uncertainty*, AIAA Standard S-071, 1995.

2.1 Overview

The word *accuracy* is generally used to indicate the relative closeness of agreement between an experimentally-determined value of a quantity and its true value. *Error* (d) is the difference between the experimentally-determined value and the truth, thus as error decreases accuracy is said to increase. Only in rare instances is the true value of a quantity known. Thus, one is forced to estimate error, and that estimate is called an uncertainty, U. Uncertainty estimates are made at some confidence level -- a 95% confidence estimate, for example, means that the true value of the quantity is expected to be within the ±U interval about the experimentally-determined value 95 times out of 100.

As shown in Figure 1(a), total error d can be considered to be composed of two components: a *precision* (random) component e and a *bias* (systematic) component b. An error is classified as precision if it contributes to the scatter of the data; otherwise, it is a bias error. It is assumed that corrections have been made for all systematic errors whose values are known. The remaining bias errors are thus equally as likely to be positive as negative.
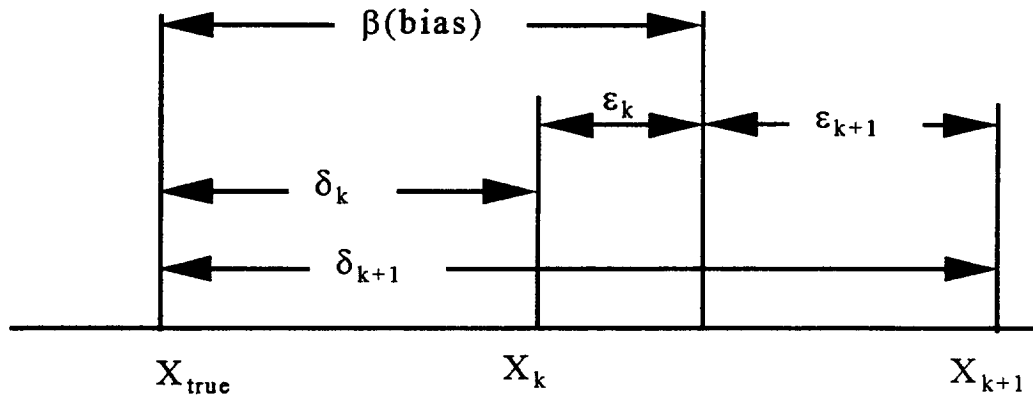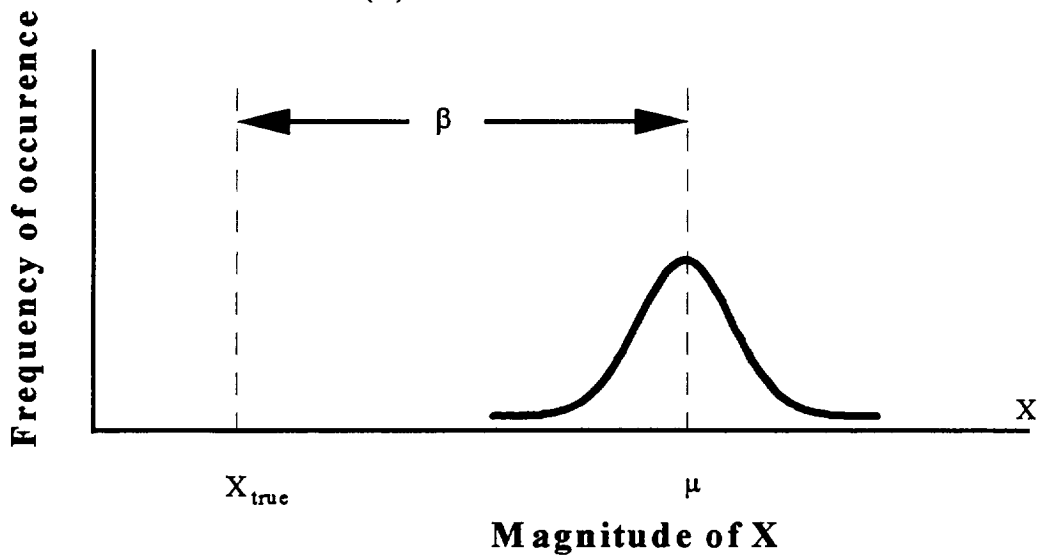
Figure 2.1 Errors in the Measurement of a Variable X:(a) two readings; (b) infinite number of readings.

Suppose that we are making a number of measurements of the value of a variable X that is absolutely steady. The k and k+1 measurements are shown in Figure 1(a). Since the bias is a fixed error, it is the same for each measurement. However, the precision error will have a different value for each measurement. It then follows that the total error in each measurement will be different, since the total error is the sum of the bias error and precision error in a measurement.

If we continued to take measurements as previously described until we had a sample of N readings, more than likely as N approached infinity the data would behave as shown in Figure 1(b). The bias error would be given by the difference between the mean (average) value m of the N readings and the true

value of X, whereas the precision errors would cause the frequency of occurrence of the readings to be distributed about the mean value.

As an estimator of β, a bias limit B is defined[8]. A 95% confidence estimate is interpreted as the experimenter being 95% confident that the true value of the bias error, if known, would fall within ±B. A useful approach to estimating the magnitude of a bias error is to assume that the bias error for a given case is a single realization drawn from some statistical parent distribution of possible bias errors. For example, suppose a thermistor manufacturer specifies that 95% of samples of a given model are within ±1.0 C of a reference resistance-temperature (R-T) calibration curve supplied with the thermistors. One might assume that the bias errors (the differences between the actual, but unknown, R-T curves of the various thermistors and the reference curve) belong to a Gaussian parent distribution with a standard deviation b=0.5 C. Then the interval defined by ±B = ± 2b = ±1.0 C would include about 95% of the possible bias errors that could be realized from the parent distribution. (The bias limit is sometimes called the "systematic uncertainty".)

As an estimator of the magnitude of the precision errors (the width of the distribution of readings in Figure 1(b)), a precision limit P is defined[8]. A 95% confidence estimate of P is interpreted to mean that the ±P interval about a single reading of X_i should cover μ 95 times out of 100. (The precision limit is sometimes called the "precision uncertainty".)

In nearly all experiments, the measured values of different variables are combined using a data reduction equation (DRE) to form some desired result. A good example is the experimental determination of mass flow rate using a venturi meter as discussed in the previous contract report[9]. Functionally, the mass flow rate is given as

$$W_e = W_e(P, T, \Delta P, d, D, \alpha, C_D) \tag{1}$$

One can envision that errors in the values of the variables on the right hand side of Eq. (1) will cause errors in the experimental result W_e.

A more general representation of a data reduction equation is

$$r = r(X_1, X_2, ..., X_J) \tag{2}$$

where r is the experimental result determined from J measured variables X_i. Each of the measured variables contains bias errors and precision errors. These errors in the measured values then propagate through the data reduction

[8] Coleman, H. W., and Steele, W. G., *Experimentation and Uncertainty Analysis for Engineers*, Wiley, New York, 1989.

[9] Coleman, Hugh W., and Brown, Kendall K., "Impact of Uncertainty on Modeling and Testing," Propulsion Research Center Report # 95-001, Final Report on NASA-Marshall Space Flight Center Contract NAS8-38609 D.O. #106, 10 January 1994 to 30 April 1995.

equation, thereby generating the bias and precision errors in the experimental result, r.

If the "large sample assumption" is made[6,7] then the 95% confidence expression for U_r becomes

$$U_r^2 = \sum_{i=1}^{J} \theta_i^2 B_i^2 + 2 \sum_{i=1}^{J-1} \sum_{k=i+1}^{J} \theta_i \theta_k B_{ik}$$
$$+ \sum_{i=1}^{J} \theta_i^2 P_i^2 + 2 \sum_{i=1}^{J-1} \sum_{k=i+1}^{J} \theta_i \theta_k P_{ik}$$

(3)

where

$$\theta_i = \frac{\partial r}{\partial X_i}$$

(4)

and where the 95% confidence precision limit for a variable X_i is estimated as

$$P_i = 2 S_i \qquad N \geq 10$$

(5)

and the sample standard deviation is calculated using

$$S_i = \left[\frac{1}{N-1} \sum_{k=1}^{N} [(X_i)_k - \overline{X}_i]^2 \right]^{1/2}$$

(6)

where the mean value is defined as

$$\overline{X}_i = \frac{1}{N} \left[\sum_{k=1}^{N} (X_i)_k \right]$$

(7)

and P_{ik} is the 95% confidence estimator of the covariance of the precision errors in X_i and X_k, and B_{ik} is the 95% confidence estimator of the covariance of the bias errors in X_i and X_k.

If we define the bias limit (systematic uncertainty) of the result as

$$B_r^2 = \sum_{i=1}^{J} \theta_i^2 B_i^2 + 2 \sum_{i=1}^{J-1} \sum_{k=i+1}^{J} \theta_i \theta_k B_{ik}$$

(8)

and the precision limit (precision uncertainty) of the result as

$$P_r^2 = \sum_{i=1}^{J} \theta_i^2 P_i^2 + 2 \sum_{i=1}^{J-1} \sum_{k=i+1}^{J} \theta_i \theta_k P_{ik}$$

(9)

then Eq. (3) can be written as

$$U_r^2 = B_r^2 + P_r^2$$

(10)

and Eqs. (8) and (9) can be viewed as propagation equations for the bias limits and precision limits, respectively.

2.2   Determining Precision Limits

Single Test. When the result is determined from a single test -- that is, at a given test condition the result is determined once using Eq. (2)

$$r = r(X_1, X_2, ..., X_J) \tag{2}$$

and when the X_i's are considered single measurements, then Eq. (9) is used to find the precision limit of the result. This situation is often encountered in large scale engineering tests in which measurements of the variables are made at a given set point over a period that is small compared to the periods of the factors causing variability in the experiment. A proper precision limit (one indicative of the dispersion of the variable over several cycles of the factors causing its variation) cannot be calculated from readings taken over such a small time interval. For such data, the measurement(s) of a variable X_i should be considered a single reading -- whether the value of X_i is the average of 10, 10^3 or 10^6 readings taken during the short measurement time. In such a test, the value for the precision limit to be associated with a single reading would have to be based on <u>previous information</u> about that measurement <u>obtained over the appropriate time interval</u>[10]. If previous readings of a variable over an appropriate interval are not available, then the experimenter must estimate a value for P_i using the best information available at that time[6,7].

For single tests in which some of the variables (X_2 and X_3, for instance) can be determined as averages from multiple readings over an appropriate time period but the other variables cannot be, then

$$r = r(X_1, \overline{X}_2, \overline{X}_3, ..., X_J) \tag{11}$$

and Eq. (9) is used to find the precision limit of the result as follows. For the variables that are single readings, the P_i's are the precision limits determined from previous information or estimated from the best available information. For the averaged variables when N_2 and N_3 are equal to or greater than 10, P_2 and P_3 should be taken as precision limits of means, $(2S_2)/(N_2)^{1/2}$ and $(2S_3)/(N_3)^{1/2}$, with the S's calculated using Eq. (6). When N_2 and N_3 are less than 10, it is the authors' recommendation that the precision limits used in Eq. (9) for the averaged variables be taken as $(P_2)/(N_2)^{1/2}$ and $(P_3)/(N_3)^{1/2}$, where P_2 and P_3 are determined from previous information, as is done for the single reading variables.

---

[10] Steele, W. G., Taylor, R.P., Burrell, R. E., and Coleman, H. W., "The Use of Data from Previous Experience to Estimate the Precision Uncertainty of Small Sample Experiments," *AIAA Journal*, Vol. 31, No. 10, 1993.

For tests in which multiple readings of *all* of the variables can be obtained over an appropriate period, the following method is recommended.

Multiple Tests. If a test is performed so that M multiple sets of measurements $(X_1, X_2, ... X_J)_k$ at the same test condition are obtained, then M results can be determined using Eq. (2) and an average result $\bar{r}$ can be determined using

$$\bar{r} = \frac{1}{M} \sum_{k=1}^{M} r_k \tag{12}$$

If the M sets of measurements were obtained over an appropriate time period, the precision limit that should be associated with a single result would be

$$P_r = t S_r \tag{13}$$

where t is determined with M-1 degrees of freedom and is taken as 2 for M≥10 and S_r is the standard deviation of the sample of M results

$$S_r = \left[\frac{1}{M-1} \sum_{k=1}^{M} (r_k - \bar{r})^2 \right]^{1/2} \tag{14}$$

The precision limit that should be associated with the average result is given by

$$P_{\bar{r}} = \frac{P_r}{\sqrt{M}} \tag{15}$$

with P_r given by Eq. (13). Using the large sample assumption, the uncertainty that should be associated with a single result would be

$$U_r^2 = B_r^2 + (2S_r)^2 \tag{16}$$

and with an average result $\bar{r}$

$$U_{\bar{r}}^2 = B_r^2 + \left(2 S_r / \sqrt{M} \right)^2 \tag{17}$$

with B_r given by Eq. (8).

Correlated Precision Uncertainties. The P_{ik} terms in Eq. (3) take into account the possibility of precision errors in different variables being correlated. These terms have traditionally been neglected[1,3,4,5,7], although precision errors in different variables caused by the same uncontrolled factor(s) are certainly possible and can have a substantial impact on the value of the precision limit[11]. In such cases, one would need to acquire sufficient data to allow a valid statistical estimate of the precision covariance terms to be made if using Eq. (3).

---

[11] Hudson, S. T., Bordelon, W., and Coleman, H. W., "Effect of Correlated Precision Errors on the Uncertainty of a Subsonic Venturi Calibration," AIAA-95-0797, 1995.

Note, however, that the multiple tests approach using Eq. (14) implicitly includes the correlated error effect -- a definite advantage when multiple sets of measurements over an appropriate time period are available.

2.3   Estimating Bias Limits

Bias Limits of Individual Variables. When attempting to estimate the bias limits B_i of the individual variables in Eq. (8), one might separate the bias errors which influence the measurement of a variable into different categories: calibration errors, data acquisition errors, data reduction errors, test technique errors, etc. Within each category, there may be several elemental sources of bias. For instance, if for the Jth variable, X_J, there are M elemental bias errors identified as significant and whose bias limits are estimated as $(B_J)_1$, $(B_J)_2$, ..., $(B_J)_M$, then the bias limit for the measurement of X_J is calculated as the root-sum-square (RSS) combination of the elemental limits

$$ B_J = \left[\sum_{k=1}^{M} (B_J)_k^2 \right]^{1/2} \tag{18} $$

The elemental bias limits, $(B_i)_k$, must be estimated for each variable X_i using the best information one has available at the time. In the design phase of an experimental program, manufacturer's specifications, analytical estimates and previous experience will typically provide the basis for most of the estimates. As the experimental program progresses, equipment is assembled, and calibrations are conducted, these estimates can be updated using the additional information gained about the accuracy of the calibration standards, errors associated with the calibration process and curvefit procedures, and perhaps analytical estimates of installation errors.

As Moffat[12] suggests, there can be additional <u>conceptual</u> bias errors resulting from not measuring the variable whose symbol appears in the data reduction equation. An example would be a point temperature measurement interpreted to be indicative of a cross-section averaged temperature, but there may be a cross-sectional variation of temperature, which may or may not have a predictable profile, causing the "average" value to be different than the point value. Hence, the inclusion of an elemental bias term for the conceptual error would be appropriate.

Correlated Bias Limits. Correlated bias limits are those that are not independent of each other, typically a result of different measured variables sharing some identical elemental error sources. It is not unusual for the uncertainties in the results of experimental programs to be influenced by the effects of correlated bias errors in the measurements of several of the variables.

---

[12] Moffat, R. J., "Describing the Uncertainties in Experimental Results," *Experimental Thermal and Fluid Science, Vol. 1, 1988.*

A typical example occurs when different variables are measured using the same transducer, such as multiple pressures sequentially ported to and measured with the same transducer or temperatures at different positions in a flow measured with a single probe that is traversed across the flow field. Obviously, the bias errors in the variables measured with the same transducer are not independent of one another. Another common example occurs when different variables are measured using different transducers all of which have been calibrated against the same standard, a situation typical of the electronically scanned pressure (ESP) measurement systems in wide use in aerospace test facilities. In such a case, at least a part of the bias error arising from the calibration procedure will be the same for each transducer, and thus some of the elemental bias error contributions in the measurements of the variables will be correlated.

The B_{ik} terms in Eq. (8) must be approximated -- there is in general no way to obtain the data with which to make a statistical estimate of the covariance of the bias errors in X_i and the bias errors in X_j. The approximation of such terms was considered in detail in Ref. 12, where it was shown that the approach that consistently gives the most satisfactory approximation for the correlated bias limits was

$$B_{ik} = \sum_{\alpha=1}^{L} (B_i)_\alpha (B_k)_\alpha \qquad (19)$$

where L is the number of elemental systematic error sources that are common for measurements of variables X_i and X_k.

If, for example,

$$r = r(X_1, X_2) \qquad (20)$$

and it is possible for portions of the bias limits B_1 and B_2 to arise from the same source(s), then Eq. (8) gives

$$B_r^2 = \theta_1^2 B_1^2 + \theta_2^2 B_2^2 + 2 \theta_1 \theta_2 B_{12} \qquad (21)$$

For a case in which the measurements of X_1 and X_2 are each influenced by 4 elemental error sources and sources 2 and 3 are the same for both X_1 and X_2, Eq. (18) gives

$$B_1^2 = (B_1)_1^2 + (B_1)_2^2 + (B_1)_3^2 + (B_1)_4^2 \qquad (22)$$

and

[13] Brown, K. K., Coleman, H. W., Steele, W. G., and Taylor, R. P., "Evaluation of Correlated Bias Approximations in Experimental Uncertainty Analysis," AIAA 94-0772, 1994.

$$B_2^2 = (B_2)_1^2 + (B_2)_2^2 + (B_2)_3^2 + (B_2)_4^2 \qquad (23)$$

while Eq. (19) gives

$$B_{12} = (B_1)_2(B_2)_2 + (B_1)_3(B_2)_3 \qquad (24)$$

Appendix 2
Baseline Data Set, Data Reduction Data, and Uncertainty Estimates

This appendix contains tables for the baseline data set (BDS), the data sets to use for data reduction and verification of the new model, and the associated uncertainty estimates. These data sets were generated by reviewing the test profiles of all Engine 3001 tests performed on the Technology Test Bed facility. The tests and time slices chosen and for inclusion in these sets have the same mixture ratios, inlet conditions, repressurization flowrates, and similar hardware configurations.

Engine Control Conditions: 104% RPL			
PTMCHB=PSMCHB?	63	MCC Pc Avg	3126.25
		mixture ratio	6.01
		O2 repress flowrate	1.10
		H@ repress flowrate	0.20
TTHTNK	1021	LPFP inlet temp lev 6B	37.02
TTVL18	1058	LPOP inlet temp lev 6A	166.27
PTHTNK	9910	LPFP INLET PR	38.43
PSVL18?	9911	LPOP INLET PR	97.56

ROCETS variable	PID #	NAME	avg	s	s (%)	B	B (%)	U	U (%)
PTFPRB=PSFPRB?	8500	FPB Pc (thru liner)	5278.81	74.86	1.4	105.58	2.0	183.20	3.5
PTOPRB=PSOPRB?	8458	OPB Pc (thru liner)	5244.05	11.21	0.2	104.88	2.0	107.25	2.0
PSPBSO	341	PBP discharge Pr NFD	7302.45	33.95	0.5	146.05	2.0	161.06	2.2
PSVL02	86	HPFP inlet Pr avg (LFDP)	237.72	4.14	1.7	4.75	2.0	9.55	4.0
PSVL19?	209/210 avg	HPOP inlet PR avg	337.20	14.97	4.4	6.74	2.0	30.69	9.1
SNFL	754	LPFTP Speed A	15668.87	28.52	0.2	313.38	2.0	318.53	2.0
SNFH	734	LPOTP speed NFD	5225.15	15.91	0.3	104.50	2.0	109.24	2.1
TTHTFD	231-232 AVG	HPFT discharge temp AVG	1801.09	26.15	1.5	36.02	2.0	63.51	3.5
TTHTOD	233-234 AVG	HPOT discharge temp AVG	1345.57	28.47	2.1	26.91	2.0	62.97	4.7
TTVL03	659	HPFP discharge temp	93.35	0.22	0.2	1.87	2.0	1.92	2.1
TTVL12	18	MCC clnt discharge temp B	429.56	3.56	0.8	8.59	2.0	11.15	2.6
WFOPB?	8805	OPB fuel flow (calc)	35.14	0.46	1.3	0.70	2.0	1.15	3.3
WLPFT	8801	LPFT inlet flow (calc)	29.51	0.34	1.2	0.59	2.0	0.90	3.1
XRFPOV	42	FPOV act pos A (FPV1)	82.94	1.29	1.6	0.83	1.0	2.72	3.3
XROPOV	40	OPOV act pos A (OPV1)	67.23	1.23	1.8	0.67	1.0	2.56	3.8

Table 1 Baseline Data Set for 104% rated power level.

Rocets Var	Pid #	Measurement Name	Test 21					Test 31				
	9903	SLICE START TIME	87	88	89	90	91	54	55	56	58	58
	9904	SLICE END TIME	88	89	90	91	92	55	56	57	58	59
	9906	MCC PC CONTROL	3126.25	3126.25	3126.25	3126.25	3126.25	3126.25	3126.25	3126.25	3126.25	3126.25
Data Reduction Measurements												
PTFPRB	8500	FPB Pc (thru liner)	5292.16	5286.79	5286.98	5773.48	5315.98	5245.12	5238.32	5244.72	5243	5240.67
PTOPRB	8458	OPB Pc (thru liner)	5227.96	5224.66	5222.16	5303.1	5268.42	5239	5224.06	5227.35	5224.67	5223.98
PTPBSO	341	PBP discharge Pr NFD	7344.22	7336.53	7341.87	7356.28	7335.17	7291.94	7279.96	7290.5	7289.63	7290.13
PTVL02	86	HPFP inlet Pr avg (LFDP)	231.89	231.41	231.37	232.46	231.38	239.66	239.66	238.93	238.94	239.36
PTVL20	209/210 avg	HPOP inlet PR	342.295	342.7	343.375	343.43	343.35	344.51	343.965	344.945	345.175	344.97
SNFL	754	LPFTP Speed A	15706.7	15687.64	15692.53	15710.43	15681.86	15660.83	15658.16	15650.89	15650.94	15652.05
SNOL	734	LPOTP speed NFD						5207.08	5204.37	5210.57	5208.67	5209.42
TTHTFD	231/232 avg	HPFT discharge temp avg	1770.755	1767.335	1765.095	1764.82	1763.485	1814.205	1810.11	1807.675	1810.45	1806.91
TTHTOD	233/234 avg	HPOT discharge temp avg	1313.36	1312.705	1319.19	1317.66	1321.58	1343.405	1349.415	1348.855	1344.93	1341.765
TTVL03	659	HPFP discharge temp	93.72	93.67	93.65	93.74	93.63	93.24	93.22	93.23	93.23	93.21
TTVL12	18	MCC clnt discharge temp B	433.39	432.72	432.99	433.26	433.78	425	425	425	425	425
WFOPB	8805	OPB fuel flow (calc)	35.93	35.68	35.56	35.94	35.68	35.01	35.02	35.04	34.98	34.93
WLPFT	8801	LPFT inlet flow (calc)	30.07	30.01	30.01	30.05	29.96	29.3	29.27	29.28	29.3	29.31
XROPOV	40	OPOV act pos A (OPV1)	65.75	65.74	65.59	65.44	65.35	67.16	67.14	67.25	67.28	67.34
XRFPOV	42	FPOV act pos A (FPV1)	81.1	81.05	81.07	80.96	81.04	83.38	83.42	83.43	83.29	83.26
Control Point Measurements												
PTMCHB	63	MCC Pc Avg	3129.9	3126.9	3127.43	3130.65	3125.09	3127.84	3123.97	3127.23	3125.86	3125.24
W01	9908	FACILITY FUEL FLOW						154.57	154.6	154.57	154.8	154.58
WLPFP	9909	FACILITY OXYGEN FLOW						925.99	925.66	926.12	924.73	926.22
		mixture ratio										
		O2 REPRESS FLOWRATE										
		H2 REPRESS FLOWRATE										
TTHTNK	1021	LPFP inlet temp lev 6B	36.98	36.97	36.99	36.98	36.98	37.04	37.04	37.04	37.04	37.04
TTVL18	1058	LPOP inlet temp lev 6A	167.02	167.03	167.02	167.02	167.02	164.67	164.72	164.69	164.7	164.72
PTHTNK	9910	LPFP INLET PR	35.64	35.67	35.74	35.64	35.68	39.3	39.24	39.27	39.28	39.36
PSVL18?	9911	LPOP INLET PR	97.63	97.87	97.77	97.68	97.95	95.89	95.81	95.77	95.87	95.99
Additional Measurements												
TTVL02	15	HPFP inlet temp avg	42.64	42.63	42.64	42.65	42.64	42.75	42.75	42.74	42.74	42.74
	639	LPFP DIS TEMP	47.77	47.76	47.76	47.79	47.78	43.62	43.62	43.63	43.62	43.63
PSVL03	459	HPFP DISCH PR NFD	6192.86	6185.23	6181.99	6194.29	6176.48	6184.88	6178.84	6181.06	6180.82	6178.73
PSVL21?	8751	HPOP DIS VENTURI IN PR	4158.62	4153.15	4154.17	4157.48	4150.93	4123.63	4118.52	4123.85	4122.26	4123.45
PSVL21?	334	HPOP discharge Pr NFD	4100.28	4096.31	4098.29	4100.07	4096.4	4095.83	4091.09	4096.82	4095.43	4096.36
PSVL13?	437	LPFT discharge Pr	3519.41	3516.44	3516.66	3520.99	3514.13	3512.16	3509.51	3511.79	3511.2	3510.76
PSVL21?	8684	MINJ LOX INJ PR 2	3633.41	3612.77	3589.74	3602.39	3583.06	3709.49	3692.87	3689.46	3686.24	3685.91
	8014	LPFT VENTURI PR	4502.18	4496.26	4497.19	4502.7	4494.02	4482.86	4478.68	4481.04	4480.04	4479.76
	8016	LPFT VENTURI TEMP	432.78	433.25	433.23	433.25	433.66	428.31	428.25	428.58	428.18	428.18
TTPBSO	93	PBP discharge temp ch A	208.4	208.37	208.4	208.46	208.39	207.17	207.11	207.17	207.16	207.18
PSVL04	356	MFV discharge Pr	5810.34	5803.32	5798.79	5815.18	5794.43	5827.87	5822.04	5823.7	5823	5821.86
PSVL12	17	MCC coolant discharge Pr A	4458.92	4454.12	4455.92	4461.32	4448.7	4472.38	4467.55	4469.98	4469.38	4466.34
WCCV	8818	CCV inlet flow (calc)	73.95	73.08	74.17	73.41	73.87	71.99	71.95	72.17	72.12	72.06
	8815	Nozzle clnt inlet flow-1 (calc)	14.26	14.25	14.21	14.21	14.35	14.33	14.24	14.35	14.26	14.21
	8816	Nozzle clnt inlet flow-2 (calc)	11.83	11.79	11.99	11.7	11.9	12.58	12.62	12.59	12.6	12.56
	8817	Nozzle clnt inlet flow-3 (calc)	14.38	14.33	14.79	14.39	14.61					
WF2		TOTAL NOZZLE FLOW	40.47	40.37	40.99	40.3	40.86					
WLPOT	8802	LPOT inlet flow (calc)	190.14	191.71	191.68	190.73	189.8	192.33	192.15	192.32	192.31	192.25
WHPOP-...	8819	HPOP discharge flow (calc)	897.49	896.23	894.75	897.59	897.96	895.92	895.26	895.72	895.33	894.77
WLPOV	8804	OPB LOX flow (calc)	26.72	26.79	26.65	26.62	26.88	26.69	26.65	26.65	26.66	26.7
WFPOV	8810	FPB LOX flow (calc)	76.06	75.66	76.66	76.17	75.1	74.76	74.65	74.83	74.68	74.62

Table 2. Data Reduction Data Sets, Tests TTB021 and TTB031, 104% RPL

Rocets Var	Pid #	Measurement Name	Test 34					Test 35				
	9903	SLICE START TIME	85	86	87	88	89	100	101	102	103	104
	9904	SLICE END TIME	86	87	88	89	90	101	102	103	104	105
	9906	MCC PC CONTROL	3126.25	3126.25	3126.25	3126.25	3126.25	3126.25	3126.25	3126.25	3126.25	3126.25
		Data Reduction Measurements										
PTFPRB	8500	FPB Pc (thru liner)	5236.44	5240.71	5239.96	5246.64	5248.59	5240.23	5239.51	5236.87	5239.46	5240.5
PTOPRB	8458	OPB Pc (thru liner)	5246.53	5252.03	5249.48	5256.98	5260.53	5246.12	5247.46	5243.82	5245.07	5247.7
PTPBSO	341	PBP discharge Pr NFD	7255.93	7263.66	7257.74	7266.36	7275.97	7315.48	7315.84	7308.52	7309.89	7323.35
PTVL02	86	HPFP inlet Pr avg (LFDP)	240.86	241.28	241.04	241.19	241.31	238.51	238.96	238.76	238.85	238.62
PTVL20	209/210 avg	HPOP inlet PR	313.825	313.33	313.3	312.81	312.425	347.96	348.195	347.855	347.985	347.6
SNFL	754	LPFTP Speed A	15675.19	15690.27	15684.83	15694.82	15701.25	15634.3	15642.48	15633.59	15636.38	15632.3
SNOL	734	LPOTP speed NFD	5236.18	5238.45	5238.25	5240.93	5243.53	5228.44	5228.57	5226.61	5227.73	5228.49
TTHTFD	231/232 avg	HPFT discharge temp avg	1808.455	1808.795	1807.435	1812.065	1811.91	1818.71	1818.805	1816.475	1818.425	1819.885
TTHTOD	233/234 avg	HPOT discharge temp avg	1372.05	1374.25	1377.875	1373.725	1370.64	1344.175	1346.25	1344.285	1345.6	1349.595
TTVL03	659	HPFP discharge temp	93.16	93.21	93.21	93.25	93.29	93.25	93.26	93.23	93.25	93.25
TTVL12	18	MCC clnt discharge temp B	431.01	431.42	431.95	429.97	432.08	428.9	428.64	428.62	428.36	429.02
WFOPB	8805	OPB fuel flow (calc)	34.62	34.63	34.65	34.74	34.74	35.16	35.16	35.11	35.14	35.11
WLPFT	8801	LPFT inlet flow (calc)	29.29	29.36	29.36	29.38	29.38	29.38	29.39	29.38	29.42	29.41
XROPOV	40	OPOV act pos A (OPV1)	68.44	68.56	68.62	68.64	68.47	67.66	67.49	67.59	67.54	67.43
XRFPOV	42	FPOV act pos A (FPV1)	83.84	83.94	84.11	83.99	83.8	83.55	83.45	83.44	83.43	83.32
		Control Point Measurements										
PTMCHB	63	MCC Pc Avg	3123.55	3126.85	3124.3	3127.75	3129.02	3127.55	3126.56	3126.25	3127.31	3128.14
W01	9908	FACILITY FUEL FLOW	154.36	154.51	154.4	154.54	154.55	154.72	154.78	154.68	154.69	154.63
WLPFP	9909	FACILITY OXYGEN FLOW	924.69	926.18	926.53	925.28	925.58	923.77	925.27	925.09	924.78	925.48
		mixture ratio										
		O2 REPRESS FLOWRATE										
		H2 REPRESS FLOWRATE										
TTHTNK	1021	LPFP inlet temp lev 6B	37.01	37.01	37.01	37.01	37.01	37.06	37.05	37.06	37.06	37.06
TTVL18	1058	LPOP inlet temp lev 6A	166.4	166.42	166.41	166.39	166.39	166.95	166.96	166.99	166.95	166.98
PTHTNK	9910	LPFP INLET PR	39.45	39.38	39.33	39.39	39.27	39.47	39.39	39.41	39.46	39.31
PSVL18?	9911	LPOP INLET PR	58	57.4	56.89	56.33	55.76	99.13	99.06	99.02	99.04	98.84
		Additional Measurements										
TTVL02	15	HPFP inlet temp avg	42.71	42.72	42.72	42.72	42.72	42.74	42.74	42.75	42.74	42.74
	839	LPFP DIS TEMP	43.54	43.52	43.54	43.51	43.54	43.36	43.34	43.29	43.27	43.25
PSVL03	459	HPFP DISCH PR NFD	6188.72	6196.67	6195.75	6203.11	6206.27	6181.46	6183.36	6178.11	6180.85	6181.69
PSVL21?	8751	HPOP DIS VENTURI IN PR	4127.57	4132.15	4128.61	4134.25	4137.48	4135.67	4134.57	4132.84	4134.2	4137.59
PSVL21?	334	HPOP discharge Pr NFD	4095.04	4096.81	4095.57	4100.92	4104.32	4101.72	4101.1	4099.01	4100.31	4103.47
PSVL13?	437	LPFT discharge Pr	3514.27	3516.51	3514.85	3518.94	3520.88	3519.1	3518.71	3516.19	3517.62	3518.02
PSVL21?	8684	MINJ LOX INJ PR 2	3628.03	3636.24	3631.92	3634.64	3648.95	3642.96	3641.65	3638.77	3642.1	3639.3
	8014	LPFT VENTURI PR	4484.08	4488.04	4486.1	4491.42	4493.93	4481.58	4482.37	4478.8	4480.82	4481.75
	8016	LPFT VENTURI TEMP	432.68	432.3	432.15	431.83	432.49	430.78	430.74	430.32	430	430.2
TTPBSO	93	PBP discharge temp ch A	210.25	210.3	210.28	210.33	210.44	210.19	210.22	210.19	210.2	210.25
PSVL04	356	MFV discharge Pr	5823.31	5830.96	5830.03	5836.09	5839.32	5822.53	5825.12	5819.56	5821.26	5822.59
PSVL12	17	MCC coolant discharge Pr A	4467.19	4470.81	4467.79	4475.67	4478.06	4454.84	4456.69	4453.05	4455.44	4453.04
WCCV	8818	CCV inlet flow (calc)	71.91	71.89	72	71.96	71.94	72.21	72.12	72.2	72.25	72.27
	8815	Nozzle clnt inlet flow-1 (calc)	13.73	13.7	13.65	13.63	13.7	13.88	13.86	13.84	13.8	13.79
	8816	Nozzle clnt inlet flow-2 (calc)	12.19	12.26	12.22	12.23	12.26	12.13	12.16	12.12	12.17	12.12
	8817	Nozzle clnt inlet flow-3 (calc)	14.27	14.3	14.34	14.43	14.39	14.27	14.31	14.25	14.29	14.3
WF2		TOTAL NOZZLE FLOW	40.19	40.26	40.21	40.29	40.35	40.28	40.33	40.21	40.26	40.21
WLPOT	8802	LPOT inlet flow (calc)	191.85	192.03	191.97	192.03	192.08	191.55	191.64	191.61	191.58	191.61
WHPOP-...	8819	HPOP discharge flow (calc)	898.45	899.68	899.29	899.9	900.17	924.06	924.21	924.46	924.35	925.42
WLPOV	8804	OPB LOX flow (calc)	27.27	27.3	27.25	27.3	27.33	27.92	27.88	27.9	27.89	27.94
WFPOV	8810	FPB LOX flow (calc)	74.94	75.14	75.06	75.17	75.26	75.33	75.31	75.24	75.38	75.32

Table 3. Data Reduction Data Sets, Tests TTB034 and TTB035, 104% RPL

| Rocets Var	Pid #	Measurement Name		Avg	s	s (%)	B	B (%)	U	U (%)
	9903	SLICE START TIME								
	9904	SLICE END TIME								
	9906	MCC PC CONTROL		3126.25						
Data Reduction Measurements										
PTFPRB	8500	FPB Pc (thru liner)		5278.81	118.67	2.2	79.18	1.5	250.20	4.7
PTOPRB	8458	OPB Pc (thru liner)		5244.05	19.53	0.4	78.66	1.5	87.82	1.7
PTPBSO	341	PBP discharge Pr NFD		7302.45	30.82	0.4	146.05	2.0	158.53	2.2
PTVL02	86	HPFP inlet Pr avg (LFDP)		237.72	3.69	1.6	4.75	2.0	8.78	3.7
PTVL20	209/210 avg	HPOP inlet PR		337.20	14.37	4.3	6.74	2.0	29.53	0.8
SNFL	754	LPFTP Speed A		15668.87	26.51	0.2	156.69	1.0	165.41	1.1
SNOL	734	LPOTP speed NFD		5225.15	13.60	0.3	52.25	1.0	58.91	1.1
TTHTFD	231/232 avg	HPFT discharge temp avg		1801.09	24.94	1.4	36.02	2.0	61.53	3.4
TTHTOD	233/234 avg	HPOT discharge temp avg		1345.56	27.22	2.0	26.91	2.0	60.74	4.5
TTVL03	659	HPFP discharge temp		93.35	0.20	0.2	1.87	2.0	1.91	2.0
TTVL12	18	MCC clnt discharge temp B		429.56	3.19	0.7	8.59	2.0	10.70	2.5
WFOPB	8805	OPB fuel flow (calc)		35.14	0.41	1.2	0.70	2.0	1.08	3.1
WLPFT	8801	LPFT inlet flow (calc)		29.52	0.30	1.0	0.62	2.1	0.87	2.9
XROPOV	40	OPOV act pos A (OPV1)		67.22	1.10	1.6	0.34	0.5	2.23	3.3
XRFPOV	42	FPOV act pos A (FPV1)		82.94	1.15	1.4	0.41	0.5	2.34	2.8
Control Point Measurements										
PTMCHB	63	MCC Pc Avg		3126.87	5.27	0.2	62.54	2.0	63.42	2.0
W01	9908	FACILITY FUEL FLOW		154.61	0.14	0.1	3.09	2.0	3.10	2.0
WLPFP	9909	FACILITY OXYGEN FLOW		925.42	0.74	0.1	18.51	2.0	18.57	2.0
		mixture ratio		6.01						
		O2 REPRESS FLOWRATE		1.10						
		H2 REPRESS FLOWRATE		0.20						
TTHTNK	1021	LPFP inlet temp lev 6B		37.02	0.03	0.1	0.74	2.0	0.74	2.0
TTVL18	1058	LPOP inlet temp lev 6A		166.27	0.96	0.6	3.33	2.0	3.84	2.3
PTHTNK	9910	LPFP INLET PR		38.43	1.64	4.3	0.77	2.0	3.36	8.7
PSVL18?	9911	LPOP INLET PR		87.39	18.11	20.7	1.75	2.0	36.27	41.5
Additional Measurements										
TTVL02	15	HPFP inlet temp avg		42.71	0.04	0.1	0.85	2.0	0.86	2.0
	639	LPFP DIS TEMP		44.56	1.91	4.3	0.89	2.0	3.92	8.8
PSVL03	459	HPFP DISCH PR NFD		6186.56	8.67	0.1	123.73	2.0	124.94	2.0
PSVL21?	8751	HPOP DIS VENTURI IN PR		4136.05	12.43	0.3	82.72	2.0	86.38	2.1
PSVL21?	334	HPOP discharge Pr NFD		4098.36	3.24	0.1	81.97	2.0	82.22	2.0
PSVL13?	437	LPFT discharge Pr		3515.91	3.45	0.1	70.32	2.0	70.66	2.0
PSVL21?	8684	MINJ LOX INJ PR 2		3644.00	33.57	0.9	72.88	2.0	99.09	2.7
	8014	LPFT VENTURI PR		4487.18	7.95	0.2	89.74	2.0	91.14	2.0
	8016	LPFT VENTURI TEMP		431.06	1.96	0.5	8.62	2.0	9.47	2.2
TTPBSO	93	PBP discharge temp ch A		209.02	1.35	0.6	4.18	2.0	4.98	2.4
PSVL04	356	MFV discharge Pr		5820.57	11.45	0.2	116.41	2.0	118.64	2.0
PSVL12	17	MCC coolant discharge Pr A		4462.86	8.62	0.2	89.26	2.0	90.91	2.0
WCCV	8818	CCV inlet flow (calc)		72.48	0.76	1.0	2.17	3.0	2.65	3.7
	8815	Nozzle clnt inlet flow-1 (calc)		14.01	0.27	1.9	0.29	2.1	0.62	4.4
	8816	Nozzle clnt inlet flow-2 (calc)		12.20	0.28	2.3	0.26	2.1	0.61	5.0
	8817	Nozzle clnt inlet flow-3 (calc)		14.38	0.15	1.0	0.30	2.1	0.42	2.9
WF2		TOTAL NOZZLE FLOW		40.37	0.24	0.6	0.85	2.1	0.97	2.4
WLPOT	8802	LPOT inlet flow (calc)		191.67	0.69	0.4	4.03	2.1	4.26	2.2
WHPOP-...	8819	HPOP discharge flow (calc)		904.05	12.23	1.4	18.99	2.1	30.96	3.4
WLPOV	8804	OPB LOX flow (calc)		27.15	0.51	1.9	0.57	2.1	1.18	4.3
WFPOV	8810	FPB LOX flow (calc)		75.27	0.53	0.7	1.51	2.0	1.84	2.4

Table 4. Data Reduction Data Sets, Average Values and Uncertainties, 104% RPL.

ROCETS vAR	Pid #	Measurement Name	Avg	s	s (%)	B	B (%)	U	U (%)
		SLICE START TIME							
		SLICE END TIME							
		MCC PC CONTROL	3276.5						
		Data Reduction Measurements							
PTFPRB	8500	FPB Pc (thru liner)	5578.6	4.1	0.1	83.7	1.5	84.1	1.5
PTOPRB	8458	OPB Pc (thru liner)	5591.4	15.2	0.3	83.9	1.5	89.2	1.6
PTPBSO	341	PBP discharge Pr NFD	7712.7	16.8	0.2	154.3	2.0	157.9	2.0
PTVL02	86	HPFP inlet Pr avg (LFDP)	247.9	1.3	0.5	5.0	2.0	5.6	2.3
PTVL20	209/210 avg	HPOP inlet Pr avg	335.9	20.9	6.2	6.7	2.0	42.4	12.6
SNFL	754	LPFTP Speed A	16158.2	26.6	0.2	161.6	1.0	170.1	1.1
SNOL	734	LPOTP speed NFD	5381.6	15.3	0.3	53.8	1.0	61.9	1.2
TTHTFD	231/232 avg	HPFT discharge temp avg	1851.6	5.9	0.3	37.0	2.0	38.9	2.1
TTHTOD	233/234 avg	HPOT discharge temp avg	1420.2	22.4	1.6	28.4	2.0	53.0	3.7
TTVL03	659	HPFP discharge temp	96.1	0.0	0.0	1.9	2.0	1.9	2.0
TTVL12	18	MCC clnt discharge temp B	424.0	1.6	0.4	8.5	2.0	9.1	2.1
WFOPB	8805	OPB fuel flow (calc)	36.1	0.3	0.8	0.7	2.0	0.9	2.5
WLPFT	8801	LPFT inlet flow (calc)	31.2	0.1	0.2	0.7	2.1	0.7	2.1
XROPOV	40	OPOV act pos A (OPV1)	72.1	0.8	1.1	0.4	0.5	1.6	2.2
XRFPOV	42	FPOV act pos A (FPV1)	86.3	0.3	0.3	0.4	0.5	0.7	0.8
		Control Point Measurements							
PTMCHB	63	MCC Pc Avg	3276.3	1.5	0.0	65.5	2.0	65.6	2.0
W01	9908	FACILITY FUEL FLOW	162.1	0.1	0.1	3.2	2.0	3.2	2.0
WLPFP	9909	FACILITY OXYGEN FLOW	969.2	1.1	0.1	19.4	2.0	19.5	2.0
		mixture ratio	6.0	0.0	0.1	0.1	2.0	0.0	0.3
		O2 REPRESS FLOWRATE	1.1						
		H2 REPRESS FLOWRATE	0.2						
TTHTNK	1021	LPFP inlet temp lev 6B	37.1	0.0	0.1	0.7	2.0	0.7	2.0
TTVL18	1058	LPOP inlet temp lev 6A	166.0	1.0	0.6	3.3	2.0	3.9	2.3
PTHTNK	9910	LPFP INLET PR	38.7	0.1	0.2	0.8	2.0	0.8	2.0
PSVL18?	9911	LPOP INLET PR	97.0	2.1	2.2	1.9	2.0	4.7	4.8
		Additional Measurements							
TTVL02	15	HPFP inlet temp avg	42.9	0.0	0.0	0.9	2.0	0.9	2.0
	639	LPFP DIS TEMP	43.7	0.1	0.2	0.9	2.0	0.9	2.0
PSVL03	459	HPFP DISCH PR NFD	6587.7	9.1	0.1	131.8	2.0	133.0	2.0
PSVL21?	8751	HPOP DIS VENTURI IN PR	4369.9	6.6	0.2	87.4	2.0	88.4	2.0
PSVL21?	334	HPOP discharge Pr NFD	4336.9	4.2	0.1	86.7	2.0	87.1	2.0
PSVL13?	437	LPFT discharge Pr	3683.2	3.9	0.1	73.7	2.0	74.1	2.0
PSVL21?	8684	MINJ LOX INJ PR 2	3846.4	27.5	0.7	76.9	2.0	94.6	2.5
	8014	LPFT VENTURI PR	4740.6	4.7	0.1	94.8	2.0	95.3	2.0
	8016	LPFT VENTURI TEMP	427.0	1.9	0.4	8.5	2.0	9.3	2.2
TTPBSO	93	PBP discharge temp ch A	212.8	1.6	0.8	4.3	2.0	5.4	2.5
PSVL04	356	MFV discharge Pr	6195.9	6.5	0.1	123.9	2.0	124.6	2.0
PSVL12	17	MCC coolant discharge Pr A	4720.7	8.2	0.2	94.4	2.0	95.8	2.0
WCCV	8818	CCV inlet flow (calc)	74.8	0.2	0.3	2.2	3.0	2.3	3.1
	8815	Nozzle clnt inlet flow-1 (calc)	14.7	0.3	1.9	0.3	2.1	0.6	4.4
	8816	Nozzle clnt inlet flow-2 (calc)	13.0	0.2	1.8	0.3	2.1	0.6	4.3
	8817	Nozzle clnt inlet flow-3 (calc)	15.2	0.1	0.3	0.3	2.1	0.3	2.2
WF2		TOTAL NOZZLE FLOW	42.6	0.1	0.1	0.9	2.1	0.9	2.1
WLPOT	8802	LPOT inlet flow (calc)	197.5	0.3	0.2	4.1	2.1	4.2	2.1
WHPOP-...	8819	HPOP discharge flow (calc)	950.5	13.7	1.4	20.0	2.1	33.9	3.6
WLPOV	8804	OPB LOX flow (calc)	29.8	0.5	1.8	0.6	2.1	1.2	4.2
WFPOV	8810	FPB LOX flow (calc)	81.0	0.4	0.4	1.6	2.0	1.8	2.2

Table 5. Data Reduction Data Sets, Average Values and Uncertainties, 109% RPL.

Rocets Var	Pid #	Measurement Name		Avg	s	s (%)	B	B (%)	U	U (%)
	9903	SLICE START TIME								
	9904	SLICE END TIME								
	9906	MCC PC CONTROL		3006						
		Data Reduction Measurements								
PTFPRB	8500	FPB Pc (thru liner)		4986.36	20.76	0.4	1.50	74.79533	85.55	1.7
PTOPRB	8458	OPB Pc (thru liner)		4963.12	11.71	0.2	1.50	74.44679	78.04	1.6
PTPBSO	341	PBP discharge Pr NFD		6970.15	41.70	0.6	2.00	139.4	162.45	2.3
PTVL02	86	HPFP inlet Pr avg (LFDP)		230.76	3.43	1.5	2.00	4.6	8.27	3.6
PTVL20	209/210 avg	HPOP inlet PR		342.61	1.71	0.5	2.00	6.9	7.66	2.2
SNFL	754	LPFTP Speed A		15228.81	35.10	0.2	1.00	152.3	167.69	1.1
SNOL	734	LPOTP speed NFD		5096.70	7.79	0.2	1.00	51.0	53.29	1.0
TTHTFD	231/232 avg	HPFT discharge temp avg		1766.23	25.26	1.4	2.00	35.3	61.65	3.5
TTHTOD	233/234 avg	HPOT discharge temp avg		1296.59	12.11	0.9	2.00	25.9	35.48	2.7
TTVL03	659	HPFP discharge temp		90.99	0.19	0.2	2.00	1.8	1.86	2.0
TTVL12	18	MCC clnt discharge temp B		431.60	3.70	0.9	2.00	8.6	11.37	2.6
WFOPB	8805	OPB fuel flow (calc)		34.09	0.34	1.0	2.00	0.7	0.96	2.8
WLPFT	8801	LPFT inlet flow (calc)		28.11	0.29	1.0	2.10	0.590342	0.83	3.0
XROPOV	40	OPOV act pos A (OPV1)		64.54	0.51	0.8	0.50	0.322703	1.07	1.7
XRFPOV	42	FPOV act pos A (FPV1)		80.85	1.00	1.2	0.50	0.404248	2.04	2.5
		Control Point Measurements								
PTMCHB	63	MCC Pc Avg		3005.70	4.74	0.2	2.00	60.1	60.86	2.0
W01	9908	FACILITY FUEL FLOW		148.43	0.20	0.1	2.00	3.0	3.00	2.0
WLPFP	9909	FACILITY OXYGEN FLOW		890.55	1.30	0.1	2.00	17.8	18.00	2.0
		mixture ratio					(6.01 mr)			
		O2 REPRESS FLOWRATE					(1.1 lb/sec)			
		H2 REPRESS FLOWRATE					(0.2 lb/sec)			
TTHTNK	1021	LPFP inlet temp lev 6B		37.01	0.03	0.1	2.00	0.7	0.74	2.0
TTVL18	1058	LPOP inlet temp lev 6A		166.31	0.97	0.6	2.00	3.3	3.85	2.3
PTHTNK	9910	LPFP INLET PR		39.01	1.52	3.9	2.00	0.8	3.14	8.1
PSVL18?	9911	LPOP INLET PR		98.51	0.96	1.0	2.00	2.0	2.75	2.8
		Additional Measurements								
TTVL02	15	HPFP inlet temp avg		42.56	0.05	0.1	2.00	0.9	0.86	2.0
	639	LPFP DIS TEMP		44.48	1.90	4.3	2.00	0.9	3.90	8.8
PSVL03	459	HPFP DISCH PR NFD		5873.75	5.50	0.1	2.00	117.5	117.99	2.0
PSVL21?	8751	HPOP DIS VENTURI IN PR		3946.85	11.08	0.3	2.00	78.9	81.99	2.1
PSVL21?	334	HPOP discharge Pr NFD		3911.84	5.09	0.1	2.00	78.2	78.90	2.0
PSVL13?	437	LPFT discharge Pr		3363.04	2.80	0.1	2.00	67.3	67.49	2.0
PSVL21?	8684	MINJ LOX INJ PR 2		3489.10	80.16	2.3	2.00	69.8	174.85	5.0
	8014	LPFT VENTURI PR		4280.82	7.32	0.2	2.00	85.6	86.86	2.0
	8016	LPFT VENTURI TEMP		432.80	2.40	0.6	2.00	8.7	9.90	2.3
TTPBSO	93	PBP discharge temp ch A		206.42	1.12	0.5	2.00	4.1	4.69	2.3
PSVL04	356	MFV discharge Pr		5530.18	9.40	0.2	2.00	110.6	112.19	2.0
PSVL12	17	MCC coolant discharge Pr A		4256.53	6.74	0.2	2.00	85.1	86.19	2.0
WCCV	8818	CCV inlet flow (calc)		70.17	0.60	0.9	3.00	2.10501	2.42	3.5
	8815	Nozzle clnt inlet flow-1 (calc)		13.22	0.41	3.1	2.10	0.277526	0.86	6.5
	8816	Nozzle clnt inlet flow-2 (calc)		11.42	0.27	2.4	2.10	0.239862	0.59	5.2
	8817	Nozzle clnt inlet flow-3 (calc)		13.65	0.14	1.0	2.10	0.286706	0.40	2.9
WF2		TOTAL NOZZLE FLOW		38.13	0.54	1.4	2.10	0.800632	1.34	3.5
WLPOT	8802	LPOT inlet flow (calc)		187.61	0.84	0.4	2.10	3.939884	4.28	2.3
WHPOP-...	8819	HPOP discharge flow (calc)		870.76	12.24	1.4	2.10	18.28594	30.56	3.5
WLPOV	8804	OPB LOX flow (calc)		25.14	0.68	2.7	2.10	0.5	1.45	5.8
WFPOV	8810	FPB LOX flow (calc)		70.777	0.384052	0.542622	2	1.41554	1.610508	2.275468

Table 6. Data Reduction Data Sets, Average Values and Uncertainties, 100% RPL.
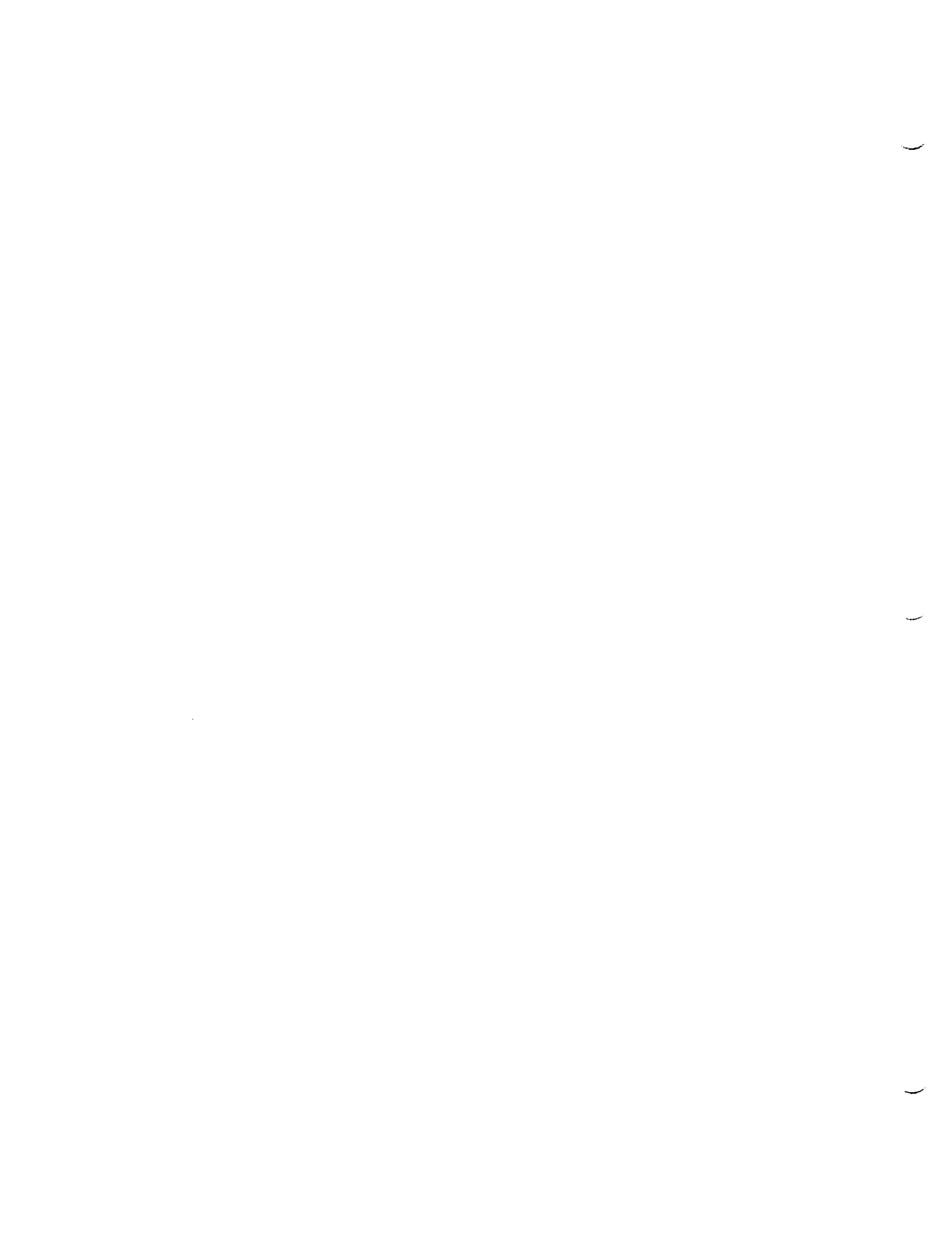
Appendix 3

Uncertainty in Linear Regression

Introduction

When experimental information is used in a model in the form of a curvefit an uncertainty due to the original experimental program is introduced. Currently there is no accepted methodology to assess this uncertainty. The work reported here is a continuation of a previous effort[1] to develop a methodology to assess the uncertainty in linear regression analysis, or curvefits, when the experimental uncertainties contain precision, systematic, and correlated systematic uncertainties.. The work reported in reference [1] developed a methodology to assess the uncertainty in the regression coefficients, slope and y-intercept, for a 1st order linear regression. The most common forms of regression models used are straight lines and polynomial curvefits where both the X and Y axes are functional relationships containing uncertain experimental information. While multivariate regressions are also important models, they were not studied in this effort.

In using the basic regression models with typical engineering data many of the underlying assumptions used in the statistical development of the regression models are violated. The underlying assumptions assume that the errors " (1) are unbiased; (2) have constant variance; (3) are uncorrelated, and (4) are normally distributed."[2] In a typical experimental program the first three assumptions will usually be violated. Seber[2] and Montgomery[3] discuss these assumptions and provide methods to deal with some of the violations, however their methods are mathematically rigorous and do not readily lend themselves to the propagation of experimental uncertainties. Violation of these assumptions does not preclude using the regression models to obtain a model for the data, but the model must be used with the realization that it only represents the "best fit" of a curve through the data. Any confidence interval then used with that curvefit must properly account for any violation of the underlying assumptions.

The methodology presented in this report is an extention of accepted uncertainty propagation techniques to the linear regression equations. The effectiveness of this new methodology was evaluated using Monte Carlo-type simulations. This report will briefly discuss the uncertainty analysis techniques and then present its application to linear regression analysis, first for 1st order (straight line) regressions and then for higher order (polynomial) regressions followed by a summary of the Monte Carlo simulation technique employed to evaluate the methodology. The report concludes with the application of the curvefit uncertainty methodology to compressor map characteristics.

Regression Analysis Uncertainty Methodology for Slope and y-Intercept

The uncertainties in the slope, m, and the Y-intercept, c, are functions of the uncertainties in the determinations of the X and Y variables. The values of m and c are obtained by minimizing the sum of the squares of the deviations between the line and the data points, commonly known as the method of least squares. The development of the equations to calculate m and c can be found in statistics books[2,3,9] and only the equations will be presented here. For N (X_i, Y_i) data pairs, the slope of the line, m, is determined from

$$m = \frac{N \sum_{i=1}^{N} X_i Y_i - \sum_{i=1}^{N} X_i \sum_{i=1}^{N} Y_i}{N \sum_{i=1}^{N} (X_i^2) - \left(\sum_{i=1}^{N} X_i \right)^2}$$

(1)

and the intercept, c, is determined from

$$c = \frac{\sum_{i=1}^{N} (X_i^2) \sum_{i=1}^{N} Y_i - \sum_{i=1}^{N} X_i \sum_{i=1}^{N} (X_i Y_i)}{N \sum_{i=1}^{N} (X_i^2) - \left(\sum_{i=1}^{N} X_i \right)^2}$$

(2)

In this paper we present a methodology to determine the uncertainties in linear regression coefficients. The effectiveness of this methodology was analyzed using a Monte Carlo-type simulation assuming the true relationship between the X and Y variables is in fact linear.

The approach presented in this paper is an application of the uncertainty analysis methodology presented above to the regression equations for slope and intercept

Considering Eq.s (2) and (3) to be data reduction equations of the form

$$m = m(X_1, X_2, ..., X_N, Y_1, Y_2, ..., Y_N)$$

(3)

and

$$c = c(X_1, X_2, ..., X_N, Y_1, Y_2, ..., Y_N)$$

(4)

and applying the uncertainty analysis equations, Eq.s (5)-(13), the most general form of the expression for the uncertainty in the slope of the line, m, is

$$U_m^2 = \sum_{i=1}^{J}\left(\frac{\partial m}{\partial Y_i}\right)^2 B_{Y_i}^2 + 2\sum_{i=1}^{J-1}\sum_{k=i+1}^{J}\left(\frac{\partial m}{\partial Y_i}\right)\left(\frac{\partial m}{\partial Y_k}\right)B_{Y_iY_k} + \sum_{i=1}^{J}\left(\frac{\partial m}{\partial Y_i}\right)^2 P_{Y_i}^2$$

$$+ \sum_{i=1}^{J}\left(\frac{\partial m}{\partial X_i}\right)^2 B_{X_i}^2 + 2\sum_{i=1}^{J-1}\sum_{k=i+1}^{J}\left(\frac{\partial m}{\partial X_i}\right)\left(\frac{\partial m}{\partial X_k}\right)B_{X_iX_k} + \sum_{i=1}^{J}\left(\frac{\partial m}{\partial X_i}\right)^2 P_{X_i}^2 \qquad (5)$$

$$+ 2\sum_{i=1}^{J}\sum_{k=1}^{J}\left(\frac{\partial m}{\partial X_i}\right)\left(\frac{\partial m}{\partial Y_k}\right)B_{X_iY_k}$$

where B_{Y_i} is the systematic uncertainty for the Y_i variable, B_{X_i} is the systematic uncertainty for the X_i variable, $B_{Y_iY_k}$ is the covariance estimator for the correlated bias uncertainties in the Y_i and Y_k variables, $B_{X_iX_k}$ is the covariance estimator for correlated bias uncertainties in the X_i and X_k variables, P_{Y_i} is the random uncertainty for the Y_i variable and P_{X_i} is the random uncertainty for the X_i variable, and $B_{X_iY_i}$ is the covariance estimator for the correlated bias uncertainties between X_i and Y_i.

A similar expression for the uncertainty in the intercept is

$$U_c^2 = \sum_{i=1}^{J}\left(\frac{\partial c}{\partial Y_i}\right)^2 B_{Y_i}^2 + 2\sum_{i=1}^{J-1}\sum_{k=i+1}^{J}\left(\frac{\partial c}{\partial Y_i}\right)\left(\frac{\partial c}{\partial Y_k}\right)B_{Y_iY_k} + \sum_{i=1}^{J}\left(\frac{\partial c}{\partial Y_i}\right)^2 P_{Y_i}^2$$

$$+ \sum_{i=1}^{J}\left(\frac{\partial c}{\partial X_i}\right)^2 B_{X_i}^2 + 2\sum_{i=1}^{J-1}\sum_{k=i+1}^{J}\left(\frac{\partial c}{\partial X_i}\right)\left(\frac{\partial c}{\partial X_k}\right)B_{X_iX_k} + \sum_{i=1}^{J}\left(\frac{\partial c}{\partial X_i}\right)^2 P_{X_i}^2 \qquad (6)$$

$$+ 2\sum_{i=1}^{J}\sum_{k=1}^{J}\left(\frac{\partial c}{\partial X_i}\right)\left(\frac{\partial c}{\partial Y_k}\right)B_{X_iY_k}$$

The partial derivatives are

$$\frac{\partial m}{\partial X_i} = \frac{NX_i - \sum_{i=1}^{N}X_i}{N\sum_{i=1}^{N}(X_i^2) - \left(\sum_{i=1}^{N}X_i\right)^2} \qquad (7)$$

$$\frac{\partial c}{\partial Y_i} = \frac{\sum_{i=1}^{N}(X_i^2) - X_i\sum_{i=1}^{N}X_i}{N\sum_{i=1}^{N}(X_i^2) - \left(\sum_{i=1}^{N}X_i\right)^2} \qquad (8)$$

$$\frac{\partial m}{\partial X_i} = \frac{NY_i - \sum_{i=1}^{N}Y_i}{N\sum_{i=1}^{N}(X_i^2) - \left(\sum_{i=1}^{N}X_i\right)^2} - \frac{\left(N\sum_{i=1}^{N}X_iY_i - \sum_{i=1}^{N}X_i\sum_{i=1}^{N}Y_i\right)\left(2NX_i - 2\sum_{i=1}^{N}X_i\right)}{\left(N\sum_{i=1}^{N}(X_i^2) - \left(\sum_{i=1}^{N}X_i\right)^2\right)^2} \qquad (9)$$

and
$$\frac{\partial c}{\partial X_i} = \frac{2X_i \sum_{i=1}^{N} Y_i - \sum_{i=1}^{N} X_i Y_i - Y_i \sum_{i=1}^{N} X_i}{N \sum_{i=1}^{N} (X_i^2) - \left(\sum_{i=1}^{N} X_i\right)^2} - \frac{\left(\sum_{i=1}^{N} (X_i^2) \sum_{i=1}^{N} Y_i - \sum_{i=1}^{N} X_i \sum_{i=1}^{N} X_i Y_i\right)\left(2NX_i - 2\sum_{i=1}^{N} X_i\right)}{\left(N \sum_{i=1}^{N} (X_i^2) - \left(\sum_{i=1}^{N} X_i\right)^2\right)^2} \quad (10)$$

Equations above show the most general form of the equations for the uncertainty in the slope and the y-intercept, allowing for correlation of bias errors among the different X's, among the different Y's and also among the X's and Y's.. If none of the systematic error sources are common between the X variables and the Y variables, the last term of the equations, the X-Y covariance estimator, is zero and the equations reduce to

$$U_m^2 = \sum_{i=1}^{J} \left(\frac{\partial m}{\partial Y_i}\right)^2 B_{Y_i}^2 + 2\sum_{i=1}^{J-1}\sum_{k=i+1}^{J} \left(\frac{\partial m}{\partial Y_i}\right)\left(\frac{\partial m}{\partial Y_k}\right) B_{Y_i Y_k} + \sum_{i=1}^{J} \left(\frac{\partial m}{\partial Y_i}\right)^2 P_{Y_i}^2$$
$$+ \sum_{i=1}^{J} \left(\frac{\partial m}{\partial X_i}\right)^2 B_{X_i}^2 + 2\sum_{i=1}^{J-1}\sum_{k=i+1}^{J} \left(\frac{\partial m}{\partial X_i}\right)\left(\frac{\partial m}{\partial X_i}\right) B_{X_i X_k} + \sum_{i=1}^{J} \left(\frac{\partial m}{\partial X_i}\right)^2 P_{X_i}^2 \quad (11)$$

and

$$U_c^2 = \sum_{i=1}^{J} \left(\frac{\partial c}{\partial Y_i}\right)^2 B_{Y_i}^2 + 2\sum_{i=1}^{J-1}\sum_{k=i+1}^{J} \left(\frac{\partial c}{\partial Y_i}\right)\left(\frac{\partial c}{\partial Y_k}\right) B_{Y_i Y_k} + \sum_{i=1}^{J} \left(\frac{\partial c}{\partial Y_i}\right)^2 P_{Y_i}^2$$
$$+ \sum_{i=1}^{J} \left(\frac{\partial c}{\partial X_i}\right)^2 B_{X_i}^2 + 2\sum_{i=1}^{J-1}\sum_{k=i+1}^{J} \left(\frac{\partial c}{\partial X_i}\right)\left(\frac{\partial c}{\partial X_i}\right) B_{X_i X_k} + \sum_{i=1}^{J} \left(\frac{\partial c}{\partial X_i}\right)^2 P_{X_i}^2 \quad (12)$$

Regression Analysis Methodology for Predicted Value; Straight Line

The expression for the uncertainty in the predicted value, Y, at a given X variable

$$Y(\mathbf{X}) = m\mathbf{X} + c \quad (13)$$

(where X is assumed to have no uncertainty) is determined in a similar manner by applying Eq.s (2) through (8) to equation (21) to obtain

$$U_{Y(X)}^2 = \sum_{i=1}^{J} \left(\frac{\partial Y}{\partial Y_i}\right)^2 B_{Y_i}^2 + 2\sum_{i=1}^{J-1}\sum_{k=i+1}^{J} \left(\frac{\partial Y}{\partial Y_i}\right)\left(\frac{\partial Y}{\partial Y_k}\right) B_{Y_i Y_k} + \sum_{i=1}^{J} \left(\frac{\partial Y}{\partial Y_i}\right)^2 P_{Y_i}^2$$
$$+ \sum_{i=1}^{J} \left(\frac{\partial Y}{\partial X_i}\right)^2 B_{X_i}^2 + 2\sum_{i=1}^{J-1}\sum_{k=i+1}^{J} \left(\frac{\partial Y}{\partial X_i}\right)\left(\frac{\partial Y}{\partial X_k}\right) B_{X_i X_k} + \sum_{i=1}^{J} \left(\frac{\partial Y}{\partial X_i}\right)^2 P_{X_i}^2$$
$$+ 2 \quad \frac{\partial Y}{}$$

and
$$\frac{\partial Y}{\partial Y_i} = \frac{\partial m}{\partial Y_i} X + \frac{\partial c}{\partial Y_i} \qquad (16)$$

and where the partial derivatives for m and c are as defined in Eq.s (15) through (18). The partial derivatives can also be determined numerically, as will be discussed later.

Calibration Problem

If the value of X being used in the regression model is measured with the same apparatus as the X_i data, and thus shares the same systematic error sources the uncertainty expression must be expanded to include these uncertainties and correlations. This problem is often encountered in calibration processes and the uncertainty expression is

$$
\begin{aligned}
U_Y^2 &= \sum_{i=1}^{J} \left(\frac{\partial Y}{\partial Y_i}\right)^2 B_{Y_i}^2 + 2\sum_{i=1}^{J-1}\sum_{k=i+1}^{J} \left(\frac{\partial Y}{\partial Y_i}\right)\left(\frac{\partial Y}{\partial Y_k}\right) B_{Y_i Y_k} + \sum_{i=1}^{J} \left(\frac{\partial Y}{\partial Y_i}\right)^2 P_{Y_i}^2 \\
&+ \sum_{i=1}^{J} \left(\frac{\partial Y}{\partial X_i}\right)^2 B_{X_i}^2 + 2\sum_{i=1}^{J-1}\sum_{k=i+1}^{J} \left(\frac{\partial Y}{\partial X_i}\right)\left(\frac{\partial Y}{\partial X_k}\right) B_{X_i X_k} + \sum_{i=1}^{J} \left(\frac{\partial Y}{\partial X_i}\right)^2 P_{X_i}^2 \qquad (17) \\
&+ \sum_{i=1}^{J} \left(\frac{\partial Y}{\partial X}\right)^2 B_X^2 + 2\sum_{i=1}^{J} \left(\frac{\partial Y}{\partial X}\right)\left(\frac{\partial Y}{\partial X_i}\right) B_{X X_i} + \sum_{i=1}^{J} \left(\frac{\partial Y}{\partial X}\right)^2 P_X^2 \\
&+ 2\sum_{i=1}^{J}\sum_{k=1}^{J} \left(\frac{\partial Y}{\partial X_i}\right)\left(\frac{\partial Y}{\partial Y_k}\right) B_{X_i Y_k} + 2\sum_{i=1}^{J} \left(\frac{\partial Y}{\partial X}\right)\left(\frac{\partial Y}{\partial Y_i}\right) B_{X Y_i}
\end{aligned}
$$

If no errors sources are common between the X and Y_i variables, the X-Y_i correlation terms are omitted, these terms comprise the last line of the above expression.

Numerical Partial Derivative Determination

The partial derivatives can be approximated directly using a finite difference numerical technique, often referred to as a "jitter-routine."[4] A simple forward-difference partial derivative, which has accuracy of order h is

$$\frac{\partial r}{\partial X_1} = \frac{f(X_1+h, X_2,...,X_n) - f(X_1, X_2,...,X_n)}{h} \qquad (18)$$

It was determined during this effort that round-off errors could be significant, so double precision arithmetic was used. Accuracy was also enhanced by using a second order accurate central-differencing scheme[9], such as:

$$\frac{\partial r}{\partial X_1} = \frac{f(X_1+h, X_2,...,X_n) - f(X_1-h, X_2,...,X_n)}{2h} \qquad (19)$$

Traditional Statistical Regression Uncertainties; Straight Line

To demonstrate the value of the uncertainty propagation methodology presented above a comparison to the confidence intervals provided by traditional statistical techniques is needed. The form of the statistical intervals used in this study was taken from Natrella[10], more discussion of these intervals and additional forms of the intervals can also be found in references [2] and [3]. The variance of the slope is given as

$$s_m^2 = \frac{s_Y^2}{S_{xx}}$$
(20)

with the 95% confidence interval represented by

$$m \pm \lambda s_m$$
(21)

where the 95% coverage factor, λ, is determined using the two-tailed Student's t-distribution, with n-2 degrees of freedom, as

$$\lambda = t_{.95}(n-2)$$
(22)

Similarly, the variance for the y-intercept is given by

$$s_c^2 = s_Y^2 \left\{ \frac{1}{n} + \frac{\overline{X}^2}{S_{xx}} \right\}$$
(23)

and the 95% confidence interval is determined as

$$c \pm \lambda s_c$$
(24)

A confidence interval about any point along the regression line, what has been referred to as the predicted value is obtained with the interval W_i as

$$W_i = \lambda s_Y \left\{ \frac{1}{n} + \frac{(X_i - \overline{X})^2}{S_{xx}} \right\}^{1/2}$$
(25)

and the 95% confidence region is expressed as

$$Y_i \pm W_i$$
(26)

Where the sum of squares statistics used in the determination of these intervals are defined as

$$S_{xx} = \sum_{i=1}^{n} X_i^2 - \frac{\left(\sum_{i=1}^{n} X_i \right)^2}{n} = \sum_{i=1}^{n} (X - \overline{X})^2$$
(27)

and

$$S_{yy} = \sum_{i=1}^{n} Y_i^2 - \frac{\left(\sum_{i=1}^{n} Y_i \right)^2}{n} = \sum_{i=1}^{n} (Y - \overline{Y})^2$$
(28)

and
$$S_{xy} = \sum_{i=1}^{n} X_i Y_i - \frac{\sum_{i=1}^{n} X_i \sum_{i=1}^{n} Y_i}{n} = \sum_{i=1}^{n} (X_i - \bar{X})(Y_i - \bar{Y})$$
(29)

and
$$s_Y^2 = \frac{1}{n-2} \left\{ S_{yy} - \frac{(S_{xy})^2}{S_{xx}} \right\}$$
(30)

X and Y as Functional Relations

In many, if not most instances, the test data will be expressed in some form of functional relationship. In these cases, the data will not be the variables used in the regression, instead the result from the functional relationships will be used. Examples of common functional relations are Reynolds number, flow coefficient, pressure coefficient, specific fuel consumption, etc. This can be expressed for a general example as

$$X_i = f(VAR1_i, VAR2_i)$$
(31)

and
$$Y_i = f(VAR1_i, VAR4_i, VAR5_i)$$
(32)

so the expression for the uncertainty in the predicted value becomes

$$U_Y^2 = \sum_{i=1}^{n} \sum_{j=1}^{5} \left(\frac{\partial Y}{\partial VARj_i} \right)^2 P_{VARj_i}^2 + \sum_{i=1}^{n} \sum_{j=1}^{5} \left(\frac{\partial Y}{\partial VARj_i} \right)^2 B_{VARj_i}^2$$

$$+ 2 \sum_{i=1}^{n-1} \sum_{k=i+1}^{n} \sum_{j=1}^{5} \left(\frac{\partial Y}{\partial VARj_i} \right) \left(\frac{\partial Y}{\partial VARj_k} \right) B_{VARj_i VARj_k}$$
(33)

$$+ 2 \sum_{i=1}^{n} \sum_{k=1}^{n} \sum_{j=1}^{4} \sum_{l=j+1}^{5} \left(\frac{\partial Y}{\partial VARj_i} \right) \left(\frac{\partial Y}{\partial VARl_k} \right) B_{VARj_i VARl_k}$$

where the second term accounts for correlated systematic uncertainty sources within each variable and the third term accounts for systematic uncertainty sources common between variables. Similar expressions for the uncertainty in the slope and y-intercept are readily obtained. The complexity introduced by the transformation necessitates determining the partial derivatives numerically.

Another important form of transformation is when one or both of the variables are represented in logarithmic space. A similar technique is used whereby the functional relationship as expressed in Eq.s (39) and (40) become the logarithmic function desired, such as

$$X_i = \ln(VAR1_i) \quad \text{and} \quad Y_i = \ln(VAR2_i)$$
(34)

The partial derivatives then account for the transformation and the uncertainties in the measured variables are propagated in the units of the measurand without transformation.

Methodology Development and Monte Carlo Simulations

The methodology for assessing the uncertainty in linear regressions was developed using Monte Carlo-type simulations. Monte Carlo-type simulations are often used in uncertainty analysis to determine the effectiveness of a particular uncertainty model. For this work, what is referred to as a Monte Carlo-type simulation simply means generating numbers to represent experimental data with some amount of error randomly obtained from predefined error distribution populations.

The Monte Carlo simulations were conducted in the following manner. *"True"* values for data from a relationship with specified coefficients were determined. The word *true* is emphasized to indicate that it represents the actual physical quantity of the parameter if it could be measured without any bias error or precision error, which is always an unobtainable value. The two-sigma (2 standard deviation or 95% confidence) bias limits and precision limits for each variable were then specified. The errors in each variable were assumed to come from these normally distributed error populations with the specified standard deviations. A random value for each bias error and precision error was found from a Gaussian random deviate generator subroutine using the specified standard deviations. The Gaussian deviates have a mean of zero and an equal probability of being positive or negative. The bias errors within each variable were assumed to be from the same source, and were assigned the same random deviate from the Gaussian distribution. In some cases these bias errors were a fixed amount and in some cases they were a percent of reading type error. Precision errors were obtained by sampling the precision error populations repeatedly to obtain independent random deviates for each variable. The individual error values, bias errors and precision errors were then summed and added to the *true* value to obtain a data point with errors from the specified error populations. These data points were then used in the linear least squares equations to obtain the value of the regression coefficients and the curvefit model. These coefficients and the curvefit model represent the "best fit" of the experimental data when the bias and precision errors are present.

A 95% confidence uncertainty interval for the result was calculated from the uncertainty propagation analysis equations for m, c, and Y. A $\pm U_m$ interval was placed around the slope coefficient value, m, and if the true value of the slope was found to be within the interval a counter was incremented. A similar procedure was used with the y-intercept and the predicted value from the curvefit expression. This procedure was repeated 10,000 times and the percent coverage, or number of times the true result was within the estimated interval, was determined. Using this procedure,

the effectiveness of the uncertainty propagation equation could be investigated by checking whether or not the *true* value is within the 95% confidence uncertainty interval about the measured result 95% of the time, we can determine how well our uncertainty approximation equations work.

In the previous work[1] the precision uncertainties used in the propagation equations were determined using the "large sample approximation" and calculating a standard at each setpoint. The effect of sample size, i.e. the number of setpoints and the number of data taken at each setpoint, was thus studied. The conclusion drawn from this analysis was that when the "correct" precision limit is used in the propagation equations the desired confidence interval is obtained. Thus, all the work in this report will assume that the correct precision uncertainties have been estimated based upon prior information and experience with the test rig so that the simulations will evaluate the methodology only.

A useful statistic from the simulation is the uncertainty ratio, the ratio of the average uncertainty intervals for the regression coefficients from the 10,000 iterations divided by the true 95% confidence intervals. The *true* 95% uncertainties are calculated as twice the sample standard deviations, S_m, S_c, and S_Y, from the 10,000 samples of the regression coefficients {not to be confused with the standard deviations of the curvefit, s_m, s_c, and W, as defined in Eq.s (28), (31), and (33)}. The sample standard deviations from the 10,000 sample population can be expected to be good representations of the actual standard deviations of the infinite population with the elemental uncertainty sources as defined. An uncertainty ratio near unity shows that the uncertainty methodology works for the particular case, with values greater than one meaning an over-prediction and values less than one meaning an under-prediction.

1st Order Regression Uncertainty Simulation and Results

Case 1: Dominant Systematic Uncertainties $B_{X1}= 2.5$ $B_{X2}= 2.5\%$ $B_{X3}=B_{Y3}= 2.5$ $B_{Y1}= 2.5$ $B_{Y2}= 2.5$ $P_X= 0.0$ $P_Y= 0.1$								
			Uncertainty Propagation			Classical Statistics		
pt	X_i	Y_i	$U_{Y (avg)}$	Cov (%)	Ratio	$W_{(avg)}$	Cov (%)	Ratio
1	80.0	90.0	4.58	95.4%	0.99	0.15	3.9	0.02
2	90.0	100.0	4.81	95.3%	0.99	0.11	2.5	0.02
3	100.0	110.0	5.06	95.4%	0.99	0.09	1.8	0.01
4	110.0	120.0	5.32	95.3%	0.99	0.11	2.3	0.02
5	120.0	130.0	5.59	95.4%	0.99	0.15	3.0	0.02
Coefficient Uncertainties			U_m	Cov (%)	Ratio	tS	Cov (%)	Ratio
true slope, m=1.0			0.036	95.6	1.01	0.005	21.1%	0.13
true y-intercept, c=10.0			3.56	95.3	0.99	0.47	20.2%	0.13

Table 1. 1st Order Regression Simulation and Results; Dominant Systematic Uncertainties.

Case 2: Comparable Uncertainties								
B_{X1}= 2.5		B_{X2}= 0.0%	B_{X3}=B_{Y3}= 0.0					
B_{Y1}= 2.5		B_{Y2}= 0.0%						
P_X = 2.5		P_Y = 2.5						

			Uncertainty Propagation			Classical Statistics		
pt	X_i	Y_i	$U_{Y (avg)}$	Cov (%)	Ratio	$W_{(avg)}$	Cov (%)	Ratio
1	80.0	90.0	4.47	95.3	0.99	3.42	85.3	0.89
2	90.0	100.0	4.02	95.4	0.99	2.41	77.6	0.70
3	100.0	110.0	3.87	95.4	0.99	1.98	71.4	0.60
4	110.0	120.0	4.03	95.4	0.99	2.42	77.4	0.70
5	120.0	130.0	4.47	95.6	0.99	3.43	84.9	0.89
Coefficient Uncertainties			$U_{m (avg)}$	Cov (%)	Ratio	$tS_{(avg)}$	Cov (%)	Ratio
true slope, m=1.0			0.112	95.1	1.00	0.164	94.4	1.464
true y-intercept, c=10.0			11.84	95.0	1.00	16.5	94.0	1.394

Table 2. 1st Order Regression Simulation and Results; Comparable Systematic and Precision Uncertainties.

Case 3: Dominant Precision Uncertainties								
B_{X1}= 0.0		B_{X2}= 0.0	B_{X3}=B_{Y3}= 0.0					
B_{Y1}= 0.0		B_{Y2}= 0.0						
P_X = 2.5		P_Y = 2.5						

			Uncertainty Propagation			Classical Statistics		
pt	X_i	Y_i	$U_{Y (avg)}$	Cov (%)	Ratio	$W_{(avg)}$	Cov (%)	Ratio
1	80.0	90.0	2.74	95.6	1.00	3.15	95.0	1.46
2	90.0	100.0	1.96	95.3	1.00	2.25	94.8	1.46
3	100.0	110.0	1.59	95.3	1.00	1.84	94.6	1.46
4	110.0	120.0	1.98	95.4	1.00	2.28	94.9	1.46
5	120.0	130.0	2.76	95.4	1.00	3.17	94.8	1.46
Coefficient Uncertainties			$U_{m (avg)}$	Cov (%)	Ratio	$tS_{(avg)}$	Cov (%)	Ratio
true slope, m=1.0			0.112	95.4	1.01	0.163	94.94	1.48
true y-intercept, c=10.0			11.31	95.5	1.01	16.5	94.79	1.47

Table 3. 1st Order Regression Simulation and Results; Dominant Precision Uncertainties.

Calibration Problem Results

The calibration problem was simulated, wherein the systematic uncertainty associated with the X variable in the curvefit expression was correlated with the systematic uncertainty in the X data used in the curvefit. Equation (18) was used with the X-Y correlation terms omitted. The same true linear expression was used as in the previous simulations, however the curvefit was evaluated at calibration points between the curvefit data. The input data, uncertainty information, and simulation results are shown in Table 4.

Calibration Problem Case 1: Dominant Systematic Uncertainties $B_X= 2.5$ $P_X= 2.5$ $B_Y = 2.5$ $P_Y= 2.5$					
			Uncertainty Propagation		
pt	X_i/X_i(cal)	Y_i	U_Y	Cov (%)	Ratio
1	80.0/ 85.0	90.0	4.24	95.2	1.00
2	90.0/ 95.0	100.0	3.91	95.2	0.99
3	100.0/ 105.0	110.0	3.87	95.0	1.00
4	110.0/ 115.0	120.0	4.12	95.0	0.99
5	120.0/ 125.0	130.0	4.68	95.1	0.99

Table 4. Calibration Problem Simulation and Results; Comparable Systematic and Precision Uncertainties.

Table 4 again demonstrates that the appropriate uncertainty interval is obtained with the proposed methodology. The regression coefficient results and the traditional statistics results are similar to Tables 1, 2, and 3. They have been omitted because they are not affected by the calibration problem.

Polynomial Regression Uncertainty Simulation Results

A 2nd order polynomial curve was used to generate "true" (X,Y) data pairs and the uncertainty propagation methodology was evaluated using the Monte Carlo simulation technique. The methodology provided the appropriate coverage for the curves simulated. Several different curves have been modeled and simulated, and the methodology appears to work in most curvefit applications. A few areas need further work before the methodology can be fully recommended, these areas are discussed in the next section.

In lieu of presenting the results of the polynomial simulations performed, a polynomial curvefit for the High Pressure Fuel Turbopump turbine efficiency map will be discussed in Appendix 4.

Future Research

A number of areas of continued research are identified as a result of this effort In all of the Monte Carlo simulations performed, the precision limits used in the propagation equations were the exact (2σ) values. Work similar to that presented in reference [1] needs to be performed and extended to study the effect of sample size. the large sample approximation, data location, the use of prior information, and the use of other precision limit estimates. The polynomial curvefit results indicated that the methodology provides the appropriate uncertainty intervals in a well defined and well behaved problem. However, if the data and the curvefit using that data do not represent the "true" phenomena being investigated incorrect uncertainty intervals will be obtained. This could happen due to over-fitting or under-fitting the data. In general, the limitations of using this method to assess the uncertainties in polynomial curvefits must be investigated, and any underlying assumptions identified.

Since the primary motivation of this work is the assessment of uncertainties in propulsion system models, and since multivariate regression models are often used in engine system models a means of assessing the associated uncertainties is needed. Thus extension of this methodology to multivariate regressions is necessary.

Another important area for future research is the engineering application of this methodology. For example, how should it be integrated into data acquisition and test data reduction systems. How should the uncertainty information be documented so that others reading a report have the necessary information. And finally, an algorithm or flowchart describing how to implement this methodology would be very useful.

Conclusion

The work presented in this appendix provides a new methodology for assessing the uncertainty associated with curvefits of experimental information. This methodology is based upon the propagation of experimental uncertainties using accepted techniques. In the analysis it was shown that the methodology provided the appropriate uncertainty intervals when correlated systematic uncertainties are present, and that traditional statistical confidence intervals do not provide the appropriate intervals in these situations. The methodology was shown to extend to cases where the curvefit variables are functional relations of experimental data.

References

1.   Brown, Kendall K., Coleman, Hugh W., and Steele, W. Glenn, Estimating Uncertainty Intervals for Linear Regression, AIAA Paper 95-0796, 33rd Aerospace Sciences Meeting and Exhibit, January 1995.

2.   Seber, G.A.F., *Linear Regression Analysis*, John Wiley & Sons, New York, 1977.

3.   Montgomery, Douglas C. and Peck, Elizabeth A., *Introduction to Linear Regression Analysis*, 2nd Ed., John Wiley & Sons, New York, 1992.

4.   Coleman, Hugh W. and Steele, Glenn W., *Experimentation and Uncertainty Analysis for Engineers*, John Wiley & Sons, New York, 1989.

5.   *Guide to the Expression of Uncertainty in Measurement*, International Organization for standardization, Beneve, Switzerland, 1993.

6.   "Quality Assessment for Wind Tunnel Testing," AGARD-AR-304, 1994.

7.   American National Standards Institute/American Society of Mechanical Engineers, *Measurement Uncertainty*, PTC 19.1-1985, American Society of Mechanical Engineers, New York, 1986.

8.   Brown, Kendall K., Coleman, Hugh W., Steele, W.G., and Taylor, Robert P., "Evaluation of Correlated Bias Error Effects in Experimental Uncertainty Analysis," *AIAA Journal*, (in press).

9.   Burden, Richard L., and Faires, J. Douglas, *Numerical Methods*, 5th Ed., PWS Publishing Company, Boston, 1993.

10.   Natrella, M.G., *Experimental Statistics*, NBS Handbook 91, National Bureau of Standards, United States Department of Commerce, 1963.

11.   Press, William H., Flannery, Brian P., Teukolsky, and Vetterling, William T., *Numerical Recipes; The Art of Scientific Computing*, Cambridge University Press, Cambridge, 1986.

12.   Hale, A.A., and Davis, M.W., "DYNamic Turbine Engine Compressor Code DYNTECC - Theory and Capabilities," AIAA Paper 92-3190, AIAA/SAE/ASME/ASEE 28th Joint Propulsion Conference and Exhibit, Nashville, TN, July 1992.

13.   Bevington, Philip R., and Robinson, D. Keith, *Data Reduction and Error Analysis for the Physical Sciences*, 2nd Ed, McGraw Hill, New York, 1992.
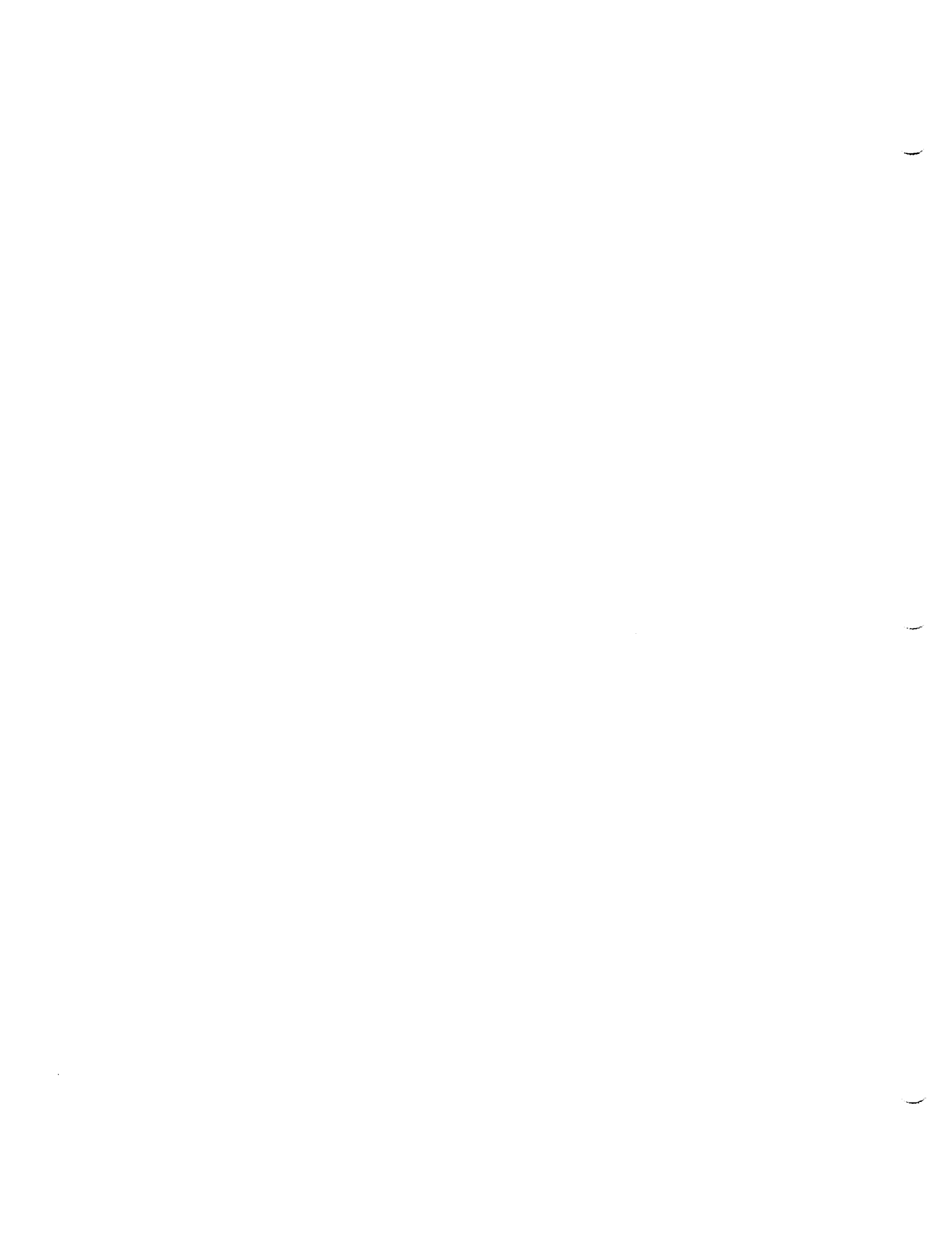
Appendix - 4

Monte Carlo Simulation of HPFT Efficiency Map

Appendix 3 introduced the proposed methodology to assess the uncertainty of nth order linear regressions when the regression parameters are functional relations. To verify the methodology was applicable to the type of component performance maps used in the SSME model, a Monte Carlo simulation of the turbine efficiency map for the High Pressure Fuel Turbopump Turbine (HPFT) was conducted. This simulation is also important as another demonstration of the regression uncertainty methodology.

As discussed in Section 3.3.1, the uncertainty to associate with a value from the HPFT efficiency parameter versus speed parameter map is being estimated from the cold-flow testing of the HPFT in the MSFC air flow Turbine Test Equipment facility[1] and the adjustments to engine operating conditions.

The information used to obtain the HPFT turbine efficiency map was obtained from a July 1991, Rocketdyne Internal Letter[2]. This memo only contains the reduced data, and not the measured inlet and exit total pressures, total temperatures, and mass flowrates. Using information from this memo, and discussions with MSFC personnel involved in the HPFTP model testing[3], information to set up the Monte Carlo simulation was generated.

For the purposes of the Monte Carlo simulation a fourth order linear regression was obtained from the data in the Rocketdyne memo. The fourth order curvefit used to model the efficiency map was

$$ETA_{map} = 6.281 \left(\frac{U}{C_0} \right)^4 - 18.866 \left(\frac{U}{C_0} \right)^3 + 29.101 \left(\frac{U}{C_0} \right)^2 - 22.961 \left(\frac{U}{C_0} \right)^1 + 6.609 \tag{1}$$

Information about the inlet test conditions and the test profile from Ms. Hudson was used to generate a set of data which yields values on this curve. This information is shown in Table A-4.1. She also stated that the overall uncertainty associated with the temperature measurements is 1.0°R, consisting mostly of bias uncertainty, the overall uncertainty in the pressure

---

[1] Hudson, Susan T., Gaddis, Stephen W., Johnson, P., Dean, and Boynton, James, L., "Cold Flow Testing of the Space Shuttle Main Engine High Pressure Fuel Turbine Model," AIAA Technical Paper 91-2503, AIAA/SAE/ASME/ASEE 27th Joint Propulsion Conference, June 24-26, 1991, Sacramento, CA.

[2] Boynton, J.,and Daumann, A., "Revision of SSME HPFTP Turbine Performance Based on NASA/MSFC Baseline Air Test Results," July 23, 1991.

[3] Personal Communication with Ms. Susan Hudson, Experimental Branch, Structures and Dynamics Lab, NASA- Marshall Space Flight Center.

measurements is 0.25 psia, consisting mostly of precision uncertainty, and the overall uncertainty in speed measurement is approximately 15 rpm, consisting mostly of precision uncertainty. Using this information the uncertainties to use in the Monte Carlo simulation were chosen.

T01	T02	P01	P02	N	PR	U	U/C0	ETA	ETA/U/C0
549.69	519.30	100	62.5	2000	1.6	87.870	0.096	0.440	4.562
549.69	524.96	100	71.4	2000	1.4	87.870	0.113	0.491	4.346
549.69	533.25	100	83.3	2000	1.2	87.870	0.152	0.589	3.883
549.69	508.37	100	66.7	4000	1.5	175.739	0.207	0.687	3.324
549.69	499.32	100	62.5	5000	1.6	219.674	0.241	0.729	3.025
549.69	504.84	100	66.7	5000	1.5	219.674	0.258	0.746	2.887
549.69	496.52	100	62.5	6000	1.6	263.609	0.289	0.770	2.661
549.69	502.67	100	66.7	6000	1.5	263.609	0.310	0.782	2.522
549.69	494.85	100	62.5	6982	1.6	306.753	0.337	0.794	2.359
549.69	501.48	100	66.7	6982	1.5	306.753	0.361	0.802	2.222
549.69	517.67	100	76.9	6000	1.3	263.609	0.382	0.807	2.113
549.69	508.95	100	71.4	6982	1.4	306.753	0.394	0.809	2.051
549.69	517.47	100	76.9	6982	1.3	306.753	0.444	0.812	1.828
549.69	527.06	100	83.3	6000	1.2	263.609	0.455	0.811	1.782
549.69	517.74	100	76.9	8000	1.3	351.478	0.509	0.805	1.582
549.69	527.36	100	83.3	6982	1.2	306.753	0.530	0.800	1.511
549.69	528.15	100	83.3	8000	1.2	351.478	0.607	0.772	1.272
549.69	531.65	100	83.3	10000	1.2	439.348	0.759	0.647	0.852

Table A-4.1. Input "Data" used in HPFT Efficiency Map Monte Carlo Simulation

The x-axis of the turbine efficiency map is the velocity ratio, defined as the disk tangential speed, U, divided by the isentropic spouting velocity, C_0. Where the velocity ratio is determined from

$$U = \frac{D_{pitch} \times N}{229.18} \quad \text{ft}/\text{sec}$$

(2)

and the isentropic spouting velocity is found from

$$C_0 = \sqrt{2 g_c \, J \, \Delta H_{T-T(isen)}} \quad \text{ft}/\text{sec}$$

(3)

and the delta-enthalpy is calculated as

$$\Delta H_{T-T(isen)} = T_{01}\left[1 - \left(\frac{P_{02}}{P_{01}}\right)^{\frac{\gamma-1}{\gamma}}\right]$$

(4)

where g_c is the gravitational constant, J is the Joules Constant, and the 229.18 in the denominator of the U is a unit conversion constant. The data reduction equation for the turbine model efficiency is

$$\eta = \frac{T_{01} - T_{02}}{T_{01}\left[1 - \left(P_{02}/P_{01}\right)^{\frac{\gamma-1}{\gamma}}\right]} \tag{5}$$

However, the map efficiency, the y-axis, is plotted in terms of the efficiency divided by the velocity ratio,

$$\eta_{map} = \eta \Big/ \left(U/C_0\right) \tag{6}$$

Using these data reduction equations and the generated test measurements the *true* values of map efficiency and velocity ratio were calculated, shown in Table A-4.1.

The uncertainty to associate with the fourth-order regression is obtained by applying Eq. (33) in Appendix 3. The resulting expression is

$$U^2_{\eta_{map}} = \sum_{i=1}^{n}\left(\frac{\partial \eta_{map}}{\partial T_1(i)}\right)P^2_{T_1}(i) + \sum_{i=1}^{n}\left(\frac{\partial \eta_{map}}{\partial T_2(i)}\right)P^2_{T_2}(i) + \sum_{i=1}^{n}\left(\frac{\partial \eta_{map}}{\partial P_1(i)}\right)P^2_{P_1}(i) + \sum_{i=1}^{n}\left(\frac{\partial \eta_{map}}{\partial P_2(i)}\right)P^2_{P_2}(i)$$

$$+ \sum_{i=1}^{n}\left(\frac{\partial \eta_{map}}{\partial N(i)}\right)P^2_{N}(i) + \sum_{i=1}^{n}\left(\frac{\partial \eta_{map}}{\partial T_1(i)}\right)B^2_{T_1}(i) + \sum_{i=1}^{n}\left(\frac{\partial \eta_{map}}{\partial T_2(i)}\right)B^2_{T_2}(i) + \sum_{i=1}^{n}\left(\frac{\partial \eta_{map}}{\partial P_1(i)}\right)B^2_{P_1}(i)$$

$$+ \sum_{i=1}^{n}\left(\frac{\partial \eta_{map}}{\partial P_2(i)}\right)B^2_{P_2}(i) + \sum_{i=1}^{n}\left(\frac{\partial \eta_{map}}{\partial W(i)}\right)B^2_{N}(i)$$

$$+ 2\sum_{i=1}^{n-1}\sum_{k=i+1}^{n}\left(\frac{\partial \eta_{map}}{\partial T_1(i)}\right)\left(\frac{\partial \eta_{map}}{\partial T_1(k)}\right)B_{T1_i\,T1_k} + 2\sum_{i=1}^{n-1}\sum_{k=i+1}^{n}\left(\frac{\partial \eta_{map}}{\partial T_2(i)}\right)\left(\frac{\partial \eta_{map}}{\partial T_2(k)}\right)B_{T2_i\,T2_k}$$

$$+ 2\sum_{i=1}^{n}\sum_{k=1}^{n}\left(\frac{\partial \eta_{map}}{\partial T_1(i)}\right)\left(\frac{\partial \eta_{map}}{\partial T_2(k)}\right)B_{T1_i\,T2_k} + 2\sum_{i=1}^{n-1}\sum_{k=i+1}^{n}\left(\frac{\partial \eta_{map}}{\partial P_1(i)}\right)\left(\frac{\partial \eta_{map}}{\partial P_1(k)}\right)B_{P1_i\,P1_k}$$

$$+ 2\sum_{i=1}^{n-1}\sum_{k=i+1}^{n}\left(\frac{\partial \eta_{map}}{\partial P_2(i)}\right)\left(\frac{\partial \eta_{map}}{\partial P_2(k)}\right)B_{P2_i\,P2_k} + 2\sum_{i=1}^{n}\sum_{k=1}^{n}\left(\frac{\partial \eta_{map}}{\partial P_1(i)}\right)\left(\frac{\partial \eta_{map}}{\partial P_2(k)}\right)B_{P1_i\,P2_k}$$

$$+ 2\sum_{i=1}^{n-1}\sum_{k=i+1}^{n}\left(\frac{\partial \eta_{map}}{\partial N(i)}\right)\left(\frac{\partial \eta_{map}}{\partial N(k)}\right)B_{W_i\,W_k} + \left\{\begin{array}{l}\text{correlation terms for } B_{T1\,P1}, B_{T2\,P1}, \\ B_{T1N}, B_{T2N,} B_{P1N} \text{ ,etc. are neglected here}\end{array}\right\} \tag{7}$$

U/C0	ETA/(U/C0)	U avg	Coverge %	σ	RATIO
0.096	4.7119	0.053	95.54	0.0266	0.995
0.113	4.4896	0.0435	95.51	0.0219	0.994
0.152	4.0116	0.0337	95.28	0.017	0.993
0.207	3.4338	0.0282	95.34	0.0142	0.995
0.241	3.1246	0.0231	95.21	0.0116	0.996
0.258	2.9824	0.0202	95.14	0.0102	0.996
0.289	2.7489	0.0155	95.23	0.0078	0.997
0.310	2.6055	0.0134	95.33	0.0067	0.999
0.337	2.4365	0.0127	95.51	0.0064	1.002
0.361	2.2957	0.0137	95.51	0.0068	1.002
0.382	2.1834	0.0149	95.37	0.0074	1.001
0.394	2.1191	0.0156	95.29	0.0078	1.001
0.444	1.8881	0.0167	95.28	0.0084	0.996
0.455	1.8411	0.0167	95.22	0.0084	0.994
0.509	1.6342	0.0176	95.22	0.0089	0.986
0.530	1.5608	0.0194	95.12	0.0098	0.984
0.607	1.3141	0.0322	95.21	0.0163	0.989
0.759	0.880	0.036	95.79	0.018	1.000

Table A-4.2. Results of HPFT Efficiency Map Monte Carlo Simulation

The average uncertainty ranges from 1.1% at U/C0=0.096 to 4.1% at U/C0=0.759. At the general mainstage operating regime of the SSME the uncertainty in the efficiency parameter is approximately 0.5% - 0.75%.

Appendix - 5

Balance Relation Uncertainty Calculations

Table 5.1 contains the balance relation equations and the balance relation uncertainty estimates. The remainder of this appendix is the output from a MathCAD version 6.0+ file which performs the calculations for the balance relation uncertainty estimates. This file is being provided to the COTR, Mr. John P. Butas, NASA/MSFC, Propulsion Laboratory, EP-14. As better estimates for the hardware characteristic are obtained this file can be quickly modified to obtain the updated balance relation uncertainty estimates.

Balance relation uncertainties for balance relations 50-69 and 79-93 are essentially default values, these uncertainties are only slightly better than pure guesses. These value are intentionally over-estimated so that when the balance relation uncertainties are used in the solution methodology the solution will work to resolve the balance relations for which more information is known. When additional information is obtained to allow the estimation of uncertainties for these subcomponent models these balance relation uncertainties should be updated.

BAL#	MODULE	NAME	RELATION	TYPE	U_{BAL} %	Note
1	VOLM01	VL01	WLPFP=WF1	continuity	5.0	1
2			WLPFP*HTHTINK+QDOTLPFP=WF1*HTVL01	energy	5.0	1
3	VOLM00	VL02	WF1=WHPFP	continuity	5.0	1
4			WF1*HTVL01+QDOTVL02=WHPFP*HTVL02	energy	5.0	1
5	VOLM01	VL03	WHPFP=WMFV+WFTC	continuity	4.9	1
6			WHPFP*HTVL02+QDOTHPFP=(WMFV+WFTC)*HTVL03	energy	13.1	1
7	VOLQ01	VL04	WMFV=WF2+WF6+WF8+WFIG+WFFI+WFOI	continuity	5.8	1
8			WMFV*(HTVL03-UTVL04)=(WF2+WF6+WF8+WFIG+WFFI+WFOI)*(HTVL04-UTVL04)	energy	5.8	
9	VOLQ00	VL05	WF2=WF3	continuity	7.1	1
10			WF2*HTVL04+QDOTVL05=WF3*HTVL05	energy	7.1	1
11	VOLQ01	VL06	WF3=WF4+WNLK1	continuity	7.1	1
12			WF3*(HTVL05-UTVL06)=(WF4+WNLK1)*(HTVL06-UTVL06)	energy	7.0	1
13	VOLQ03	VL07	WF4=WF5	continuity	7.1	1
14			WF4*HTVL06+QDOTVL07+QAMBVL07=WF5*HTVL07	energy	23.6	1
15	VOLQ01	VL08	WF5+WCCV=WF7	continuity	7.0	1
16			WF5*(HTVL07-UTVL08)+WCCV*(HTVL09-UTVL08)=WF7*(HTVL08-UTVL08)	energy	8.7	
17	VOLQ00	VL09	WF6=WCCV	continuity	7.1	1
18			WF6*HTVL04+QDOTVL09=WCCV*HTVL09	energy	7.1	1
19	VOLQ00	VL10	WF8=WF9	continuity	7.1	1
20			WF8*HTVL04+QDOTVL10=WF9*HTVL10	energy	7.1	1
21	VOLQ01	VL11	WF9=WF10+WMLKI	continuity	7.1	1
22			WF9*(HTVL10-UTVL11)=(WF10+WMLKI)*(HTVL11-UTVL11)	energy	7.1	1
23	VOLQ04	VL12	WF10=WLPFT	continuity	7.1	1
24			WF10*(HTVL11-UTVL12)+QDOTVL12=WLPFT*(HTVL12-UTVL12)	energy	6.0	1
25	VOLM01	VL13	WLPFT=WF11+WF13+WFRPR	continuity	40.7	1
26			WLPFT*HTLTFD+QDOTVL13=(WF11+WF13+WFRPR)*HTVL13	energy	7.3	1
27	VOLM01	VL16	WF11+WF13=WFSLV+WF15	continuity	7.3	1
28			(WF11+WF13)*HTVL13+QDOTOMCI=(WFSLV+WF15)*HTVL16	energy	6.6	1
29	VOLQ01	PBSF	WF7=WFFPB+WFOPB+WOTC	continuity	7.4	1
30			WF7*(HTVL08-UTPBSF)=(WFFPB+WFOPB+WOTC)*(HTPBSF-UTPBSF)	energy	7.3	1

Table 5.1 Balance Relations and Balance Relation Uncertainty Estimates.

BAL#	MODULE	NAME	RELATION	TYPE	U$_{BAL}$,%	Note
31	POGO01	POGO	WPDIPOGO=WPDOPOGO	recirc line continuity	14.1	1
32			QINPOGO=QOUTPOGO	energy	14.1	1
33			WLXIPOGO=WLXOPOGO	LOX continuity	14.1	1
34			WGXIPOGO=WGXTPOGO	GOX continuity	2.1	1
35			WHEIPOGO=WHEOPOGO	He species continuity	10.0	1
36	VOLM01	VL17	WO1+WRIV=WO2	continuity	7.06	1
37			(WO1+WRIV)*HTOTNK+QDOTVL17=WO2*HTVL17	energy	7.06	1
38	VOLM00	VL18	WO2=WLPOP	continuity	5.00	1
39			WO2*HTVL17+QDOTVL18=WLPOP*HTVL18	energy	5.001	1
40	VOLM01	VL19	WLPOP+WLPOT=WO3	continuity	5.07	1
41			WLPOP*HTVL18+WLPOT*HTLTOD+QDOTLPOP=WO3*HTVL19	energy	5.09	1
42	VOLM01	VL20	WO3+WO6+WPOGL+WPOGG+WO4=WHPOP	continuity	4.96	1
43			WO3*HTVL19+WO6*HTPBSO+(WPOGL+WPOFF)*HTVL20 +WO4*HTVL21+QDOTVL20=WHPOP*HTVL20	energy	4.94	1
44	VOLM01	VL21	WHPOP=WO4+WO5+WHX+WMOV+WPRBP+WORPR	continuity	3.8	1
45			WHPOP*HTVL20+QDOTHPOP=(WO4+WO5+WHX+WMOV+WPRBP +WORPR)*HTVL21	energy	3.9	1
46	VOLM00	VL22	WO5=WLPOT	continuity	7.1	1
47			WO5*HTVL21+QDOTVL22=WLPOT*HTVL22	energy	5.0	1
48	VOLM01	PBSO	WPRBP=WO6+WOPOV+WFPOV	continuity	3.6	1
49			WPRBP*HTVL21+QDOTPRBP=(WO6+WOPOV+WFPOV)*HTPBSO	energy	3.7	1
50	PBRN01	OPRB	WOOPB+WOPBF+WHE2=WHG2	continuity	10	2
51			(WOOPB+WOPBF+WHE2)*(GAMA(PTOPRB,OFROPRB,HFROPRB, TTHETK,TTOPBF,TTOPBI)*TTCBST(PTOPRB,OFROPRB, HFROPRB,TTHETK,TTOPBF,TTOPBI)-TTOPRB) =WHG2*(GAMA(PTOPRB,OFROPRB,HFROPRB,TTHETK, TTOPBF,TTOPBI)-1)*TTOPRB	energy	20	2
52			WOOPB=OFROPRB*(WOOPB+WOPBF+WHE2)	O2 species continuity	20	2

Table 5.1, continued.   Balance Relations and Balance Relation Uncertainty Estimates.

BAL#	MODULE	NAME	RELATION	TYPE	U$_{BAL}$%	
53			WHE2=HFROPRB*(WOOPB+WOPBF+WHE2)	He species continuity	5	2
54	VOLM02	OSF	HFRHTOD*WHPOT+HFROTBP*WHG4+HFRPBSF*WOTC =HFROSF*(WHPOT+WHG4+WOTC)	H2 species continuity	20	2
55			OFRHTOD*WHPOT+OFROTBP*WHG4+OFRPBSF*WOTC =OFROSF*(WHPOT+WHG4+WOTC)	O2 species continuity	20	2
56			WHPOT+WHG4+WOTC=WHG6+WOLK	continuity	20	2
57			WHPOT*GAMAHTOD*(TTHTOD-TTOSF)+WHG4*GAMAOTBP*(TTOTBP -TTOSF)+WOTC*GAMAPBSF*(TTPBSF-TTOSF)+QDOTOSF *GAMAOSF/CPOSF=(WHG6+WOLK)*(GAMAOSF-1)*TTOSF	energy	20	2
58	PBRN01	FPRB	WOFPB+WFPBF+WHE1=WHG1	continuity	20	2
59			(WOFPB+WFPBF+WHE1)*(GAMA(PTFPRB,OFRFPRB,HFRFPRB, TTHETK,TTFPBF,TTFPBI)*TTCBST(PTFPRB,OFRFPRB, HFRFPRB,TTHETK,TTFPBF,TTFPBI)-TTFPRB) =WHG1*(GAMA(PTFPRB,OFRFPRB,HFRFPRB,TTHETK, TTFPBF,TTFPBI)-1)*TTFPRB	energy	20	
60			WOFPB=OFRFPRB*(WOFPB+WFPBF+WHE1)	O2 species continuity	20	2
61			WHE1=HFRFPRB*(WOFPB+WFPBF+WHE1)	He species continuity	5	2
62	VOLM02	FSF	HFRHTFD*WHPFT+HFRFTBP*WHG3+HFRVL03*WFTC =HFRFSF*(WHPFT+WHG3+WFTC)	H2 species continuity	20	2
63			OFRHTFD*WHPFT+OFRFTBP*WHG3+OFRVL03*WFTC =OFRFSF*(WHPFT+WHG3+WFTC)	O2 species continuity	20	2
64			WHPFT+WHG3+WFTC=WHG5	continuity	20	2
65			WHPFT*GAMAHTFD*(TTHTFD-TTFSF)+WHG3*GAMAFTBP*(TTFTBP -TTFSF)+WFTC*GAMAVL03*(TTVL03-TTFSF)+QDOTFSF *GAMAFSF/CPFSF=WHG5*(GAMAFSF-1)*TTFSF	energy	20	2
66	VOLM02	MFI	HFRFSF*WHG5+HFROSF*WHG6+HFRVL16*WFSLV =HFRMFI*(WHG5+WHG6+WFSLV)	H2 species continuity	20	2

Table 5.1, continued. Balance Relations and Balance Relation Uncertainty Estimates.

BAL#	MODULE	NAME	RELATION	TYPE	U_{BAL}%	Note
67			OFRFSF*WHG5+OFROSF*WHG6+OFRVL16*WFSLV =OFRMFI*(WHG5+WHG6+WFSLV)	O2 species continuity	20	2
68			WHG5+WHG6+WFSLV=WFINJ	continuity	20	2
69			WHG5*GAMAFSF*(TTFSF-TTMFI)+WHG6*GAMAOSF*(TTOSF-TTMFI) +WFSLV*GAMAVL16*(TTVL16-TTMFI)+(QDOTFMCO +QDOTOMCO)*GAMAMFI/CPMFI =WFINJ*(GAMAMFI-1)*TTMFI	energy	20	2
70	ROTR00	FL	TRQPFL=TRQNFL	mechanical energy	11.0	1
71	ROTR00	FH	TRQPFH=TRQNFH	mechanical energy	11.0	1
72	ROTR00	OL	TRQPOL=TRQN0L	mechanical energy	17.8	1
73	ROTR00	OH	TRQPOH=TRQNOH	mechanical energy	21.8	1
74	CFG		PTLPFP=PTVL01	map-system balance	2.5	1
75	CFG		PTHPFP=PTVL03	map-system balance	6.7	1
76	CFG		PTLPOP=PTVL19	map-system balance	4.1	1
77	CFG		PTHPOP=PTVL21	map-system balance	5.5	1
78	CFG		PTPRBP=PTPBSO	map-system balance	2.1	1
79	CFG		XROPV=XROPOV	control match	5	2
80	CFG		PTHG2=PTOPRB	map-system balance	20	2
81	CFG		PTHG6=PTOSF	map-system balance	20	2

Table 5.1, continued. Balance Relations and Balance Relation Uncertainty Estimates.

A5–5

BAL#	MODULE	NAME	RELATION	TYPE	U$_{BAL}$	Note
82	CFG		PTHG1=PTFPRB	map-system balance	20	2
83	CFG		PTHG5=PTFSF	map-system balance	20	2
84	CFG		PTFINJ=PTMFI	map-system balance	20	2
85	CFG		WMCHB=WNOZL	map-system balance	20	2
86	CFG		WHG1=WFTBP	map-system balance	20	2
87	CFG		WHG2=WOTBP	map-system balance	20	2
88	RUN		PTMCHB=PCREQ	control match	20	2
89	RUN		EMRFCNTR=OFREQ	control match	20	2
90	RUN		QOUTNOZX=QINNOZX	energy	20	2
91	RUN		QOUTNOZU=QINNOZU	energy	20	2
92	RUN		QOUTCHML=QINCHML	energy	20	2
93	RUN		QOUTCHMU=QINCHMU	energy	20	2

Table 5.1, continued.   Balance Relations and Balance Relation Uncertainty Estimates.

Notes: 1. Balance Uncertainty Calculations Shown in Appendix

2. These balance relation uncertainties are essentially default values, these uncertainties are only slightly better than pure guesses. These value are intentionally over-estimated so that when the balance relation uncertainties are used in the solution methodology the solution will work to resolve the balance relations for which more information is known.

Balance Relation Equations, Calcuations, and Uncertainty Calculations

Constants and information used throughout the equations.

Joules Constant $\quad$ RJ $:= 9337.92$

CLEN $:= 1.0$

CMASS $:= 1.0$

CFORCE $:= 1.0$

CTEMP $:= 1.0$

GC $:= 386.088$

FLOCON $:= 0.53531$

The turbopump speeds are:

$$SNRADFL := SNFL \cdot \frac{\pi}{30} \qquad SNRADFL = 1.444 \cdot 10^3$$

$$SNRADFH := SNFH \cdot \frac{\pi}{30} \qquad SNRADFH = 3.524 \cdot 10^3$$

$$SNRADOL := SNOL \cdot \frac{\pi}{30} \qquad SNRADOL = 537.135$$

$$SNRADOH := SNOH \cdot \frac{\pi}{30} \qquad SNRADOH = 2.885 \cdot 10^3$$

SNFL $:= 13785.63$

SNFH $:= 33655.01$

SNOL $:= 5129.258$

SNOH $:= 27553.1$

Balance Relation 1: WLPFP=WF1
* WLPFP is an iteration variable
* WF1 is the flow in fuel line 1, calculated in FLOW00

First, look at the calculation of WF1 and it's uncertainty

$$WF1 = \sqrt{\Delta P \cdot \frac{RHOVL01}{RF1}}$$

$WLPFP := 149.0299$

$WF1 := 149.0299$

$RF1 := 3.81 \cdot 10^{-6}$

$U_{RF1} := 0.10 \cdot RF1$

$RHOVL01 := 2.56 \cdot 10^{-3}$

$U_{RHOVL01} := 0.001 \cdot RHOVL01$

Consider uncertainties in the resistance and
the density from the property routine.

$$U_{WF1} = \sqrt{\left(\Theta_{RF1} \cdot U_{RF1}\right)^2 + \left(\Theta_{RHOVL01} \cdot U_{RHOVL01}\right)^2}$$

Evaluating the partial derivatives and dividing by WF1 to obtain
the uncertainty as a percentage.

$$U\%_{WF1} := \sqrt{\left(-\frac{1}{2} \cdot \frac{U_{RF1}}{RF1}\right)^2 + \left(\frac{1}{2} \cdot \frac{U_{RHOVL01}}{RHOVL01}\right)^2}$$

$$U\%_{WF1} = 5 \cdot \%$$

$$U_{WF1} := WF1 \cdot U\%_{WF1}$$

$$U_{WF1} = 7.452$$

Now rewrite the balance relation as $BAL1 := WF1 - WLPFP$

$$U_{BAL1} := U_{WF1}$$ $BAL1 = 0$

$$U_{BAL1} = 7.452$$

Now write the uncertainty as a percentage of the right-hand side of the balance relation:

$$U\%_{BAL1} := \frac{U_{BAL1}}{WF1}$$

$$U\%_{BAL1} = 5 \cdot \%$$

Balance relation 2: WLPFP*HTHTNK+QDOTLPFP=WF1*HTVL01
* WLPFP is an iteration variable
* HTHTNK is the H2 tank enthalpy and is an iteration variable
* QDOTLPFP is the power required by the pump, calc'd in SPUMP
* WF1 is the flow in fuel line 1
* HTVL01 is the volume 1 enthalpy and is an iteration variable

Now rewrite the balance relation and determine the uncertainty

$$BAL2 = WF1 \cdot HTVL01 - WLPFP \cdot HTHTNK - QDOTLPFP$$

The LPFP torque is calculated in SPUMP and uses a map for TAU vs PHI

$$TORQLPFP = -TAULPFP \cdot TORQMLPFP \cdot RHOVL01 \cdot SNRADFL^2$$

$$TORQLPFP := -10521.79$$

$$TRQPFL := TORQLPFP$$

$$HTVL01 := -96.92439$$

$$HTHTNK := -107.8393$$

$$WLPFP := 149.0299$$

$$TAULPFP := 1.971925$$

$$SNFL = 1.379 \cdot 10^4$$

$$SNRADFL = 1.444 \cdot 10^3$$

Considering an uncertainty associated with the torque coefficient vs flow coefficient map, and an uncertainty in density due to the property routine.

$$U\%_{TORQLPFP} := \sqrt{\left(\frac{U_{TAULPFP}}{TAULPFP}\right)^2 + \left(\frac{U_{RHOVL01}}{RHOVL01}\right)^2}$$

$$U_{TAULPFP} = 0.05 \cdot TAULPFP$$

$$U\%_{TORQLPFP} = 5.001 \cdot \%$$

$$U_{TORQLPFP} := |U\%_{TORQLPFP} \cdot TORQLPFP|$$

$$U_{TORQLPFP} = 526.195$$

$$QDOTLPFP := -TORQLPFP \cdot \frac{SNRADFL}{RJ}$$

$$QDOTLPFP = 1.627 \cdot 10^3$$

$$\theta_{TORQLPFP} := \frac{-SNRADFL}{RJ}$$

$$U_{QDOTLPFP} := \sqrt{\left(\theta_{TORQLPFP} \cdot U_{TORQLPFP}\right)^2}$$

$$U_{QDOTLPFP} = 81.349$$

$$U\%_{QDOTLPFP} := \frac{U_{QDOTLPFP}}{QDOTLPFP}$$

$$U\%_{QDOTLPFP} = 5.001 \cdot \%$$

Returning to the balance relation uncertainty,
and noting that the uncertainty sources are U_{WF1} AND $U_{QDOTLPFP}$

$$BAL2 := WF1 \cdot HTVL01 - WLPFP \cdot HTHTNK - QDOTLPFP$$

$$\theta_{WF1} := HTVL01 \qquad\qquad BAL2 = -0.004$$

$$\theta_{QDOTLPFP} := -1$$

$$U_{BAL2} := \sqrt{\left(\theta_{WF1} \cdot U_{WF1}\right)^2 + \left(\theta_{QDOTLPFP} \cdot U_{QDOTLPFP}\right)^2}$$

$$U_{BAL2} = 726.834$$

Now writing the uncertainty as a percentage of the RHS of the balance relation:

$$U\%_{BAL2} := \frac{U_{BAL2}}{|WF1 \cdot HTVL01|}$$

$$U\%_{BAL2} = 5.032 \cdot \%$$

Balance Relation 3: WF1=WHPFP
* WHPFP is an iteration variable
* WF1 is the flow in fuel line 1, calculated in FLOW00

$$WHPFP := 149.0299$$

Recalling the WF1 uncertainty

$$U\%_{WF1} = 5 \cdot \%$$

$$U_{WF1} = 7.452$$

Now rewrite the balance relation as $BAL3 := WHPFP - WF1$ $BAL3 = 0$

$$U_{BAL3} := U_{WF1}$$

$$U_{BAL3} = 7.452$$

Now write the uncertainty as a percentage of the RHS of the balance relation"

$$U\%_{BAL3} := \frac{U_{BAL3}}{WHPFP}$$

$$U\%_{BAL3} = 5 \cdot \%$$

Balance relation 4: WF1*HTVL01+QDOTVL02=WHPFP*HTVL02
* WHPFP is an iteration variable
* HTVL01 is the volume 2 enthalpy and is an iteration variable
* QDOTHPFP is the power required by the pump, calc'd in SPUMP
* WF1 is the flow in fuel line 1
* HTVL01 is the volume 1 enthalpy and is an iteration variable

Now rewrite the balance relation and determine the uncertainty

$$HTVL02 := -96.92438$$

$$QDOTVL02 := 0$$

$$BAL4 := WHPFP \cdot HTVL02 - WF1 \cdot HTVL01 - QDOTVL02$$

$$BAL4 = 0.001$$

$$\theta_{WF1} := -HTVL01$$

$$U_{BAL4} := \sqrt{\left(\theta_{WF1} \cdot U_{WF1}\right)^2}$$

$$U_{BAL4} = 722.268$$

Now write the uncertainty as a percentage of the RHS of the balance relation"

$$U\%_{BAL4} := \frac{U_{BAL4}}{|WHPFP \cdot HTVL02|}$$

$$U\%_{BAL4} = 5 \cdot \%$$

Balance Relation 5: WHPFP=WMFV+WFTC
* WHPFP is an iteration variable
* WMFV is the main fuel valve flow, calculated in FLOW00

Now rewrite the balance relation as: WMFV+WFTC-WHPFP

$$WMFV := 145.1001$$

Looking at the flow and uncertainty calculations for the MFV

$$RMFV := 1.53 \cdot 10^{-5}$$

$$U_{RMFV} := 0.10 \cdot RMFV$$

$$WMFV = \sqrt{\Delta P \cdot \frac{RHOVL03}{RMFV}}$$

Consider uncertainties in the resistance and
the density from the property routine.

$$RHOVL03 := 2.89 \cdot 10^{-3}$$

$$U_{RHOVL03} := 0.001 \cdot RHOVL03$$

$$U_{WF1} = \sqrt{\left(\theta_{RMFV} \cdot U_{RMFV}\right)^2 + \left(\theta_{RHOVL03} \cdot U_{RHOVL03}\right)^2}$$

Evaluating the partial derivatives and dividing by WF1 to obtain
the uncertainty as a percentage.

$$U\%_{WMFV} := \sqrt{\left(-\frac{1}{2} \cdot \frac{U_{RMFV}}{RMFV}\right)^2 + \left(\frac{1}{2} \cdot \frac{U_{RHOVL03}}{RHOVL03}\right)^2}$$

$$U\%_{WMFV} = 5 \cdot \%$$

$$U_{WMFV} := WMFV \cdot U\%_{WMFV}$$

$$U_{WMFV} = 7.255$$

Looking at the flow and uncertainty calculations for the FTC

$$WFTC := 3.929894$$

$$WFTC = \sqrt{\Delta P \cdot RHOVL03 \cdot CFFTC^2 \cdot FLOCON}$$

$$CFFTC := 2.025$$

Consider uncertainties in the resistance and
the density from the property routine.

$$U_{CFFTC} := 0.10 \cdot CFFTC$$

$$RHOVL03 := 2.89 \cdot 10^{-3}$$

$$U_{WFTC} = \sqrt{\left(\theta_{CFFTC} \cdot U_{CFFTC}\right)^2 + \left(\theta_{RHOVL03} \cdot U_{RHOVL03}\right)^2}$$

$$U_{RHOVL03} := 0.06 \cdot RHOVL03$$

Evaluating the partial derivatives and dividing by WF1 to obtain
the uncertainty as a percentage.

$$U\%_{WFTC} := \sqrt{\left(\frac{U_{CFFTC}}{CFFTC}\right)^2 + \left(\frac{1}{2} \cdot \frac{U_{RHOVL03}}{RHOVL03}\right)^2}$$

$$U\%_{WFTC} = 10.44 \cdot \%$$

$$U_{WFTC} := WFTC \cdot U\%_{WFTC}$$

$$U_{WFTC} = 0.41$$

Rewriting the balance relation and determining the uncertainty

$$BAL5 := WMFV + WFTC - WHPFP$$

$$BAL5 = 9.4 \cdot 10^{-5}$$

$$U_{BAL5} := \sqrt{U_{WMFV}^2 + U_{WFTC}^2}$$

$$U_{BAL5} = 7.267$$

Now write the uncertainty as a percentage of the RHS of the balance relation"

$$U\%_{BAL5} := \frac{U_{BAL5}}{|WMFV + WFTC|}$$

$$U\%_{BAL5} = 4.876 \cdot \%$$

Balance relation 6: WHPFP*HTVL02+QDOTHPFP=(WMFV+WFTC)*HTVL03
* WHPFP is an iteration variable
* HTVL02 is the volume 2 enthalpy and is an iteration variable
* QDOTHPFP is the power required by the HPFTP pump, calc'd in SPUMP
* WMFV is the flow through the MFV
* WFTC is the flow through the fuel turbine cooling line
* HTVL03 is the volume 3 enthalpy and is an iteration variable

Now rewrite the balance relation and determine the uncertainty

$$HTVL03 := 176.0563$$

BAL6=(WMFV+WFTC)*HTVL03-WHPFP*HTVL02-QDOTHPFP

The required pump power is determined from the SPUMP module and the pump map uncertainties.

$$QDOTHPFP = TORQHPFP \cdot \frac{SNRADFH}{RJ}$$

TORQHPFP is calculated using TAUHPFP from the torque
parameter vs flow coefficient map.

$$TAUHPFP := 3.003558$$

$$TORQHPFP = -\ TAUHPFP \cdot TORQMHPFP \cdot RHOVL03 \cdot SNRADFH^2$$

$$SNFH = 3.366 \cdot 10^4$$

$$TORQHPFP := -107789.8$$

$$SNRADFH = 3.524 \cdot 10^3$$

$$TRQPFH := |TORQHPFP|$$

Considering an uncertainty associated with the torque coefficient vs flow coefficient map, and an
uncertainty in density due to the property routine.

$$U\%_{TORQHPFP} := \sqrt{\left(\frac{U_{TAUHPFP}}{TAUHPFP}\right)^2 + \left(\frac{U_{RHOVL03}}{RHOVL03}\right)^2}$$

$$U_{TAUHPFP} := 0.05 \cdot TAUHPFP$$

$$U\%_{TORQHPFP} = 7.81 \cdot \%$$

$$U_{TORQHPFP} := |U\%_{TORQHPFP} \cdot TORQHPFP|$$

$$U_{TORQHPFP} = 8.419 \cdot 10^3$$

$$U_{TRQPFH} := U_{TORQHPFP}$$

$$SNFH := 33655.01$$

$$U_{TRQPFH} = 8.419 \cdot 10^3$$

$$SNRADFH := SNFH \cdot \frac{\pi}{30}$$

$$SNRADFH = 3.524344 \cdot 10^3$$

$$QDOTHPFP := -\ TORQHPFP \cdot \frac{SNRADFH}{RJ}$$

$$QDOTHPFP = 4.068 \cdot 10^4$$

$$\theta_{TORQHPFP} := \frac{-SNRADFH}{RJ}$$

$$U_{QDOTHPFP} := \sqrt{\left(\Theta_{TORQHPFP} \cdot U_{TORQHPFP}\right)^2}$$

$$U_{QDOTHPFP} = 3.177 \cdot 10^3$$

$$U\%_{QDOTHPFP} := \frac{U_{QDOTHPFP}}{QDOTHPFP}$$

$$U\%_{QDOTHPFP} = 7.81 \cdot \%$$

Returning to the balance relation and its uncertainty

$$BAL6 := (WMFV + WFTC) \cdot HTVL03 - WHPFP \cdot HTVL02 - QDOTHPFP$$

$$BAL6 = -0.034$$

The partial derivatives, Θ's, are

$$\Theta_{WMFV} := HTVL03$$

$$\Theta_{WFTC} := HTVL03$$

$$\Theta_{QDOTHPFP} := -1$$

so that the uncertainty expression for balance relation 6 becomes

$$U_{BAL6} := \sqrt{\left(\Theta_{WMFV} \cdot U_{WMFV}\right)^2 + \left(\Theta_{WFTC} \cdot U_{WFTC}\right)^2 + \left(\Theta_{QDOTHPFP} \cdot U_{QDOTHPFP}\right)^2}$$

$$U_{BAL6} = 3.425 \cdot 10^3$$

Now write the uncertainty as a percentage of the RHS of the balance relation"

$$U\%_{BAL6} := \frac{U_{BAL6}}{\left|(WMFV + WFTC) \cdot HTVL03\right|}$$

$$U\%_{BAL6} = 13.055 \cdot \%$$

Balance Relation 7: WMFV=WF2+WF6+WF8+WFIG+WFFI+WFOI
* WMFV is the main fuel valve flow, calculated in FLOW00
* WF2 is the flow through fuel line 2, calculated in FLOW00
* WF6 is the flow through fuel line 6, calculated in FLOW00
* WF8 is the flow through fuel line 6, calculated in FLOW00
* WFIG is the flow through fuel line, calculated in PIPE01
* WFFI is the flow through fuel line, calculated in PIPE01
* WFOI is the flow through fuel line, calculated in PIPE01

Now rewrite the balance relation as: BAL7=WMFV-WF2-WF6-WF8-WFIG-WFFI-WFOI

First, look at the calculation of WF2 and it's uncertainty

$$WF2 = \sqrt{\Delta P \cdot \frac{RHOVL04}{RF2}}$$

$$WF2 := 56.02199$$

$RF2 := 4.59 \cdot 10^{-5}$

$RF6 := 3.00 \cdot 10^{-4}$

$RF8 := 4.43 \cdot 10^{-4}$

$CFFIG := 0.42$

Consider uncertainties in the resistance and
the density from the property routine.

$CFFFI := 0.745$

$CFFOI := 0.799$

$$U_{WF2} = \sqrt{\left(\Theta_{RF2} \cdot U_{RF2}\right)^2 + \left(\Theta_{RHOVL04} \cdot U_{RHOVL04}\right)^2}$$

Evaluating the partial derivatives and dividing by WF2 to obtain
the uncertainty as a percentage.

$U_{RF2} := 0.1 \cdot RF2$

$RHOVL04 := 2.87 \cdot 10^{-3}$

$$U\%_{WF2} := \sqrt{\left(-\frac{1}{2} \cdot \frac{U_{RF2}}{RF2}\right)^2 + \left(\frac{1}{2} \cdot \frac{U_{RHOVL04}}{RHOVL04}\right)^2}$$

$U_{RHOVL04} := 0.001 \cdot RHOVL04$

$$U\%_{WF2} = 5 \cdot \%$$

$$U_{WF2} := WF2 \cdot U\%_{WF2}$$

$$U_{WF2} = 2.801$$

First, look at the calculation of WF6 and it's uncertainty

$$WF6 = \sqrt{\Delta P \cdot \frac{RHOVL04}{RF6}}$$

$$WF6 := 54.64435$$

Consider uncertainties in the resistance and
the density from the property routine.

$$U_{WF6} = \sqrt{\left(\Theta_{RF6} \cdot U_{RF6}\right)^2 + \left(\Theta_{RHOVL04} \cdot U_{RHOVL04}\right)^2}$$

Evaluating the partial derivatives and dividing by WF6 to obtain the uncertainty as a percentage.

$$U\%_{WF6} := \sqrt{\left(-\frac{1}{2} \cdot \frac{U_{RF6}}{RF6}\right)^2 + \left(\frac{1}{2} \cdot \frac{U_{RHOVL04}}{RHOVL04}\right)^2}$$

$$U\%_{WF6} = 0.05$$

$$U_{WF6} := WF6 \cdot U\%_{WF6}$$

$$U_{WF6} = 2.732$$

First, look at the calculation of WF8 and it's uncertainty

$$WF8 = \sqrt{\Delta P \cdot \frac{RHOVL04}{RF8}}$$

Consider uncertainties in the resistance and the density from the property routine.

$$U_{WF8} = \sqrt{\left(\Theta_{RF8} \cdot U_{RF8}\right)^2 + \left(\Theta_{RHOVL04} \cdot U_{RHOVL04}\right)^2}$$

Evaluating the partial derivatives and dividing by WF8 to obtain the uncertainty as a percentage.

$$U\%_{WF8} := \sqrt{\left(-\frac{1}{2} \cdot \frac{U_{RF8}}{RF8}\right)^2 + \left(\frac{1}{2} \cdot \frac{U_{RHOVL04}}{RHOVL04}\right)^2}$$

$$U\%_{WF8} = 0.05$$

$$U_{WF8} := WF8 \cdot U\%_{WF8}$$

$$U_{WF8} = 1.595$$

Looking at the flow and uncertainty calculations for the FIG

$$WFIG = \sqrt{\Delta P \cdot RHOVL04 \cdot CFFIG^2 \cdot FLOCON}$$

Consider uncertainties in the resistance and the density from the property routine.

$$U_{WFIG} = \sqrt{\left(\Theta_{CFFIG} \cdot U_{CFFIG}\right)^2 + \left(\Theta_{RHOVL04} \cdot U_{RHOVL04}\right)^2}$$

Evaluating the partial derivatives and dividing by WFIG to obtain the uncertainty as a percentage.

$$U\%_{WFIG} := \sqrt{\left(\frac{U_{CFFIG}}{CFFIG}\right)^2 + \left(\frac{1}{2} \cdot \frac{U_{RHOVL04}}{RHOVL04}\right)^2}$$

$$U\%_{WFIG} = 10 \cdot \%$$

$$U_{WFIG} := WFIG \cdot U\%_{WFIG}$$

$$U_{WFIG} = 0.086$$

$$U_{RF6} := 0.1 \cdot RF6$$

$$WF8 := 31.90515$$

$$U_{RF8} := 0.1 \cdot RF8$$

$$WFIG := 0.85539$$

$$U_{CFFIG} := 0.1 \cdot CFFIG$$

A5-18

Looking at the flow and uncertainty calculations for the FFI

$$WFFI = \sqrt{\Delta P \cdot RHOVL04 \cdot CFFFI^2 \cdot FLOCON}$$

Consider uncertainties in the resistance and
the density from the property routine.

$$U_{WFFI} = \sqrt{\left(\Theta_{CFFFI} \cdot U_{CFFFI}\right)^2 + \left(\Theta_{RHOVL04} \cdot U_{RHOVL04}\right)^2}$$

Evaluating the partial derivatives and dividing by WF1 to obtain
the uncertainty as a percentage.

$$U\%_{WFFI} := \sqrt{\left(\frac{U_{CFFFI}}{CFFFI}\right)^2 + \left(\frac{1}{2} \cdot \frac{U_{RHOVL04}}{RHOVL04}\right)^2}$$

$$U\%_{WFFI} = 10 \cdot \%$$

$$U_{WFFI} := WFFI \cdot U\%_{WFFI}$$

$$U_{WFFI} = 0.086$$

Looking at the flow and uncertainty calculations for the FOI

$$WFOI = \sqrt{\Delta P \cdot RHOVL04 \cdot CFFOI^2 \cdot FLOCON}$$

Consider uncertainties in the resistance and
the density from the property routine.

$$U_{WFOI} = \sqrt{\left(\Theta_{CFFOI} \cdot U_{CFFOI}\right)^2 + \left(\Theta_{RHOVL04} \cdot U_{RHOVL04}\right)^2}$$

Evaluating the partial derivatives and dividing by WF1 to obtain
the uncertainty as a percentage.

$$U\%_{WFOI} := \sqrt{\left(\frac{U_{CFFOI}}{CFFOI}\right)^2 + \left(\frac{1}{2} \cdot \frac{U_{RHOVL04}}{RHOVL04}\right)^2}$$

$$U\%_{WFOI} = 0.1$$

$$U_{WFOI} := WFOI \cdot U\%_{WFOI}$$

$$U_{WFOI} = 0.086$$

The uncertainty expression for BAL7 reduces to

$$U_{BAL7} := \sqrt{U_{WF2}^2 + U_{WF6}^2 + U_{WF8}^2 + U_{WFIG}^2 + U_{WFFI}^2 + U_{WFOI}^2 + U_{WMFV}^2}$$

$$U_{BAL7} = 8.398$$

Now write the uncertainty as a percentage of the RHS of the balance relation"

$$U\%_{BAL7} := \frac{U_{BAL7}}{|WF2 + WF6 + WF8 + WFIG + WFFI + WFOI|}$$

$$U\%_{BAL7} = 5.786 \cdot \%$$

$$WFFI := 0.85539$$

$$U_{CFFFI} := 0.1 \cdot CFFFI$$

$$WFOI := 0.85539$$

$$U_{CFFOI} := 0.1 \cdot CFFOI$$

A5-19

Balance relation 8:
WMFV*(HTVL03-UTVL04)=(WF2+WF6+WF8+WFIG+WFFI+WFOI)*(HTVL04-UTVL04)
* WMFV, WF2,WF6,WF8 are calculated in FLOW00 and have uncertainties
* WFIG, WFFI, WFOI are calculated in PIPE01 and have uncertainties
* HTVL03, HTVL04 are iteration variables
* UTVL04 is calculated in SSME3.CFG

HTVL04 and PTVL04 are iteration variables:

$$HTVL04 := 176.0563$$

$$UTVL04 := HTVL04 - \frac{1}{RJ} \cdot \frac{PTVL04}{RHOVL04}$$

$$PTVL04 := 5709.895$$

$$UTVL04 = -37.001$$

Thus UTVL04 has uncertainty due to the uncertainty from the property routine.

**this value for UTVL04 is slightly different that the value in the output file used of -37.34206

$$\Theta_{RHOVL04} := \frac{1}{RJ} \cdot \frac{PTVL04}{RHOVL04^2}$$

$$U_{UTVL04} := \sqrt{\left(\Theta_{RHOVL04} \cdot U_{RHOVL04}\right)^2}$$

$$U_{UTVL04} = 0.213$$

Balance relation 8 is rewritten as:

$$BAL8 := (WF2 + WF6 + WF8 + WFIG + WFFI + WFOI) \cdot (HTVL04 - UTVL04) - WMFV \cdot (HTVL03 - UTVL04)$$

$$BAL8 = 8.002$$

$$\Theta_{WF2} := HTVL04 - UTVL04 \qquad \Theta_{WFIG} := HTVL04 - UTVL04$$

$$\Theta_{WF6} := HTVL04 - UTVL04 \qquad \Theta_{WFFI} := HTVL04 - UTVL04$$

$$\Theta_{WF8} := HTVL04 - UTVL04 \qquad \Theta_{WFOI} := HTVL04 - UTVL04$$

$$\Theta_{UTVL04} := -WF2 - WF6 - WF8 - WFIG - WFFI - WFOI + WMFV$$

$$\Theta_{WMFV} := -HTVL03 + UTVL04$$

$$U_{BAL8} := \sqrt{\begin{aligned}&\left(\Theta_{WF2} \cdot U_{WF2}\right)^2 + \left(\Theta_{WF6} \cdot U_{WF6}\right)^2 + \left(\Theta_{WF8} \cdot U_{WF8}\right)^2 + \left(\Theta_{WFIG} \cdot U_{WFIG}\right)^2 \cdots \\ &+ \left(\Theta_{WFFI} \cdot U_{WFOI}\right)^2 + \left(\Theta_{WMFV} \cdot U_{WMFV}\right)^2 + \left(\Theta_{UTVL04} \cdot U_{UTVL04}\right)^2\end{aligned}}$$

$$U_{BAL8} = 1.789 \cdot 10^3$$

Now write the uncertainty as a percentage of the RHS of the balance relation"

$$U\%_{BAL8} := \frac{U_{BAL8}}{\left|(WF2 + WF6 + WF8 + WFIG + WFFI + WFOI) \cdot (HTVL04 - UTVL04)\right|}$$

$$U\%_{BAL8} = 5.786 \cdot \%$$

Balance Relation 9: WF2=WF3
* WF2 and WF3 are calculated in FLOW00

First, look at the calculation of WF3 and it's uncertainty

$$WF3 = \sqrt{\Delta P \cdot \frac{RHOVL05}{RF3}}$$

$WF3 := 56.0222$

$RF3 := 4.89 \cdot 10^{-5}$

$U_{RF3} := 0.1 \cdot RF3$

Consider uncertainties in the resistance and
the density from the property routine.

$$U_{WF3} = \sqrt{\left(\Theta_{RF3} \cdot U_{RF3}\right)^2 + \left(\Theta_{RHOVL05} \cdot U_{RHOVL05}\right)^2}$$

Evaluating the partial derivatives and dividing by WF2 to obtain
the uncertainty as a percentage.

$RHOVL05 := 2.89 \cdot 10^{-3}$

$U_{RHOVL05} := 0.001 \cdot RHOVL05$

$$U\%_{WF3} := \sqrt{\left(-\frac{1}{2} \cdot \frac{U_{RF3}}{RF3}\right)^2 + \left(\frac{1}{2} \cdot \frac{U_{RHOVL05}}{RHOVL05}\right)^2}$$

$U\%_{WF3} = 5 \cdot \%$

$U_{WF3} := WF3 \cdot U\%_{WF3}$

$U_{WF3} = 2.801$

Rewriting the balance relation and determining the uncertainty

$BAL9 := WF3 - WF2$

$BAL9 = 2.1 \cdot 10^{-4}$

$$U_{BAL9} := \sqrt{U_{WF2}^2 + U_{WF3}^2}$$

$U_{BAL9} = 3.962$

Now write the uncertainty as a percentage of the RHS of the balance relation

$$U\%_{BAL9} := \frac{U_{BAL9}}{|WF3|}$$

$U\%_{BAL9} = 7.071 \cdot \%$

Balance Relation 10: WF2*HTVL04+QDOTVL05=WF3*HTVL05
* WF2, WF3 are calculated in FLOW00 and uncertainties as above
* HTVL04, HTVL05 are iteration variables
* QDOTVL05 is defined as zero for this relation

$HTVL05 := 176.0564$

Rewriting the balance relation and determining the uncertainty:

$QDOTVL05 := 0$

$$BAL10 := WF3 \cdot HTVL05 - WF2 \cdot HTVL04 - QDOTVL05$$

$$BAL10 = 0.043$$

$$\theta_{WF3} := HTVL05$$

$$\theta_{WF2} := -HTVL04$$

$$U_{BAL10} := \sqrt{\left(\theta_{WF3} \cdot U_{WF3}\right)^2 + \left(\theta_{WF2} \cdot U_{WF2}\right)^2}$$

$$U_{BAL10} = 697.458$$

Now write the uncertainty as a percentage of the RHS of the balance relation"

$$U\%_{BAL10} := \frac{U_{BAL10}}{|WF3 \cdot HTVL05|}$$

$$U\%_{BAL10} = 7.071 \cdot \%$$

Balance Relation 11: WF3=WF4+WNLK1
* WF3, WF4 are calculated in FLOW00
* WNLK1 is the nozzle leakage flow and is currently zeroed out. $WNLK1 := 0$

Rewrite the balance relation as: BAL11=WF4+WNLK1-WF3

First, look at the calculation of WF3 and it's uncertainty

$$WF4 = \sqrt{\Delta P \cdot \frac{RHOVL06}{RF4}}$$

$$WF4 := 56.02217$$

Consider uncertainties in the resistance and
the density from the property routine.

$$U_{WF3} = \sqrt{\left(\Theta_{RF4} \cdot U_{RF4}\right)^2 + \left(\Theta_{RHOVL06} \cdot U_{RHOVL06}\right)^2}$$

Evaluating the partial derivatives and dividing by WF2 to obtain
the uncertainty as a percentage.

$$U\%_{WF4} := \sqrt{\left(-\frac{1}{2} \cdot \frac{U_{RF4}}{RF4}\right)^2 + \left(\frac{1}{2} \cdot \frac{U_{RHOVL06}}{RHOVL06}\right)^2}$$

$$U\%_{WF4} = 5 \cdot \%$$

$$U_{WF4} := WF4 \cdot U\%_{WF4}$$

$$U_{WF4} = 2.801$$

Rewriting the balance relation and determining the uncertainty

$$BAL11 := WF4 + WNLK1 - WF3$$

$$BAL11 = -3 \cdot 10^{-5}$$

$$U_{BAL11} := \sqrt{U_{WF4}^2 + U_{WF3}^2}$$

$$U_{BAL11} = 3.962$$

Now write the uncertainty as a percentage of the RHS of the balance relation"

$$U\%_{BAL11} := \frac{U_{BAL11}}{|WF4 + WNLK1|}$$

$$U\%_{BAL11} = 7.071 \cdot \%$$

$RF4 := 1.05 \cdot 10^{-4}$

$U_{RF4} := 0.1 \cdot RF4$

$RHOVL06 = 2.84 \cdot 10^{-3}$

$U_{RHOVL06} := 0.001 \cdot RHOVL06$

Balance Relation 12: WF3*(HTVL05-UTVL06)=(WF4+WNLK1)*(HTVL06-UTVL06)
* WF3, WF4 are calculated in FLOW00, as shown above
* WNLK1 is defined as zero at this point
* HTVL05,HTVL06 are iteration variables
* UTVL06 is calculated in the configuration file

HTVL06 and PTVL06 are iteration variables:

$$\text{UTVL06} := \text{HTVL06} - \frac{1}{\text{RJ}} \cdot \frac{\text{PTVL06}}{\text{RHOVL06}}$$

$$\text{HTVL06} := 176.0591$$

$$\text{PTVL06} := 5605.869$$

$$\text{UTVL06} = -35.326$$
**this value for UTVL06 is slightly different that the value in the output file used of -35.09946

Thus UTVL06 has uncertainty due to the uncertainty from the property routine.

$$\Theta_{\text{RHOVL06}} := \frac{1}{\text{RJ}} \cdot \frac{\text{PTVL06}}{\text{RHOVL06}^2}$$

$$U_{\text{UTVL06}} := \sqrt{\left(\Theta_{\text{RHOVL06}} \cdot U_{\text{RHOVL06}}\right)^2}$$

$$U_{\text{UTVL06}} = 0.211$$

Now rewriting the balance relation and determining the uncertainty

$$\text{BAL12} := (\text{WF4} + \text{WNLK1}) \cdot (\text{HTVL06} - \text{UTVL06}) - \text{WF3} \cdot (\text{HTVL05} - \text{UTVL06})$$

$$\text{BAL12} = 0.145$$

$$\Theta_{\text{WF4}} := \text{HTVL06} - \text{UTVL06}$$

$$\Theta_{\text{WF3}} := -\text{HTVL05} + \text{UTVL06}$$

$$\Theta_{\text{UTVL06}} := -\text{WF4} - \text{WNLK1} + \text{WF3}$$

$$U_{\text{BAL12}} := \sqrt{\left(\Theta_{\text{WF4}} \cdot U_{\text{WF4}}\right)^2 + \left(\Theta_{\text{WF3}} \cdot U_{\text{WF3}}\right)^2 + \left(\Theta_{\text{UTVL06}} \cdot U_{\text{UTVL06}}\right)^2}$$

$$U_{\text{BAL12}} = 837.411$$

Now write the uncertainty as a percentage of the RHS of the balance relation"

$$U\%_{\text{BAL12}} := \frac{U_{\text{BAL12}}}{|(\text{WF4} + \text{WNLK1}) \cdot (\text{HTVL06} - \text{UTVL06})|}$$

$$U\%_{\text{BAL12}} = 7.071 \cdot \%$$

Balance Relation 13: WF4=WF5
* WF4,WF5 are calculated in FLOW00

First, look at the calculation of WF5 and it's uncertainty

$$WF5 = \sqrt{\Delta P \cdot \frac{RHOVL07}{RF4}}$$

Consider uncertainties in the resistance and
the density from the property routine.

$$U_{WF5} = \sqrt{\left(\Theta_{RF4} \cdot U_{RF4}\right)^2 + \left(\Theta_{RHOVL07} \cdot U_{RHOVL07}\right)^2}$$

Evaluating the partial derivatives and dividing by WF5 to obtain
the uncertainty as a percentage.

$$U\%_{WF5} := \sqrt{\left(-\frac{1}{2} \cdot \frac{U_{RF5}}{RF5}\right)^2 + \left(\frac{1}{2} \cdot \frac{U_{RHOVL07}}{RHOVL07}\right)^2}$$

$$U\%_{WF5} = 5.831 \cdot \%$$

$$U_{WF5} := WF5 \cdot U\%_{WF5}$$

$$U_{WF5} = 3.267$$

Rewriting the balance relation and determining the uncertainty

$$BAL13 := WF5 - WF4$$

$$BAL13 = -1.5 \cdot 10^{-4}$$

$$U_{BAL13} := \sqrt{U_{WF5}^2 + U_{WF4}^2}$$

$$U_{BAL13} = 4.303$$

Now write the uncertainty as a percentage of the RHS of the balance relation"

$$U\%_{BAL13} := \frac{U_{BAL13}}{|WF5|}$$

$$U\%_{BAL13} = 7.681 \cdot \%$$

$$WF5 := 56.02202$$

$$RF5 := 1.13 \cdot 10^{-4}$$

$$U_{RF5} := 0.1 \cdot RF5$$

$$RHOVL07 := 1.46 \cdot 10^{-3}$$

$$U_{RHOVL07} := 0.06 \cdot RHOVL07$$

Balance Relation 14: WF4*HTVL06+QDOTVL07+QAMBVL07=WF5*HTVL07

* WF4,WF5 are shown above
* HTVL06,HTVL07 are the volume 6 and 7 enthalpies and are iteration variables
* QHOTVL07 is the heat transfer from the nozzle to the coolant flow
* QAMBVL07 is the heat transfer from the ambient to the coolant flow

$$HTVL06 := 176.0591 \qquad\qquad QDOTVL07 := 41579.38$$

$$HTVL07 := 918.2539$$
$$QAMBVL07 := 0$$

Heat transfers, Q's, are calculated in VOLQ03 by calling the QH2 subroutines, which calculates the heat flux, QDOT, through the areas, AHOTVL07 AND AAMBVL07.

$$AAMBVL07 := 28670$$

$$AHOTVL07 := 14490$$

QDOT is calculated in QH2 with the heat transfer correlation equation:

$$QDOT = \frac{0.0303}{D^{1.8}} \cdot \frac{W}{W^{.2}} \cdot \left(\frac{TF}{TM}\right)^{.55} \cdot \left(\frac{C_P}{\mu}\right)^{.4} \cdot k^6 \qquad\qquad QDOT_{HOT} := \frac{QDOTVL07}{AHOTVL07}$$

This equation is highly empirical and trying to base an uncertainty by propagating the estimated uncertainties of the individual terms would not be advisable. Some of the areas which contribute to the heat flux uncertainty are:
* There is no way to assess an uncertainty for the constants and exponents.
* The specific heat, viscosity, and thermal conductivity are difficult to obtain for super-critical hydrogen, so they will have considerable uncertainty.
* Values used for the temperature of the fluid, TF, and metal temperature, TM, are difficult to model.

Thus, the best way to estimate an uncertainty for the heat transfer flux is to examine the information upon which the flux equation was developed. There are no comment lines in the subroutine discussing the development of the equation and no other information is available at this time. Hense, an uncertainty of 20% will be assigned to the heat flux, until information is obtained upon which a better estimate can be made.

$$U\%_{QDOT} := 0.20 \qquad\qquad U_{QDOTHOT} := U\%_{QDOT} \cdot QDOT_{HOT}$$

$$U_{QDOTHOT} = 0.574$$

AHOTVL07 is the heat transfer area representing the hot wall of the nozzle. The nature of the design and manufacture of the nozzle and the multiple tubes which make up the nozzle coolant passages make an acurate determination of the heat transfer area difficult. Thus an uncertainty of 20% is being assigned.

$$QDOTVL07 := QDOT_{HOT} \cdot AHOTVL07 \qquad\qquad U_{AHOT} := 0.20 \cdot AHOTVL07$$

$$\Theta_{AREA} := QDOT_{HOT}$$
$$\Theta_{FLUX} := AHOTVL07$$

$$U_{QDOTVL07} := \sqrt{\left(\Theta_{FLUX} \cdot U_{QDOTHOT}\right)^2 + \left(\Theta_{AREA} \cdot U_{AHOT}\right)^2}$$

$$U_{QDOTVL07} = 1.176 \cdot 10^4$$

Rewriting the balance relation and propagating the uncertainties:

$$BAL14 := WF5 \cdot HTVL07 - WF4 \cdot HTVL06 - QDOTVL07 - QAMBVL07$$

$$BAL14 = -0.154$$

The partial derivatives needed are:

$$\Theta_{WF5} := HTVL07$$

$$\Theta_{QDOTVL07} := -1$$

$$\Theta_{WF4} := -HTVL06$$

$$U_{BAL14} := \sqrt{\left(\Theta_{WF5} \cdot U_{WF5}\right)^2 + \left(\Theta_{WF4} \cdot U_{WF4}\right)^2 + \left(\Theta_{QDOTVL07} \cdot U_{QDOTVL07}\right)^2}$$

$$U_{BAL14} = 1.215 \cdot 10^4$$

Now write the uncertainty as a percentage of the RHS of the balance relation"

$$U\%_{BAL14} := \frac{U_{BAL14}}{|WF5 \cdot HTVL07|}$$

$$U\%_{BAL14} = 23.613 \cdot \%$$

Balance Relation 15: WF5+WCCV=WF7
* WF5,WF7 are fuel line flows and calculated in FLOW00
* WCCV is the flow through the coolant control valve and is calculated in FLOW00

Now rewrite the balance relation as: BAL15=WF7-WF5-WCCV

$$WF7 := 110.667$$
$$RHOVL08 := 1.85 \cdot 10^{-3}$$
$$RF7 := 4.02 \cdot 10^{-6}$$

First, look at the calculation of WF7 and it's uncertainty

$$WF7 = \sqrt{\Delta P \cdot \frac{RHOVL08}{RF7}}$$

Consider uncertainties in the resistance and the density from the property routine. Estimate 10% uncertainty in resistance and 2% uncertainty in density from the property routine.

$$U_{WF7} = \sqrt{\left(\Theta_{RF7} \cdot U_{RF7}\right)^2 + \left(\Theta_{RHOVL08} \cdot U_{RHOVL08}\right)^2}$$

Evaluating the partial derivatives and dividing by WF8 to obtain the uncertainty as a percentage.

$$U_{RF7} := 0.1 \cdot RF7$$
$$U_{RHOVL08} := 0.06 \cdot RHOVL08$$

$$U\%_{WF7} := \sqrt{\left(-\frac{1}{2} \cdot \frac{U_{RF7}}{RF7}\right)^2 + \left(\frac{1}{2} \cdot \frac{U_{RHOVL08}}{RHOVL08}\right)^2}$$

$$U\%_{WF7} = 5.831 \cdot \%$$

$$U_{WF7} := WF7 \cdot U\%_{WF7}$$

$$U_{WF7} = 6.453$$

And similarly for the Coolant Control Valve.

$$RHOVL09 := 2.8 \cdot 10^{-3}$$
$$RCCV := 6.49 \cdot 10^{-5}$$
$$WCCV := 54.64416$$

$$WCCV = \sqrt{\Delta P \cdot \frac{RHOVL09}{RCCV}}$$

Consider uncertainties in the resistance and the density from the property routine. Estimate 10% uncertainty in resistance and 0.2% uncertainty in density from the property routine.

$$U_{WCCV} = \sqrt{\left(\Theta_{RCCV} \cdot U_{RCCV}\right)^2 + \left(\Theta_{RHOVL09} \cdot U_{RHOVL09}\right)^2}$$

Evaluating the partial derivatives and dividing by WCCV to obtain the uncertainty as a percentage.

$$U_{RCCV} := 0.1 \cdot RCCV$$
$$U_{RHOVL09} := 0.001 \cdot RHOVL09$$

$$U\%_{WCCV} := \sqrt{\left(-\frac{1}{2} \cdot \frac{U_{RCCV}}{RCCV}\right)^2 + \left(\frac{1}{2} \cdot \frac{U_{RHOVL09}}{RHOVL09}\right)^2}$$

$$U\%_{WCCV} = 5 \cdot \%$$

$$U_{WCCV} := WCCV \cdot U\%_{WCCV}$$

$$U_{WCCV} = 2.732$$

Now, rewriting the balance relation as

$$BAL15 := WF7 - WF5 - WCCV$$

$$BAL15 = 8.2 \cdot 10^{-4}$$

$$\Theta_{WF5} := 1$$
$$\Theta_{WCCV} := -1$$
$$\Theta_{WF7} := 1$$

$$U_{BAL15} := \sqrt{\left(\Theta_{WF7} \cdot U_{WF7}\right)^2 + \left(\Theta_{WF5} \cdot U_{WF5}\right)^2 + \left(\Theta_{WCCV} \cdot U_{WCCV}\right)^2}$$

$$U_{BAL15} = 7.732$$

Now write the uncertainty as a percentage of the RHS of the balance relation

$$U\%_{BAL15} := \frac{U_{BAL15}}{|WF7|}$$

$$U\%_{BAL15} = 6.986 \cdot \%$$

Balance Relation 16: WF5*(HTVL07-UTVL08)+WCCV*(HTVL09-UTVL08)=WF7*(HTVL08-UTVL08)
* WF5,WCCV,WFV are discussed above
* HTVL07,HTVL08,HTVL09 are iteration variables
* UTVL08 is calculated from available information.

$HTVL08 := 551.7748$

HTVL08 and PTVL08 are iteration variables:

$HTVL09 := 176.0563$

$PTVL08 := 5328.137$

$$UTVL08 := HTVL08 - \frac{1}{RJ} \cdot \frac{PTVL08}{RHOVL08}$$

$UTVL08 = 243.347$

Thus UTVL08 has uncertainty due to the uncertainty from the property routine.

**this value for UTVL08 is slightly different that the value in the output file of 243.9922

$$\theta_{RHOVL08} := \frac{1}{RJ} \cdot \frac{PTVL08}{RHOVL08^2}$$

$$U_{UTVL08} := \sqrt{\left(\theta_{RHOVL08} \cdot U_{RHOVL08}\right)^2}$$

$$U_{UTVL08} = 18.506$$

Now rewriting the balance relation and determining the uncertainty

$$BAL16 := WF7 \cdot (HTVL08 - UTVL08) - WF5 \cdot (HTVL07 - UTVL08) - WCCV \cdot (HTVL09 - UTVL08)$$

$$BAL16 = 0.175$$

The partial derivatives are:

$$\theta_{WF7} := HTVL08 - UTVL08$$

$$\theta_{WF5} := -HTVL07 + UTVL08$$

$$\theta_{WCCV} := -HTVL09 + UTVL08$$

$$\theta_{UTVL08} := -WF7 + WF5 + WCCV$$

$$U_{BAL16} := \sqrt{\left(\theta_{WF7} \cdot U_{WF7}\right)^2 + \left(\theta_{WF5} \cdot U_{WF5}\right)^2 + \left(\theta_{WCCV} \cdot U_{WCCV}\right)^2 + \left(\theta_{UTVL08} \cdot U_{UTVL08}\right)^2}$$

$$U_{BAL16} = 2.976 \cdot 10^3$$

Now write the uncertainty as a percentage of the RHS of the balance relation"

$$U\%_{BAL16} := \frac{U_{BAL16}}{|WF7 \cdot (HTVL08 - UTVL08)|}$$

$$U\%_{BAL16} = 8.718 \cdot \%$$

Balance Relation 17: WF6=WCCV
* WF6,WCCV are calculated in FLOW00

First, look at the calculation of WF6 and it's uncertainty

$$WF6 = \sqrt{\Delta P \cdot \frac{RHOVL04}{RF6}}$$

Consider uncertainties in the resistance and
the density from the property routine.

$$U_{WF6} = \sqrt{\left(\Theta_{RF6} \cdot U_{RF6}\right)^2 + \left(\Theta_{RHOVL04} \cdot U_{RHOVL04}\right)^2}$$

Evaluating the partial derivatives and dividing by WF6 to obtain
the uncertainty as a percentage.

$$U\%_{WF6} := \sqrt{\left(-\frac{1}{2} \cdot \frac{U_{RF6}}{RF6}\right)^2 + \left(\frac{1}{2} \cdot \frac{U_{RHOVL04}}{RHOVL04}\right)^2}$$

$$U\%_{WF6} = 5 \cdot \%$$

$$U_{WF6} := WF6 \cdot U\%_{WF6}$$

$$U_{WF6} = 2.732$$

Rewriting the balance relation and determining the uncertainty

$$BAL17 := WCCV - WF6$$

$$BAL17 = -1.9 \cdot 10^{-4}$$

$$U_{BAL17} := \sqrt{U_{WCCV}^2 + U_{WF6}^2}$$

$$U_{BAL17} = 3.864$$

Now write the uncertainty as a percentage of the RHS of the balance relation"

$$U\%_{BAL17} := \frac{U_{BAL17}}{|WCCV|}$$

$$U\%_{BAL17} = 7.071 \cdot \%$$

WF6 := 54.64435

RF6 := 1.13·10⁻⁴

$$U_{RF6} := 0.1 \cdot RF5$$

RHOVL04 := 2.84·10⁻³

$$U_{RHOVL04} := 0.001 \cdot RHOVL04$$

Balance Relation 18: WF6*HTVL04+QDOTVL09=WCCV*HTVL09
* WF6, WCCV are discussed above
* HTVL04, HTVL09 are iteration variables
* QDOTVL09 is zeroed in this model version

$$QDOTVL09 := 0$$

Rewriting the balance relation and determining the uncertainty

$$BAL18 := WCCV \cdot HTVL09 - WF6 \cdot HTVL04 - QDOTVL09$$

$$BAL18 = -0.033$$

The partial derivatives are:

$$\theta_{WCCV} := HTVL09$$

$$\theta_{WF6} := -HTVL04$$

$$U_{BAL18} := \sqrt{\left(\theta_{WCCV} \cdot U_{WCCV}\right)^2 + \left(\theta_{WF6} \cdot U_{WF6}\right)^2}$$

$$U_{BAL18} = 680.304$$

Now write the uncertainty as a percentage of the RHS of the balance relation"

$$U\%_{BAL18} := \frac{U_{BAL18}}{|WCCV \cdot HTVL09|}$$

$$U\%_{BAL18} = 7.071 \cdot \%$$

Balance Relation 19: WF8=WF9
* WF8,WF9 are calculated in FLOW00

First, look at the calculation of WF9 and it's uncertainty

$$WF9 = \sqrt{\Delta P \cdot \frac{RHOVL10}{RF9}}$$

Consider uncertainties in the resistance and the density from the property routine.

$$U_{WF9} = \sqrt{\left(\Theta_{RF9} \cdot U_{RF9}\right)^2 + \left(\Theta_{RHOVL10} \cdot U_{RHOVL10}\right)^2}$$

Evaluating the partial derivatives and dividing by WF9 to obtain the uncertainty as a percentage.

$$U\%_{WF9} := \sqrt{\left(-\frac{1}{2} \cdot \frac{U_{RF9}}{RF9}\right)^2 + \left(\frac{1}{2} \cdot \frac{U_{RHOVL10}}{RHOVL10}\right)^2}$$

$$U\%_{WF9} = 5 \cdot \%$$

$$U_{WF9} := WF9 \cdot U\%_{WF9}$$

$$U_{WF9} = 1.595$$

Rewriting the balance relation and determining the uncertainty

$$BAL19 := WF9 - WF8$$

$$BAL19 = -1 \cdot 10^{-5}$$

$$U_{BAL19} := \sqrt{U_{WF9}^2 + U_{WF8}^2}$$

$$U_{BAL19} = 2.256$$

Now write the uncertainty as a percentage of the RHS of the balance relation"

$$U\%_{BAL19} := \frac{U_{BAL19}}{|WF9|}$$

$$U\%_{BAL19} = 7.071 \cdot \%$$

$$WF9 := 31.90514$$
$$RF9 := 10. \cdot 10^{-4}$$
$$U_{RF9} := 0.1 \cdot RF9$$
$$RHOVL10 = 2.83 \cdot 10^{-3}$$
$$U_{RHOVL10} := 0.001 \cdot RHOVL10$$

Balance Relation 20: WF8*HTVL04+QDOTVL10=WF9*HTVL10
* WF8, WF9 are discussed above
* HTVL04, HTVL10 are iteration variables
* QDOTVL10 is zeroed in this model version

$$QDOTVL10 := 0$$
$$HTVL10 := 176.0562$$

Rewriting the balance relation and determining the uncertainty

$$BAL20 := WF9 \cdot HTVL10 - WF8 \cdot HTVL04 - QDOTVL10$$

$$BAL20 = -0.005$$

The partial derivatives are:
$$\Theta_{WF9} := HTVL10$$
$$\Theta_{WF8} := -HTVL04$$

$$U_{BAL20} := \sqrt{\left(\Theta_{WF9} \cdot U_{WF9}\right)^2 + \left(\Theta_{WF8} \cdot U_{WF8}\right)^2}$$

$$U_{BAL20} = 397.209$$

Now write the uncertainty as a percentage of the RHS of the balance relation"

$$U\%_{BAL20} := \frac{U_{BAL20}}{|WF9 \cdot HTVL10|}$$

$$U\%_{BAL20} = 7.071 \cdot \%$$

Balance Relation 21: WF9=WF10+WMLK1
* WF9,WF10 are calculated in FLOW00
* WMLK1 is a leakage flow, zeroed out in this model

First, look at the calculation of WF9 and it's uncertainty

$$WF10 = \sqrt{\Delta P \cdot \frac{RHOVL11}{RF10}} \qquad WF10 := 31.90514$$

$$RF10 := 21.7596 \cdot 10^{-4}$$

$$U_{RF10} := 0.1 \cdot RF10$$

Consider uncertainties in the resistance and the density from the property routine.

$$RHOVL11 := 2.75 \cdot 10^{-3}$$

$$U_{RHOVL11} := 0.001 \cdot RHOVL11$$

$$WMLK1 := 0$$

$$U_{WF10} = \sqrt{\left(\Theta_{RF10} \cdot U_{RF10}\right)^2 + \left(\Theta_{RHOVL11} \cdot U_{RHOVL11}\right)^2}$$

Evaluating the partial derivatives and dividing by WF10 to obtain the uncertainty as a percentage.

$$U\%_{WF10} := \sqrt{\left(-\frac{1}{2} \cdot \frac{U_{RF10}}{RF10}\right)^2 + \left(\frac{1}{2} \cdot \frac{U_{RHOVL11}}{RHOVL11}\right)^2}$$

$$U\%_{WF10} = 5 \cdot \%$$

$$U_{WF10} := WF10 \cdot U\%_{WF10}$$

$$U_{WF10} = 1.595$$

Rewriting the balance relation and determining the uncertainty

$$BAL21 := WF10 + WMLK1 - WF9$$

$$BAL21 = 0$$

$$U_{BAL21} := \sqrt{U_{WF10}^2 + U_{WF9}^2}$$

$$U_{BAL21} = 2.256$$

Now write the uncertainty as a percentage of the RHS of the balance relation"

$$U\%_{BAL21} := \frac{U_{BAL21}}{|WF10 + WMLK1|}$$

$$U\%_{BAL21} = 7.071 \cdot \%$$

Balance Relation 22: WF9*(HTVL10-UTVL11)=(WF10+WMLK1)*(HTVL11-UTVL11)
* WF9, WF10 are calculated in FLOW00, as shown above
* WMLK1 is defined as zero at this point
* HTVL10,HTVL11 are iteration variables
* UTVL11 is calculated in the configuration file

HTVL11 and PTVL11 are iteration variables:

$$HTVL11 := 176.0558$$

$$PTVL11 := 5193.024$$

$$UTVL11 := HTVL11 - \frac{1}{RJ} \cdot \frac{PTVL11}{RHOVL11}$$

$$UTVL11 = -26.17$$

**this value for UTVL11 is slightly different that the value in the output file used of -25.93668

Thus UTVL11 has uncertainty due to the uncertainty from the property routine.

$$\theta_{RHOVL11} := \frac{1}{RJ} \cdot \frac{PTVL11}{RHOVL11^2}$$

$$U_{UTVL11} := \sqrt{\left(\theta_{RHOVL11} \cdot U_{RHOVL11}\right)^2}$$

$$U_{UTVL11} = 0.202$$

Now rewriting the balance relation and determining the uncertainty

$$BAL22 := (WF10 + WMLK1) \cdot (HTVL11 - UTVL11) - WF9 \cdot (HTVL10 - UTVL11)$$

$$BAL22 = -0.013$$

$$\theta_{WF10} := HTVL11 - UTVL11$$

$$\theta_{WF9} := -HTVL10 + UTVL11$$

$$\theta_{UTVL11} := -WF10 - WMLK1 + WF9$$

$$U_{BAL22} := \sqrt{\left(\theta_{WF10} \cdot U_{WF10}\right)^2 + \left(\theta_{WF9} \cdot U_{WF9}\right)^2 + \left(\theta_{UTVL11} \cdot U_{UTVL11}\right)^2}$$

$$U_{BAL22} = 456.253$$

Now write the uncertainty as a percentage of the RHS of the balance relation"

$$U\%_{BAL22} := \frac{U_{BAL22}}{(WF10 + WMLK1) \cdot (HTVL11 - UTVL11)}$$

$$U\%_{BAL22} = 7.071 \cdot \%$$

Balance Relation 23: WF10=WLPFT
* WF10 is the fuel line 10 flow and is discussed above
* WLPFT is the flow through the Low Pressure Fuel Turbine
  and is calculated in TURB02 and uses the flow area map in TBMP04

$$W = \sqrt{RHOIN \cdot \frac{DP}{RHOMAP \cdot GC} \cdot \frac{XAREA}{\left(SFAREA \cdot CLEN^2\right)}}$$

$WLPFT := 31.90515$

$RHOVL12 := 1.31 \cdot 10^{-3}$

$XAREA := 1$

$PTVL12 := 4388.501$ $\qquad$ $PTIN := PTVL12$

$PTLTFD := 3288.016$ $\qquad$ $PTOUT := PTLTFD$

$DP := PTIN - PTOUT$

$RHOIN := RHOVL12$

$$W = \sqrt{RHOIN \cdot \frac{DP}{RHOMAP \cdot GC} \cdot \frac{XAREA}{\left(SFAREA \cdot CLEN^2\right)}}$$

$U\%_{XAREA} := 0.05$

$U\%_{RHOIN} := 0.02$

$$U\%_{WLPFT} := \sqrt{\left[\left(\frac{U_{XAREA}}{XAREA}\right) + \left(\frac{1}{2} \cdot \frac{U_{RHOIN}}{RHOIN}\right)\right]^2}$$

$U_{XAREA} := U\%_{XAREA} \cdot XAREA$

$U_{RHOIN} := U\%_{RHOIN} \cdot RHOIN$

$U\%_{WLPFT} = 6 \cdot \%$

$U_{WLPFT} := WLPFT \cdot U\%_{WLPFT}$

$\quad U_{WLPFT} = 1.914$

$BAL23 := WLPFT - WF10$

$\quad BAL23 = 1 \cdot 10^{-5}$

$U_{BAL23} := U_{WLPFT}$

$\quad U_{BAL23} = 1.914$

Now write the uncertainty as a percentage of the RHS of the balance relation"

$$U\%_{BAL23} := \frac{U_{BAL23}}{WLPFT}$$

$\quad U\%_{BAL23} = 6 \cdot \%$

Balance Relation 24: WF10*(HTVL11-UTVL12)+QDOTVL12=WLPFT*HTVL12
* WF10, WLPFT discussed above
* HTVL11,HTVL12 are iteration variables
* UTVL12 is calculated using enthalpy, pressure, and density
* QDOTVL12 is the heat transfer for the chamber wall cooling

$$HTVL12 := 832.1201$$

$$PTVL12 := 4388.501$$

HTVL12 and PTVL12 are iteration variables:

$$UTVL12 := HTVL12 - \frac{1}{RJ} \cdot \frac{PTVL12}{RHOVL12}$$

$$UTVL12 = 473.368$$
**this value for UTVL12 is slightly different that the value in the output file used of 473.8838

Thus UTVL11 has uncertainty due to the uncertainty from the property routine.

$$\theta_{RHOVL12} := \frac{1}{RJ} \cdot \frac{PTVL12}{RHOVL12^2}$$

$$U_{RHOVL12} := 0.06 \cdot RHOVL12$$

$$U_{UTVL12} := \sqrt{\left(\theta_{RHOVL12} \cdot U_{RHOVL12}\right)^2}$$

$$U_{UTVL12} = 21.525$$

Now look at the uncertainty in QDOTVL12, the chamber wall heat transfer.
As discussed in balance relation14, the uncertainty in the heat transfer calculations is estimated by combining an uncertainty associated with the heat flux calculation and an uncertainty associated with the heat transfer area. The heat transfer subroutine, QH2 includes a second heat transfer correlation to account for coolant boiling and two-phase flow. Again, no information is available at this time to assess whether this heat flux model correctly models the actual physical phenomena, so an overall uncertainty estimate, based upon engineering judgment, of 25% will be used.

The area through which the heat transfer is occurring should be easier to determine for the main combustion chamber, so an uncertainty of 10% will be used.

$$AHOTVL12 := 3912$$

$$QDOTVL12 = AHOTVL12 \cdot Q_{HOTVL12}$$

$$QDOTVL12 := 20931.83$$

Determining the uncertainty expression on a percentage basis:

$$U\%_{AHOTVL12} := 0.1$$

$$U\%_{QDOTVL12} := \sqrt{U\%_{AHOTVL12}^2 + U\%_{QHOTVL12}}$$

$$U\%_{QHOTVL12} := 0.25$$

$$U\%_{QDOTVL12} = 0.51$$

$$U_{QDOTVL12} := QDOTVL12 \cdot U\%_{QDOTVL12}$$

$$U_{QDOTVL12} = 1.067 \cdot 10^4$$

Rewriting the balance relation and propagating the uncertainties:

$$BAL24 := WLPFT \cdot (HTVL12 - UTVL12) - WF10 \cdot (HTVL11 - UTVL12) - QDOTVL12$$

$$BAL24 = -0.003$$

$$\Theta_{WLPFT} := HTVL12$$

$$\Theta_{WF10} := -HTVL11 + UTVL12$$

$$\Theta_{UTVL12} := WF10$$

$$\Theta_{QDOTVL12} := -1$$

$$U_{BAL24} := \sqrt{\left(\Theta_{WLPFT} \cdot U_{WLPFT}\right)^2 + \left(\Theta_{WF10} \cdot U_{WF10}\right)^2 + \left(\Theta_{UTVL12} \cdot U_{UTVL12}\right)^2 \cdots + \left(\Theta_{QDOTVL12} \cdot U_{QDOTVL12}\right)^2}$$

$$U_{BAL24} = 1.082 \cdot 10^4$$

Now write the uncertainty as a percentage of the RHS of the balance relation"

$$U\%_{BAL24} := \frac{U_{BAL24}}{WLPFT \cdot HTVL12}$$

$$U\%_{BAL24} = 40.769 \cdot \%$$

Balance Relation 25: WLPFT=WF11+WF13+WFRPR
* WLPFT, WF11 are discussed above
* WF13 is the flow through fuel line 13 and is calculated in FLOW00
* WFRPR is the fuel repressurization flow and is set at 0.2 lb/s

First, look at the calculation of WF11 and it's uncertainty

$$WF11 = \sqrt{\Delta P \cdot \frac{RHOVL13}{RF11}} \qquad WF11 := 13.43799$$

$RF11 := 2.55 \cdot 10^{-4}$

$U_{RF11} := 0.1 \cdot RF11$

Consider uncertainties in the resistance and
the density from the property routine.

$RHOVL13 := 1.09 \cdot 10^{-3}$

$U_{RHOVL13} := 0.06 \cdot RHOVL13$

$WFRPR := 0.2$

$$U_{WF11} = \sqrt{\left(\theta_{RF11} \cdot U_{RF11}\right)^2 + \left(\theta_{RHOVL13} \cdot U_{RHOVL13}\right)^2}$$

Evaluating the partial derivatives and dividing by WF11 to obtain
the uncertainty as a percentage.

$$U\%_{WF11} := \sqrt{\left(-\frac{1}{2} \cdot \frac{U_{RF11}}{RF11}\right)^2 + \left(\frac{1}{2} \cdot \frac{U_{RHOVL13}}{RHOVL13}\right)^2}$$

$U\%_{WF11} = 5.831 \cdot \%$

$U_{WF11} := WF11 \cdot U\%_{WF11}$

$U_{WF11} = 0.784$

Now, look at the calculation of WF13 and it's uncertainty

$$WF13 = \sqrt{\Delta P \cdot \frac{RHOVL13}{RF13}}$$

$WF13 := 18.26689$

$RF13 := 1.38 \cdot 10^{-4}$

$U_{RF13} := 0.1 \cdot RF13$

Consider uncertainties in the resistance and
the density from the property routine.

$RHOVL13 := 1.09 \cdot 10^{-3}$

$U_{RHOVL13} := 0.06 \cdot RHOVL13$

$$U_{WF13} = \sqrt{\left(\theta_{RF13} \cdot U_{RF13}\right)^2 + \left(\theta_{RHOVL13} \cdot U_{RHOVL13}\right)^2}$$

Evaluating the partial derivatives and dividing by WF13 to obtain
the uncertainty as a percentage.

$$U\%_{WF13} := \sqrt{\left(-\frac{1}{2} \cdot \frac{U_{RF13}}{RF13}\right)^2 + \left(\frac{1}{2} \cdot \frac{U_{RHOVL13}}{RHOVL13}\right)^2}$$

$U\%_{WF13} = 0.058$

$U_{WF13} := WF13 \cdot U\%_{WF13}$

$U_{WF13} = 1.065$

Including a 10% uncertainty for the fuel repress flow.

$U_{WFRPR} := 0.10 \cdot WFRPR$

$U_{WFRPR} = 0.02$

Rewriting the balance relation and determining the uncertainty

$$BAL25 := WF11 + WF13 + WFRPR - WLPFT$$

$$BAL25 = -2.7 \cdot 10^{-4}$$

$$U_{BAL25} := \sqrt{U_{WF11}^2 + U_{WF13}^2 + U_{WLPFT}^2 + U_{WFRPR}^2}$$

$$U_{BAL25} = 2.327$$

Now write the uncertainty as a percentage of the RHS of the balance relation"

$$U\%_{BAL25} := \frac{U_{BAL25}}{|WF11 + WF13 + WFRPR|}$$

$$U\%_{BAL25} = 7.293 \cdot \%$$

Balance Relation 26: WLPFT*HTLTFD+QDOTVL13=(WF11+WF13+WFRPR)*HTVL13
* WLPFT, WF11,WF13,WFRPR are discussed above
* HTLTFD,HTVL13 are iteration variables
* QDOTVL13 is defined as zero

Rewriting the balance relation and determining the uncertainty

$$QDOTVL13 := 0$$

$$HTVL13 := 781.1489$$

$$HTLTFD := 781.1362$$

$$BAL26 := (WF11 + WF13 + WFRPR) \cdot HTVL13 - WLPFT \cdot HTLTFD - QDOTVL13$$

$$BAL26 = 0.194$$

$$\Theta_{WF11} := HTVL13$$

$$\Theta_{WF13} := HTVL13$$

$$\Theta_{WFRPR} := HTVL13$$

$$\Theta_{WLPFT} := -HTLTFD$$

$$U_{BAL26} := \sqrt{\left(\Theta_{WF11} \cdot U_{WF11}\right)^2 + \left(\Theta_{WF13} \cdot U_{WF13}\right)^2 + \left(\Theta_{WFRPR} \cdot U_{WFRPR}\right)^2 + \left(\Theta_{WLPFT} \cdot U_{WLPFT}\right)^2}$$

$$U_{BAL26} = 1.817 \cdot 10^3$$

Now write the uncertainty as a percentage of the RHS of the balance relation"

$$U\%_{BAL26} := \frac{U_{BAL26}}{\left|(WF11 + WF13 + WFRPR) \cdot HTVL13\right|}$$

$$U\%_{BAL26} = 7.292 \cdot \%$$

Balance Relation 27: WF11+WF13=WFSLV+WF15
* WF11,WF13 are discussed above
* WFSLV is the flow through the fuel line to the main fuel injector
* WF15 is the flow through fuel line 15.

First, look at the calculation of WFSLV and it's uncertainty

$$WFSLV = \sqrt{\Delta P \cdot \frac{RHOVL16}{RFSLV}}$$

$WFSLV := 4.179799$

$RFSLV := 23.5 \cdot 10^{-4}$

$U_{RFSLV} := 0.1 \cdot RFSLV$

$RHOVL16 := 9.97 \cdot 10^{-4}$

$U_{RHOVL16} := 0.06 \cdot RHOVL16$

Consider uncertainties in the resistance and
the density from the property routine.

$$U_{WFSLV} = \sqrt{\left(\Theta_{RFSLV} \cdot U_{RFSLV}\right)^2 + \left(\Theta_{RHOVL16} \cdot U_{RHOVL16}\right)^2}$$

Evaluating the partial derivatives and dividing by WFSLV to obtain
the uncertainty as a percentage.

$$U\%_{WFSLV} := \sqrt{\left(-\frac{1}{2} \cdot \frac{U_{RFSLV}}{RFSLV}\right)^2 + \left(\frac{1}{2} \cdot \frac{U_{RHOVL16}}{RHOVL16}\right)^2}$$

$U\%_{WFSLV} = 5.831 \cdot \%$

$U_{WFSLV} := WFSLV \cdot U\%_{WFSLV}$

$U_{WFSLV} = 0.244$

Now, look at the calculation of WF15 and it's uncertainty

$$WF15 = \sqrt{\Delta P \cdot \frac{RHOVL16}{RF15}}$$

$WF15 := 27.52525$

$RF15 := 3.16 \cdot 10^{-4}$

$U_{RF15} := 0.1 \cdot RF15$

Consider uncertainties in the resistance and
the density from the property routine.

$$U_{WF15} = \sqrt{\left(\Theta_{RF15} \cdot U_{RF15}\right)^2 + \left(\Theta_{RHOVL16} \cdot U_{RHOVL16}\right)^2}$$

Evaluating the partial derivatives and dividing by WF13 to obtain
the uncertainty as a percentage.

$$U\%_{WF15} := \sqrt{\left(-\frac{1}{2} \cdot \frac{U_{RF15}}{RF15}\right)^2 + \left(\frac{1}{2} \cdot \frac{U_{RHOVL16}}{RHOVL16}\right)^2}$$

$U\%_{WF15} = 5.831 \cdot \%$

$U_{WF15} := WF15 \cdot U\%_{WF15}$

$U_{WF15} = 1.605$

Rewriting the balance relation and determining the uncertainty

$$BAL27 := WFSLV + WF15 - WF11 - WF13$$

$$BAL27 = 1.69 \cdot 10^{-4}$$

$$U_{BAL27} := \sqrt{U_{WFSLV}^2 + U_{WF15}^2 + U_{WF11}^2 + U_{WF13}^2}$$

$$U_{BAL27} = 2.094$$

Now write the uncertainty as a percentage of the RHS of the balance relation:

$$U\%_{BAL27} := \frac{U_{BAL27}}{|WFSLV + WF15|}$$

$$U\%_{BAL27} = 6.604 \cdot \%$$

Balance Relation 28: (WF11+WF13)*HTVL13+QDOTOMCI+QDOTFMCI=(WFSLV+WF15)*HTVL16
* WF11,WF13,WFSLV,WF15 are discussed previously
* HTVL13,WHVL16 are iteration variables
* QDOTOMCI, QDOTFMCI are manifold cooling heat transfers

From the configuration file

$HTVL16 := 886.4781$

$TTMFI := 1549.379$

$TKMCO := 0.00167$

$TTVL13 := 267.5007$

$TKMCF := 0.00131$

$AHTMCO := 728.0$

$AHTMCF := 872.0$

$WF13 = 18.267$

$$QDOTFMCI := TKMCO \cdot AHTMCO \cdot (TTMFI - TTVL13) \cdot \sqrt{\frac{WF13}{11.36}}$$

$QDOTOMCO := - QDOTFMCI$

$WF11 = 13.438$

$$QDOTOMCI := TKMCF \cdot AHTMCF \cdot (TTMFI - TTVL13) \cdot \sqrt{\frac{WF11}{15.50}}$$

$QDOTOMCO := QDOTOMCI$

$QDOTOMCI = 1.363 \cdot 10^3$

$QDOTFMCI = 1.976 \cdot 10^3$

Using the same logic and justification as discussed in balance relations 16 & 24, the heat transfer uncertainty is estimated by estimating an uncertainty for the heat transfer area and an uncertainty for the heat flux.

$QDOTOMCI = AHTMCF \cdot QDOT_{OMCI}$

Determining the uncertainty expression on a percentage basis:

$U\%_{AHTMCF} := 0.1$

$$U\%_{QDOTOMCI} := \sqrt{U\%_{AHTMCF}^2 + U\%_{QOMCI}}$$

$U\%_{QOMCI} := 0.20$

$U\%_{QDOTOMCI} = 45.826 \cdot \%$

$U_{QDOTOMCI} := QDOTOMCI \cdot U\%_{QDOTOMCI}$

$U_{QDOTOMCI} = 624.806$

$QDOTFMCI = AHTMCO \cdot QDOT_{FMCI}$

Determining the uncertainty expression on a percentage basis: $U\%_{AHTMCO} := 0.1$

$$U\%_{QDOTFMCI} := \sqrt{U\%_{AHTMCO}^2 + U\%_{QFMCI}}$$

$U\%_{QFMCI} := 0.20$

$$U\%_{QDOTFMCI} = 45.826 \cdot \%$$

$$U_{QDOTFMCI} := QDOTFMCI \cdot U\%_{QDOTFMCI}$$

$$U_{QDOTFMCI} = 905.623$$

Rewriting the balance relation and determining the uncertainty:

$$BAL28 := (WFSLV + WF15) \cdot HTVL16 - (WF11 + WF13) \cdot HTVL13 - QDOTOMCI - QDOTFMCI$$

$$BAL28 = -0.071$$

$$\Theta_{WFSLV} := HTVL16$$
$$\Theta_{WF15} := HTVL16$$
$$\Theta_{WF11} := -HTVL13$$
$$\Theta_{WF13} := -HTVL13$$
$$\Theta_{QDOTOMCI} := -1$$
$$\Theta_{QDOTFMCI} := -1$$

$$U_{BAL28} := \sqrt{\begin{array}{l}\left(\Theta_{WFSLV} \cdot U_{WFSLV}\right)^2 + \left(\Theta_{WF15} \cdot U_{WF15}\right)^2 + \left(\Theta_{WF11} \cdot U_{WF11}\right)^2 + \left(\Theta_{WF13} \cdot U_{WF13}\right)^2 \cdots \\ + \left(\Theta_{QDOTOMCI} \cdot U_{QDOTOMCI}\right)^2 + \left(\Theta_{QDOTFMCI} \cdot U_{QDOTFMCI}\right)^2\end{array}}$$

$$U_{BAL28} = 2.085 \cdot 10^3$$

Now write the uncertainty as a percentage of the RHS of the balance relation:

$$U\%_{BAL28} := \frac{U_{BAL28}}{\left|(WFSLV + WF15) \cdot HTVL16\right|}$$

$$U\%_{BAL28} = 7.419 \cdot \%$$

Balance Relation 29: WF7=WFFPB+WFOPB+WOTC
* WF7 is discussed above
* WFFPB is the fuel flow through the line to the fuel preburner
* WFOPB is the fuel flow through the line to the oxidizer preburner
* WOTC is the fuel flow through the oxidizer cooling line

First, look at the calculation of WFFPB and it's uncertainty

$$WFFPB = \sqrt{\Delta P \cdot \frac{RHOPBSF}{RFFPB}}$$

$$WFFPB := 75.21584$$

$$RFFPB := 1.243 \cdot 10^{-4}$$
$$U_{RFFPB} := 0.1 \cdot RFFPB$$

$$RHOPBSF := 9.97 \cdot 10^{-4}$$
$$U_{RHOPBSF} := 0.06 \cdot RHOPBSF$$

Consider uncertainties in the resistance and the density from the property routine.

$$U_{WFFPB} = \sqrt{\left(\Theta_{RFFPB} \cdot U_{RFFPB}\right)^2 + \left(\Theta_{RHOPBSF} \cdot U_{RHOPBSF}\right)^2}$$

Evaluating the partial derivatives and dividing by WFSLV to obtain the uncertainty as a percentage.

$$U\%_{WFFPB} := \sqrt{\left(-\frac{1}{2} \cdot \frac{U_{RFFPB}}{RFFPB}\right)^2 + \left(\frac{1}{2} \cdot \frac{U_{RHOPBSF}}{RHOPBSF}\right)^2}$$

$$U\%_{WFFPB} = 5.831 \cdot \%$$

$$U_{WFFPB} := WFFPB \cdot U\%_{WFFPB}$$

$$U_{WFFPB} = 4.386$$

Now, look at the calculation of WFOPB and it's uncertainty

$$WFOPB = \sqrt{\Delta P \cdot \frac{RHOPBSF}{RFOPB}}$$

$$WFOPB := 34.52161$$

$$RFOPB := 5.383 \cdot 10^{-4}$$
$$U_{RFOPB} := 0.1 \cdot RFOPB$$

$$RHOPBSF := 1.85 \cdot 10^{-3}$$
$$U_{RHOPBSF} := 0.06 \cdot RHOPBSF$$

Consider uncertainties in the resistance and the density from the property routine.

$$U_{WFOPB} = \sqrt{\left(\Theta_{RFOPB} \cdot U_{RFOPB}\right)^2 + \left(\Theta_{RHOPBSF} \cdot U_{RHOPBSF}\right)^2}$$

Evaluating the partial derivatives and dividing by WFSLV to obtain the uncertainty as a percentage.

$$U\%_{WFOPB} := \sqrt{\left(-\frac{1}{2} \cdot \frac{U_{RFOPB}}{RFOPB}\right)^2 + \left(\frac{1}{2} \cdot \frac{U_{RHOPBSF}}{RHOPBSF}\right)^2}$$

$$U\%_{WFOPB} = 5.831 \cdot \%$$

$$U_{WFOPB} := WFOPB \cdot U\%_{WFOPB}$$

$$U_{WFOPB} = 2.013$$

Looking at the flow and uncertainty calculations for the oxidizer turbine cooling line, WOTC

$$WOTC = \sqrt{\Delta P \cdot RHOPBSF \cdot CFOTC^2 \cdot FLOCON}$$

$WOTC := 0.929067$

Consider uncertainties in the resistance and the density from the property routine.

$CFOTC := 0.661$

$U_{CFOTC} := 0.1 \cdot CFOTC$

$$U_{WOTC} = \sqrt{\left(\Theta_{CFOTC} \cdot U_{CFOTC}\right)^2 + \left(\Theta_{RHOPBSF} \cdot U_{RHOPBSF}\right)^2}$$

Evaluating the partial derivatives and dividing by WFIG to obtain the uncertainty as a percentage.

$$U\%_{WOTC} := \sqrt{\left(\frac{U_{CFOTC}}{CFOTC}\right)^2 + \left(\frac{1}{2} \cdot \frac{U_{RHOPBSF}}{RHOPBSF}\right)^2}$$

$U\%_{WOTC} = 10.44 \cdot \%$

$U_{WOTC} := WOTC \cdot U\%_{WOTC}$

$U_{WOTC} = 0.097$

Rewriting the balance relation and determining the uncertainty

$BAL29 := WFFPB + WFOPB + WOTC - WF7$

$BAL29 = -4.83 \cdot 10^{-4}$

$$U_{BAL29} := \sqrt{U_{WFFPB}^2 + U_{WFOPB}^2 + U_{WOTC}^2 + U_{WF7}^2}$$

$U_{BAL29} = 8.058$

Now write the uncertainty as a percentage of the RHS of the balance relation:

$$U\%_{BAL29} := \frac{U_{BAL29}}{|WFFPB + WFOPB + WOTC|}$$

$U\%_{BAL29} = 7.282 \cdot \%$

Balance Relation 30: WF7*(HTVL08-UTPBSF)=(WFFPB+WFOPB+WOTC)*(HTPBSF-UTPBSF)
* WF7, WFFPB,WFOPB, WOTC are discussed above
* HTVL08, HTPBSF are iteration variables
* UTPBSF is determined from HTPBSF, PTPBSF, RHOPBSF

HTVL12 and PTVL12 are iteration variables:

$$\text{HTPBSF} := 551.7749$$

$$\text{PTPBSF} := 5301.58$$

$$\text{UTPBSF} := \text{HTPBSF} - \frac{1}{\text{RJ}} \cdot \frac{\text{PTPBSF}}{\text{RHOPBSF}}$$

$$\text{UTPBSF} = 244.884$$

**this value for UTPBSF is slightly different that the value in the output file used of 244.5773

Thus UTPBSF has uncertainty due to the uncertainty from the property routine.

$$\Theta_{\text{RHOPBSF}} := \frac{1}{\text{RJ}} \cdot \frac{\text{PTPBSF}}{\text{RHOPBSF}^2}$$

$$U_{\text{UTPBSF}} := \sqrt{\left(\Theta_{\text{RHOPBSF}} \cdot U_{\text{RHOPBSF}}\right)^2}$$

$$U_{\text{UTPBSF}} = 18.413$$

Rewriting the balance relation and determining the uncertainty

$$\text{BAL30} := (\text{WFFPB} + \text{WFOPB} + \text{WOTC}) \cdot (\text{HTPBSF} - \text{UTPBSF}) - \text{WF7} \cdot (\text{HTVL08} - \text{UTPBSF})$$

$$\text{BAL30} = -0.137$$

$$\Theta_{\text{WFFPB}} := \text{HTPBSF} - \text{UTPBSF}$$

$$\Theta_{\text{WFOPB}} := \text{HTPBSF} - \text{UTPBSF}$$

$$\Theta_{\text{WOTC}} := \text{HTPBSF} - \text{UTPBSF}$$

$$\Theta_{\text{WF7}} := -\text{HTVL08} + \text{UTPBSF}$$

$$\Theta_{\text{UTPBSF}} := -\text{WFFPB} - \text{WFOPB} - \text{WOTC} + \text{WF7}$$

$$U_{\text{BAL30}} := \sqrt{\begin{array}{l}\left(\Theta_{\text{WFFPB}} \cdot U_{\text{WFFPB}}\right)^2 + \left(\Theta_{\text{WFOPB}} \cdot U_{\text{WFOPB}}\right)^2 + \left(\Theta_{\text{WOTC}} \cdot U_{\text{WOTC}}\right)^2 \cdots \\ + \left(\Theta_{\text{WF7}} \cdot U_{\text{WF7}}\right)^2 + \left(\Theta_{\text{UTPBSF}} \cdot U_{\text{UTPBSF}}\right)^2\end{array}}$$

$$U_{\text{BAL30}} = 2.473 \cdot 10^3$$

Now write the uncertainty as a percentage of the RHS of the balance relation:

$$U\%_{\text{BAL30}} := \frac{U_{\text{BAL30}}}{|(\text{WFFPB} + \text{WFOPB} + \text{WOTC}) \cdot (\text{HTPBSF} - \text{UTPBSF})|}$$

$$U\%_{\text{BAL30}} = 7.282 \cdot \%$$

Balance Relation 31: WPDIPOGO=WPDOPOGO
recirc line continuity

$WPDIPOGO := 2.723936$

$WPDOPOGO := 2.723936$

$BAL31 := WPDOPOGO - WPDIPOGO$

$BAL31 = 0$

$U_{WPDOPOGO} := 0.10 \cdot WPDOPOGO$

$U_{WPDIPOGO} := 0.1 \cdot WPDIPOGO$

$U_{BAL31} := \sqrt{U_{WPDOPOGO}^2 + U_{WPDIPOGO}^2}$

$U_{BAL31} = 0.385$

Now write the uncertainty as a percentage of the RHS of the balance relation:

$U\%_{BAL31} := \dfrac{U_{BAL31}}{|WPDOPOGO|}$

$U\%_{BAL31} = 14.142 \cdot \%$

Balance Relation 32: QINPOGO=QOUTPOGO
energy

$QINPOGO := 21.79906$

$QOUTPOGO := 21.80359$

$BAL32 := QOUTPOGO - QINPOGO$

$BAL32 = 0.005$

$U_{QOUTPOGO} := 0.10 \cdot QOUTPOGO$

$U_{QINPOGO} := 0.1 \cdot QINPOGO$

$$U_{BAL32} := \sqrt{U_{QOUTPOGO}^2 + U_{QINPOGO}^2}$$

$U_{BAL32} = 3.083$

Now write the uncertainty as a percentage of the RHS of the balance relation:

$$U\%_{BAL32} := \frac{U_{BAL32}}{|QOUTPOGO|}$$

$U\%_{BAL32} = 14.141 \cdot \%$

Balance Relation 33: WLXIPOGO=WLXOPOGO
LOX continuity

$\text{WLXIPOGO} := 2.398129$

$\text{WLXOPOGO} := 2.398129$

$\text{BAL33} := \text{WLXOPOGO} - \text{WLXIPOGO}$

$\text{BAL33} = 0$

$U_{\text{WLXOPOGO}} := 0.10 \cdot \text{WLXOPOGO}$

$U_{\text{WLXIPOGO}} := 0.1 \cdot \text{WLXIPOGO}$

$U_{\text{BAL33}} := \sqrt{U_{\text{WLXOPOGO}}^2 + U_{\text{WLXIPOGO}}^2}$

$U_{\text{BAL33}} = 0.339$

Now write the uncertainty as a percentage of the RHS of the balance relation:

$U\%_{\text{BAL33}} := \dfrac{U_{\text{BAL33}}}{|\text{WLXOPOGO}|}$

$U\%_{\text{BAL33}} = 14.142 \cdot \%$

Balance Relation 34: WGXIPOGO=WGXOPOGO
GOX continuity

$$\text{WGXIPOGO} := 0.3511104$$

$$\text{WGXOPOGO} := 0.3511104$$

$$\text{BAL34} := \text{WGXOPOGO} - \text{WGXIPOGO}$$

$$\text{BAL34} = 0$$

$$\text{U}_{\text{WGXOPOGO}} := 0.10 \cdot \text{WGXOPOGO}$$

$$\text{U}_{\text{WGXIPOGO}} := 0.1 \cdot \text{WGXIPOGO}$$

$$\text{U}_{\text{BAL34}} := \sqrt{\text{U}_{\text{WGXOPOGO}}^2 + \text{U}_{\text{WGXIPOGO}}^2}$$

$$\text{U}_{\text{BAL34}} = 0.05$$

Now write the uncertainty as a percentage of the RHS of the balance relation:

$$\text{U\%}_{\text{BAL34}} := \frac{\text{U}_{\text{BAL34}}}{|\text{WLXOPOGO}|}$$

$$\text{U\%}_{\text{BAL34}} = 2.071 \cdot \%$$

Balance Relation 35: WHEIPOGO=WHEOPOGO
He continuity

$$WHEIPOGO := 0$$

$$BAL35 := WHEOPOGO - WHEIPOGO$$

$$WHEOPOGO := 8.7810^{-9}$$

$$BAL35 = 3.222 \cdot 10^{-9}$$

$$U_{WHEOPOGO} := 0.10 \cdot WHEOPOGO$$

$$U_{WHEIPOGO} := 0.1 \cdot WHEIPOGO$$

$$U_{BAL35} := \sqrt{U_{WHEOPOGO}^2 + U_{WHEIPOGO}^2}$$

$$U_{BAL35} = 3.222 \cdot 10^{-10}$$

Now write the uncertainty as a percentage of the RHS of the balance relation:

$$U\%_{BAL35} := \frac{U_{BAL35}}{|WHEOPOGO|}$$

$$U\%_{BAL35} = 10 \cdot \%$$

Balance Relation 36: WO1+WRIV=WO2
* WO1 is the flow through oxidizer line 1
* WRIV is the recirculation flow, somehow related to the pogo
* WO2 is the flow through oxidizer line 2

First, look at the calculation of WO1 and it's uncertainty

$$WO1 = \sqrt{\Delta P \cdot \frac{RHOOTNK}{RO1}}$$

Consider uncertainties in the resistance and
the density from the property routine.

$$U_{WO1} = \sqrt{\left(\Theta_{RO1} \cdot U_{RO1}\right)^2 + \left(\Theta_{RHOOTNK} \cdot U_{RHOOTNK}\right)^2}$$

Evaluating the partial derivatives and dividing by WO1 to obtain
the uncertainty as a percentage.

$$U\%_{WO1} := \sqrt{\left(-\frac{1}{2} \cdot \frac{U_{RO1}}{RO1}\right)^2 + \left(\frac{1}{2} \cdot \frac{U_{RHOOTNK}}{RHOOTNK}\right)^2}$$

$$U\%_{WO1} = 5.001 \cdot \%$$

$$U_{WO1} := WO1 \cdot U\%_{WO1}$$

$$U_{WO1} = 45.17$$

Now, look at the calculation of WO2 and it's uncertainty

$$WO2 = \sqrt{\Delta P \cdot \frac{RHOVL17}{RO2}}$$

Consider uncertainties in the resistance and
the density from the property routine.

$$U_{WO2} = \sqrt{\left(\Theta_{RO2} \cdot U_{RO2}\right)^2 + \left(\Theta_{RHOVL17} \cdot U_{RHOVL17}\right)^2}$$

Evaluating the partial derivatives and dividing by WO2 to obtain
the uncertainty as a percentage.

$$U\%_{WO2} := \sqrt{\left(-\frac{1}{2} \cdot \frac{U_{RO2}}{RO2}\right)^2 + \left(\frac{1}{2} \cdot \frac{U_{RHOVL17}}{RHOVL17}\right)^2}$$

$$U\%_{WO2} = 5.001 \cdot \%$$

$$U_{WO2} := WO2 \cdot U\%_{WO2}$$

$$U_{WO2} = 45.306$$

$WO1 := 903.2136$

$RHOOTNK := 4.09 \cdot 10^{-2}$

$U_{RHOOTNK} := 0.002 \cdot RHOOTNK$

$RO1 := 1.00 \cdot 10^{-6}$

$U_{RO1} := 0.1 \cdot RO1$

$WO2 := 905.9374$

$RHOVL17 := 4.09 \cdot 10^{-2}$

$U_{RHOVL17} := 0.002 \cdot RHOOTNK$

$RO2 := 2.23 \cdot 10^{-7}$

$U_{RO2} := 0.1 \cdot RO2$

Sufficient information to determine an uncertainty for WRIV was not found, so an uncertainty will be estimated as the same percentage uncertainty as determined for the majority of the other ducts.

$$U\%_{WRIV} := 0.05 \qquad\qquad WRIV := 2.723989$$

$$U_{WRIV} := U\%_{WRIV} \cdot WRIV$$

$$U_{WRIV} = 0.136$$

Rewriting the balance relation and determining the uncertainty

$$BAL36 := WO2 - WO1 - WRIV$$

$$BAL36 = -1.89 \cdot 10^{-4}$$

$$U_{BAL36} := \sqrt{U_{WO2}^2 + U_{WO1}^2 + U_{WRIV}^2}$$

$$U_{BAL36} = 63.976$$

Now write the uncertainty as a percentage of the RHS of the balance relation:

$$U\%_{BAL36} := \frac{U_{BAL36}}{|WO2|}$$

$$U\%_{BAL36} = 7.062 \cdot \%$$

Balance Relation 37: (WO1+WRIV)*HTOTNK+QDOTVL17=WO2*HTVL17
* WO1,WRIV,WO2 are discussed above
* HTOTNK, HTVL17 are iteration variables
* QDOTVL17 is zeroed out in this version

$$QDOTVL17 := 0$$
$$HTOTNK := 63.04315$$
$$HTVL17 := 63.04316$$

Rewriting the balance relation and determining the uncertainty

$$BAL37 := WO2 \cdot HTVL17 - (WO1 + WRIV) \cdot HTOTNK + QDOTVL17$$

$$BAL37 = -0.003$$

$$\theta_{WO2} := HTVL17$$
$$\theta_{WO1} := -HTOTNK$$
$$\theta_{WRIV} := -HTOTNK$$

$$U_{BAL37} := \sqrt{\left(\theta_{WO2} \cdot U_{WO2}\right)^2 + \left(\theta_{WO1} \cdot U_{WO1}\right)^2 + \left(\theta_{WRIV} \cdot U_{WRIV}\right)^2}$$

$$U_{BAL37} = 4.033 \cdot 10^3$$

Now write the uncertainty as a percentage of the RHS of the balance relation:

$$U\%_{BAL37} := \frac{U_{BAL37}}{|WO2 \cdot HTVL17|}$$

$$U\%_{BAL37} = 7.062 \cdot \%$$

Balance Relation 38: WO2=WLPOP
* WO2 is discussed above
* WLPOP is the flow through the Low Pressure Oxidizer Turbine, and is an iteration variable

Rewriting the balance relation and determining the uncertainty:

$BAL38 := WLPOP - WO2$

$WLPOP := 905.9375$

$BAL38 = 1 \cdot 10^{-4}$

$U_{BAL38} := U_{WO2}$

$U_{BAL38} = 45.306$

Now write the uncertainty as a percentage of the RHS of the balance relation:

$$U\%_{BAL38} := \frac{U_{BAL38}}{|WLPOP|}$$

$$U\%_{BAL38} = 5.001 \cdot \%$$

Balance Relation 39: WO2*HTVL17+QDOTVL18=WLPOP*HTVL18
* WO2,WLPOP are discussed above
* HTVL17, HTVL18 are iteration variables
* QDOTVL18 is heat transfer and is zeroed out in this model version

$$QDOTVL18 := 0$$

$$HTVL18 := 63.04316$$

Rewriting the balance relation and determining the uncertainty

$$BAL39 := WLPOP \cdot HTVL18 - WO2 \cdot HTVL17 - QDOTVL18$$

$$BAL39 = 0.006$$

$$\Theta_{WO2} := -HTVL17$$

$$U_{BAL39} := \sqrt{\left(\Theta_{WO2} \cdot U_{WO2}\right)^2}$$

$$U_{BAL39} = 2.856 \cdot 10^3$$

Now write the uncertainty as a percentage of the RHS of the balance relation:

$$U\%_{BAL39} := \frac{U_{BAL39}}{|WLPOP \cdot HTVL18|}$$

$$U\%_{BAL39} = 5.001 \cdot \%$$

Balance Relation 40: WLPOP+WLPOT=WO3
* WLPOP is discussed previously
* WLPOT is the flow through the Low Pressure Oxidizer Turbine (LPOT),
  uses TURB02 and the map in TBMP06
* WO3 is the flow through oxidizer line 3

The LPOT flow is calculated using the equation

$$WLPOT = WMAP \cdot \frac{SFW}{CMASS \cdot \sqrt{SFRHO}}$$

where WMAP is the value from the flow parameter vs pressure ratio and speed map
       SFW is the turbine area scale factor
       CMASS is a mass conversion parameter
       SFRHO is a density scale factor

$$AREAMAP := 1.0$$

$$RHOMAP := 0.040509$$

$$WLPOT = WMAP \cdot \left(\frac{AREAMAP}{AREA \cdot CLEN^2}\right) \cdot \frac{1}{CMASS} \cdot \frac{1}{\sqrt{\dfrac{RHOMAP}{RHOIN \cdot CMASS \cdot CLEN^3}}}$$

Consider uncertainties for the hardware characteristics WMAP and AREA, and for the inlet density density uncertainty from the physical property routine.

Taking the partial derivatives with respect to each uncertainty source and dividing by WLPOT

$$\theta\% \; WMAP = \frac{1}{WMAP}$$

$$\theta\% \; RHOIN = \frac{\dfrac{1}{2} \cdot WMAP \cdot \dfrac{AREAMAP}{\left[AREA \cdot \left[\sqrt{CLEN} \cdot \left[\sqrt{CMASS} \cdot \left(\sqrt{RHOMAP} \cdot \sqrt{RHOIN}\right)\right]\right]\right]}}{WMAP \cdot \left(\dfrac{AREAMAP}{AREA \cdot CLEN^2}\right) \cdot \dfrac{1}{CMASS} \cdot \dfrac{1}{\sqrt{\dfrac{RHOMAP}{RHOIN \cdot CMASS \cdot CLEN^3}}}}$$

simplifying

$$\theta\% \; RHOIN := \frac{1}{(2 \cdot RHOIN)}$$

$$\Theta\%_{AREA}=\cfrac{-WMAP\cdot\cfrac{AREAMAP}{\left[AREA^2\cdot\left[\sqrt{CLEN}\cdot\left(\sqrt{CMASS}\cdot\sqrt{RHOMAP}\right)\right]\right]}\cdot\sqrt{RHOIN}}{WMAP\cdot\left(\cfrac{AREAMAP}{AREA\cdot CLEN^2}\right)\cdot\cfrac{1}{CMASS}\cdot\cfrac{1}{\sqrt{\cfrac{RHOMAP}{RHOIN\cdot CMASS\cdot CLEN^3}}}}$$

simplifying

$$\Theta\%_{AREA}=\frac{-1}{AREA}$$

$$\Theta_{WMAP}:=1$$

$$\Theta_{AREALPOT}:=\frac{-1}{AREALPOT}$$

$$\Theta_{RHOVL19}:=\frac{1}{(2\cdot RHOVL19)}$$

$$RHOVL19:=4.04\cdot10^{-2}$$

$$U_{RHOVL19}:=0.002\cdot RHOOTNK$$

$$WLPOT:=178.7272$$

$$AREALPOT:=1.$$

$$U\%_{WMAP}:=0.05$$

$$U\%_{AREALPOT}:=0.01$$

$$U\%_{RHOVL19}:=\frac{U_{RHOVL19}}{RHOVL19}$$

The uncertainty expression then becomes

$$U\%_{WLPOT}:=\sqrt{\left(U\%_{WMAP}\right)^2+\left(-U\%_{AREALPOT}\right)^2+\left(\frac{U\%_{RHOVL19}}{2}\right)^2}$$

$$U\%_{WLPOT}=5.1\cdot\%$$

$$U_{WLPOT}:=U\%_{WLPOT}\cdot WLPOT$$

$$U_{WLPOT}=9.115$$

Now, look at the calculation of WO3 and it's uncertainty

$$WO3=\sqrt{\Delta P\cdot\frac{RHOVL19}{RO3}}$$

Consider uncertainties in the resistance and
the density from the property routine.

$$U_{WO3}=\sqrt{\left(\Theta_{RO3}\cdot U_{RO3}\right)^2+\left(\Theta_{RHOVL19}\cdot U_{RHOVL19}\right)^2}$$

$$WO3:=1084.665$$

$$RO3:=2.23\cdot10^{-7}$$

$$U_{RO3}:=0.1\cdot RO3$$

Evaluating the partial derivatives and dividing by WO3 to obtain
the uncertainty as a percentage.

$$U\%_{WO3} := \sqrt{\left(-\frac{1}{2} \cdot \frac{U_{RO3}}{RO3}\right)^2 + \left(\frac{1}{2} \cdot \frac{U_{RHOVL19}}{RHOVL19}\right)^2}$$

$$U\%_{WO3} = 5.001 \cdot \%$$

$$U_{WO3} := WO3 \cdot U\%_{WO3}$$

$$U_{WO3} = 54.244$$

Now, rewrite the balance relation and determine the uncertainty

$$BAL40 := WO3 - WLPOP - WLPOT$$

$$BAL40 = 3 \cdot 10^{-4}$$

$$U_{BAL40} := \sqrt{U_{WO3}^2 + U_{WLPOT}^2}$$

$$U_{BAL40} = 55.005$$

Now write the uncertainty as a percentage of the RHS of the balance relation:

$$U\%_{BAL40} := \frac{U_{BAL40}}{|WO3|}$$

$$U\%_{BAL40} = 5.071 \cdot \%$$

Balance Relation 41: WLPOP*HTVL18+WLPOT*HTLTOD+QDOTLPOP=WO3*HTVL19
* WLPOP, WLPOT, WO3 are flowrates discussed above
* HTVL18, HTVL19, HTLTOD are iteration variables
* QDOTLPOP is the power required to drive the pump

The required pump power is determined from the SPUMP module and the pump map uncertainties.

The LPOP torque is calculated in SPUMP and uses a map for TAU vs PHI $\text{TAULPOP} := 1.658089$

$$\text{SNOL} = 5.129 \cdot 10^3$$

$$\text{TORQLPOP} = -\text{TAULPOP} \cdot \text{TORQMLPOP} \cdot \text{RHOVL01} \cdot \text{SNRADOL}^2 \qquad \text{SNRADOL} = 537.135$$

$$\text{TORQLPOP} := -10521.79$$

$$\text{TRQPOL} := |\text{TORQLPOP}|$$

Considering an uncertainty associated with the torque coefficient vs flow coefficient map, and an uncertainty in density due to the property routine.

$$\text{U\%}_{\text{TORQLPOP}} := \sqrt{\left(\frac{\text{U}_{\text{TAULPOP}}}{\text{TAULPOP}}\right)^2 + \left(\frac{\text{U}_{\text{RHOVL19}}}{\text{RHOVL19}}\right)^2} \qquad \text{U}_{\text{TAULPOP}} := 0.05 \cdot \text{TAULPOP}$$

$$\text{U\%}_{\text{TORQLPOP}} = 5.004 \cdot \%$$

$$\text{U}_{\text{TORQLPOP}} := |\text{U\%}_{\text{TORQLPOP}} \cdot \text{TORQLPOP}|$$

$$\text{U}_{\text{TORQLPOP}} = 526.521$$

$$\text{U}_{\text{TRQPOL}} := \text{U}_{\text{TORQLPOP}} \qquad\qquad \text{U}_{\text{TRQPOL}} = 526.521$$

$$\text{QDOTLPOP} := -\text{TORQLPOP} \cdot \frac{\text{SNRADOL}}{\text{RJ}}$$

$$\text{QDOTLPOP} = 605.233$$

$$\theta_{\text{TORQLPOP}} := -\frac{\text{SNRADOL}}{\text{RJ}}$$

$$\text{U}_{\text{QDOTLPOP}} := \sqrt{\left(\theta_{\text{TORQLPOP}} \cdot \text{U}_{\text{TORQLPOP}}\right)^2}$$

$$\text{U}_{\text{QDOTLPOP}} = 30.286$$

Rewriting the balance relation and determining the uncertainty

$HTLTOD := 74.48289$

$BAL41 := WO3 \cdot HTVL19 - WLPOP \cdot HTVL18 - WLPOT \cdot HTLTOD - QDOTLPOP$

$HTVL19 := 65.95411$

$BAL41 = 507.601$

$\Theta_{WO3} := HTVL19$

$\Theta_{WLPOT} := -HTLTOD$

$\Theta_{QDOTLPOP} := -1$

$$U_{BAL41} := \sqrt{\left(\Theta_{WO3} \cdot U_{WO3}\right)^2 + \left(\Theta_{WLPOT} \cdot U_{WLPOT}\right)^2 + \left(\Theta_{QDOTLPOP} \cdot U_{QDOTLPOP}\right)^2}$$

$U_{BAL41} = 3.642 \cdot 10^3$

Now write the uncertainty as a percentage of the RHS of the balance relation:

$$U\%_{BAL41} := \frac{U_{BAL41}}{\left| WO3 \cdot HTVL19 \right|}$$

$U\%_{BAL41} = 5.09 \cdot \%$

Balance Relation 42: WO3+WO6+WPOGL+WPOGG+WO4=WHPOP
* WO3 is discussed previously
* WO4,WO6 are the flows through oxidizer lines four and six, cal'd in PIPE01
* WPOGG, WPOGL are pogo related flows, WPOGG is zeroed out, WPOGL has
  a value. A large uncertainty for WPOGL will be assigned.
* WHPOP is the flow through the High Pressure Oxidizer Pump and is an iteration variable

Looking at the flow and uncertainty calculations for oxidizer line four, WO4

$$WO4 = \sqrt{\Delta P \cdot RHOVL21 \cdot CFO4^2 \cdot FLOCON}$$

Consider uncertainties in the resistance and
the density from the property routine.

$$U_{WO4} = \sqrt{\left(\Theta_{CFO4} \cdot U_{CFO4}\right)^2 + \left(\Theta_{RHOVL21} \cdot U_{RHOVL21}\right)^2}$$

Evaluating the partial derivatives and dividing by WO4 to obtain
the uncertainty as a percentage.

$$U\%_{WO4} := \sqrt{\left(\frac{U_{CFO4}}{CFO4}\right)^2 + \left(\frac{1}{2} \cdot \frac{U_{RHOVL21}}{RHOVL21}\right)^2}$$

$$U\%_{WO4} = 10 \cdot \%$$

$$U_{WO4} := WO4 \cdot U\%_{WO4}$$

$$U_{WO4} = 0.2$$

Assigning a 50% uncertainty to the WPOGL flowrate because no information is available.

$$U_{WPOGL} := 0.5 \cdot WPOGL$$

$$U_{WPOGL} = -1.19$$

Looking at the flow and uncertainty calculations for oxidizer line six, WO6

$$WO6 = \sqrt{\Delta P \cdot RHOPBSO \cdot CFO6^2 \cdot FLOCON}$$

Consider uncertainties in the resistance and
the density from the property routine.

$$U_{WO6} = \sqrt{\left(\Theta_{CFO6} \cdot U_{CFO6}\right)^2 + \left(\Theta_{RHOPBSO} \cdot U_{RHOPBSO}\right)^2}$$

WHPOP := 1094.372
WPOGG := 0
WPOGL := -2.38062
WO4 := 1.99514
WO6 := 10.08544
CFO4 := 0.221
$U_{CFO4} := 0.1 \cdot CFO4$
CFO6 := 0.8416
$U_{CFO6} := 0.1 \cdot CFO6$
RHOVL21 := $4.05 \cdot 10^{-2}$
$U_{RHOVL21} := 0.002 \cdot RHOVL21$

RHOPBSO := $4.08 \cdot 10^{-2}$
$U_{RHOPBSO} := 0.002 \cdot RHOPBSO$

Evaluating the partial derivatives and dividing by WO6 to obtain the uncertainty as a percentage.

$$U\%_{WO6} := \sqrt{\left(\frac{U_{CFO6}}{CFO6}\right)^2 + \left(\frac{1}{2} \cdot \frac{U_{RHOPBSO}}{RHOPBSO}\right)^2}$$

$$U\%_{WO6} = 10 \cdot \%$$

$$U_{WO6} := WO6 \cdot U\%_{WO6}$$

$$U_{WO6} = 1.009$$

Rewriting the balance relation and determining the uncertainty

$$BAL42 := WHPOP - WO3 - WO6 - WPOGL - WPOGG - WO4$$

$$BAL42 = 0.007$$

$$U_{BAL42} := \sqrt{U_{WO3}^2 + U_{WO6}^2 + U_{WPOGL}^2 + U_{WO4}^2}$$

$$U_{BAL42} = 54.267$$

Now write the uncertainty as a percentage of the RHS of the balance relation:

$$U\%_{BAL42} := \frac{U_{BAL42}}{|WHPOP|}$$

$$U\%_{BAL42} = 4.959 \cdot \%$$

Balance Relation 43:

WO3*HTVL19+WO6*HTPBSO+(WPOGL+WPOGG)*HTVL20+WO4*HTVL21+QDOTVL20
=WHPOP*HTVL20

* WO3,WO4,WO6, WHPOP, WPOGL, WPOGG are discussed above
* HTVL19,HTVL20,HTVL21,HTPBSO are iteration variables
* QDOTVL20 is zeroed out in this version

$$HTVL19 = 65.954$$
$$HTVL20 := 66.20525$$
$$HTVL21 := 80.70924$$
$$HTPBSO := 90.34464$$
$$QDOTVL20 := 0$$

$$BAL43 := WHPOP \cdot HTVL20 - WO3 \cdot HTVL19 - WO6 \cdot HTPBSO - (WPOGL + WPOGG) \cdot HTVL20 \ldots$$
$$+ - WO4 \cdot HTVL21 - QDOTVL20$$

$$BAL43 = 0.475$$

$$\theta_{WO3} := -HTVL19$$
$$\theta_{WO6} := -HTPBSO$$
$$\theta_{WPOGL} := -HTVL20$$
$$\theta_{WO4} := -HTVL21$$

$$U_{BAL43} := \sqrt{\left(\theta_{WO3} \cdot U_{WO3}\right)^2 + \left(\theta_{WO6} \cdot U_{WO6}\right)^2 \ldots \\ + \left(\theta_{WPOGL} \cdot U_{WPOGL}\right)^2 + \left(\theta_{WO4} \cdot U_{WO4}\right)^2}$$

$$U_{BAL43} = 3.58 \cdot 10^3$$

Now write the uncertainty as a percentage of the RHS of the balance relation:

$$U\%_{BAL43} := \frac{U_{BAL43}}{|WHPOP \cdot HTVL20|}$$

$$U\%_{BAL43} = 4.941 \cdot \%$$

Balance Relation 44: WHPOP=WO4+WO5+WHX+WMOV+WPRBP+WORPR
* WHPOP is an iteration variable
* WO4,WO5 are discussed above.
* WHX is a flow to the POGO accumulator (?) No information is available in the configuration file upon which to calculate an uncertianty. Estimate an uncertainty of 25%
* WMOV is the flow through the main oxidizer valve.
* WPRBP is the flow through the Preburner Pump, and is an iteration variable.
* WORPR is the oxygen repressurization flow, and is a setpoint.

Now, look at the calculation of WMOV and it's uncertainty

$$WMOV = \sqrt{\Delta P \cdot \frac{RHOVL21}{RMOV}}$$

Consider uncertainties in the resistance and the density from the property routine.

$$U_{WMOV} = \sqrt{\left(\theta_{RMOV} \cdot U_{RMOV}\right)^2 + \left(\theta_{RHOVL21} \cdot U_{RHOVL21}\right)^2}$$

Evaluating the partial derivatives and dividing by WMOV to obtain the uncertainty as a percentage.

$$U\%_{WMOV} := \sqrt{\left(-\frac{1}{2} \cdot \frac{U_{RMOV}}{RMOV}\right)^2 + \left(\frac{1}{2} \cdot \frac{U_{RHOVL21}}{RHOVL21}\right)^2}$$

$$U\%_{WMOV} = 0.05$$

$$U_{WMOV} := WMOV \cdot U\%_{WMOV}$$

$$U_{WMOV} = 40.213$$

$WMOV := 804.09$

$RMOV := 7.0 \cdot 10^{-5}$

$U_{RMOV} := 0.1 \cdot RMOV$

$WHX := 0.3511104$

$WPRBP := 108.1089$

$WORPR := 1.1$

$WO5 := 178.7268$

Now, look at the calculation of WO5 and it's uncertainty

$$WO5 = \sqrt{\Delta P \cdot \frac{RHOVL21}{RO5}}$$

Consider uncertainties in the resistance and the density from the property routine.

$$U_{WO5} = \sqrt{\left(\theta_{RO5} \cdot U_{RO5}\right)^2 + \left(\theta_{RHOVL21} \cdot U_{RHOVL21}\right)^2}$$

Evaluating the partial derivatives and dividing by WMOV to obtain the uncertainty as a percentage.

$$U\%_{WO5} := \sqrt{\left(-\frac{1}{2} \cdot \frac{U_{RO5}}{RO5}\right)^2 + \left(\frac{1}{2} \cdot \frac{U_{RHOVL21}}{RHOVL21}\right)^2}$$

$$U\%_{WO5} = 5.001 \cdot \%$$

$$U_{WO5} := WO5 \cdot U\%_{WO5}$$

$$U_{WO5} = 8.938$$

$RO5 := 0.86 \cdot 10^{-4}$

$U_{RO5} := 0.1 \cdot RO5$

Include a 10% uncertainty for the oxygen repressurization flow

$$U_{WORPR} := 0.10 \cdot WORPR$$

$$U_{WORPR} = 0.11$$

Include a 25% uncertainty for the POGO flow

$$U_{WHX} := 0.25 \cdot WHX$$

$$U_{WHX} = 0.088$$

Rewriting the balance relation and determining the uncertainty.

$$BAL44 := WO4 + WO5 + WHX + WMOV + WPRBP + WORPR - WHPOP$$

$$BAL44 = -4.96 \cdot 10^{-5}$$

$$U_{BAL44} := \sqrt{U_{WO4}^2 + U_{WO5}^2 + U_{WHX}^2 + U_{WMOV}^2 + U_{WORPR}^2}$$

$$U_{BAL44} = 41.195$$

Now write the uncertainty as a percentage of the RHS of the balance relation:

$$U\%_{BAL44} := \frac{U_{BAL44}}{|WO4 + WO5 + WHX + WMOV + WPRBP + WORPR|}$$

$$U\%_{BAL44} = 3.764 \cdot \%$$

Balance Relation 45:

WHPOP*HTVL20+QDOTHPOP=(WO4+WO5+WHX+WMOV+WPRBP+WORPR)*HTVL21
* WHPOP, WO4,WO5,WHX,WMOV,WPRBP,WORPR are discussed above
* HTVL20,HTVL21 are iteration variables
* QDOTHPOP is the power required by the High Pressure Oxidizer Pump, calculated in SPUMP

The required pump power is determined from the SPUMP module and the pump map uncertainties.

The HPOP torque is calculated in SPUMP and uses a map for TAU vs PHI

$$\text{TORQHPOP} := -\text{TAUHPOP} \cdot \text{TORQMHPOP} \cdot \text{RHOVL21} \cdot \text{SNRADOH}^2$$

$$\text{TORQHPOP} := -51369.37$$

$$\text{TAUHPOP} := 0.1524294$$

$$\text{SNOH} = 2.755 \cdot 10^4$$

$$\text{SNRADOH} = 2.885 \cdot 10^3$$

Considering an uncertainty associated with the torque coefficient vs flow coefficient map, and an uncertainty in density due to the property routine.

$$U\%_{\text{TORQHPOP}} := \sqrt{\left(\frac{U_{\text{TAUHPOP}}}{\text{TAUHPOP}}\right)^2 + \left(\frac{U_{\text{RHOVL21}}}{\text{RHOVL21}}\right)^2}$$

$$U_{\text{TAUHPOP}} = 0.05 \cdot \text{TAUHPOP}$$

$$U\%_{\text{TORQHPOP}} = 5.004 \cdot \%$$

$$U_{\text{TORQHPOP}} := \left| U\%_{\text{TORQHPOP}} \cdot \text{TORQHPOP} \right|$$

$$U_{\text{TORQHPOP}} = 2.571 \cdot 10^3$$

$$\text{QDOTHPOP} := -\text{TORQHPOP} \cdot \frac{\text{SNRADOH}}{\text{RJ}}$$

$$\text{QDOTHPOP} = 1.587279 \cdot 10^4$$

$$\Theta_{\text{TORQHPOP}} := -\frac{\text{SNRADOH}}{\text{RJ}}$$

$$U_{\text{QDOTHPOP}} := \sqrt{\left(\Theta_{\text{TORQHPOP}} \cdot U_{\text{TORQHPOP}}\right)^2}$$

$$U_{\text{QDOTHPOP}} = 794.274$$

$$U\%_{\text{QDOTHPOP}} := \frac{U_{\text{QDOTHPOP}}}{\text{QDOTHPOP}}$$

$$U\%_{\text{QDOTHPOP}} = 5.004 \cdot \%$$

Rewriting the balance relation and determining the uncertainty

$$BAL45 := (WO4 + WO5 + WHX + WMOV + WPRBP + WORPR) \cdot HTVL21 - WHPOP \cdot HTVL20 - QDOTHPOP$$

$$BAL45 = -0.03$$

$$\theta_{WO4} := HTVL21$$

$$\theta_{WO5} := HTVL21$$

$$\theta_{WHX} := HTVL21$$

$$\theta_{WMOV} := HTVL21$$

$$\theta_{WORPR} := HTVL21$$

$$\theta_{QDOTHPOP} := -1$$

$$U_{BAL45} := \sqrt{ \begin{array}{l} \left(\theta_{WO4} \cdot U_{WO4}\right)^2 + \left(\theta_{WO5} \cdot U_{WO5}\right)^2 + \left(\theta_{WHX} \cdot U_{WHX}\right)^2 + \left(\theta_{WMOV} \cdot U_{WMOV}\right)^2 \cdots \\ + \left(\theta_{WORPR} \cdot U_{WORPR}\right)^2 + \left(\theta_{QDOTHPOP} \cdot U_{QDOTHPOP}\right)^2 \end{array} }$$

$$U_{BAL45} = 3.418 \cdot 10^3$$

Now write the uncertainty as a percentage of the RHS of the balance relation:

$$U\%_{BAL45} := \frac{U_{BAL45}}{\left| (WO4 + WO5 + WHX + WMOV + WPRBP + WORPR) \cdot HTVL21 \right|}$$

$$U\%_{BAL45} = 3.87 \cdot \%$$

Balance Relation 46: WO5=WLPOT
* WO5, WLPOT are discussed above

Rewriting the balance relation and determining the uncertainty

$$BAL46 := WLPOT - WO5$$

$$BAL46 = 4 \cdot 10^{-4}$$

$$U_{BAL46} := \sqrt{U_{WLPOT}^2 + U_{WO5}^2}$$

$$U_{BAL46} = 12.766$$

Now write the uncertainty as a percentage of the RHS of the balance relation:

$$U\%_{BAL46} := \frac{U_{BAL46}}{|WLPOT|}$$

$$U\%_{BAL46} = 7.143 \cdot \%$$

Balance Relation 47: WO5*HTVL21+QDOTVL22=WLPOT*HTVL22
* WO5, WLPOT are discussed above
* HTVL21, HTVL22 are iteration variables
* QDOTVL22 is zeroed out in this model version

$HTVL22 := 80.70924$

$QDOTVL22 := 0$

$BAL47 := WLPOT \cdot HTVL22 - WO5 \cdot HTVL21 - QDOTVL22$

$BAL47 = 0.032$

$\theta_{WO5} := -HTVL21$

$U_{BAL47} := \sqrt{\left(\theta_{WO5} \cdot U_{WO5}\right)^2}$

$U_{BAL47} = 721.389$

Now write the uncertainty as a percentage of the RHS of the balance relation:

$U\%_{BAL47} := \dfrac{U_{BAL47}}{|WLPOT \cdot HTVL22|}$

$U\%_{BAL47} = 5.001 \cdot \%$

Balance Relation 48: WPRBP=WO6+WOPOV+WFPOV
* WPRBP is the flow through the Preburner Pump and is an iteration variable
* WO6 is the flow through oxidizer line six, and calculated in PIPE01
* WOPOV is the flow through the oxidizer preburner oxidizer valve, cal'd in FLOW00
* WFPOV is the flow through the fuel preburner fuel valve, cal'd in FLOW00

Looking at the flow and uncertainty calculations for oxidizer line six, WO6

$$WO6 = \sqrt{\Delta P \cdot RHOPBSO \cdot CFO6^2 \cdot FLOCON}$$

$WO6 := 10.08544$
$CFO6 := 0.8416$
$RHOPBSO = 0.041$

Consider uncertainties in the resistance and
the density from the property routine.

$$U_{WO6} = \sqrt{\left(\Theta_{CFO6} \cdot U_{CFO6}\right)^2 + \left(\Theta_{RHOPBSO} \cdot U_{RHOPBSO}\right)^2}$$

Evaluating the partial derivatives and dividing by WO4 to obtain the uncertainty as a percentage.

$$U\%_{WO6} := \sqrt{\left(\frac{U_{CFO6}}{CFO6}\right)^2 + \left(\frac{1}{2} \cdot \frac{U_{RHOPBSO}}{RHOPBSO}\right)^2}$$

$$U\%_{WO6} = 10 \cdot \%$$

$$U_{WO6} := WO6 \cdot U\%_{WO6}$$

$$U_{WO6} = 1.009$$

Now, look at the calculation of WOPOV and it's uncertainty

$$WOPOV = \sqrt{\Delta P \cdot \frac{RHOPBSO}{RLINOPOV}}$$

$WOPOV := 28.04103$
$RLINOPOV := 0.0635$
$U_{RLINOPOV} := 0.1 \cdot RLINOPOV$

Consider uncertainties in the resistance and
the density from the property routine.

$$U_{WOPOV} = \sqrt{\left(\Theta_{RLINOPOV} \cdot U_{RLINOPOV}\right)^2 + \left(\Theta_{RHOPBSO} \cdot U_{RHOPBSO}\right)^2}$$

Evaluating the partial derivatives and dividing by WOPOV to obtain
the uncertainty as a percentage.

$$U\%_{WOPOV} := \sqrt{\left(-\frac{1}{2} \cdot \frac{U_{RLINOPOV}}{RLINOPOV}\right)^2 + \left(\frac{1}{2} \cdot \frac{U_{RHOPBSO}}{RHOPBSO}\right)^2}$$

$$U\%_{WOPOV} = 5.001 \cdot \%$$

$$U_{WOPOV} := WOPOV \cdot U\%_{WOPOV}$$

$$U_{WOPOV} = 1.402$$

Now, look at the calculation of WFPOV and it's uncertainty

$$WFPOV = \sqrt{\Delta P \cdot \frac{RHOPBSO}{RLINFPOV}}$$

Consider uncertainties in the resistance and the density from the property routine.

$$WFPOV := 69.98241$$

$$RLINFPOV := 0.00905$$

$$U_{RLINFPOV} := 0.1 \cdot RLINFPOV$$

$$U_{WFPOV} = \sqrt{\left(\Theta_{RLINFPOV} U_{RLINFPOV}\right)^2 + \left(\Theta_{RHOPBSO} U_{RHOPBSO}\right)^2}$$

Evaluating the partial derivatives and dividing by WOPOV to obtain the uncertainty as a percentage.

$$U\%_{WFPOV} := \sqrt{\left(-\frac{1}{2} \cdot \frac{U_{RLINFPOV}}{RLINFPOV}\right)^2 + \left(\frac{1}{2} \cdot \frac{U_{RHOPBSO}}{RHOPBSO}\right)^2}$$

$$U\%_{WFPOV} = 5.001 \cdot \%$$

$$U_{WFPOV} := WFPOV \cdot U\%_{WFPOV}$$

$$U_{WFPOV} = 3.5$$

Rewriting the balance relation and determining the uncertainty

$$BAL48 := WO6 + WOPOV + WFPOV - WPRBP$$

$$BAL48 = -2 \cdot 10^{-5}$$

$$U_{BAL48} := \sqrt{U_{WO6}^2 + U_{WOPOV}^2 + U_{WFPOV}^2}$$

$$U_{BAL48} = 3.903$$

Now write the uncertainty as a percentage of the RHS of the balance relation:

$$U\%_{BAL48} := \frac{U_{BAL48}}{|WO6 + WOPOV + WFPOV|}$$

$$U\%_{BAL48} = 3.61 \cdot \%$$

Balance Relation 49: WPRBP*HTVL21+QDOTPRBP=(WO6+WOPOV+WFPOV)*HTPBSO
* WPRBP, WO6,WOPOV,WFPOV are discussed above
* HTVL21, HTPBSO are iteration variables
* QDOTPRBP is the power required by the preburner pump, cal'd in SPUMP.

The required pump power is determined from the SPUMP module and the pump map uncertainties.

The PRBP torque is calculated in SPUMP and uses a map for TAU vs PHI

$$\text{TORQPRBP} = -\text{TAUPRBP} \cdot \text{TORQMHPOP} \cdot \text{RHOVLPBSO} \cdot \text{SNRADOH}^2 \qquad \text{TAUPRBP} := 0.00992$$

$$\text{TORQPRBP} := -3371.18 \qquad \text{SNOH} = 2.755 \cdot 10^4$$

$$\text{SNRADOH} = 2.885 \cdot 10^3$$

Considering an uncertainty associated with the torque coefficient vs flow coefficient map, and an uncertainty in density due to the property routine.

$$U\%_{\text{TORQPRBP}} := \sqrt{\left(\frac{U_{\text{TAUPRBP}}}{\text{TAUPRBP}}\right)^2 + \left(\frac{U_{\text{RHOPBSO}}}{\text{RHOPBSO}}\right)^2} \qquad U_{\text{TAUPRBP}} := 0.05 \cdot \text{TAUPRBP}$$

$$U\%_{\text{TORQPRBP}} = 5.004 \cdot \%$$

$$U_{\text{TORQPRBP}} := \left| U\%_{\text{TORQPRBP}} \cdot \text{TORQPRBP} \right|$$

$$U_{\text{TORQPRBP}} = 168.694$$

$$U_{\text{TRQPOH}} := \sqrt{U_{\text{TORQHPOP}}^2 + U_{\text{TORQPRBP}}^2}$$

$$U_{\text{TRQPOH}} = 2.576 \cdot 10^3$$

$$\text{QDOTPRBP} := -\text{TORQPRBP} \cdot \frac{\text{SNRADOH}}{\text{RJ}}$$

$$\text{QDOTPRBP} = 1.0417 \cdot 10^3$$

$$\Theta_{\text{TORQPRBP}} := -\frac{\text{SNRADOH}}{\text{RJ}}$$

$$U_{\text{QDOTPRBP}} := \sqrt{\left(\Theta_{\text{TORQPRBP}} \cdot U_{\text{TORQPRBP}}\right)^2}$$

$$U_{\text{QDOTPRBP}} = 52.125$$

$$U\%_{\text{QDOTPRBP}} := \frac{U_{\text{QDOTPRBP}}}{\text{QDOTPRBP}}$$

$$U\%_{\text{QDOTPRBP}} = 5.004 \cdot \%$$

Rewriting the balance relation and determining the uncertainty

$$BAL49 := (WO6 + WOPOV + WFPOV) \cdot HTPBSO - WPRBP \cdot HTVL21 - QDOTPRBP$$

$$BAL49 = -0.001$$

$$\Theta_{WO6} := HTPBSO$$

$$\Theta_{WOPOV} := HTPBSO$$

$$\Theta_{WFPOV} := HTPBSO$$

$$\Theta_{QDOTPRBP} := -1$$

$$U_{BAL49} := \sqrt{\left(\Theta_{WO6} \cdot U_{WO6}\right)^2 + \left(\Theta_{WOPOV} \cdot U_{WOPOV}\right)^2 + \left(\Theta_{WFPOV} \cdot U_{WFPOV}\right)^2 \cdots + \left(\Theta_{QDOTPRBP} \cdot U_{QDOTPRBP}\right)^2}$$

$$U_{BAL49} = 356.437$$

Now write the uncertainty as a percentage of the RHS of the balance relation:

$$U\%_{BAL49} := \frac{U_{BAL49}}{\left|(WO6 + WOPOV + WFPOV) \cdot HTPBSO\right|}$$

$$U\%_{BAL49} = 3.649 \cdot \%$$

Balance Relation 50: WOOPB+WOPBF+WHE2=WHG2
* WOOPB is the oxidizer to the OPB
* WOPBF is the fuel to the OPB
* WHE2 is the He dilutant to the OPB
* WHG2 is the hot gas out from the OPB

$$BAL50 := WHG2 - WOOPB - WOPBF - WHE2$$

$$BAL50 = -3 \cdot 10^{-5}$$

$$WOOPB := 28.04103$$

$$WOPBF := 35.37508$$

$$WHE2 := 0$$

$$WHG2 := 63.41608$$

BAL51=WHG2*(GAMA(PTOPRB,OFROPRB,HFROPRB,TTHETK,TTOPBF,TTOPBI)-1)*TTOPRB
    -(WOOPB+WOPBF+WHE2)*(GAMA(PTOPRB,OFROPRB,HFROPRB,TTHETK,
    TTOPBF,TTOPBI)*TTCBST(PTOPRB,TTHETK,TTOPBF,TTOPBI)-TTOPRB)

Balance Relation 52: WOOPB=OFROPRB*(WOOPB+WOPBF+WHE2)

$$BAL52 = OFROPRB \cdot (WOOPB + WOPBF + WHE2) - WOOPB$$

Balance Relation 53: WHE2=HFROPRB*(WOOPB+WOPBF+WHE2)

$$BAL53 = HFROPRB \cdot (WOOPB + WOPBF + WHE2) - WHE2$$

Balance Relation 54:
HFRHTOD*WHPOT+HFROTBP*WHG4+HFRPBSF*WOTC=HFROSF*(WHPOT+WHG4+WOTC)

$$BAL54 = HFROSF \cdot (WHPOT + WHG4 + WOTC) - HFRHTOD \cdot WHPOT - HFROTBP \cdot WHG4 - HFRPBSF \cdot WOTC$$

Balance Relation 55:
OFRHTOD*WHPOT+OFROTBP*WHG4+OFRPBSF*WOTC=OFROSF*(WHPOT+WHG4+WOTC)

$$BAL55 = OFROSF \cdot (WHPOT + WHG4 + WOTC) - OFRHTOD \cdot WHPOT - OFROTBP \cdot WHG4 - OFRPBSF \cdot WOTC$$

Balance Relation 56: WHPOT+WHG4+WOTC=WHG6+WOLK

$$BAL56 = WHG6 + WOLK - WHPOT - WHG4 - WOTC$$

Balance Relation 57:
WHPOT*GAMAHTOD*(TTHTOD-TTOSF)+WHG4*GAMAOTBP*(TTOTBP-TTOSF)
+WOTC*GAMAPBSF*(TTPBSF-TTOSF)+QDOTOSF*GAMAOSF/CPOSF
=(WHG6+WOLK)*(GAMAOSF-1)*TTOSF

$$BAL57 = (WHG6 + WOLK) \cdot (GAMAOSF - 1) \cdot TTOSF - WHPOT \cdot GAMAHTOD \cdot (TTHTOD - TTOSF) \dots$$
$$+ - WHG4 \cdot GAMAOTBP \cdot (TTOTBP - TTOSF) - WOTC \cdot GAMAPBSF \cdot (TTPBSF - TTOSF) \dots$$
$$+ - QDOTOSF \cdot \frac{GAMAOSF}{CPOSF}$$

Balance Relation 58: WOFPB+WFPBF+WHE1=WHG1

$$BAL58 = WHG1 - WOFPB - WFPBF - WHE1$$

Balance Relation 59:
(WOFPB+WFPBF+WHE1)*(GAMA(PTFPRB,OFRFPRB,HFRFPRB,
TTHETK,TTFPBF,TTFPBI)*TTCBST(PTFPRB,OFRFPRB,HFRFPRB,TTHETK,TTFPBF,
TTFPBI)-TTFPRB)=WHG1*(GAMA(PTFPRB,OFRFPRB,HFRFPRB,TTHETK,TTFPBF,
TTFPBI)-1)*TTFPRB

Balance Relation 60: WOFPB=OFRFPRB*(WOFPB+WFPBF+WHE1)

$$BAL60 = OFRFPRB \cdot (WOFPB + WFPBF + WHE1) - WOFPB$$

Balance Relation 61: WHE1+HFRFPRB*(WOFPB+WFPBF+WHE1)

$$BAL61 = HFRFPRB \cdot (WOFPB + WFPBF + WHE1) - WHE1$$

Balance Relation 62:
HFRHTFD*WHPFT+HFRFTBP*WHG3+HFRVL03*WFTC=HFRFSF*(WHPFT+WHG3+WFTC)

$$BAL62 = HFRFSF \cdot (WHPFT + WHG3 + WFTC) - HFRHTFD \cdot WHPFT - HFRFTBP \cdot WHG3 - HFRVL03 \cdot WFTC$$

Balance Relation 63: OFRHTFD*WHPFT+OFRFTBP*WHG3+OFRVL03*WFTC
=OFRFSF*(WHPFT+WHG3+WFTC)

$$BAL63 = OFRFSF \cdot (WHPFT + WHG3 + WFTC) - OFRHTFD \cdot WHPFT - OFRFTBP \cdot WHG3 - OFRVL03 \cdot WFTC$$

Balance Relation 64: WHPFT+WHG3+WFTC=WHG5

$$BAL64 = WHG5 - WHPFT - WHG3 - WFTC$$

Balance Relation 65:
WHPFT*GAMAHTFD*(TTHTFD-TTFSF)+WHG3*GAMAFTBP*(TTFTBP-TTFSF)
+WFTC*GAMAVL03*(TTVL03-TTFSF)+QDOTFSF*GAMAFSF/CPFSF
=WHG5*(GAMAFSF-1)*TTFSF

Balance Relation 66:
HFRFSF*WHG5+HFROSF*WHG6+HFRVL16*WFSLV=HFRMFI*(WHG5+WHG6+WFSLV)

$$BAL66 = HFRMFI \cdot (WHG5 + WHG6 + WFSLV) - HFRFSF \cdot WHG5 - HFROSF \cdot WHG6 - HFRVL16 \cdot WFSLV$$

Balance Relation 67: OFRFSF*WHG5+OFROSF*OFROSF*WHG6+OFRVL16*WFSLV=
OFRMFI*(WHG5+WHG6+WFSLV)

$$BAL67 = OFRMFI \cdot (WHG5 + WHG6 + WFSLV) - OFRFSF \cdot WHG5 + OFROSF \cdot WHG6 - OFRVL16 \cdot WFSLV$$

Balance Relation 68: WHG5+WHG6+WFSLV=WFINJ

$$BAL68 = WFINJ - WHG5 - WHG6 - WFSLV$$

Balance Relation 69:

WHG5*GAMAFSF*(TTFSF-TTMFI)+WHG6*GAMAOSF*(TTOSF-TTMFI)
+WFSLV*GAMAVL16*(TTVL16-TTMFI)+(QDOTFMCO+QDOTOMCO)*GAMAMFI/CPMFI
=WFINJ*(GAMAMFIR-1)*TTMFI

Balance Relation 70: TRQPFL:TRQNFL
* TRQPFL is the torque required by the Low Pressure Fuel Pump
* TRQNFL is the torque produced by the Low Pressure Fuel Turbine
Both routines use speed as an iteration variable

$$TAULPFP := 1.971925$$

The LPFP torque is calculated in SPUMP and uses a map for TAU vs PHI $\quad$ $SNFL = 1.379 \cdot 10^4$

$$TORQLPFP = -TAULPFP \cdot TORQMLPFP \cdot RHOVL01 \cdot SNRADFL^2$$

$$SNRADFL = 1.444 \cdot 10^3$$

$$TORQLPFP := -10521.79$$

$$TRQPFL := -TORQLPFP$$

Considering an uncertainty associated with the torque coefficient vs flow coefficient map, and an uncertainty in density due to the property routine.

$$U\%_{TORQLPFP} := \sqrt{\left(\frac{U_{TAULPFP}}{TAULPFP}\right)^2 + \left(\frac{U_{RHOVL01}}{RHOVL01}\right)^2}$$

$$U_{TAULPFP} := 0.05 \cdot TAULPFP$$

$$U\%_{TORQLPFP} = 0.05$$

$$U_{TORQLPFP} := |U\%_{TORQLPFP} \cdot TORQLPFP|$$

$$U_{TORQLPFP} = 526.195$$

$$U_{TRQPFL} := U_{TORQLPFP}$$

$$U_{TRQPFL} = 526.195$$

Now consider the torque calculation for the LPFT, modules TURB02 and TBMP04.

Uncertainties are introduced through the turbine flow, WLPFT, as discussed in balance relation 23, and the turbine efficiency map. The DH is determined in TBMP04 by calling the H2 property routine for the exit pressure (an iteration variable) and inlet entropy, since this value is so closely related to the iteration variable no uncertainty will be assigne to DHLPFT.

A 2.5% uncertainty for ETALPFT is being assigned based upon engineering judgment since no information was obtained.

$$U\%_{ETALPFT} := 0.025$$

$$TORQLPFT = DHLPFT \cdot WLPFT \cdot \frac{RJ}{SNRADFL}$$

$$TORQLPFT := 10521.78$$

$$DHLPFT = ETALPFT \cdot DHIDLLPFT$$

$$TORQLPFT = ETALPFT \cdot DHIDLLPFT \cdot WLPFT \cdot \frac{RJ}{SNRADFL}$$

$$TRQNFL := TORQLPFT$$

$$U\%_{TORQLPFT} := \sqrt{U\%_{ETALPFT}^2 + U\%_{WLPFT}^2}$$

$$U\%_{TORQLPFT} = 0.065$$

$$U_{TORQLPFT} := TORQLPFT \cdot U\%_{TORQLPFT}$$

$$U_{TORQLPFT} = 683.916$$

$$U_{TRQNFL} := U_{TORQLPFT}$$

$$U_{TRQNFL} = 683.916$$

Rewriting the balance relation and determining the uncertainty

$$BAL70 := TRQNFL - TRQPFL$$

$$BAL70 = -0.01$$

$$U_{BAL70} := \sqrt{U_{TRQNFL}^2 + U_{TRQPFL}^2}$$

$$U_{BAL70} = 862.915$$

Now write the uncertainty as a percentage of the RHS of the balance relation:

$$U\%_{BAL70} := \frac{U_{BAL70}}{|TRQNFL|}$$

$$U\%_{BAL70} = 8.201 \cdot \%$$

Balance Relation 71: TRQPFH:TRQNFH
* TRQPFH is the torque required by the High Pressure Fuel Pump
* TRQNFH is the torque produced by the High Pressure Fuel Turbine
Both routines use speed as an iteration variable

The HPFP torque is calculated in SPUMP and uses a map for TAU vs PHI

$TAUHPFP := 3.003558$

$$TORQHPFP = -TAUHPFP \cdot TORQMHPFP \cdot RHOVL03 \cdot SNRADFH^2$$

$SNFH = 3.366 \cdot 10^4$

$$TORQHPFP := -107789.8$$

$SNRADFH = 3.524 \cdot 10^3$

$$TRQPFH := |TORQHPFP|$$

Considering an uncertainty associated with the torque coefficient vs flow coefficient map, and an uncertainty in density due to the property routine.

$$U\%_{TORQHPFP} := \sqrt{\left(\frac{U_{TAUHPFP}}{TAUHPFP}\right)^2 + \left(\frac{U_{RHOVL03}}{RHOVL03}\right)^2}$$

$U_{TAUHPFP} := 0.05 \cdot TAUHPFP$

$$U\%_{TORQHPFP} = 0.078$$

$$U_{TORQHPFP} := |U\%_{TORQHPFP} \cdot TORQHPFP|$$

$$U_{TORQHPFP} = 8.419 \cdot 10^3$$

$$U_{TRQPFH} := U_{TORQHPFP} \qquad U_{TRQPFH} = 8.419 \cdot 10^3$$

Now consider the torque calculation for the HPFT, modules TURB01 and TBMP03.

Uncertainties are introduced through the turbine flow, WHPFT, as discussed in balance relation 64, and the turbine efficiency map. The DH is calculated in TBMP03 as a function of the inlet and exit pressures, the inlet temperature, and the gas constant. The pressures are iteration variables, since DH is so closely related to the iteration variable no uncertainty will be assigne to DHLPFT.

A 5% uncertainty for ETAHPFT is being assigned based upon engineering judgment since no information was obtained.

$$TORQHPFT = DHHPFT \cdot WHPFT \cdot \frac{RJ}{SNRADFH}$$

$U\%_{ETAHPFT} := 0.05$

$TORQHPFT := 107789.8$

$$DHHPFT = ETAHPFT \cdot DHIDLHPFT$$

$$TORQHPFT = ETAHPFT \cdot DHIDLHPFT \cdot WHPFT \cdot \frac{RJ}{SNRADFH}$$

Since this balance relation is being worked prior to working #64 uncertainties for WHPFT is being estimated

$$TRQNFH := TORQHPFT$$

$$U\%_{TORQHPFT} := \sqrt{U\%_{ETAHPFT}^2 + U\%_{WHPFT}^2} \qquad\qquad U\%_{WHPFT} := U\%_{WLPFT}$$

$$U\%_{TORQHPFT} = 0.078$$

$$U_{TORQHPFT} := TORQHPFT \cdot U\%_{TORQHPFT}$$

$$U_{TORQHPFT} = 8.419 \cdot 10^3$$

$$U_{TRQNFH} := U_{TORQHPFT}$$

$$U_{TRQNFH} = 8.419 \cdot 10^3$$

Rewriting the balance relation and determining the uncertainty

$$BAL71 := TRQNFH - TRQPFH$$

$$BAL71 = 0$$

$$U_{BAL71} := \sqrt{U_{TRQNFH}^2 + U_{TRQPFH}^2}$$

$$U_{BAL71} = 1.191 \cdot 10^4$$

Now write the uncertainty as a percentage of the RHS of the balance relation:

$$U\%_{BAL71} := \frac{U_{BAL71}}{|TRQNFH|}$$

$$U\%_{BAL71} = 11.045 \cdot \%$$

Balance Relation 72: TRQPOL:TRQNOL
* TRQPOL is the torque required by the Low Pressure Oxidizer Pump
* TRQNOL is the torque produced by the Low Pressure Oxidizer Turbine
Both routines use speed as an iteration variable

The LPOP torque is calculated in SPUMP and uses a map for TAU vs PHI

$$TAULPOP := 1.658089$$

$$SNOL = 5.129 \cdot 10^3$$

$$TORQLPOP = TAULPOP \cdot TORQMLPOP \cdot RHOVL01 \cdot SNRADOL^2$$

$$SNRADOL = 537.135$$

$$TORQLPOP := -10521.79$$

$$TRQPOL := |TORQLPOP|$$

Considering an uncertainty associated with the torque coefficient vs flow coefficient map, and an uncertainty in density due to the property routine.

$$U\%_{TORQLPOP} := \sqrt{\left(\frac{U_{TAULPOP}}{TAULPOP}\right)^2 + \left(\frac{U_{RHOVL01}}{RHOVL01}\right)^2}$$

$$U_{TAULPOP} = 0.05 \cdot TAULPOP$$

$$U\%_{TORQLPOP} = 0.05$$

$$U_{TORQLPOP} := |U\%_{TORQLPOP} \cdot TORQLPOP|$$

$$U_{TORQLPOP} = 526.195$$

$$U_{TRQPOL} := U_{TORQLPOP}$$

$$U_{TRQPOL} = 526.195$$

Now consider the torque calculation for the LPOT, modules TURB02 and TBMP06.

Uncertainties are introduced through the turbine flow, WLPOT, as discussed in balance relation 46, and the the torque correlation in TBMP06. The ideal "delta-enthalpy" is determined in TBMP06 by calling the O2 property routine for the exit pressure (an iteration variable) and inlet entropy, since this value is so closely related to the iteration variable no uncertainty will be assigned to DHIDL.

The torque produced by the LPOT is calculated in TBMP04 using a "torque correlation" equation

where AOT1,BOT1, ctqot1 are defined constants
     PHIOT1 is a function of turbine speed and turbine flowrate
and   CLEN,CFORCE, CFORCE are unit conversion constants

$$AOT1 := 1.0998 \quad SFW := 1$$

$$BOT1 := 0.16443 \quad CTQOT1 := 1$$

$$PHIOT1 := \frac{SNRADOL}{(WLPOT \cdot SFW \cdot CMASS + 1 \cdot 10^{-10})}$$

$$PHIOT1 = 3.005$$

$$TORQLPOT := (AOT1 - BOT1 \cdot PHIOT1) \cdot WLPOT \cdot |WLPOT| \cdot CTQOT1 \cdot \frac{SFW}{(CLEN \cdot CFORCE)} \cdot CMASS^2$$

$$TORQLPOT := \left[AOT1 - BOT1 \cdot \frac{SNRADOL}{(WLPOT \cdot SFW \cdot CMASS + 1 \cdot 10^{-10})}\right] \cdot WLPOT \cdot |WLPOT| \ldots$$
$$+ CTQOT1 \cdot \frac{SFW}{(CLEN \cdot CFORCE)} \cdot CMASS^2$$

$$\Theta_{AOT1} := WLPOT \cdot |WLPOT| \cdot CTQOT1 \cdot \frac{SFW}{(CLEN \cdot CFORCE)} \cdot CMASS^2$$

$$\Theta_{BOT1} := \frac{-SNRADOL}{\left(WLPOT \cdot SFW \cdot CMASS + \frac{1}{10000000000}\right)} \cdot WLPOT \cdot |WLPOT| \cdot CTQOT1 \cdot \frac{SFW}{(CLEN \cdot CFORCE)} \cdot CMASS^2$$

$$\Theta_{WLPOT} := BOT1 \cdot \frac{SNRADOL}{\left(WLPOT \cdot SFW \cdot CMASS + \frac{1}{10000000000}\right)^2} \cdot SFW^2 \cdot CMASS^3 \cdot WLPOT \cdot |WLPOT| \ldots$$
$$+ \frac{CTQOT1}{CLEN \cdot CFORCE} + 2 \cdot \left[AOT1 - BOT1 \cdot \frac{SNRADOL}{\left(WLPOT \cdot SFW \cdot CMASS + \frac{1}{10000000000}\right)} \right] \cdot |WLPOT| \ldots$$
$$+ CTQOT1 \cdot \frac{SFW}{(CLEN \cdot CFORCE)} \cdot CMASS^2$$

$$U_{AOT1} := 0.05 \cdot AOT1 \quad U_{BOT1} := 0.05 \cdot BOT1$$

$$U_{TORQLPOT} := \sqrt{\left(\Theta_{AOT1} \cdot U_{AOT1}\right)^2 + \left(\Theta_{BOT1} \cdot U_{BOT1}\right)^2 + \left(\Theta_{WLPOT} \cdot U_{WLPOT}\right)^2}$$

$$U_{TORQLPOT} = 3.395 \cdot 10^3$$

$$U\%_{TORQLPOT} := \frac{U_{TORQLPOT}}{TORQLPOT}$$

$$U\%_{TORQLPOT} = 17.551 \cdot \%$$

$$TORQLPOT = 1.934699 \cdot 10^4$$

$$TRQNOL := TORQLPOT$$

$$U_{TRQNOL} := U_{TORQLPOT}$$

Rewriting the balance relation and determining the uncertainty

$$BAL72 := TRQNOL - TRQPOL$$

$$BAL72 = 8.825 \cdot 10^3$$

$$U_{BAL72} := \sqrt{U_{TRQNOL}^2 + U_{TRQPOL}^2}$$

$$U_{BAL72} = 3.436 \cdot 10^3$$

Now write the uncertainty as a percentage of the RHS of the balance relation:

$$U\%_{BAL72} := \frac{U_{BAL72}}{|TRQNOL|}$$

$$U\%_{BAL72} = 17.76 \cdot \%$$

Balance Relation 73: TRQPOH:TRQNOH
* TRQPOH is the torque required by the High Pressure Oxidizer Pump and the Preburner Pump
* TRQNOH is the torque produced by the High Pressure Oxidizer Turbine
Both routines use speed as an iteration variable

The HPOP torque is calculated in SPUMP and uses a map for TAU vs PHI

$$\text{TORQHPOP} = - \text{TAUHPOP} \cdot \text{TORQMHPOP} \cdot \text{RHOVL21} \cdot \text{SNRADOH}^2$$

$$\text{TORQHPOP} := -51369.37$$

$$\text{TAUHPOP} := 0.1524294$$

$$\text{SNOH} = 2.755 \cdot 10^4$$

$$\text{SNRADOH} = 2.885 \cdot 10^3$$

Considering an uncertainty associated with the torque coefficient vs flow coefficient map, and an uncertainty in density due to the property routine.

$$U\% \text{ TORQHPOP} := \sqrt{\left(\frac{U \text{ TAUHPOP}}{\text{TAUHPOP}}\right)^2 + \left(\frac{U \text{ RHOVL21}}{\text{RHOVL21}}\right)^2}$$

$$U \text{ TAUHPOP} := 0.05 \cdot \text{TAUHPOP}$$

$$U\% \text{ TORQHPOP} = 0.05$$

$$U \text{ TORQHPOP} := \left| U\% \text{ TORQHPOP} \cdot \text{TORQHPOP} \right|$$

$$U \text{ TORQHPOP} = 2.571 \cdot 10^3$$

The PRBP torque is calculated in SPUMP and uses a map for TAU vs PHI

$$\text{TORQPRBP} = - \text{TAUPRBP} \cdot \text{TORQMHPOP} \cdot \text{RHOVLPBSO} \cdot \text{SNRADOH}^2$$

$$\text{TORQPRBP} := -3371.18$$

$$\text{TAUPRBP} := 0.00992$$

$$\text{SNOH} = 2.755 \cdot 10^4$$

$$\text{SNRADOH} = 2.885 \cdot 10^3$$

Considering an uncertainty associated with the torque coefficient vs flow coefficient map, and an uncertainty in density due to the property routine.

$$U\% \text{ TORQPRBP} := \sqrt{\left(\frac{U \text{ TAUPRBP}}{\text{TAUPRBP}}\right)^2 + \left(\frac{U \text{ RHOPBSO}}{\text{RHOPBSO}}\right)^2}$$

$$U \text{ TAUPRBP} = 0.05 \cdot \text{TAUPRBP}$$

$$U\% \text{ TORQPRBP} = 5.004 \cdot \%$$

$$U \text{ TORQPRBP} := \left| U\% \text{ TORQPRBP} \cdot \text{TORQPRBP} \right|$$

$$U \text{ TORQPRBP} = 168.694$$

$$\text{TRQPOH} := |\text{TORQHPOP} + \text{TORQPRBP}|$$

$$\text{TRQPOH} = 5.474 \cdot 10^4$$

$$U_{\text{TRQPOH}} := \sqrt{U_{\text{TORQHPOP}}^2 + U_{\text{TORQPRBP}}^2}$$

$$U_{\text{TRQPOH}} = 2.576 \cdot 10^3$$

Now consider the torque calculation for the HPOT, modules TURB01 and TBMP05.

Uncertainties are introduced through the turbine flow, WHPOT, as discussed in balance relation 54, and the turbine efficiency map. The DH is calculated in TBMP05 as a function of the inlet and exit pressures, the inlet temperature, and the gas constant. The pressures are iteration variables, since DH is so closely related to the iteration variable no uncertainty will be assigne to DHLPOT.

A 5% uncertainty for ETAHPOT is being assigned based upon engineering judgment since no information was obtained.

$$\text{TORQHPOT} = \text{DHHPOT} \cdot \text{WHPOT} \cdot \frac{\text{RJ}}{\text{SNRADOH}}$$

$$\text{DHHPOT} = \text{ETAHPOT} \cdot \text{DHIDLHPOT}$$

$$\text{TORQHPOT} = \text{ETAHPOT} \cdot \text{DHIDLHPOT} \cdot \text{WHPOT} \cdot \frac{\text{RJ}}{\text{SNRADOH}}$$

$$\text{TRQNOH} := \text{TORQHPOT}$$

$$U\%_{\text{ETAHPOT}} := 0.05$$

$$\text{TORQHPOT} := 54740.53$$

Since this balance relation is being worked prior to working #64 uncertainty for WHPOT is being estimated

$$U\%_{\text{TORQHPOT}} := \sqrt{U\%_{\text{ETAHPOT}}^2 + U\%_{\text{WHPOT}}^2}$$

$$U\%_{\text{TORQHPOT}} = 0.071$$

$$U_{\text{TORQHPOT}} := \text{TORQHPOT} \cdot U\%_{\text{TORQHPOT}}$$

$$U_{\text{TORQHPOT}} = 3.91 \cdot 10^3$$

$$U_{\text{TRQNOH}} := U_{\text{TORQHPOT}}$$

$$U_{\text{TRQNOH}} = 3.91 \cdot 10^3$$

$$U\%_{\text{WHPOT}} := U\%_{\text{WLPOT}}$$

Rewriting the balance relation and determining the uncertainty

$$BAL73 := TRQNOH - TRQPOH$$

$$BAL73 = -0.02$$

$$U_{BAL73} := \sqrt{U_{TRQNFH}^2 + U_{TRQPFH}^2}$$

$$U_{BAL73} = 1.191 \cdot 10^4$$

Now write the uncertainty as a percentage of the RHS of the balance relation:

$$U\%_{BAL73} := \frac{U_{BAL73}}{|TRQNOH|}$$

$$U\%_{BAL73} = 21.749 \cdot \%$$

Balance Relation 74: PTLPFP=PTVL01
* PTLPFP is calculated in SPUMP and utilizes the LPFP head coefficient map
* PTVL01 is an iteration variable

From the SPUMP module, the exit pressure and uncertainty are determined from

$$PTLPFP := PTHTNK + PSILPFP \cdot RHOVL01 \cdot SNRADFL^2$$

$PTHTNK := 39.01$

$PSILPFP := 0.0357$

$PTVL01 := 229.5579$

$$PTLPFP = 229.477$$ * Note: This value is slightly different than the model calculated value of PTLPFP=229.5579

Since PTHTNK is an input value and SNFL is an iteration variable, PSILPFP and RHOVL01 are the terms which contain uncertainties.

Using an uncertainty of 3% for the head coefficient from the head coefficient vs flow coefficient map. Estimate based upon information provided by Rocketdyne.

$$U_{PSILPFP} := 0.03 \cdot PSILPFP$$

$$\Theta_{RHOVL01} := PSILPFP \cdot SNRADFL^2$$
$$\Theta_{PSILPFP} := RHOVL01 \cdot SNRADFL^2$$

$$U_{PTLPFP} := \sqrt{\left(\Theta_{PSILPFP} \cdot U_{PSILPFP}\right)^2 + \left(\Theta_{RHOVL01} \cdot U_{RHOVL01}\right)^2}$$

$$U_{PTLPFP} = 5.717$$

Rewriting the balance relation and determining the uncertainty

$$BAL74 := PTVL01 - PTLPFP$$

$$BAL74 = 0.081$$

$$\Theta_{PTLPFP} := -1$$

$$U_{BAL74} := \sqrt{\left(\Theta_{PTLPFP} \cdot U_{PTLPFP}\right)^2}$$

$$U_{BAL74} = 5.717$$

Now write the uncertainty as a percentage of the RHS of the balance relation

$$U\%_{BAL74} := \frac{U_{BAL74}}{|PTVL01|}$$

$$U\%_{BAL74} = 2.491 \cdot \%$$

Balance Relation 75: PTHPFP=PTVL03
* PTHPFP is calculated in SPUMP and utilizes the HPFP head coefficient map
* PTVL03 is an iteration variable

From the SPUMP module, the exit pressure and uncertainty are determined from

$$PTVL02 := 196.507$$

$$PTHPFP := PTVL02 + PSIHPFP \cdot RHOVL03 \cdot SNRADFH^2$$

$$PSIHPFP := 0.1567331$$

$$PTVL03 := 5821.243$$

$$PTHPFP = 5.82271 \cdot 10^3$$

* Note: This value is slightly different than the model calculated value of PTHPFP=5821.24

Since PTVL03 is an input value and SNFH are iteration variables, PSIHPFP and RHOVL03 are the terms which contain uncertainties.

Using an uncertainty of 3.5% for the head coefficient from the head coefficient vs flow coefficient map. Estimate based upon information provided by Rocketdyne.

$$U_{PSIHPFP} := 0.035 \cdot PSIHPFP$$

$$\Theta_{RHOVL03} := PSIHPFP \cdot SNRADFH^2$$

$$\Theta_{PSIHPFP} := RHOVL03 \cdot SNRADFH^2$$

$$U_{PTHPFP} := \sqrt{\left(\Theta_{PSIHPFP} \cdot U_{PSIHPFP}\right)^2 + \left(\Theta_{RHOVL03} \cdot U_{RHOVL03}\right)^2}$$

$$U_{PTHPFP} = 390.808$$

Rewriting the balance relation and determining the uncertainty

$$BAL75 := PTVL03 - PTHPFP$$

$$BAL75 = -1.465$$

$$\Theta_{PTHPFP} := -1$$

$$U_{BAL75} := \sqrt{\left(\Theta_{PTHPFP} \cdot U_{PTHPFP}\right)^2}$$

$$U_{BAL75} = 390.808$$

Uncertainty as a percentage of the right-hand side of the balance relation:

$$U\%_{BAL75} := \frac{U_{BAL75}}{PTVL03} \cdot 100$$

$$U\%_{BAL75} = 6.713$$

Now write the uncertainty as a percentage of the RHS of the balance relation

$$U\%_{BAL75} := \frac{U_{BAL75}}{|PTVL03|}$$

$$U\%_{BAL75} = 6.713 \cdot \%$$

Balance Relation 76: PTLPOP=PTVL19
* PTLPOP is calculated in SPUMP and utilizes the LPOP head coefficient map
* PTVL19 is an iteration variable

From the SPUMP module, the exit pressure and uncertainty are determined from

$$PSILPOP := 0.0276 \quad PTVL18 := 74.07178$$

$$PTLPOP := PTVL18 + PSILPOP \cdot RHOVL19 \cdot SNRADOL^2 \qquad RHOVL19 := 0.0404 \quad PTVL19 := 396.0983$$

$$PTLPOP = 395.776$$ * Note: This value is slightly different
than the model calculated value of
PTLPOP=396.0983

Since PTVL18 and SNOL are iteration variables,
PSILPOP and RHOVL19 are the terms which contain uncertainties.

$$U_{RHOVL19} := 0.002 \cdot RHOVL19$$

Using an uncertainty of 5.0% for the head coefficient from the
head coefficient vs flow coefficient map. Estimate based upon
information provided by Rocketdyne.

$$U_{PSILPOP} := 0.05 \cdot PSILPOP$$

$$\Theta_{RHOVL19} := PSILPOP \cdot SNRADOL^2$$

$$\Theta_{PSILPOP} := RHOVL19 \cdot SNRADOL^2$$

$$U_{PTLPOP} := \sqrt{\left(\Theta_{PSILPOP} \cdot U_{PSILPOP}\right)^2 + \left(\Theta_{RHOVL19} \cdot U_{RHOVL19}\right)^2}$$

$$U_{PTLPOP} = 16.098$$

Rewriting the balance relation and determining the uncertainty

$$BAL76 := PTVL19 - PTLPOP$$

$$BAL76 = 0.322$$

$$\Theta_{PTLPOP} := -1$$

$$U_{BAL76} := \sqrt{\left(\Theta_{PTLPOP} \cdot U_{PTLPOP}\right)^2}$$

$$U_{BAL76} = 16.098$$

Now write the uncertainty as a percentage of the RHS of the balance relation

$$U\%_{BAL76} := \frac{U_{BAL76}}{|PTVL19|}$$

$$U\%_{BAL76} = 4.064 \cdot \%$$

Balance Relation 77: PTHPOP=PTVL21
* PTHPOP is calculated in SPUMP and utilizes the HPOP head coefficient map
* PTVL21 is an iteration variable

From the SPUMP module, the exit pressure and uncertainty are determined from

$$PTVL20 := 362.0607 \quad PTVL21 := 4123.193$$

$$PTHPOP := PTVL20 + PSIHPOP \cdot RHOVL21 \cdot SNRADOH^2 \quad PSIHPOP := 0.0112 \quad RHOVL21 := 0.0403$$

$$PTHPOP = 4.11975 \cdot 10^3$$ * Note: This value is slightly different
than the model calculated value of
PTHPOP=4123.194

Since PTVL20 and SNOH are iteration variables,
PSIHPOP and RHOVL21 are the terms which contain uncertainties.

$$U_{RHOVL21} := 0.002 \cdot RHOVL21$$

Using an uncertainty of 6% for the head coefficient from the
head coefficient vs flow coefficient map. Estimate based upon
information provided by Rocketdyne.

$$U_{PSIHPOP} := 0.06 \cdot PSIHPOP$$

$$\Theta_{RHOVL21} := PSIHPOP \cdot SNRADOH^2$$

$$\Theta_{PSIHPOP} := RHOVL21 \cdot SNRADOH^2$$

$$U_{PTHPOP} := \sqrt{\left(\Theta_{PSIHPOP} \cdot U_{PSIHPOP}\right)^2 + \left(\Theta_{RHOVL21} \cdot U_{RHOVL21}\right)^2}$$

$$U_{PTHPOP} = 225.587$$

Rewriting the balance relation and determining the uncertainty

$$BAL77 := PTVL21 - PTHPOP$$

$$BAL77 = 3.44$$

$$\Theta_{PTHPOP} := -1$$

$$U_{BAL77} := \sqrt{\left(\Theta_{PTHPOP} \cdot U_{PTHPOP}\right)^2}$$

$$U_{BAL77} = 225.587$$

Now write the uncertainty as a percentage of the RHS of the balance relation"

$$U\%_{BAL77} := \frac{U_{BAL77}}{|PTVL21|}$$

$$U\%_{BAL77} = 5.471 \cdot \%$$

Balance Relation 78: PTPRBP=PTPBSO

* PTPRBP is the preburner pump discharge pressure and calculated in SPUMP
* PTPBSO is the oxidizer splitter duct and is an iteration variable

The preburner pump inlet pressure is calculated in the configuration file using the equation:

$$PTPBPI := PTVL21 - \frac{4.47 \cdot 10^{-4}}{(RHOVL21)} \cdot WPRBP^2$$

$WPRBP := 108.1089$

$PTPBSO := 6932.563$

$PTPBPI = 3.99356 \cdot 10^3$ * Note, this value is slightly different than the value in the output of 3994.133

$RHOPBSO := 0.0408$

$U_{RHOPBSO} := 0.002 \cdot RHOPBSO$

From the SPUMP module, the exit pressure and uncertainty are determined from

$PSIPRBP := 0.00864$

$$PTPRBP := PTPBPI + PSIPRBP \cdot RHOPBSO \cdot SNRADOH^2$$

$PTPRBP = 6.92831 \cdot 10^3$ * Note: This value is slightly different than the model calculated value of PTPRBP=6932.563

Since PTPBSO and SNOH are iteration variables,
PSIPRBP and RHOPBSO are the terms which contain uncertainties.

Using an uncertainty of 5% for the head coefficient from the head coefficient vs flow coefficient map. Estimate based upon engineering judgment, since no information was provided by Rocketdyne for the Preburner Pump.

$$U_{PSIPRBP} := 0.05 \cdot PSIPRBP$$

$$\Theta_{RHOPBSO} := PSIPRBP \cdot SNRADOH^2$$

$$\Theta_{PSIPRBP} := RHOPBSO \cdot SNRADOH^2$$

$$U_{PTPRBP} := \sqrt{\left(\Theta_{PSIPRBP} \cdot U_{PSIPRBP}\right)^2 + \left(\Theta_{RHOPBSO} \cdot U_{RHOPBSO}\right)^2}$$

$$U_{PTPRBP} = 146.855$$

Rewriting the balance relation and determining the uncertainty

$$BAL78 := PTPBSO - PTPRBP$$

$$BAL78 = 4.249$$

$$\Theta_{PTPRBP} := -1$$

$$U_{BAL78} := \sqrt{\left(\Theta_{PTPRBP} \cdot U_{PTPRBP}\right)^2}$$

$$U_{BAL78} = 146.855$$

Now write the uncertainty as a percentage of the RHS of the balance relation

$$U\%_{BAL78} := \frac{U_{BAL78}}{|PTPBSO|}$$

$$U\%_{BAL78} = 2.118 \cdot \%$$

Balance Relation 79: XROPV=XROPOV

$$BAL79 = XROPOV - XROPV$$

Balance Relation 80: PTHG2=PTOPRB

$$BAL80 = PTOPRB - PTHG2$$

Balance Relation 81: PTHG6=PTOSF

$$BAL81 = PTOSF - PTHG6$$

Balance Relation 82: PTHG1=PTFPRB

$$BAL82 = PTFPRB - PTHG1$$

Balance Relation 83: PTHG5=PTFSF

$$BAL83 = PTFSF - PTHG5$$

Balance Relation 84: PTFINJ=PTMFI

$$BAL84 = PTMFI - PTFINJ$$

Balance Relation 85: WMCHB=WNOZL

$$BAL85 = WNOZL - WMCHB$$

Balance Relation 86: WHG1=WFTBP

$$BAL86 = WFTBP - WHG1$$

Balance Relation 87: WHG2=WOTBP

$$BAL87 = WOTBP - WHG2$$

Balance Relation 88: PTMCHB=PCREQ

$$BAL88 = PCREQ - PTMCHM$$

Balance Relation 89: EMRFCNTR=OFREQ

$$BAL89 = OFREQ - EMRFCNTR$$

Balance Relation 90: QNETNOZX=0

Balance Relation 91: QNETNOZU=0

Balance Relation 92: QNETCHML=0

Balance Relation 93: QNETCHMU=0

Summary of balance relation uncertainties

$U\%_{BAL1} = 5 \cdot \%$

$U\%_{BAL2} = 5.032 \cdot \%$

$U\%_{BAL3} = 5 \cdot \%$

$U\%_{BAL4} = 5 \cdot \%$

$U\%_{BAL5} = 4.876 \cdot \%$

$U\%_{BAL6} = 13.055 \cdot \%$

$U\%_{BAL7} = 5.786 \cdot \%$

$U\%_{BAL8} = 5.786 \cdot \%$

$U\%_{BAL9} = 7.071 \cdot \%$

$U\%_{BAL10} = 7.071 \cdot \%$

$U\%_{BAL11} = 7.071 \cdot \%$

$U\%_{BAL12} = 7.071 \cdot \%$

$U\%_{BAL13} = 7.681 \cdot \%$

$U\%_{BAL14} = 23.613 \cdot \%$

$U\%_{BAL15} = 6.986 \cdot \%$

$U\%_{BAL16} = 8.718 \cdot \%$

$U\%_{BAL17} = 7.071 \cdot \%$

$U\%_{BAL18} = 7.071 \cdot \%$

$U\%_{BAL19} = 7.071 \cdot \%$

$U\%_{BAL20} = 7.071 \cdot \%$

$U\%_{BAL21} = 7.071 \cdot \%$

$U\%_{BAL22} = 7.071 \cdot \%$

$U\%_{BAL23} = 6 \cdot \%$

$U\%_{BAL24} = 40.769 \cdot \%$

$U\%_{BAL25} = 7.293 \cdot \%$

$U\%_{BAL26} = 7.292 \cdot \%$

$U\%_{BAL27} = 6.604 \cdot \%$

$U\%_{BAL28} = 7.419 \cdot \%$

$U\%_{BAL29} = 7.282 \cdot \%$

$U\%_{BAL30} = 7.282 \cdot \%$

$U\%_{BAL31} = 14.142 \cdot \%$

$U\%_{BAL32} = 14.141 \cdot \%$

$U\%_{BAL33} = 14.142 \cdot \%$

$U\%_{BAL34} = 2.071 \cdot \%$

$U\%_{BAL35} = 10 \cdot \%$

$U\%_{BAL36} = 7.062 \cdot \%$

$U\%_{BAL37} = 7.062 \cdot \%$

$U\%_{BAL38} = 5.001 \cdot \%$

$U\%_{BAL39} = 5.001 \cdot \%$

$U\%_{BAL40} = 5.071 \cdot \%$

$U\%_{BAL41} = 5.09 \cdot \%$

$U\%_{BAL42} = 4.959 \cdot \%$

$U\%_{BAL43} = 4.941 \cdot \%$

$U\%_{BAL44} = 3.764 \cdot \%$

$U\%_{BAL45} = 3.87 \cdot \%$

$U\%_{BAL46} = 7.143 \cdot \%$

$U\%_{BAL47} = 5.001 \cdot \%$

$U\%_{BAL48} = 3.61 \cdot \%$

$U\%_{BAL49} = 3.649 \cdot \%$

$\blacksquare = \cdot \%$

$\blacksquare = \cdot \%$

$\blacksquare = \cdot \%$

$\blacksquare = \cdot \%$

$\blacksquare = \cdot \%$

$\blacksquare = \cdot \%$

$\blacksquare = \cdot \%$

$\blacksquare = \cdot \%$

$\blacksquare = \cdot \%$

$\blacksquare = \cdot \%$

$\blacksquare = \cdot \%$

$\blacksquare = \cdot\%$

$\blacksquare = \cdot\%$

$\blacksquare = \cdot\%$

$\blacksquare = \cdot\%$

$\blacksquare = \cdot\%$

$\blacksquare = \cdot\%$

$\blacksquare = \cdot\%$

$\blacksquare = \cdot\%$

$\blacksquare = \cdot\%$

$U\%_{BAL70} = 8.201 \cdot\%$

$U\%_{BAL71} = 11.045 \cdot\%$

$U\%_{BAL72} = 17.76 \cdot\%$

$U\%_{BAL73} = 21.749 \cdot\%$

$U\%_{BAL74} = 2.491 \cdot\%$

$U\%_{BAL75} = 6.713 \cdot\%$

$U\%_{BAL76} = 4.064 \cdot\%$

$U\%_{BAL77} = 5.471 \cdot\%$

$U\%_{BAL78} = 2.118 \cdot\%$

$\blacksquare = \cdot\%$

$\blacksquare = \cdot\%$

$\blacksquare = \cdot\%$

$\blacksquare = \cdot\%$

$\blacksquare = \cdot\%$

$\blacksquare = \cdot\%$

$\blacksquare = \cdot\%$

$\blacksquare = \cdot\%$

$\blacksquare = \cdot\%$

$\blacksquare = \cdot\%$

$\blacksquare = \cdot\%$

$\blacksquare =$

$\blacksquare =$

A5-102

Appendix - 6

AIAA Technical Paper 95-3073
"Enhancing Rocket Engine Test Analysis and Performance Models with the Incorporation of Uncertainties."

AIAA 95-3073
Enhancing Rocket Engine Test Analysis and
Performance Models with the Incorporation of
Uncertainties

Kendall K. Brown and Hugh W. Coleman
Propulsion Research Center
Department of Mechanical and Aerospace Engineering
University of Alabama in Huntsville
Huntsville, AL 35899

L. Michael Santi
Department of Mechanical Engineering
Christian Brothers University
Memphis, TN 38104

John P. Butas
Motor Systems Division
NASA/Marshall Space Flight Center
Marshall Space Flight Center, Alabama

31st AIAA/ASME/SAE/ASEE
Joint Propulsion Conference and Exhibit
July 10-12, 1995/San Diego, CA

Enhancing Rocket Engine Test Analysis and Performance Models with the Incorporation of Uncertainties

Kendall K. Brown* and Hugh W. Coleman†
University of Alabama in Huntsville, Huntsville, AL

L. Michael Santi‡
Christian Brothers University, Memphis, TN

John P. Butas§
NASA/Marshall Space Flight Center, Alabama

Abstract

Providing accurate performance predictions for a liquid rocket engine is essential to providing a safe and effective space launch system, since test programs cannot, in a cost efficient manner, provide all the necessary information. This paper discusses a new methodology which includes knowledge of the uncertainties associated with the test program as well as the uncertainties associated with the analytical model and the uncertainty associated with the solution of the model. This methodology will be used during the analysis of test data through a test data reconciliation strategy to incorporate the test data and its uncertainty within the model solution to provide the most plausible region of engine performance conditions.

This work is based around enhancing the analysis tools for the continued evolution of the Space Shuttle Main Engine (SSME) and its on-going development at the Technology Test Bed (TTB) facility at Marshall Space Flight Center. Assessment of the experimental uncertainties associated with TTB SSME test data and assessment of the uncertainties associated with the analytical model are also discussed.

* Graduate Research Assistant, Propulsion Research Center, Department of Mechanical and Aerospace Engineering. Student Member AIAA
† Eminent Scholar in Propulsion, Propulsion Research Center, Department of Mechanical and Aerospace Engineering. Senior Member AIAA
‡ Professor and Head, Department of Mechanical Engineering.
§ Senior Engineer, Motor System Division, Propulsion Laboratory.

Introduction

The conflicting demands placed upon current and future liquid rocket engine systems, maximum performance at minimum cost, require the development of new analysis tools, tools which provide more information upon which to base decisions. The uncertainties in the test results and the uncertainties in the analytical model predictions have often been neglected. Hence, a research program has been in progress, led by NASA Marshall Space Flight Center (MSFC), to develop analysis tools for use with the Space Shuttle Main Engine (SSME) which considers these uncertainties. The intent of these tools is to provide information which identifies the region of most plausible engine performance conditions.

This paper describes the combined effort of researchers from NASA/MSFC, Christian Brothers University[1], and the University of Alabama in Huntsville[2] to develop these tools. This paper presents the background and overall objective of the effort, aspects of the experimental uncertainty analysis, aspects of the data integration and modeling work, and a discussion of future work.

Background and Objective

Analytical performance models simulate the internal flow environment of a rocket engine by modeling subsystem components and integrating these components into an engine system. These performance models are essential in the support of SSME hardware design, evaluating hardware performance, predicting engine operating for off-nominal hardware conditions, and anomaly investigations. The primary purpose of these performance models is to accurately predict the performance characteristics of the individual engine components. These individual components are modeled using analytical relationships which describe turbopump characteristics, pressure losses,

and heat transfer effects. These analytical relationships are adjusted to correlate to test data. Thus, the quality and validity of the performance predictions generated rely primarily on the process in which test data is integrated with the analytical relationships. If this process is flawed, the hardware characteristics and performance predictions generated from these models will be inaccurate, unreliable, and could steer the rocket engine development program on a costly and undesirable course.

Accurately predicting the performance characteristics of the individual engine components is extremely difficult because of three factors. First, limited instrumentation exist on most rocket engines. There are approximately 700 parameters within the current SSME performance model which represent all of the predicted pressures, temperatures and flowrates within the engine. The instrumentation on the Technology Test Bed SSME provides data for only 12% of these internal flow parameters. Secondly, rocket engine testing is extremely costly. This limits the amount of data that can be attained for a specific rocket engine design. Third, most rocket engine performance analysis models integrate test information within the physical relationships by assuming that the measured test data is absolutely accurate. This, so-called, "pristine data" assumption is flawed since all measurement systems have inherent inaccuracies. In addition, rocket engine models consist of analytical relationships based upon simplified assumptions. Individual engine components are modeled assuming one-dimensional, uniform, flow-averaged conditions. Local measurements in this complicated flow network are incapable of characterizing these flow-averaged conditions with accuracy. Computational predictions are forced to agree with the data at instrumented locations, often at the expense of balancing fundamental physical relationships (mass conservation, momentum, and energy conservation). Consequently, this leads to inaccurate hardware characterization and engine system performance predictions. The first two factors are inherent within all rocket engine technology. The third factor can be significantly improved by developing new methods to integrate uncertain test information within simplified analytical relationships.

A new generalized performance analysis model, termed the Performance Reconciliation Model (PRM), is currently being developed which contains a test data integration strategy that eliminates the pristine data assumption. The solution procedure incorporates a system level nonlinear mathematical optimization strategy. The optimization strategy requires uncertainty estimates for both test measurements and the balance of the fundamental physical relationships. The optimization procedure selects values for engine variables (flow rates. pressures, temperatures, speeds. etc.) within defined measurement uncertainty limits, while satisfying the fundamental physical relationships within defined balance uncertainty limits. The objective of the optimization procedure is to minimize adjustments in the engine variables from the initial test values. The PRM generates a set of performance predictions by reconciling test data with fundamental physical relationships within specified uncertainty limits. In effect, PRM predictions provide the most plausible set of engine performance conditions, recognizing the inherent uncertainties in both fundamental physical relations and test measurements. Figure 1 schematically shows the fundamental aspects of this new computational strategy. Test data obtained from the SSME Technology Test-Bed facility at MSFC is being used to support this model development. The goal of this strategy is to get the test information and fundamental physical relationships to reinforce each other and thus, more accurately predict the performance characteristics of the individual engine components.
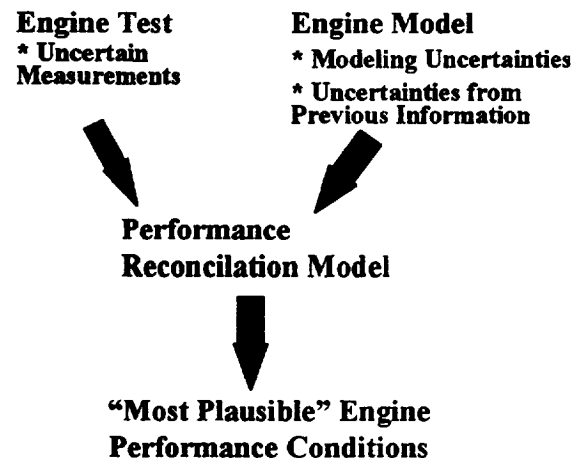
Engine Test
* Uncertain Measurements

Engine Model
* Modeling Uncertainties
* Uncertainties from Previous Information

Performance Reconcilation Model

"Most Plausible" Engine Performance Conditions

Figure 1 Schematic of Research Effort

Uncertainty Analysis in TTB Testing
The focus in this task is to identify the uncertainty that should be associated with measured variables such as temperature or pressure or with a determined result such as flowrate that is calculated using a number of measured variables.
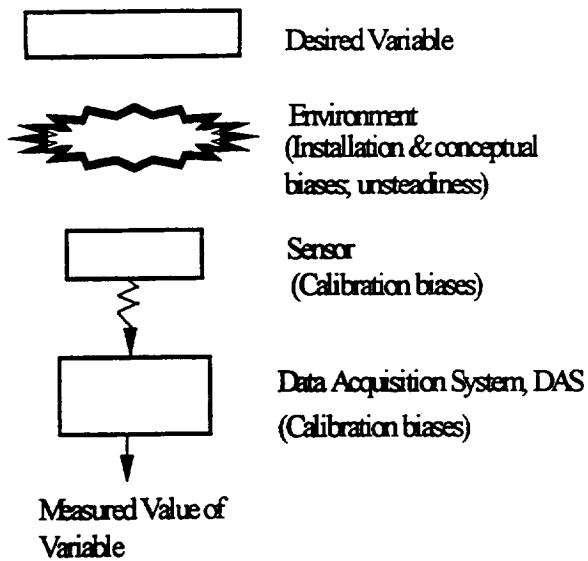
2

Desired Variable

Environment
(Installation & conceptual
biases; unsteadiness)

Sensor
(Calibration biases)

Data Acquisition System, DAS
(Calibration biases)

Measured Value of
Variable

**Figure 2 Schematic of TTB Measurement Process from an
Error Sources Viewpoint.**

Figure 2 shows a schematic of the viewpoint used in identifying error sources that contribute to the overall uncertainty. The desired variable is taken to be the one with which a model output will be compared – a cross-section averaged temperature, for example, that would usually be referred to as "the temperature" of the flow at a particular location in the engine. If the sensor responds to temperature at a point, then an installation or conceptual bias exists due to the sensor not actually responding to the desired variable (the average temperature). This is an elemental source that must be included, and it is potentially one of the dominant elemental sources in temperature and pressure data in TTB testing. The traditional "measurement uncertainty" sources are shown as biases in the sensor calibration and biases in the calibration of the data acquisition system (DAS). Additionally, the effect of unsteadiness in, and due to, the operating environment must be considered since the sensor calibrations and DAS pre-test calibration checks are not done with the engine operating, and the unsteadiness certainly can have an effect on the final system output - the measured value of the variable.

Choice of the appropriate precision uncertainty estimate (precision limit) to use with TTB data needs to be carefully done. A precision limit determined using a standard deviation from a time slice during one test gives information about the steadiness of the "steady state" at that operating condition during that particular test, but includes no effects of the test-to-test variation of the variable at that operating condition. Computing a standard deviation of a variable or result from multiple tests, all of which were at the same operating condition,

gives the appropriate precision estimate for use in discussing the uncertainty in a measured TTB variable. It is also the appropriate precision limit to consider when comparing the results from one test to results from another test in an effort to determine if a change in component, for instance, had any discernible effect on the value of the result.

An investigation to determine the experimental uncertainties associated with test measurements from the SSME Engine 3001 installed in the Technology Test Bed facility was conducted. This investigation consisted of reviewing previous analyses, discussions with NASA personnel, review of other technical literature, and new analyses. Since the thermodynamic performance analysis of the SSME was the motivation behind this contractual effort, the pressure, differential pressure, temperature, and mass flow rate measurements were the focus of the initial investigation.

Analysis of Previous TTB Test Data

To achieve a set of data to review which could be defined as from the "same" hardware, tests TTB039 through TTB 051 were chosen. These tests were conducted with Engine 3001 with the large throat combustion chamber and a consistent set of other hardware.

The mass flow rate uncertainties for the venturi flowmeters were determined using the methodology in references [3], [4], [5] and [6]. The systematic uncertainty estimates (bias limits) used in the uncertainty propagation equations were based upon the information gathered from the available documentation, discussions with TTB personnel, and engineering experience.

Potentially significant bias uncertainties yet to be evaluated in the TTB measurements are the conceptual bias uncertainties. The conceptual bias uncertainties in the temperature and pressure measurements are particularly important in this effort because of the interest in comparing the experimental results with the analytical predictions. In many of the SSME measurements the flowfield is highly complex due to the sharp turns and bends, valves, pump and turbine inlets and discharges, and other complicating factors. These factors accentuate the difference between the physical quantity at the sensor and the quantity for which the measurement is desired, typically an average value at a cross-section. These assessments will require extensive review of the measurement, the sensor and its installation, the thermodynamic and fluid dynamic flowfield, and their interaction. This detailed analysis of the measurements is currently underway.

3

The precision limits for the mass flowrate uncertainties are dependent upon the question being asked, or rather, what is purpose for the information. Precision limits can be calculated in many different ways, but the interpretation of the precision limit and the use of it depends upon data used to calculate it. The variables which must be considered for the precision limit calculation include, but are not limited to:

- engine number
- specific engine component configuration
- engine test(s)
- power level
- test profile
- specific engine adjustments
- time slice within the test
- data sample rate (data points used for standard deviation calculation)

The precision limits for the flowrate uncertainties were based upon review of the flowrate data for the chosen time slice. Precision limits were estimated in two primary ways. First, one was based upon the full sample-rate (25 or 50 samples/sec) data within each test. The second precision limit was estimated based upon averaging the full sample-rate data over a given time slice, for a given test, at a chosen power level to provide a single data point for that test condition and using similar points from other tests to form a sample from which a precision limit estimate could be calculated.

The uncertainty in the thermophysical property data must be included in the uncertainty analysis since there was some experimental uncertainty in the original experiments upon which the property tables were developed. If the property data is represented by a curve-fit of the experimental data an uncertainty associated with the data and with the curve-fit must be included. The venturi flowrate data reduction utilizes the thermophysical property routine GASP[7]. The GASP documentation shows the uncertainty in density for liquid hydrogen and liquid oxygen to be within approximately 0.25% outside of the critical region and within approximately 2.0% near the critical region. The GASP program is based upon National Bureau of Standards data for the thermodynamic properties of hydrogen and oxygen.

Calibration of Mass Flowmeters, Determination of Discharge Coefficient, C_D

The accurate determination of the mass flow rate for cryogenic rocket propellants is difficult because of the special problems presented. These problems arise because of the cryogenic

temperatures, the property data uncertainty, the differences in calibration fluids (water or air versus cryogens), and calibration limitations due to safety considerations Each of these can introduce an uncertainty in the mass flow rate determination.

The accurate determination of a mass flow rate depends upon the ability to trace the output from a given device back to a standard certified by the National Institute of Standards and Technology (NIST) or some other respected standard. The basic problem with cryogen flowmeters is that there are limited facilities which can produce an accurate standard using the actual cryogenic fluid. The facilities which do exist are limited to the calibration of liquid nitrogen flows, or have limited capacity.

The principle of dynamic similarity, matching the Reynolds number of the test fluid with the Reynolds number of the calibration fluid, has been relied upon, with corrections for the dimensional changes due to thermal contraction and other miscellaneous effects being made. A literature survey indicates that very little work has taken place to assess the accuracy of this procedure, primarily due to the cost and complexity involved with developing the necessary experiments with liquid oxygen and liquid hydrogen. The systematic uncertainty due to not calibrating the venturi flowmeters in the appropriate cryogenic fluid has been estimated to be as much as 1%.[9,10] Other assumptions and approximations are made to achieve the venturi mass flowrate data reduction equations. Two of the fundamental assumptions are that the flow through the venturi is adiabatic and one-dimensional, which is not true during engine operation. Another significant factor is that none of the venturis are installed with the recommended length of upstream straight duct. An attempt was made[8] to account for this problem by calibrating the venturis with the "as-installed" ducts connected, however they could not reproduce the other flow characteristics, such as flow swirl, turbulence, oscillations, etc.

The venturi calibration report[8] develops a polynomial curve-fit to obtain the value of the discharge coefficients where the curve-fit is based upon the Reynolds number of the flow through the venturi. For all of the venturi flowmeters calibrated with water dynamic similarity could not be obtained, that is, the flowmeters could not be calibrated at the Reynolds number expected during an engine test. In fact, most of the calibrations were performed at a fraction of the operating Reynolds number, from 1.7% to 10%, and the curve-fits were extrapolated out to the operating condition.

The extrapolation of the calibration curve-fits and the use of a different fluid for the calibration introduce an uncertainty which must be associated with the venturi discharge coefficient. In the absence of performing detailed experiments to assess these uncertainties, estimates must be made based upon the existing information. In this study, systematic uncertainties of 2-4% were estimated for the discharge coefficients.

Uncertainty in Mass Flowrate Determinations

A computer program was developed to calculate the flowrates for the venturi flowmeters and to perform the uncertainty calculations. This program accesses the raw, full sample-rate data for all of the engine measurements. The program uses the measured pressure, differential pressure, and temperature for each venturi, combined with the specific dimensional data and other constants (such as discharge coefficient), averages the data for the chosen time slice and calculates the mass flowrate. The bias limits and precision limits for the uncertainty sources for each venturi are stored in the program as constants and propagated through the data reduction equation using the uncertainty propagation equations. The only correlated bias uncertainty included in the uncertainty propagation equation is the uncertainty in the venturi dimensions. All other possible bias correlations were considered negligible, particularly with respect to the magnitude of the discharge coefficient bias uncertainty. The partial derivatives are determined numerically using a finite difference technique, often referred to as a jitter routine.

The mass flow rate uncertainties were determined to be in the 4% to 8% range, with the two dominant uncertainty contributions being the systematic uncertainty from the discharge coefficient and the precision uncertainty. Further review of the test data indicated that most of the precision uncertainty was due to the variation in the engine balance from test-to-test for a given power level. A factor which complicates the analysis of the SSME is that the engine will balance at different operating points for a given power level. Hence, the test-to-test uncertainty estimate contains this information and is the appropriate interval to use within the PRM.

Uncertainty Analysis in SSME Modeling

When comparing output of a model with experimental data, the uncertainties that should be associated with the model predictions must be considered for proper conclusions to be drawn. In the past, most of the work reported in this area has simply

considered the sensitivity of the model output to uncertainties in the input data. This obviously does not include any uncertainties in the model itself and thus is not a satisfactory approach. In this research effort, we have divided the sources that cause uncertainty in the model output into three categories: (1) uncertainties due to assumptions and approximations in the model, (2) uncertainties due to the incorporation of previous experimental data into the model, and (3) uncertainties due to the numerical solution algorithm. Consideration of the third category is considered in the next section.

The first category, uncertainties due to assumptions and approximations in the model, does not include the installation and/or conceptual bias source shown in Figure 2 and discussed above since that uncertainty is associated with the measured value. Consider the temperature at a particular position in the flow. The uncertainty associated with the measured value of the temperature includes the effect of making a point measurement but desiring a cross-sectional averaged value. The inability of the model to calculate a correct average temperature at a particular location because the one-dimensional flow approximation has been made results in an uncertainty in the predicted temperature. (Stated another way, if the model predicts the correct average temperature at a particular location, then the one-dimensional flow approximation has caused no uncertainty in the model output.)

The uncertainties due to the incorporation of previous experimental data in the model arise when material property data is used, when valve resistance characteristics are used, when pump maps are used, etc. These are all instances in which previous experimental data has been used by replacing the data with curvefits. The original data contained uncertainties, but the curvefit equations used in the predictive models have been treated as the "truth" in most previous considerations of uncertainty in model outputs. Adding further complication, there is no accepted way of estimating the influence of systematic uncertainties on the uncertainty that should be associated with a regression. This aspect has been investigated as a part of this program and is discussed later.

Modeling Assumptions and Approximations

When a model of a physical system is developed, assumptions and approximations about the system are made to simplify the system to one which mathematical expressions can describe. By making these simplifications an error is introduced and the model cannot exactly describe the physical system.

Some of the primary assumptions and approximations made within the SSME model include:

- 1-dimensional
- fully developed
- steady-state
- adiabatic
- ideal gas

If the uncertainty to associate with a particular assumption or approximation can be estimated, then sometimes the model should be improved to include this estimate instead of trying to estimate the uncertainty. For example, it was determined that a turbine exit temperature was being predicted using an ideal gas, constant specific heat approximation, which for the specific temperature range of interest was a poor approximation. Instead of trying to estimate an uncertainty to associate with that approximation, the model was altered to include a better thermodynamic description of the process.

If the models are developed based upon the soundest assumptions and approximations available, assessing the uncertainty due to these assumptions and approximations would require an effort beyond the scope of the current research program

Uncertainties From Using Previous Experimental Information

In all of the component modules, information from previous testing is used. For example, the model of the liquid oxygen flow through a given duct or through a given valve is based upon its component testing, which provides an equation for the resistance through the duct as function of the flowrate. This test information is often reduced to the form of a line or curve. The values of the polynomial constants in the thermodynamic property routines are also examples of using previously obtained uncertain test information in a model.

The methodology to assess the uncertainty in the coefficients of a linear regression were developed as part of this effort. The uncertainty analysis methodology previously discussed was applied to the expressions for the regression coefficients to develop the technique. The details of this methodology were presented at the 1995 AIAA Aerospace Sciences conference[11]. The work presented in that paper demonstrates that this technique provides a method to determine the uncertainty in linear regression coefficients, and incorporates the effects of correlated systematic uncertainties.

Recently, the methodology has been extended to provide the appropriate uncertainty interval for the predicted value using the regression model equation. Work is continuing to develop the specific techniques needed to apply this methodology

to the types of models and previous experimental information found in the SSME program.

Performance Analysis

Data integration strategies are defined by formulation, including both physical and mathematical components, and computational solution procedure. A reliable strategy requires a computationally tractable and physically consistent performance model as a fundamental starting point. In mathematical terms, the computational steady-state performance analysis problem can be stated as follows:

Problem 1   Computational Performance Analysis Problem

determine   **X**

such that $F (X ; Y) < Tol$

where

F - the column vector $[F_1 , F_2 , \ldots , F_n]^T$ composed of n independent balance relations that govern modeled engine performance

X - the column vector $[x_1 , x_2 , \ldots , x_n]^T$ composed of n independent physical characteristics that define modeled engine performance

Y - the column vector $[y_1 , y_2 , \ldots , y_m]^T$ composed of m performance parameters, assumed constant, for the modeled engine

Tol - the column vector $[tol_1 , tol_2 , \ldots , tol_n]^T$ composed of the n solution tolerances associated with the n independent balance relations governing modeled engine performance

Acceptable solutions to Problem 1 are located within the intersection of tolerance bands about the individual balance solution contours. The method for selecting individual tolerances is an important consideration which can significantly affect the solution obtained. Despite the critical nature of tolerance selection, heuristic guidelines are generally used to specify individual relation tolerances. A more systematic procedure for specifying the acceptability threshold is to define tolerance limits in terms of balance relation uncertainties. Balance relation ($F_i(X;Y)=0$) uncertainty arises from a variety of sources including model assumptions/approximations, scarce/ inaccurate

6

thermodynamic property data in ranges of interest, scatter/extrapolation of experimental data used to estimate parameters in semi-empirical relations, and secondary effects such as small scale leakage often ignored in large scale performance models.

Techniques for estimating experimental uncertainties and their propagation are well developed, as discussed previously. Although not uniformly applicable to tolerance estimation, these techniques can be expanded to provide a fundamental approach to balance uncertainty estimation. Once defined, the balance uncertainty vector $U=[\ U_1\ ,\ U_2\ ,\ \ldots\ ,\ U_n\ ]^T$ can be used in place of the tolerance vector **Tol** in Problem 1, yielding a modified computational performance analysis problem in which uncertainty band intersections define the solution feasible region as depicted conceptually in Figure 3. This type approach is logically consistent and provides consistent utilization of available information in performance modeling.

Data Reduction

The term "data reduction" indicates a specific procedure for integrating experimental test data within performance prediction models. Traditionally, data reduction has referred to data integration based on a single test firing of a specified engine. This does not, however, preclude the use of data reduction as a method for ensemble average data integration.

The data reduction procedure is a strategy for modifying engine hardware performance characteristics in order to enforce model agreement with a specified set of experimental observations. To facilitate mathematical description of the data reduction process, it is useful to define the following set partitions:

$$X\ =\ [\ x_1\ ,\ x_2\ ,...,\ x_k\ |\ x_{k+1}\ ,...,\ x_n\ ]^T\ =\ [\ X_f\ |\ X_v\ ]^T$$

$$Y\ =\ [\ y_1\ ,\ y_2\ ,...,\ y_k\ |\ y_{k+1}\ ,...,\ y_m\ ]^T\ =\ [\ Y_v\ |\ Y_f\ ]^T$$

where

X_f - a subset of X composed of the k physical characteristics that are fixed by test data

X_v - the complementary subset $(X_v=X-X_f)$of n-k physical characteristics that remain as independent data reduction solution variables
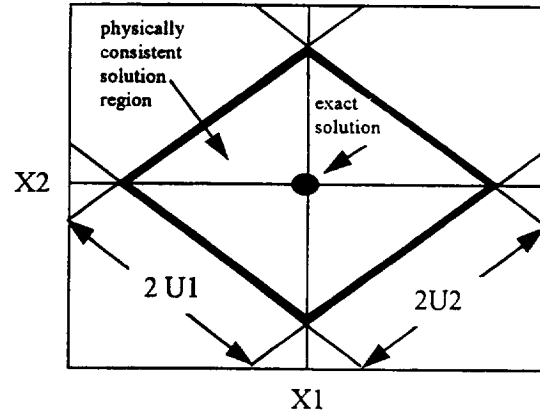
Y_v - a subset of Y composed of k hardware parameters that are treated as independent data reduction solution variables

Y_f - the complementary subset $(Y_f=Y-Y_v)$ of m-k hardware parameters that remain at assumed constant values

Using the above set partition definitions, the data reduction analysis problem can be stated as follows:

Problem 2   Data Reduction Analysis Problem

fix   k physical characteristics X_f at test data indicated values

select   k hardware parameters Y_v to treat as variable

determine X_v and Y_v

such that $F\ (\ X_v\ ,\ Y_v\ ;\ X_f\ ,\ Y_f\ )\ <\ $ **Tol**

Because there is some freedom in the selection of the elements of Y_v, the solution of the data reduction analysis problem is generally not unique. (1) This troublesome characteristics results from the fact that the system $F(X,Y)=0$ is underprescribed. (2) It places a significant burden on the model user in selecting the variable hardware components of Y_v. A logical, although not a priori correct, procedure is to select as elements of Y_v those hardware characteristics which most significantly impact corresponding fixed elements of X_f. In practice, the variable hardware characteristics are selected based on experience and related observation. This type of subjective selection provides unfortunate opportunities for systematic prediction bias.

7

A conceptual view of consistent data reduction analysis solutions, assuming absolutely accurate (pristine) test data, is presented in Figure 4. It is obvious that the set of acceptable physical solutions becomes more restricted as the dimension of X_f increases (i.e., the number of test fixed physical parameters increases).
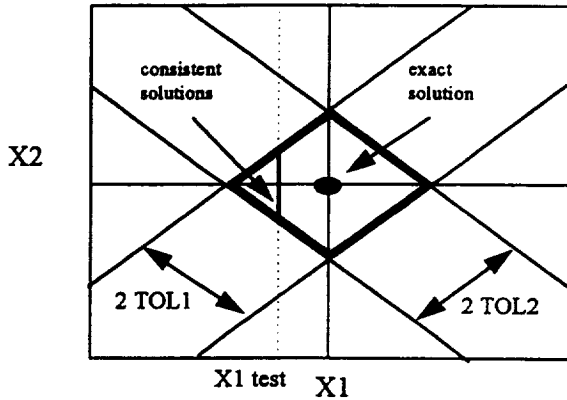

Figure 4 Data Reduction, Consistent Pristine Data Solutions

In addition, a significant problem arises when experimental observation falls outside the physically consistent solution region as displayed in Figures 5. It is an unfortunate consequence of experimental uncertainty that consistent data reduction becomes more difficult as the number of physical measurements increases. In the limit, as the number of test fixed physical characteristics approaches the total number of prediction variables, a physically consistent performance solution is unobtainable due to test data measurement uncertainty. Traditional data reduction methods do not address this fundamental problem. A logical strategy is needed to resolve the integration anomalies depicted in Figure 5.

Data Reconciliation

Three approaches can be taken to resolve the data integration problems described in the previous section. The first, and perhaps simplest, technique is to retain the pristine data assumption and increase the physical relation tolerance bands to include test values. Uncertainty bandwidths would both guide and limit the allowable tolerance relaxations. A second approach is to consider measurement uncertainty as well as balance uncertainty in data integration. The intersection of balance and measurement uncertainty bands would then define all feasible solutions. The pristine data assumption can be retained if test measurements fall within the feasible region. In addition, the second approach provides a strategy for determining feasible
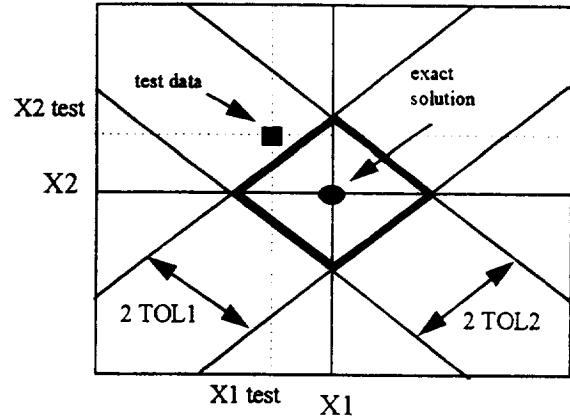
Figure 5 Data Reduction, No Consistent Pristine Data Solution

reconciliation solutions while relaxing the pristine data assumption . The third, and perhaps least desirable, approach is to simply ignore a portion of the flow physics in order to retain the pristine data assumption. This method is often used in current data reduction strategies when data restrictions preclude a consistent physical solution. This approach fails to recognize inherent measurement uncertainty and reduces physical consistency. This type of rigid adherence to the pristine data assumption is difficult to defend as a prediction enhancement strategy.

The fundamental question and problem related to test data integration is simply stated. What is the best estimate of engine performance in the presence of uncertain, non-physical test data? The available flow physics and test data are insufficient to provide a rigorous answer to this question. Therefore, the quality of performance prediction depends in large measure on effective problem formulation/solution. Since best estimates are sought for an underprescribed engine system, it is logical to assume that an effective data integration model will take the form of a mathematical programming problem. Several such formulations based on squared residual sums have been developed during the interim phase of this study. These formulations, termed data reconciliation models, are described below.

Reconciliation Formulation 1

Assumes pristine data and physical relations uncertainty band satisfaction.

$$\text{minimize } f(X, Y) = \sum_{i=1}^{n} \left[F_i(X_v, Y_v; X_f, Y_f) \right]^2$$

by selection of X_v, Y_v

subject to $\quad | F(X_v, Y_v ; X_f, Y_f) | < U$

$$X_f = \text{test value}$$

Formulation 1 is the mathematical representation of data integration approach 1. No feasible solution exists if X_f does not fall within the physical relation uncertainty band intersection.

Reconciliation Formulation 2

Assumes minimum deviation from test data and physical relations uncertainty band satisfaction.

minimize $\quad f(X, Y) = \sum_{x_i \varepsilon X_f} (x_i - x_{i,test})^2$

by selection of $\quad X, Y_v$

subject to $\quad | F(X, Y_v; Y_f) | < U$

Formulation 2 is one example of a mathematical model reflecting data integration approach 2. It seeks the physically consistent performance state closest to test data. The feasible region is the intersection of physical relation and test data uncertainty bands. In this formulation, the reconciliation solution is the point within the feasible region that deviates the least from test data.

Reconciliation Formulation 3

Assumes pristine data and minimum violation of physical relations.

minimize $\quad f(X, Y) = \sum_{i=1}^{n} \left[\dfrac{F_i(X_v, Y_v; X_f, Y_f)}{U_i} \right]^2$

by selection of $\quad X_v, Y_v$

subject to $\quad X_f = \text{test value}$

Formulation 3 presents a mathematical model related to data integration approach 2. It seeks the performance state with the highest level of physical consistency that can be attained while enforcing absolute test data agreement. The reconciliation solution selected by formulation 3 is the operating state closest to the feasible region that agrees with test data.

It is evident that reconciliation formulations 2 and 3 return data integration solutions that differ only in the perceived quality of test data relative to physical consistency. Formulation 4 described below includes both formulations 2 and 3 as specific cases.

In addition, it eliminates constraint complexity and utilizes both physical relation and test data uncertainty weighing to identify the "best" operating state prediction.

Reconciliation Formulation 4

Assume uncertainty weighing of test data and physical relations.

minimize $\quad f(X, Y) =$

$$\sum_{i=1}^{n} \left[\frac{F_i(X, Y_v; Y_f)}{U_i} \right]^2 + \sum_{x_i \varepsilon X_f} \left[\frac{(x_i - x_{i,test})}{U_i} \right]^2$$

by selection of $\quad X, Y_v$

The effect of uncertainty weighing in the above squared residuals relation is obvious. Reconciliation formulation 4, as displayed in Figure 6, provides a logical and consistent platform for combining information from the historical data base (Y and U) with single test experimental data (X_f) and physical model relations (F). It admits plausible "solutions" that approach physical and test consistency in an "optimum" fashion. In addition, it can be used to relax the requirement that the number of adjustable hardware performance parameters (in Y_v) match the number of available test measurements (in X_f) in the data integration process.

The L_2 or squared residuals formulation presented above is but one of many potential extremum formulations that can be used for effective data integration. The formulation of choice will be the one that admits the most reliable and efficient solution.
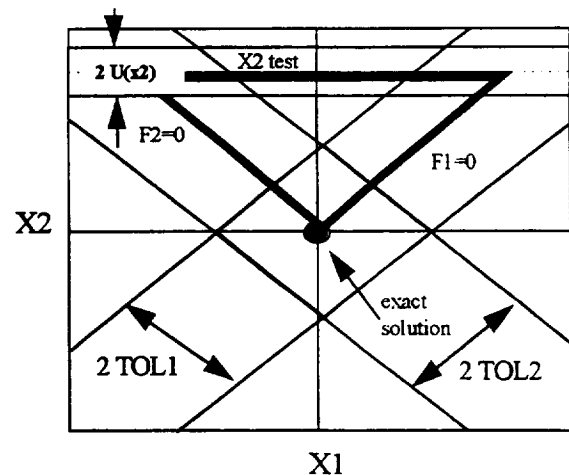

Figure 6 Data Reconciliation, Formulation 4 Feasible Region

Summary

An uncertainty analysis of the SSME test program at the Technology Test Bed facility has shown that non-negligible uncertainties exist in the determination of the mass flowrates, ranging from 2% to up to 10%, and even larger in some cases. The systematic uncertainty is dominated by the bias limit in the experimentally determined venturi discharge coefficient. The precision uncertainty is dominated by the test-to-test variation in the power balance within the engine, causing a variation in the actual flowrate in addition to the inherent flow randomness.

The uncertainty intervals provided in this report can be used for comparison to performance prediction models; however the engine configuration being modeled must be representative of the engine configuration for which the precision uncertainty was determined.

A primary source of uncertainty in the analytical modeling of the SSME is from the use of previous experimental information. This information is usually utilized in the form of regressions or curvefits. Initial research efforts to determine a methodology to properly account for the uncertainty in the regression coefficients has shown to be promising, and work is continuing to develop the methodology.

Mathematical programming formulations provide a natural analytical basis for test data integration in performance models. Plausible formulations have been developed and implemented. Computational experience with these implementations is currently being extended.

References

1. Santi, L. Michael, "Test Data Integration Procedure for General Rocket Engine Performance Models," Final Report, NASA Contract NAG8-1024, May 1995.

2. Coleman, Hugh W. and Brown, Kendall K., "Impact of Uncertainty on Modeling and Testing," Final Report, NASA Contract NAS8-38609 D.O. 106, Propulsion Research Center Report PRC 95-001, April 1995.

3. Coleman, Hugh W., and Steele. W. Glenn., *Experimentation and Uncertainty Analysis for Engineers*, John Wiley & Sons, New York, 1989.

4. *Guide to the Expression of Uncertainty in Measurement*, International Organization for Standardization, Beneve, Switzerland. 1993.

5. "Quality Assessment for Wind Tunnel Testing," AGARD-AR-304, 1994.

6. American Institute of Aeronautics and Astronautics. *Assessment of Wind Tunnel Data Uncertainty*, AIAA Standard S-071-1995, 1995.

7. Hendricks, Robert C., Baron Anne K., and Peller, Ildiko C., "GASP - A Computer Code for Calculating the Thermodynamic and Transport Properties for Ten Fluids: Parahydrogen, Helium, Neon, Methane, Nitrogen, Carbon Monoxide, Oxygen, Fluorine, Argon. and Carbon Dioxide," NASA TN D-7808, February 1975.

8. Lepore, Frank A., Space Shuttle Main Engine No. 3001, Technology Test Bed, Differential Flowmeters Calibration Final Report, Rocketdyne Division, Contract No. NAS8-27980, March 1980.

9. Brennan, J.A. LaBrecque, J.F., and Kneebone, C.H., "Progress Report on Cryogenic Flowmetering at the National Bureau of Standards," *Instrumentation in the Cryogenic Industry, Volume 1*, Proceedings of the first Biennial Symposium on Cryogenic Instrumentation, October 11-14, 1976, Held in Conjunction with the 31st Annual ISA Conference and Exhibit.

10. Szaniszlo, Andrew J., and Krause, Lloyd N., "Simulation of Liquid-Hydrogen Turbine-Type Flowmeter Calibrations using High-Pressure Gas," NASA TN D_3773.

11. Brown, Kendall K., Coleman. Hugh W., and Steele, Glenn W., "Estimating Uncertainty Intervals for Linear Regression," AIAA Paper 95-0796, 33rd Aerospace Sciences Meeting and Exhibit. January 9-12, 1995, Reno, NV.
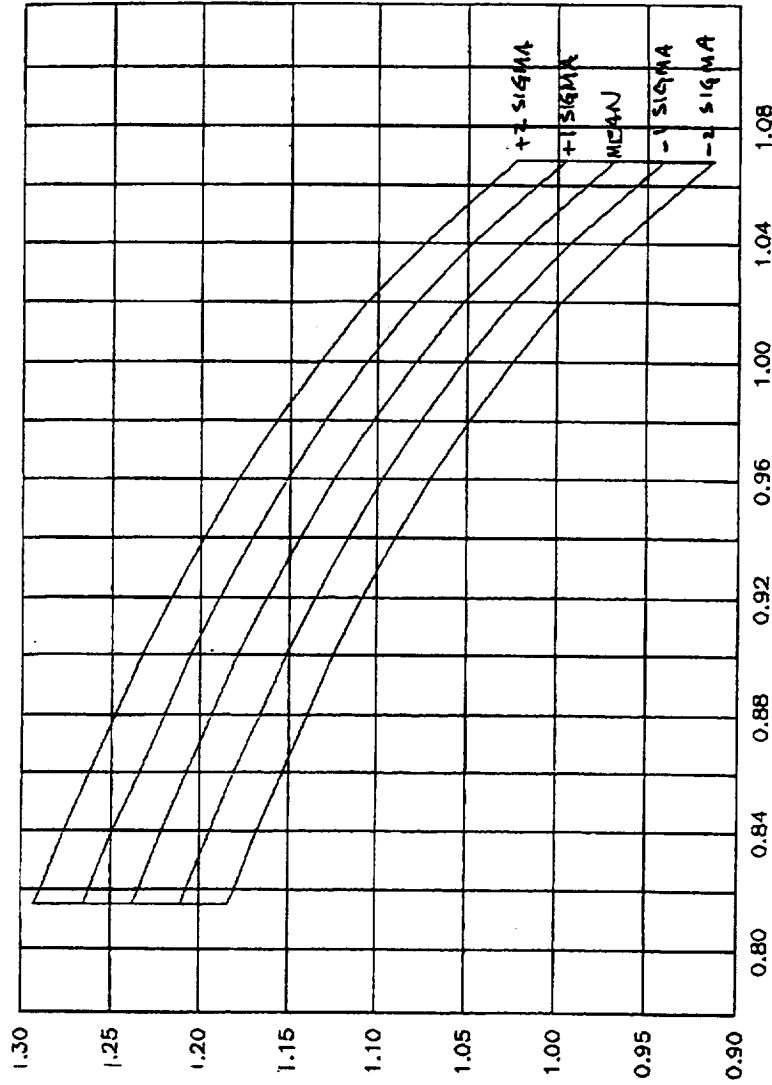
Appendix 7

Miscellaneous Background Information

The information provided in this appendix is included to assist in reviewing and updating the uncertainty estimates. They are also included as background, to used to resolve currently open issues.

The pump performance maps contained here were obtained from Rocketdyne, the proper correlation between these maps and the performance maps in ROCETS is currently not known. When the proper relationship is determined the transfer of the standard deviation bands can also be transferred.

Portions of three reports from water testing of pump inlets and exits are provided. This information can be used to estimate the conceptual bias uncertainty for the pressure measurements located near the pump inlets and exits. This information was obtained too late in the performance period include in the report.

LPOTP PUMP PERFORMANCE

FLOW COEFFICIENT

+2 SIGMA
+1 SIGMA
MEAN
-1 SIGMA
-2 SIGMA

$$\phi_N = 73.51827 \frac{Q}{D N A} \quad 0.2124$$

$$A = 3\frac{\pi}{8}(D)^2 = 11.7''$$

Kendall,

We're working to get the rest for you. Call me if you have any questions.

(only)

Rockwell Aerospace
Rocketdyne

Facsimile

To: Kendall Brown		From: Tony Eastland	
Location: U.A.H		Location:	
Fax: 205 890 7205		Fax: 818 586 0572	
Talk: 205 890 7204		Talk: 818 586 0245	
Pages: Lead + 6		Date: 4/18/96.	

HPOTP MAIN PUMP PERFORMANCE

ATLAS VS. CONTURA IMPELLER

FLOW COEFFICIENT

—— ATLAS   ········ CONTURA

+ 2 SIGMA
MEAN
+ 2 SIGMA
- 2 SIGMA
MEAN
- 2 SIGMA

$$\psi_N = \frac{\Delta H}{U_t^2/g} * \frac{1}{0.3878}$$

HEAD COEFFICIENT

$$\psi_N = \psi$$
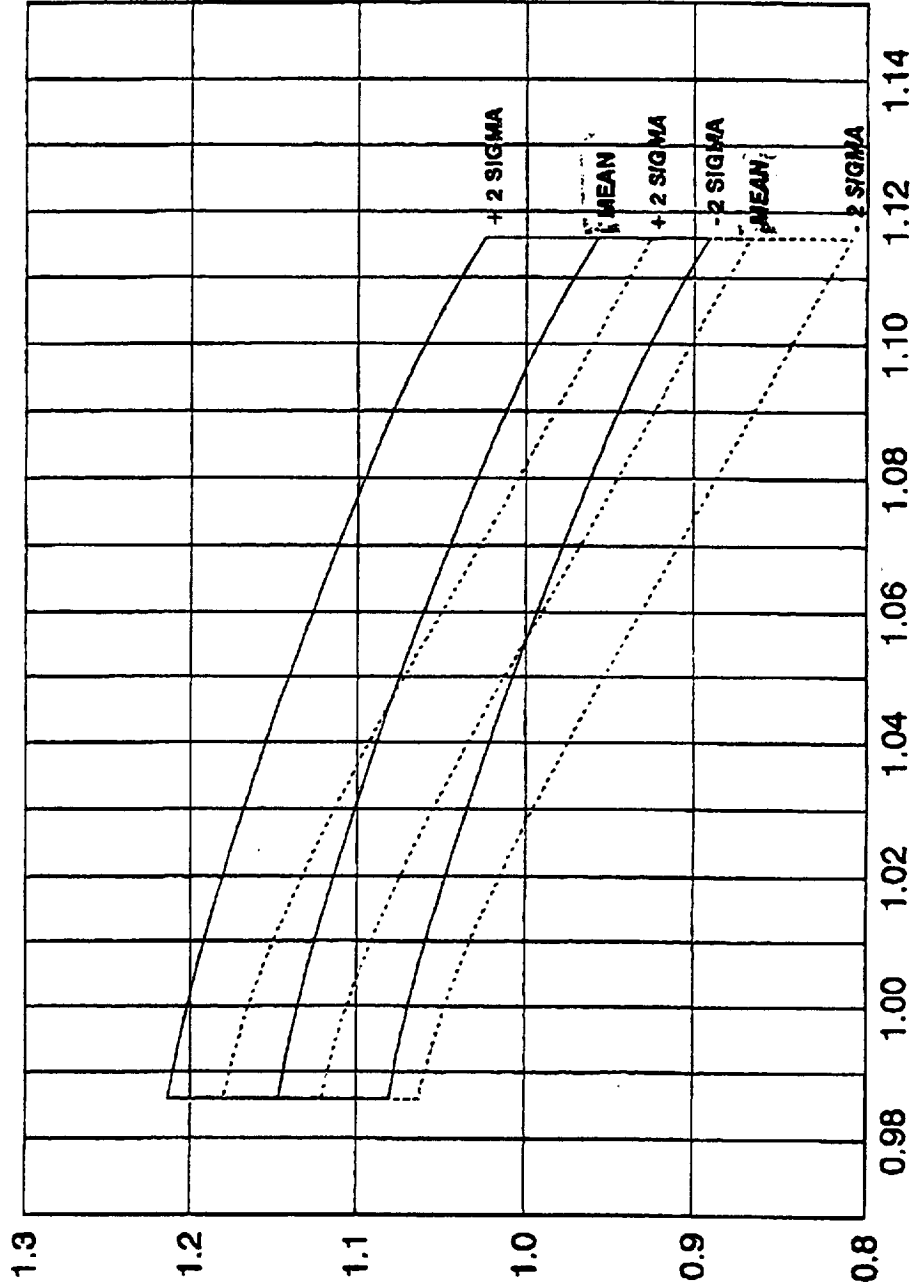
$$\phi_N = 73.51827 * \frac{Q}{DNA} * \frac{1}{0.1308}$$

$$A = 19.621 \ in^2, \ D = 6.63"$$

NORMALIZED HEAD -VS- NORMALIZED FLOW

LPFTP 2030

NORMALIZED FLOW (Thousands)
△ 901-668

NORMALIZED HEAD (Thousands)

+2 SIGMA

NOMINAL

-2 SIGMA
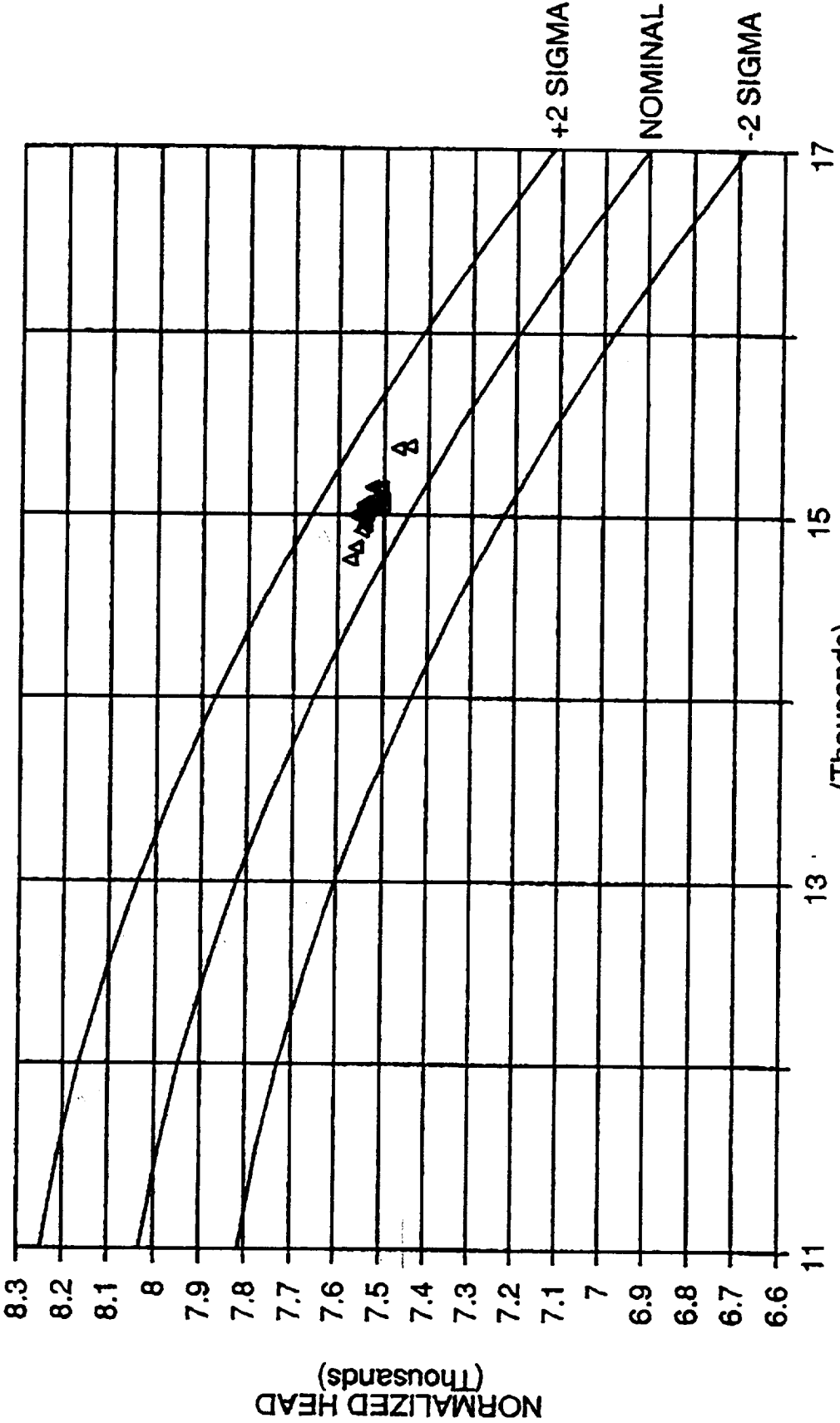
$NORMALIZED\ HEAD = HEAD * \left(\frac{14765}{N}\right)^2$

$NORMALIZED\ FLOW = FLOW * \left(\frac{14765}{N}\right)$

SSME HPFTP PERFORMANCE CURVE
PHASE II

NORMALIZED HEAD=HEAD*(35015^2)/N^2

NORMALIZED FLOW=FLOW*35015/N

+2 SIGMA

MEAN

-2 SIGMA

NORMALIZED FLOW
(Thousands)
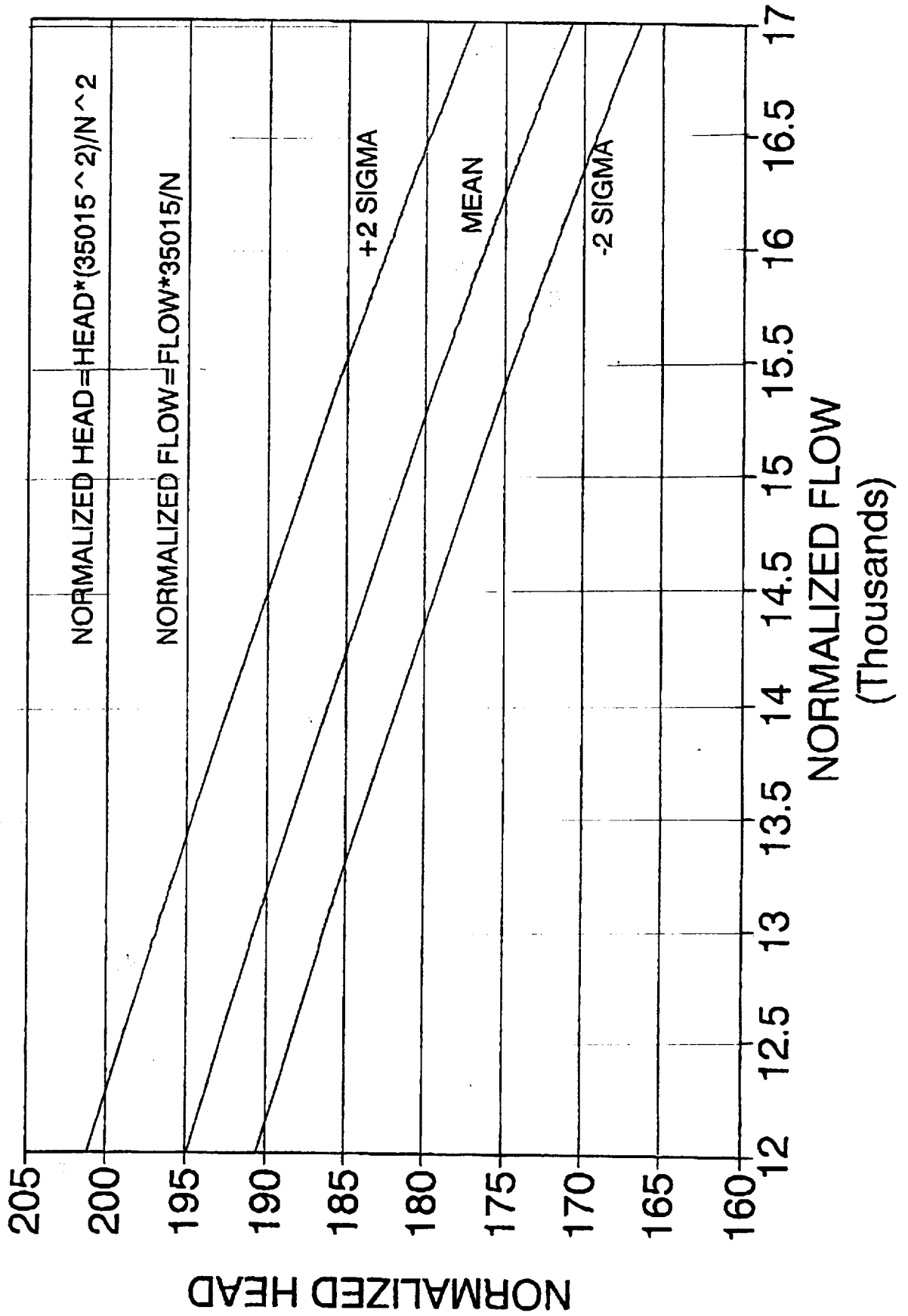
NORMALIZED HEAD

EFFICIENCY -VS- NORMALIZED FLOW

HPFTP 2035R1

+2 SIGMA

-2 SIGMA

HPFTP EFFICIENCY
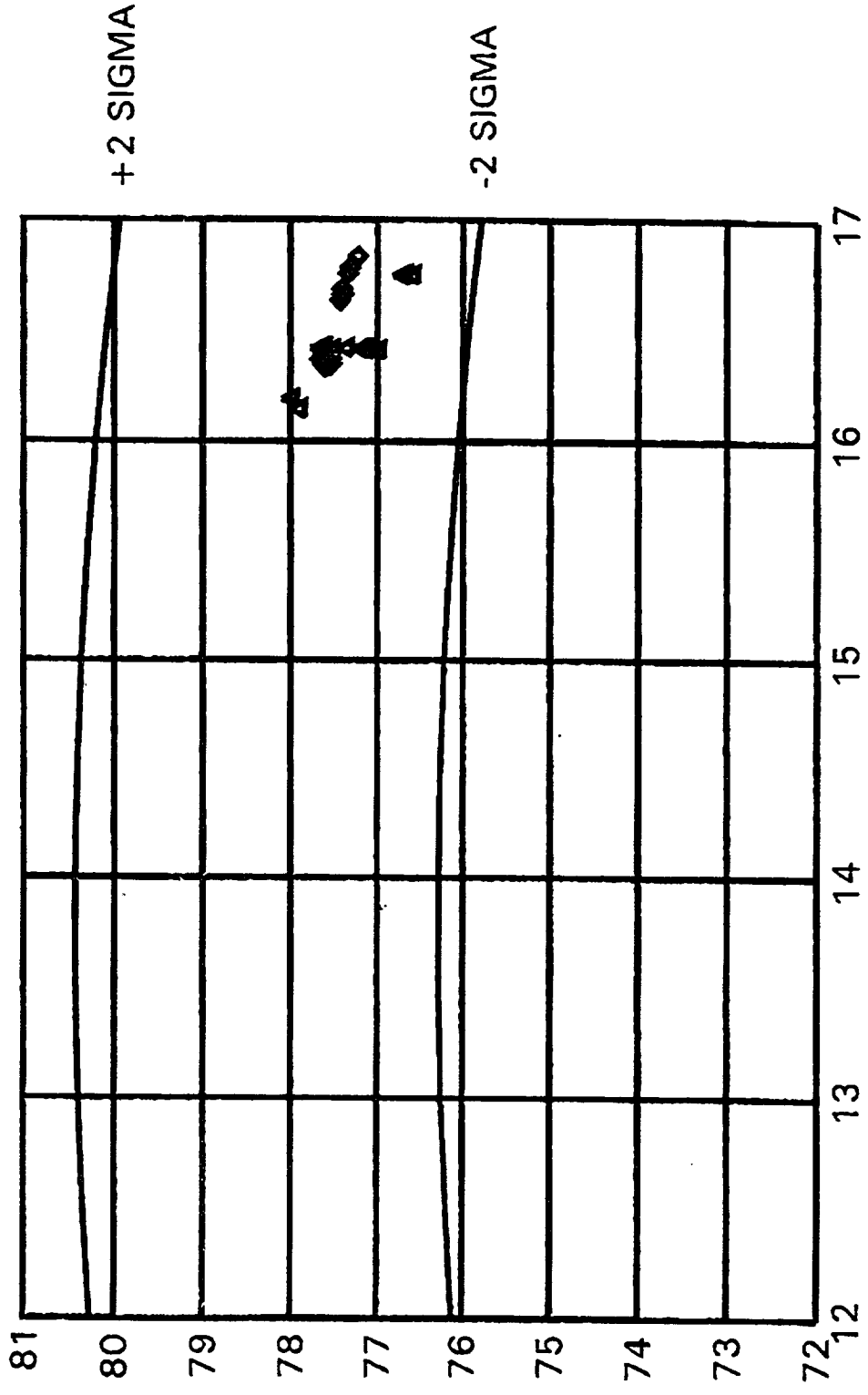
HPFTP NORMALIZED FLOW
(Thousands)

◆ 901-854   ▲ 901-855

◆ 901-854   ▲ 901-855

NORMALIZED HEAD -VS- NORMALIZED FLOW

PHASE II
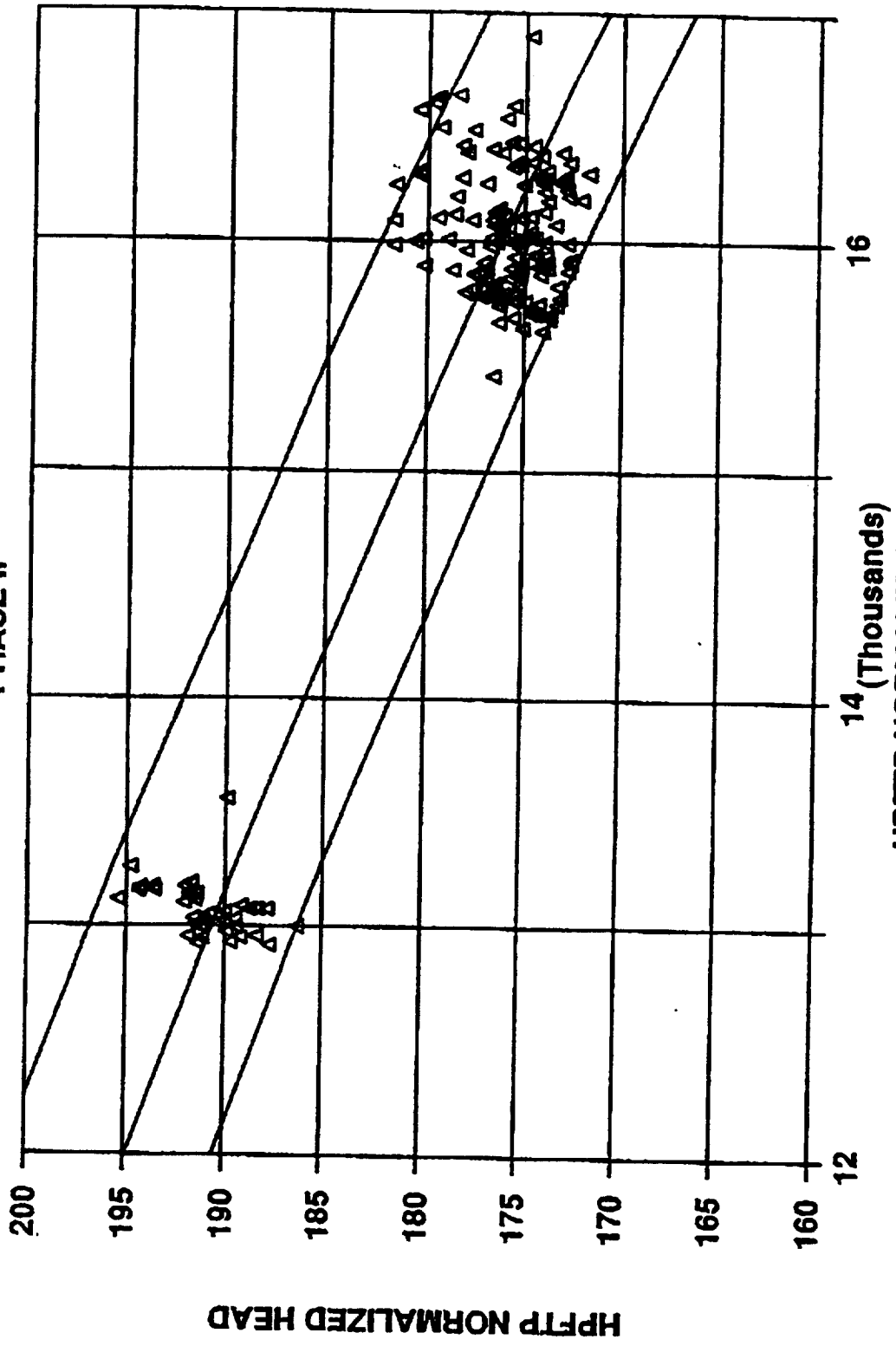
HEAD = 223.2 - 0.6104 (FLOW) - 0.1445 (FLOW)^2

HPFTP NORMALIZED FLOW

+2 SIGMA = 6.18   -2 SIGMA = 4.39

HPFTP NORMALIZED HEAD

SSME HEAD — FLOW COEFFICIENTS

$$\psi_{(PSI)} = \frac{\Delta H \cdot g}{U_T^2} \qquad \frac{\Delta P}{\rho N^2}$$

ΔH = HEAD (ft)

U_T = TIP VEL (ft/sec)

$\quad = \dfrac{D_T \cdot RPM}{229.18}$

D_T = tip diam (in)

$g = 32.172 \ ft/sec^2$

ψ = HEAD COEFFICIENT

$$\varphi_{PHI} = \frac{Q}{A_{eff} \cdot U_T} \cdot \frac{144}{448.83}$$

Q = INLET FLOW (GPM)

U_T = TIP VEL (ft/sec)

A_{eff} = effective Area (in²)

φ = flow COEFFICIENT.

	LPFTP	HPFTP	LPOTP	HPOTP	PBP
A_{eff} (in²)	26.50	15.30	33.00	19.621	3.927
D_T (in)	12.00	12.00	11.72	6.85	5.00

Tony M. Chanko
4/30/96
(ROCKETDYNE)

LEAD + 4	**ROCKETDYNE - CANOGA PARK** FAX 818-586-9644	DATE: 5/9/96

TO: Kendall Brown
UAH Propulsion Research Center

FROM: Tony Chanko
Advanced Rotating Machinery

REMARKS: Kendall - Here are torque maps that I asked our systems people to generate with ±2σ spread - The maps are based on Engine Flight Data. I hope this is helpful. If you need more info or have any questions let me know -

Tony C
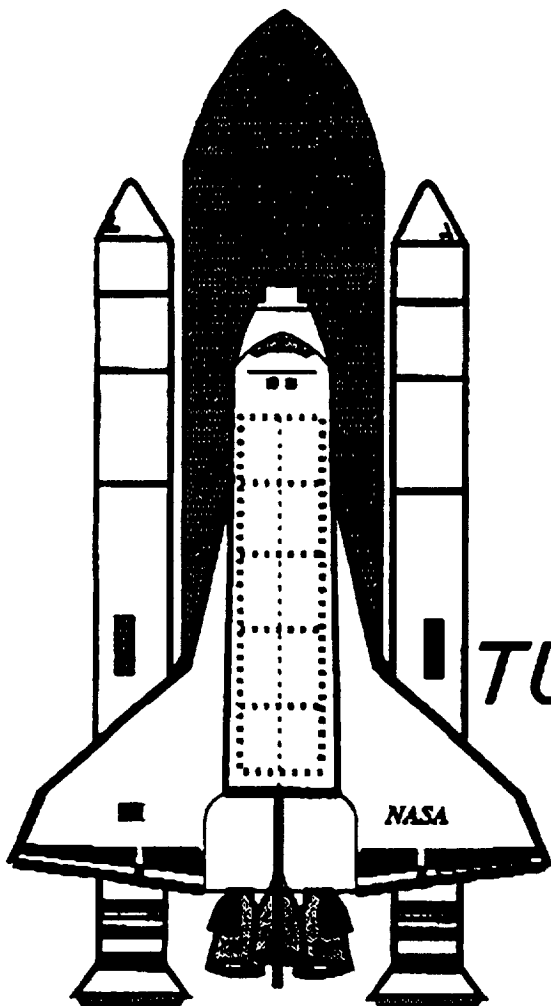
SSME

LOX AND FUEL

TURBOMACHINERY

Y:\CHARTS\FAX\DR

HPFP TORQUE VERSUS HPFP FLOW COEFFICIENT
(ANCHORED TO PHASE II 1B ENGINE FLIGHT SET - VERSION: PBM95A)
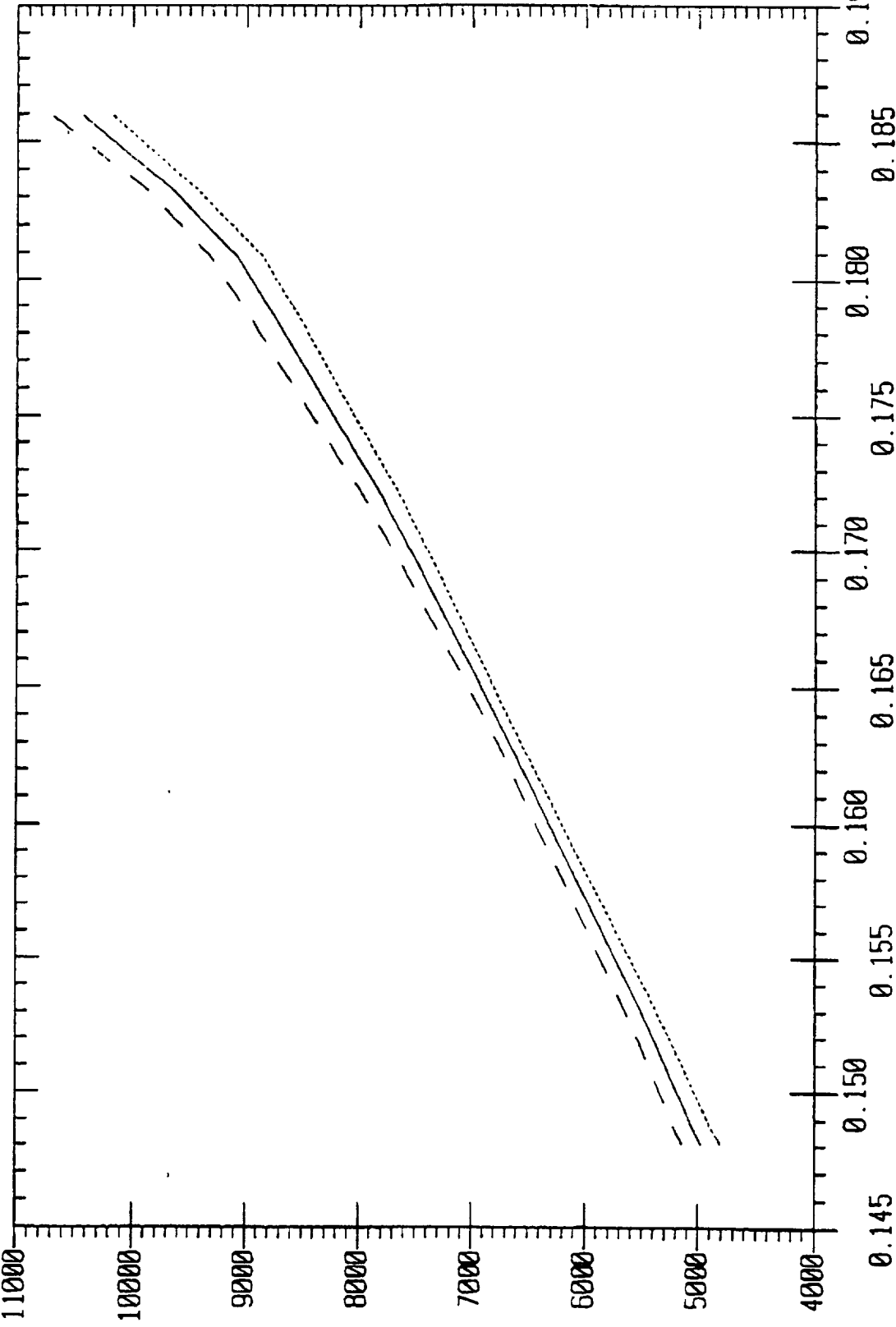
DATA FILE = TMP:TORQHPFP.AVP

HPFP Flow Coef (4428)

ROCKETDYNE
SSME SYSTEMS -- TECH SUPPORT
VAP VERSION: v3.7.0
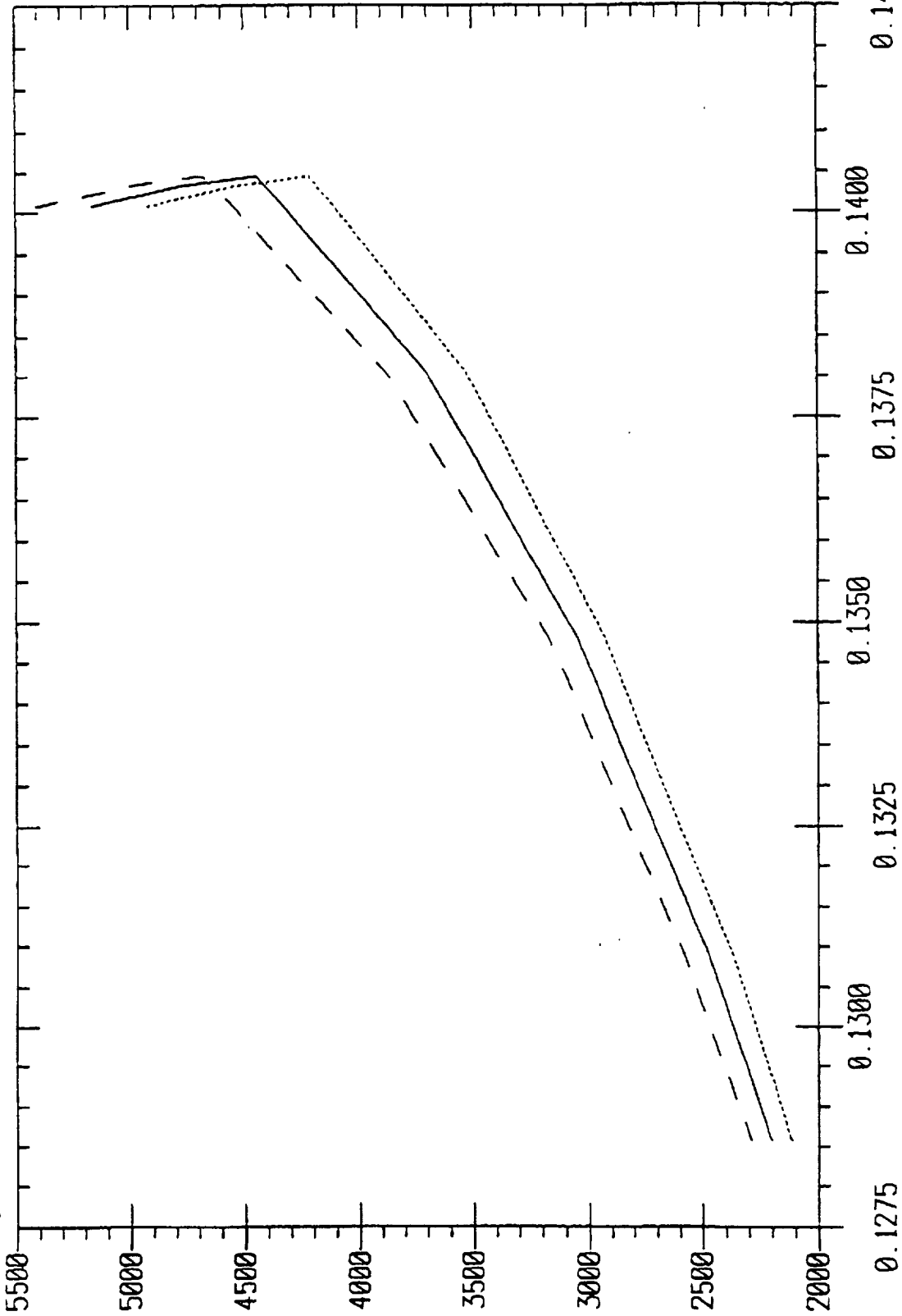96/05/09 09:46:18 DAVID

LPFP TORQUE VERSUS LPFP FLOW COEFFICIENT
(ANCHORED TO PHASE II 18 ENGINE FLIGHT SET - VERSION: PBM95A)

DATA FILE = TMP:TORQLPFP.RVP

LPFT Torque
— + 2 Sigma
‥ - 2 Sigma

{4604}
{3001}
{3002}
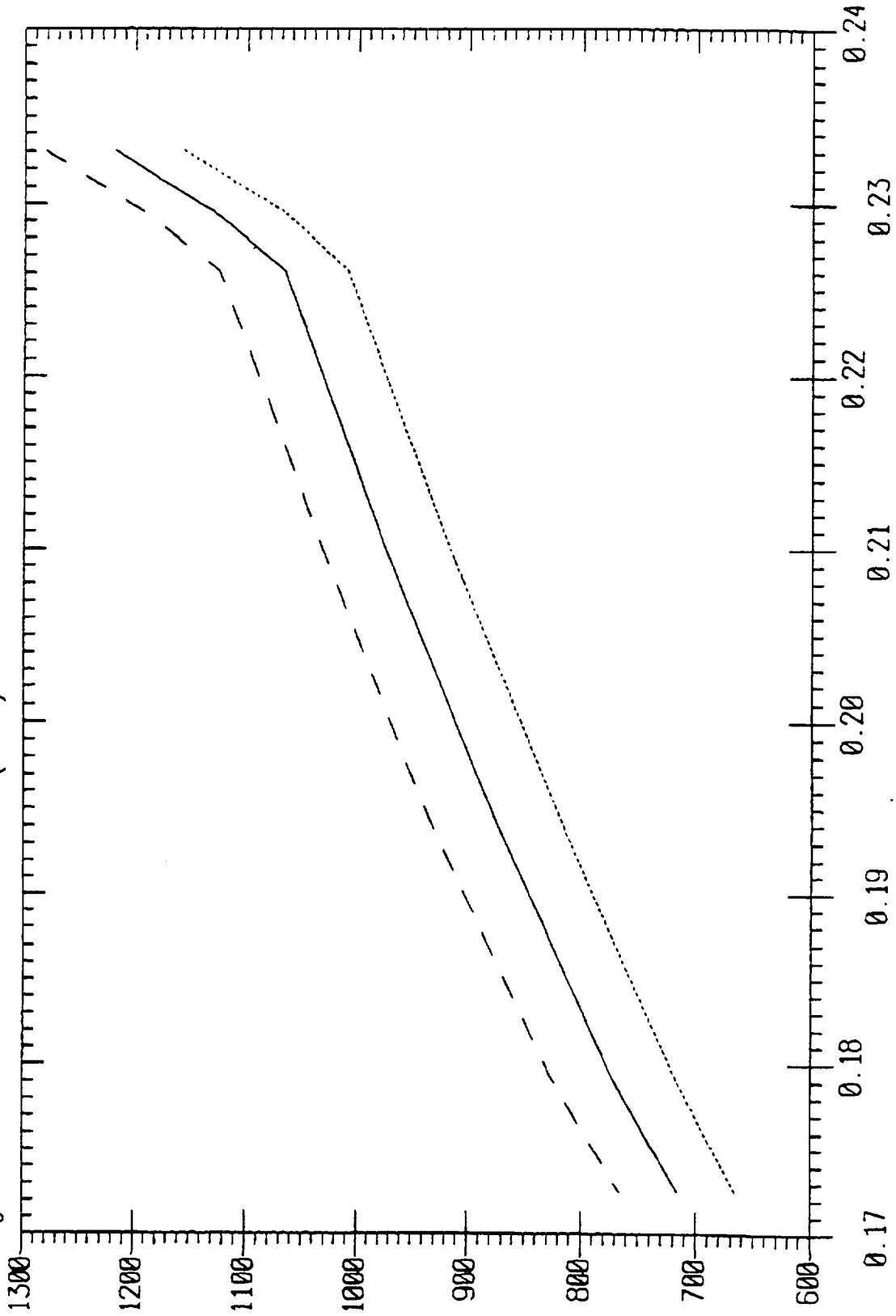
LPFP Flow Coef (4427)

0.17   0.18   0.19   0.20   0.21   0.22   0.23   0.24

600   700   800   900   1000   1100   1200   1300

ROCKETDYNE
SSME SYSTEMS -- TECH SUPPORT
VAP VERSION: v3.7.0
96/05/09 09:46:18 DAVIDSON

LPOP TORQUE VERSUS LPOP FLOW COEFFICIENT
(ANCHORED TO BABBASE 18 ENGINE FLIGHT SET - VERSION: PBM95A)

LPOT Torque
— + 2 Sigma   (4606)
— - 2 Sigma   (3001)
                (3002)
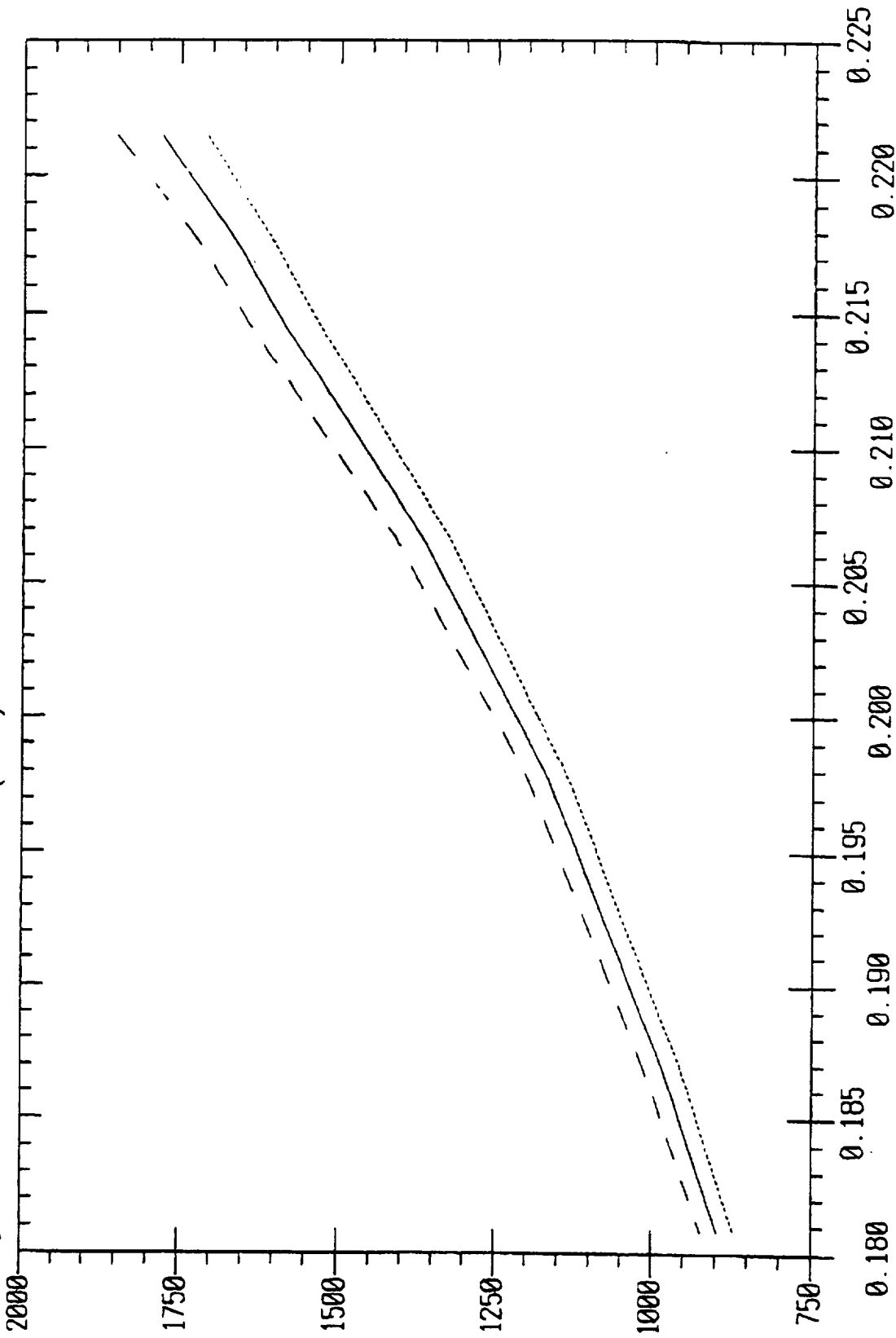
LPOP Flow Coef (4429)

DATA FILE = '   .TORQLPOP.RVP'

ROCKETDYNE
SSME SYSTEMS -- TECH SUPPORT
VRP VERSION: v3.7.0
96/05/09 09:32:04 DAVIDSON

HPOP TORQUE VERSUS HPOP FLOW COEFFICIENT
(ANCHORED TO PHASE II 18 ENGINE FLIGHT SET - VERSION: PBMJ5A)

DATA FILE = TMP:TORQHPOP.RVP

HPOP Flow Coef (4430)

ROCKETDYNE
SSME SYSTEMS -- TECH SUPPORT
VAP VERSION: v3.7.0
96/05/09 09:46:18 DAVIDSON

——— HPOT Torque (4607)
— — + 2 Sigma (3001)
.... - 2 Sigma (3002)

TOTAL & STATIC PRESSURE
DISTRIBUTIONS FOR ATD
HPFTP INLET

WJB
5/15/96

FR-20599
30 NOVEMBER 1988

SSME ALTERNATE TURBOPUMP DEVELOPMENT PROGRAM

HPFTP WATER FLOW MODEL TEST REPORT

Prepared Under
NASA Contract NAS8-36801
DRL Sequence No. SE12

Prepared for
George C. Marshall Space Flight Center
National Aeronautics and Space Administration
Marshall Space Flight Center, AL 35812

Prepared by
Pratt & Whitney
P.O. Box 109600
West Palm Beach, FL 33410-9600

Approved by:

H.C. Shubert

W.C. Shubert
ATD Project Manager

UNITED TECHNOLOGIES PRATT & WHITNEY

- Static Pressure
- Total Pressure
- Static Pressure Differentials
- Total Pressure Differentials
- Flow Angles

The locations of these probes is indicated in figure A5. There was a number of specialized probes implemented in the model; these probes are described below.

Total Pressure Kiel Probes

INSTR. RING.

Total pressure kiel probes are used at three locations. These probes are located at the inlet to the model, at the leading edge of selected inlet guide vanes, and for the dynamic test at the impeller discharge (See figures C6, C7 and C8, respectively). The total pressure probes at the model inlet were rotated from 0 degrees to +25.7, +52.4 and −25.7 to obtain the maximum number of points allowed by the model geometry of the flow profile exiting the SSME fuel supply duct.

Wedge Probes

Wedge probes are direction-sensing probes; as the name implies these probes have a wedge or triangular shaped head. There is a pressure port on each side of the wedge near the trailing edge and a total pressure port at the leading edge. The probe can be rotated about an axis perpendicular to the wedge allowing its alignment with the flow; when the pressure differential across the ports on the sides of the probe is zero the probe is aligned with the flow and the flow swirl angle can be read directly of the probe housing. Wedge probes were located slightly forward of the inlet guide vane leading edges between selected vane positions and were removed when not in use. The wedge probes provided the inlet volute discharge angle to verify inlet guide vane angle of attack.

Cobra Probes

Like the wedge probes the Cobras were used to measure flow angle and total pressure. These instruments were located 90 degrees apart with three probes across the span of the IGV discharge annulus in close proximity to the impeller inlet plane during the static induced test. Although wedge probes are a more accurate flow angle measurement instrument they require rotation capability and could not be accommodated in this location; angle is measured using the curves obtained from probe calibration. Calibration of the cobra probes used in these tests was performed at MSFC prior to the commencement of testing.

TEST DATA

Raw data and online reduced data is archived in the NASA network AFAS database at DBS1: [DBS.WFF.0034] for the static test and at DBS1: [DBS.WFF.0035] for the dynamic test. This data is also available at P&W on the interdivisional data exchange system.
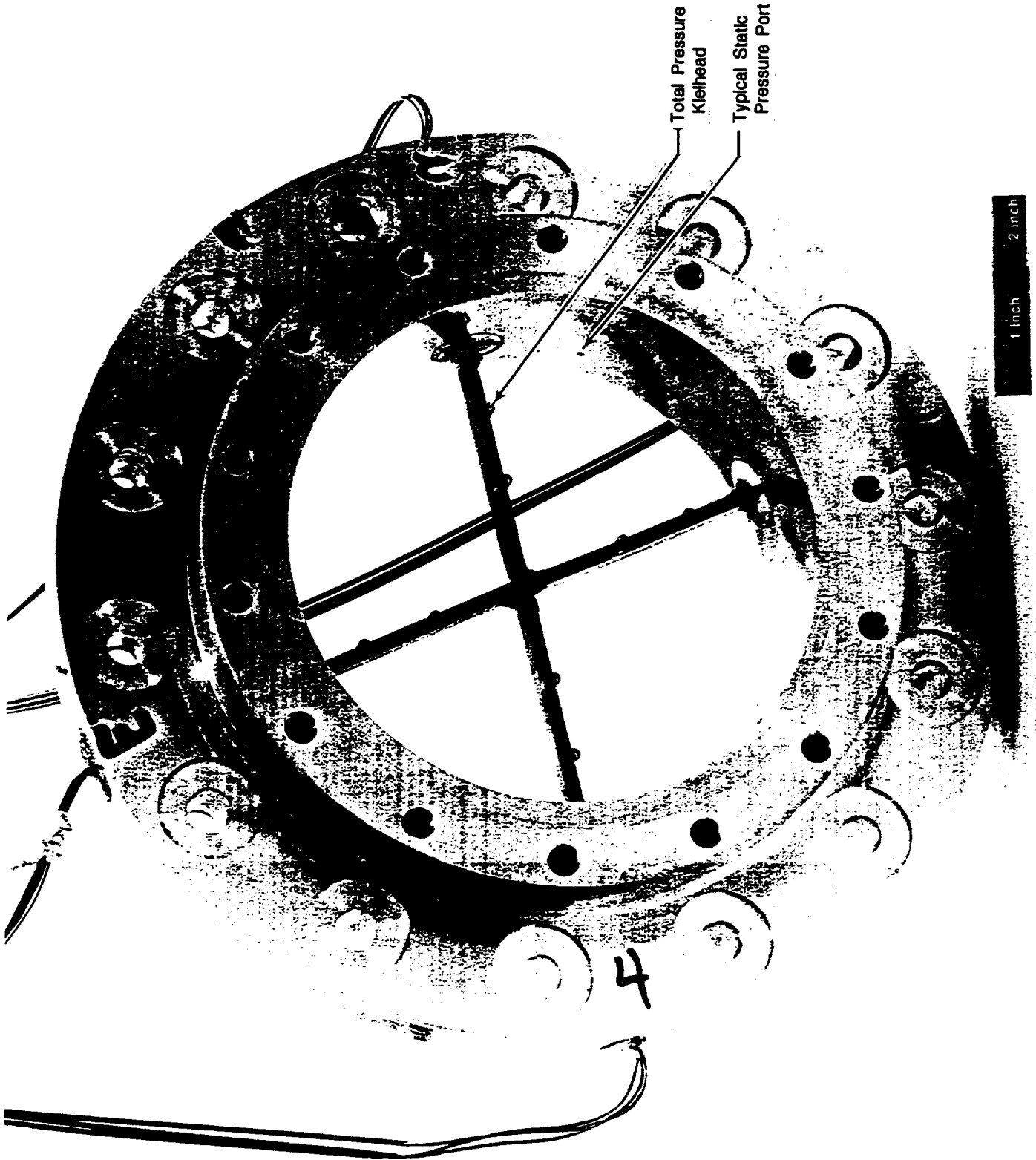
4

Total Pressure Kielhead

Typical Static Pressure Port

1 inch   2 inch

ure C6. Instrumented Inlet Ring

FD

Several differences can be observed from reviewing the two test procedures for static and dynamic tests. First it will be noted that instructions to clean the inlet screens are specified. Although, this was common practice during the static test it became critical the active test; as testing was performed debris would build up in screens and eventually produce a condition were inlet pressure would be lost during a data point (the Fluid Wafer Switches required aprox. 2 min. to scan all channels) resulting in an unacceptable non-steady state condition. Also different from the static procedure is the aforementioned valve callouts affected by the new flowpath required to maintain the highest possible inlet pressures. The addition of an oil cooled bearing box to the system resulting in the addition of instructions to check oil levels as a maintenance function as well as a set of instructions to ensure oil tank heat exchanger was operating. The attention given to the bleed procedure has also been enhanced since the hook-up to the transducer panel was not as straight forward as during the static test.

Results and Discussion

Figure B-1 shows the total and wall static pressure profiles versus circumferential position measured at the inlet flange. The instrumentation ring was clocked around the circumference of the flange to map the incoming flowfield. Total pressure measurements were taken at three different radial locations, each of which displayed similar trends, indicating peak pressures at 270 degrees and minimum pressures at 90 degrees circumferentially. The turning bend in the SSME duct upstream of the inlet flange, producing the inlet profile shown, results in higher flowrate and total pressure toward the forward side of the inlet duct and lower flowrate and pressure on the rear side near the inner wall of the bend. Radially, the data shows the lowest pressures near the center of the inlet flange with pressures increasing radially outward.

The wall static pressures were reasonably uniform around the perimeter of the inlet flange. A calculation of the resultant velocity profiles from the data is presented in Figure B-2 at three radial locations around the circumference of the inlet flange. Significant inlet flow distortion is indicated entering the model, with variation between maximum and minimum velocities of up to approximately 45 percent. A subsequent test to assess the impact of the distortion on model performance was attempted employing flow straighteners upstream of the inlet flange. Negligible changes in the inlet profile forced by the inlet duct were affected however, as indicated by the inlet instrumentation measurements.

Figure B-3 shows the top, left, and right side wall static pressures around the circumference of the volute. A diffuser section was employed in the design just downstream of the inlet flange to initially reduce the high incoming velocity from the inlet duct. The resultant diffusion is apparent from the static pressure increase relative to inlet flange values. Static pressures continue to increase along the outer wall to approximately 210 degrees circumferential location. Aft of the diffuser section the volute was designed for a constant angular momentum flowfield, which produces a gradual acceleration of the flowstreams as streamline radius is reduced. The acceleration of the flowfield, evidenced by reduced static pressures, is likewise apparent from the data through the remainder of the inlet scroll. No flow anomalies or flow separations were observed within the volute section either by test data or flow visualization. Overall the flowfield appeared steady and reasonably well behaved.

SSME/ATD HPFTP INLET WATER RIG
INLET FLANGE TOTAL AND WALL STATIC PRESSURES

RADIUS - 1.061"
RADIUS - 1.838"
RADIUS - 2.373"
RADIUS - 2.600"

NOTE: WITHOUT FLOW STRAIGHTENER
FLOWRATE = 1500 GPM

TOTAL PRESSURES

WALL STATIC PRESSURES
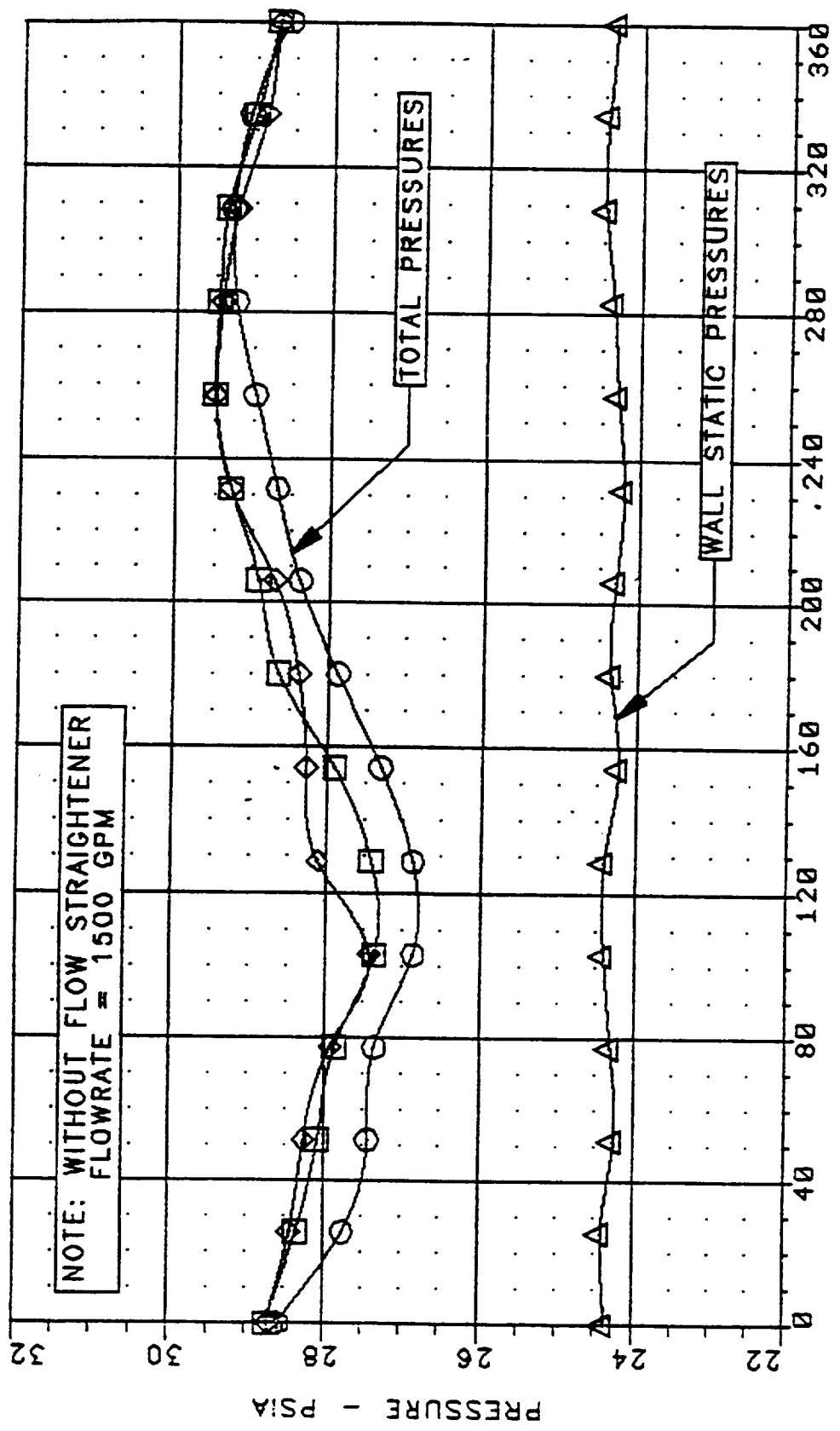
CIRCUMFERENTIAL POSITION - DEGREES

PRESSURE - PSIA

FIG

R20599/1

SSME/ATD HPFTP INLET WATER RIG
INLET FLANGE VELOCITY PROFILES

○ RADIUS = 1.061"
□ RADIUS = 1.838"
◇ RADIUS = 2.373"
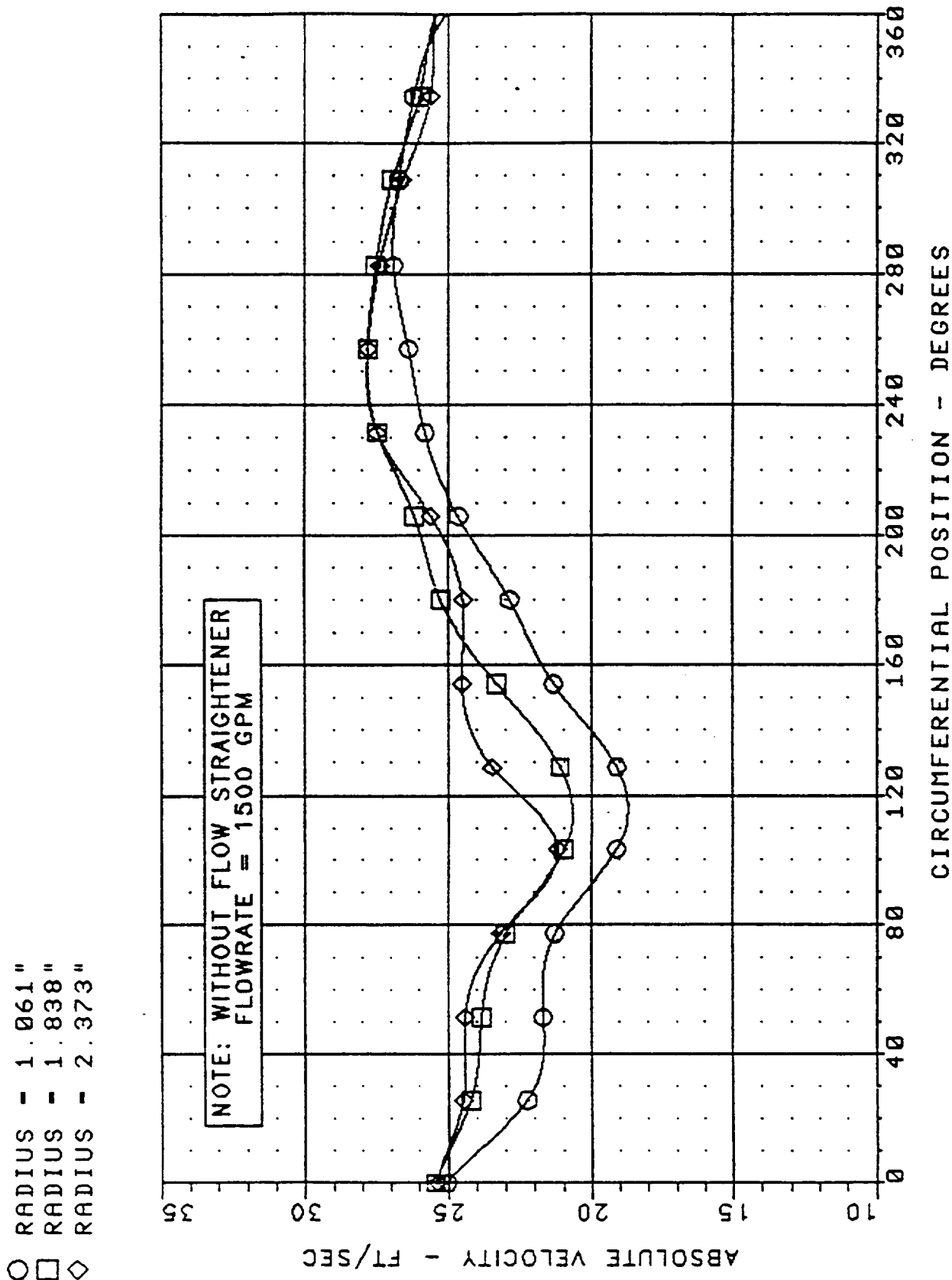
FIG B-2

32

TOTAL PRESSURE & STATIC PRESSURE
DISTRIBUTIONS FOR ATD HPOTP
INLET

FR-19847-3

WJB
5/15/96

SSME ALTERNATE TURBOPUMP
DEVELOPMENT PROGRAM

HPOTP WATER FLOW MODEL
TEST REPORT

DVS DR NO. 3.1.2.2.6.1, VM NO. 4.1.3.2.1.1B

Prepared Under
NASA Contract NAS8-36801
DRL Sequence No. SE12
WBS No. 1.5.1.2

Prepared for
George C. Marshall Space Flight Center
National Aeronautics and Space Administration
Marshall Sparce Flight Center, AL 35812

Prepared by
Pratt & Whitney
P. O. Box 109600
West Palm Beach, FL 33410-9600

Approved by:

W. C. Shubert
ATD Project Manager

UNITED
TECHNOLOGIES
PRATT&WHITNEY

R19847/1

Printed in the United States of America

SECTION III
INSTRUMENTATION

To quantify the flow phenomena observed in the Alternate Turbopump Development inlet flow models, a variety of probes and ports were used. The types of measurements obtained were as follows:

- Static pressure
- Total pressure
- Static pressure differentials
- Total pressure differentials
- Flow angles.

The locations of these probes are indicated in Figure III-1. The number of specialized probes implemented in the model are described below.

A. TOTAL PRESSURE KIEL PROBES

MEAS'S

Total pressure kiel probes are used at three locations. These probes are located at the inlet to the model (Figure III-2), at the leading edge (LE) of selected inlet guide vanes (IGVs) (Figure I-3), and for the dynamic test at the inducer discharge. The total pressure probes at the model inlet were rotated from 0 to +30 degrees, and -30 degrees to obtain an adequate number of points to map the flow profile exiting the Space Shuttle Main Engine LOX supply duct. During the dynamic test, the inducer total pressure discharge ring was also used to map the flowfield at three span-wise locations every 30 degrees.
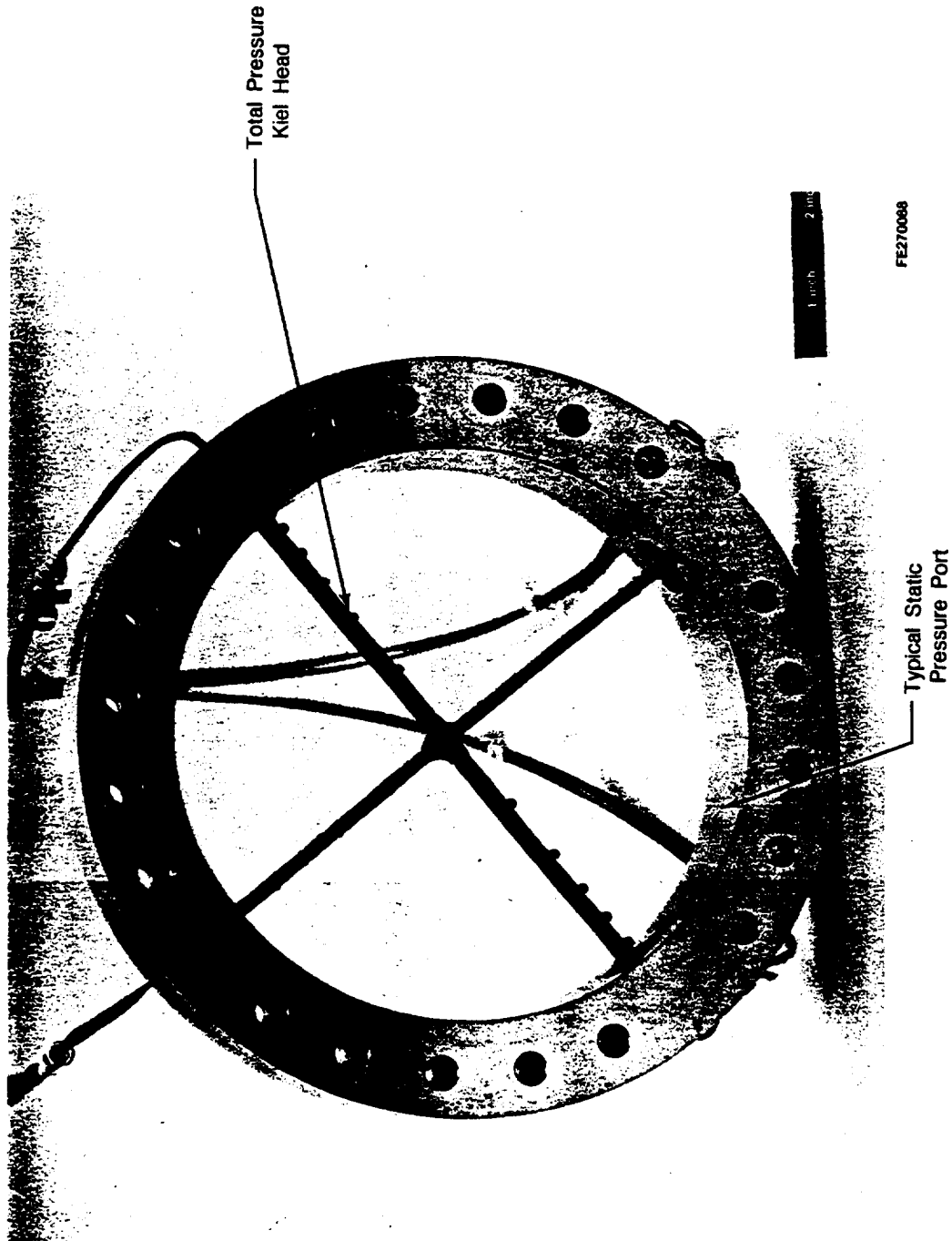
B. WEDGE PROBES

Wedge probes are direction-sensing probes. These probes have a wedge or triangular shaped head. There is a pressure port on each side of the wedge near the trailing edge (TE) and a total pressure port at the LE. The probe can be rotated about an axis perpendicular to the wedge, allowing its alignment with the flow. When the pressure differential across the ports on the sides of the probe is zero, the probe is aligned with the flow. Wedge probes were located slightly forward of the IGV LE between selected vane positions and were removed when not in use. The wedge probes provided the inlet volute discharge angle to verify IGV angle-of-attack.

C. WAKE RAKES

A wake rake is a series of total pressure impact tubes, in close proximity, used to measure the total pressure profile at the TE of a fixed body in a flow. These rakes were used in the model behind one IGV on each side of the volute to examine the characteristics of the total pressure profile at the IGV TE.

D. COBRA PROBES

Like the wedge probes, the cobras were used to measure flow angle and total pressure. These instruments were located 90 degrees apart with three probes across the span of the IGV discharge annulus in close proximity to the inducer inlet plane during the static test. Although wedge probes are a more accurate flow angle measurement instrument, they require rotation capability and cannot be accommodated in this location; angle is measured using the curves obtained from probe calibration. Calibration of the cobra probes used in these tests was performed at Marshall Space Flight Center before testing.

MEAS'S

AVL 358832

Figure III-1. High-Pressure Inlet H₂O Rig Instrumentation

III-2

R19847/3

Total Pressure
Kiel Head

Typical Static
Pressure Port

FE270088

FD 365663

Figure III-2. Instrumented Inlet Ring

(INLET INSTAL. RING FOR AFT)
(HPOTP WATER FLOW RIG)

SECTION V
TEST DATA AND RESULTS

(handwritten: USE V-2)

Figure V-1 shows the total pressure and wall static pressure profiles measured at the inlet flange versus circumferential position. The instrumentation ring was clocked around the circumference of the inlet flange to map the incoming flowfield. Total pressure measurements were taken at five different radial locations, each of which displayed similar trends. To investigate the impact of the bypass duct and the inlet bushing (employed to isolate vibrations from the inlet housing) on measured inlet profiles, a subsequent test was conducted with the model and bushing removed and straight discharge duct installed. The results indicated negligible effects on total pressures, but apparent influences from the inlet bushing on wall static readings, as well as bypass duct influences on the side opposite the inlet model (see Figure V-2). The decrease in total pressure on the model side (0 to 180 degrees) is due to losses and flow disturbances from the Pogo suppressor flange. Figure V-2 is considered to be most representative of the High-Pressure Oxidizer Turbopump (HPOTP) inlet duct static pressures. Significant inlet duct flow distortion entering the model is indicated by the data. Figure V-3 shows the velocity profiles derived from the data at varied circumferential and radial position, showing variations between maximum and minimum velocities of up to approximately 60 percent.

(handwritten left margin: INLET FLANGE RESULTS)
(handwritten right margin: DATA PLOT ON V-2)

Figure V-4 shows the front, top, and rear volute wall static pressure distributions at varied circumferential locations around both sides of the volute. Rapid acceleration and diffusion is apparent around the volute corners along the top wall, with no indication of flow separation. The measured data indicates a moderately uniform pressure distribution along the walls on both sides of the volute from the inlet to the cusp area. A moderate acceleration of flow along the side walls near the cusp, and deceleration along the top wall, are apparent within the vane channels adjoining the cusp.

Figures V-5 through V-7 show a comparison of the static pressures on each half of the volute for each wall. The profiles are similar on both sides along each wall with slightly higher pressures measured on the left half.

Flow visualization tests revealed no flow separations or anomalies within the volute except for a twin vortex formed off the inlet flow splitter that separated the test model from the bypass duct. The vortices carried into the fourth and fifth vane channels up from the cusp on both sides of the volute where they rapidly dissipated. No evidence of the vortices could be observed downstream of the inlet guide vanes (IGVs) within the discharge annulus.

Figure V-8 shows the spanwise total pressures at the leading edge (LE) of 4 of the 21 turning vanes. The pressures were reasonably uniform across the span for all four vanes, with slightly lower values for the two vanes located at 70 degrees from the top of the volute. A wedge probe was inserted upstream of two vanes on each side of the volute and traversed spanwise across the vane LE to measure the inlet swirl angle. Figure V-9 shows the measured swirl angles compared to predicted values around the volute calculated from a three-dimensional potential flow analysis. The measured swirl angles compare favorably with the predicted values as shown.
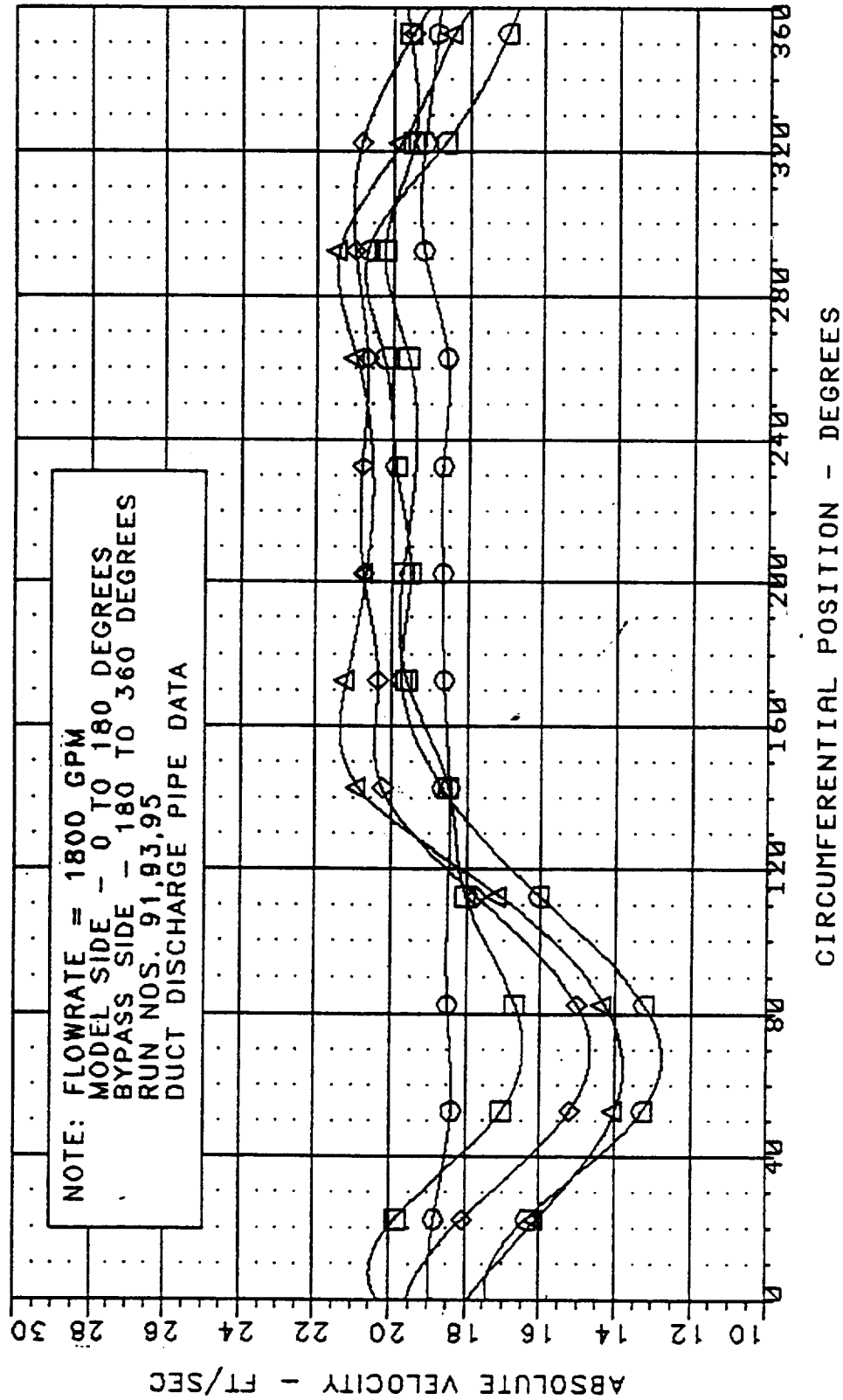
R19847/7
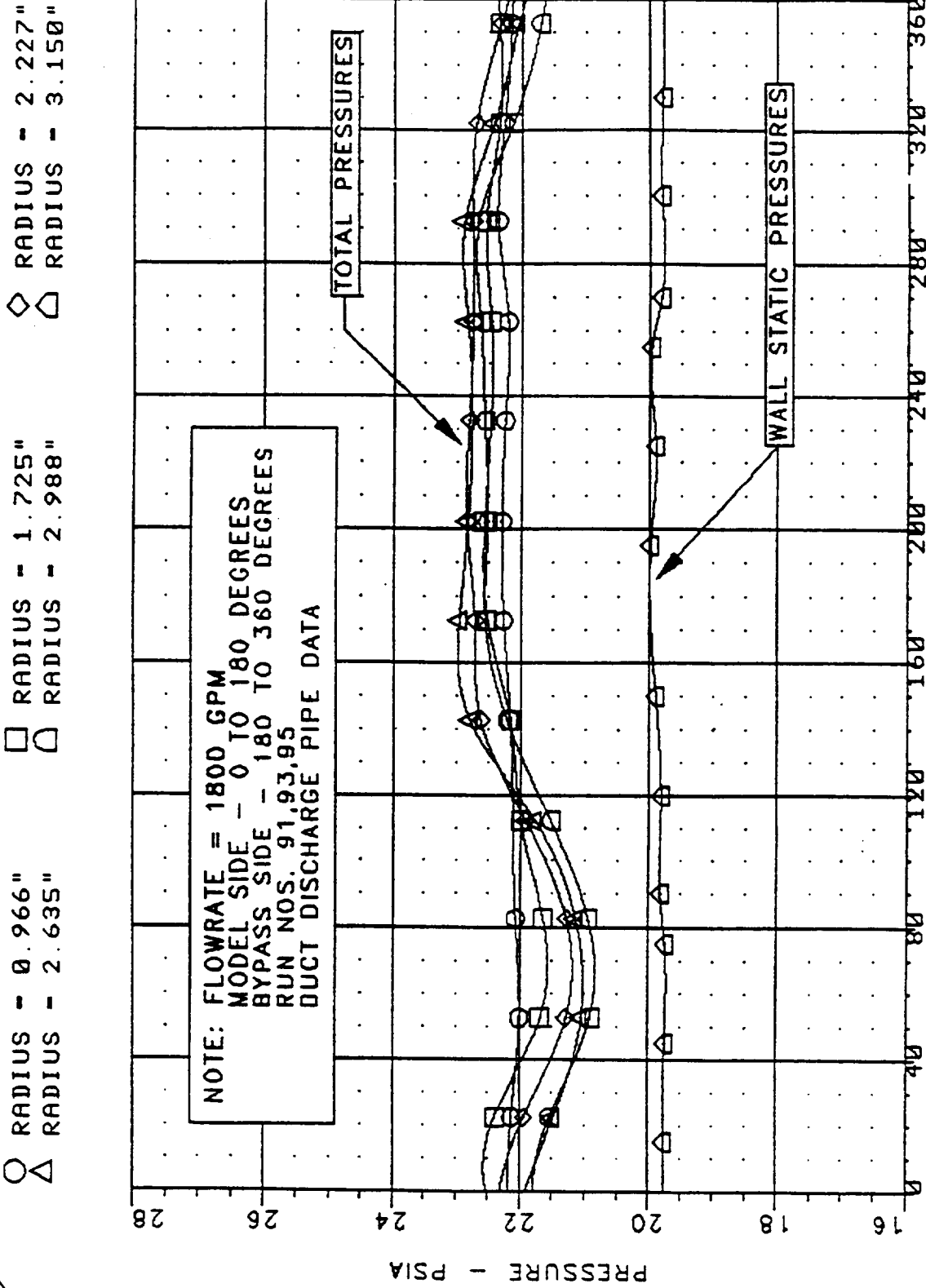
Figure V-2. Inlet Water Rig — Inlet Flange Total and Wall Static Pressures (View 2)

FD 384165

Figure V-3. Inlet Water Rig — Inlet Flange Velocity Profiles

FD 384186

R19847/7

SSME ALTERNATE TURBOPUMP DEVELOPMENT PROGRAM (HPOTP & ~~HPFTP~~)

HPOTP

MSFC RADIAL SIDELOAD RIG TESTING TEST RESULTS AND CONCLUSIONS DVS'S 29 & 30, D.R. 3.1.2.3.4.1 (NO V.M. SECTION SPECIFIED)
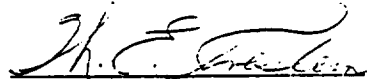
JULY 1991

Prepared under
NASA Contract NAS8-36801
DRL Sequence No. SE-12
WBS No. 1.5.1.2

Prepared for
George C. Marshall Space Flight Center
National Aeronautics and Space Administration
Marshall Space Flight Center, Al 35812

Prepared by
Pratt & Whitney
P. O. Box 109600
West Palm Beach, FL 33410-9600

Approved by:

W. E. Creslein
ATD Project Manager

UNITED TECHNOLOGIES PRATT&WHITNEY

pressure. The higher static pressure was the result of flow diffusing through the lower half of the nozzle. As will be shown later in Figure 8.19 most of the flow was being pushed out through the upper half of the nozzle. The pressure profiles were similar for all three Q/N's, but with slightly more circumferential pressure variation with increasing flows. At higher flows the main discharge leg includes more of the cutwater channel flow and more positive incidence on the splitter.
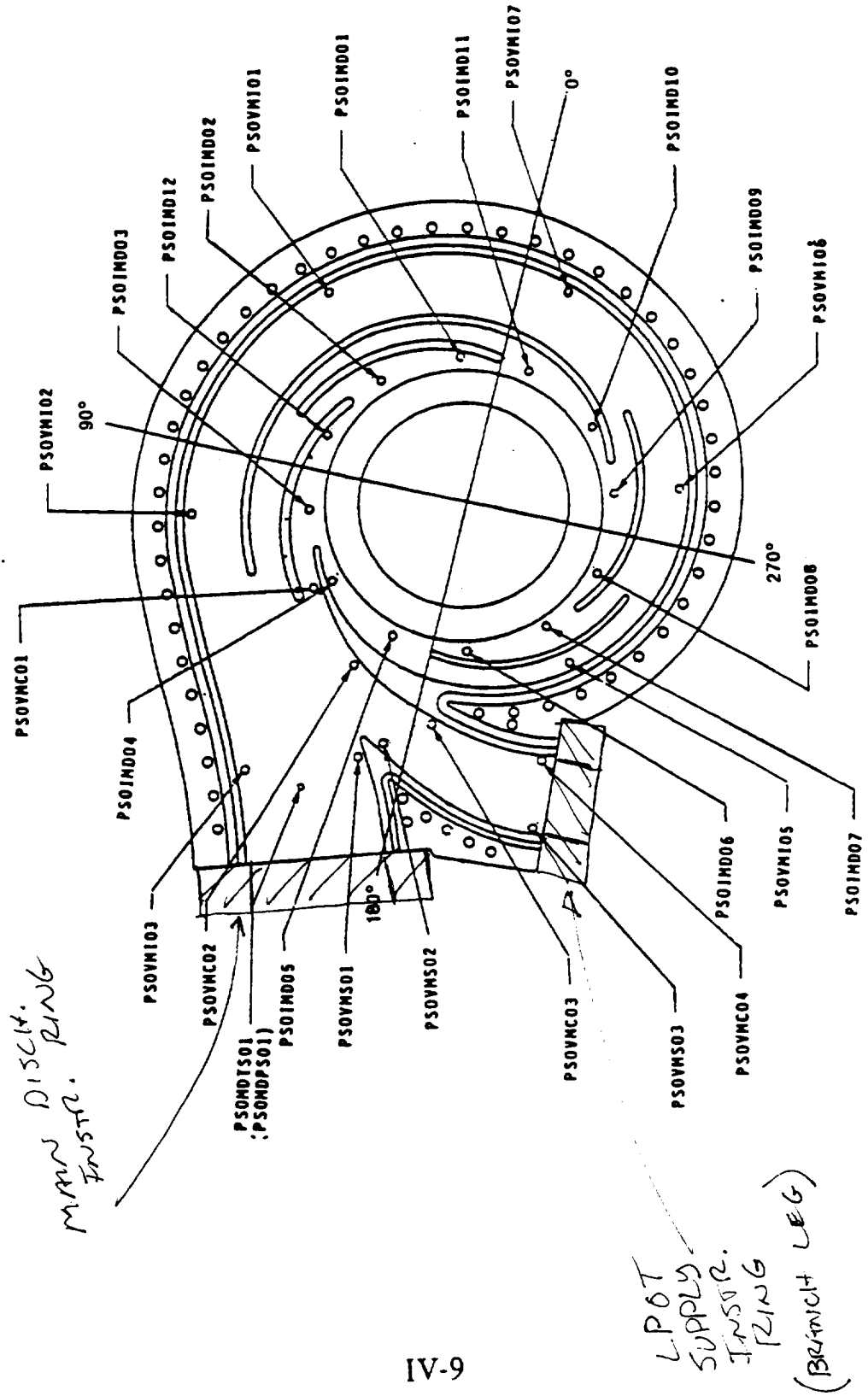
The inner and outer walls along the branch leg were instrumented to measure the amount of diffusion through the branch leg. Two static pressure taps were positioned along the outer wall and four pressure taps along the inner wall. The two outer wall taps were located at the entrance and exit of the branch leg. The four inner wall taps were located upstream of the entrance, at the entrance, part way through, and at the exit of the branch leg. Unfortunately, the static tap at the exit of the branch leg along the inner wall, where a majority of the diffusion would occur was plugged. Therefore the measurement of the complete diffusion through the branch leg along the inner wall was unobtainable. Figure 8.18 shows the static pressure along the inner and outer wall for three different Q/N's. A moderate amount of diffusion takes place along the outer wall. Once inside the branch leg, the inner wall shows a greater amount of diffusion as expected. The calculated wall loadings for design and off-design flow conditions were low. There were no signs of any flow separation on either wall.

The trends for the off-design Q/N's were very similar, although there was more diffusion along the inner wall and slightly less diffusion along the outer wall as less flow traveled through the branch leg. Higher inlet Q/N's resulted in slightly lower flows through the branch discharge leg, due to the engine cycle flow split requirements. Also at higher Q/N's less of the cutwater channel flow traveled through the branch leg, resulting in higher positive incidence angles on the main - branch leg splitter.

The discharge flanges of the main and branch legs were instrumented with a keil probe ring. Each ring contained four keil probes 90 degrees apart, to measure the total pressure profile exiting into the downstream ducting. Plotted in Figure 8.19 are the total pressures versus circumferential position, for the main and branch leg discharge flanges at the design Q/N. Approximately 84 percent of the total flow through the pump passes through the main discharge leg at the design point. The outer wall for the main discharge flange, opposite from the splitter, was located at 270 degrees. The outer wall for the branch discharge flange was located at 60 degrees. The total pressure profile at the branch leg discharge flange was quite uniform. The main discharge flange showed higher pressures on the outside wall away from the splitter. The measured profile was consistent with test data of similarly designed volutes which displayed higher total pressures and flows pushed out toward the outer wall. The total pressures measured at the branch leg discharge were slightly higher than those measured at the main leg discharge.

HPOTP MAIN COLLECTOR

ATD

Figure 4.8

g15468

MAIN DISCHARGE – TOTAL PRESSURE PROBES
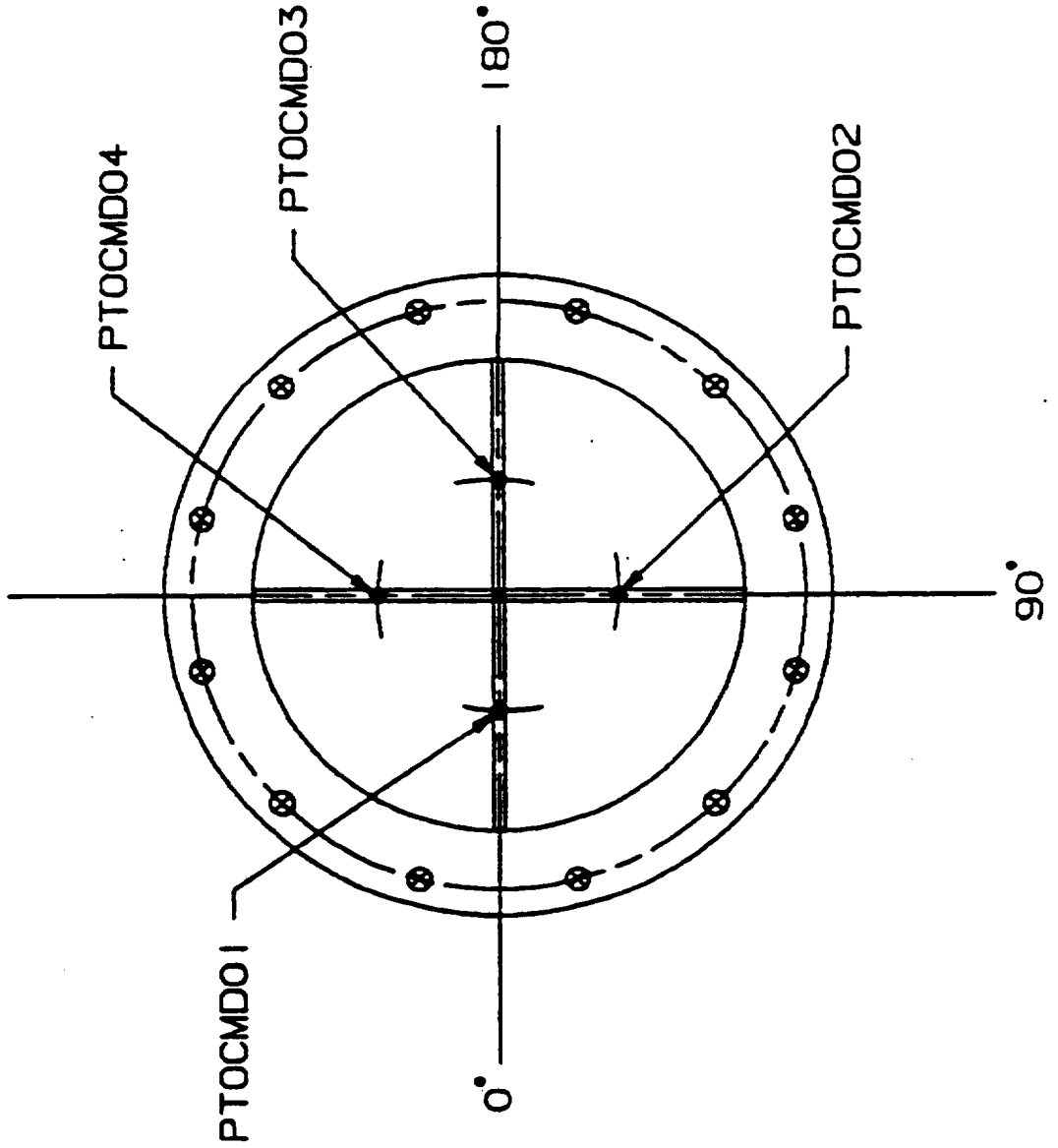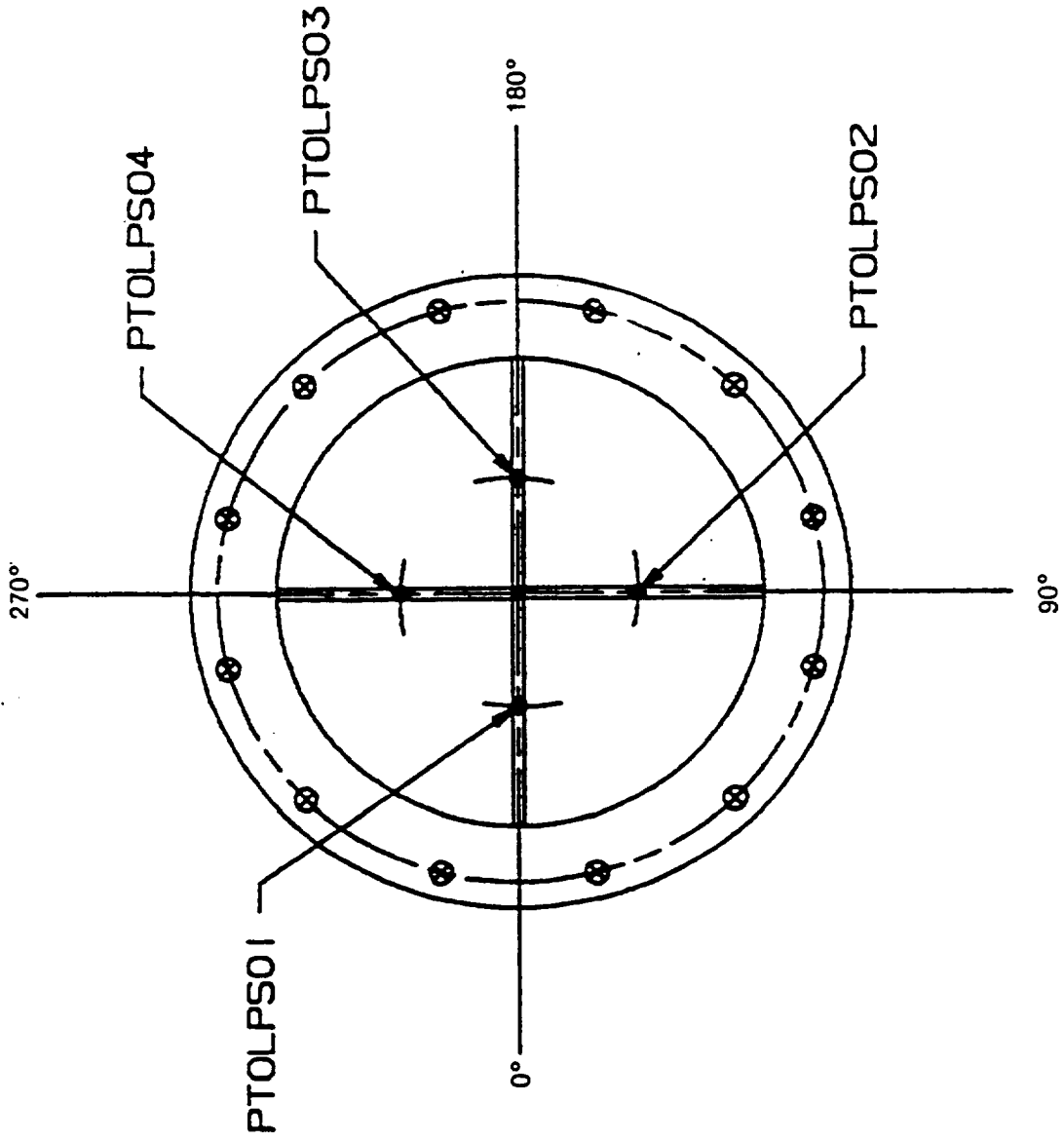
APD

270° (OUTER WALL, OPPOSITE SPLITTER)

PTOCMD04

PTOCMD03

PTOCMD02

PTOCMD01

180°

90°

0°

Figure 4.9

g15468

LPCI SUPPLY – TOTAL PRESSURE PROBES

PTOLPSO4

PTOLPSO3

PTOLPSO2

PTOLPSO1

180°

270°

90°

0°

g15468

Figure 4.10

SSME/ATD HPOTP RADIAL SIDE LOAD RIG
Flange Discharge
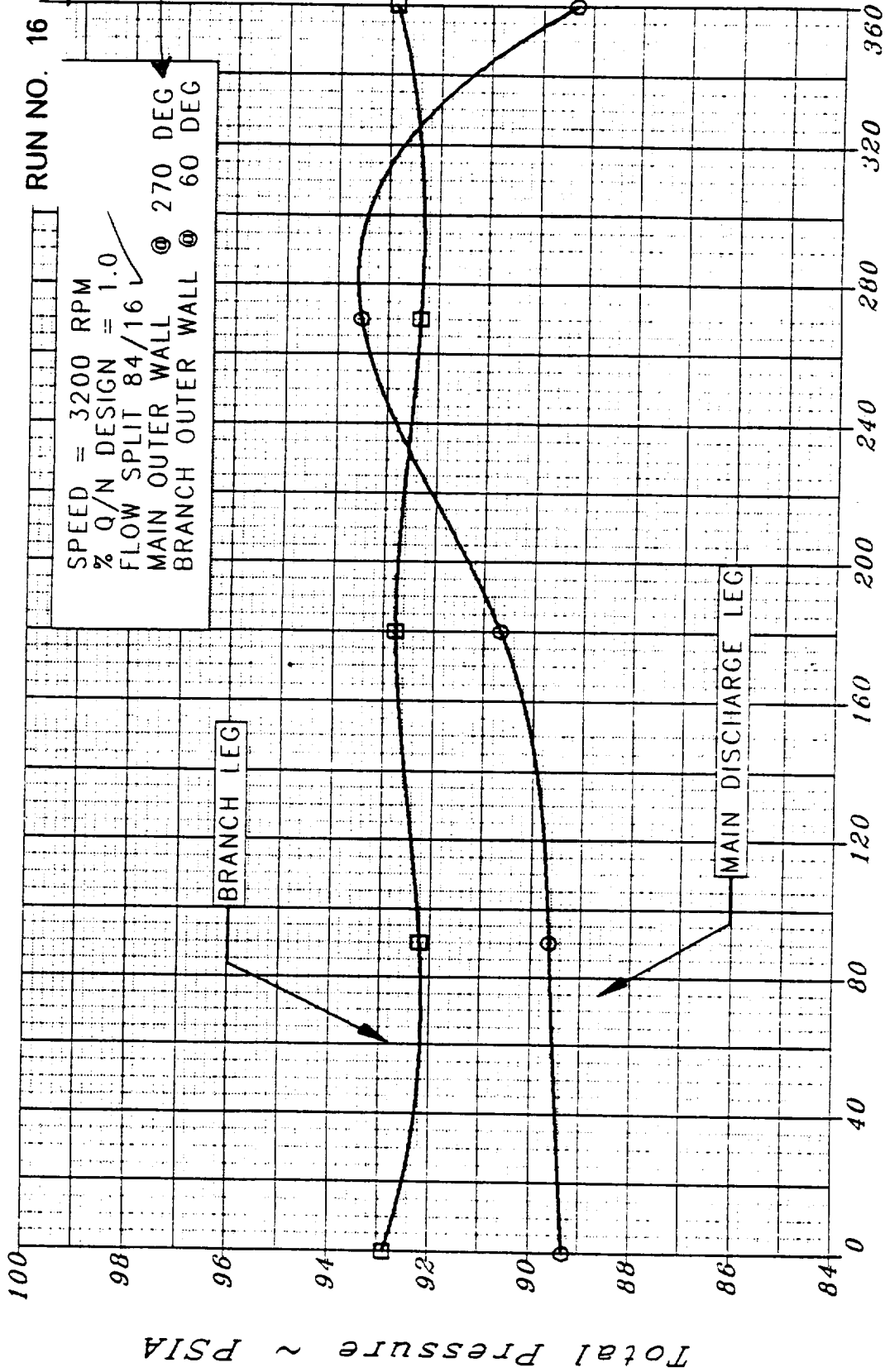
Figure 8.19

Report Document Page

1. Report No.	2. Government Accession No.	3. Recipient's Catalog No.

4. Title and Subtitle	5. Report Due
Determination of Uncertainties of the New SSME Model	16 May 96

	6. Performing Organization Code
	University of Alabama in Huntsville

7. Author(s)	8. Performing Organization Report No.
Kendall K. Brown Hugh W. Coleman	
	10. Work Unit No.

9. Performing Organization Name and Address	11. Contract or Grant No.
University of Alabama in Huntsville Huntsville, Alabama 35899	NAS8-38609 D.O. 140

12. Sponsoring Agency Name and Address	13. Type of report and Period covered
National Aeronautics and Space Administration Washington, D.C. 20546-001 Marshall Space Flight Center, AL 35812	Contractor Report Final Report, 1 May 95 –16 May 96
	14. Sponsoring Agency Code

15. Supplementary Notes

16. Abstract

This report discusses the uncertainty analysis performed in support of a new test analysis and performance prediction model for the Space Shuttle Main Engine. The new model utilizes uncertainty estimates for experimental data and for the analytical model to obtain the most plausible operating condition for the engine system. This report discusses the development of the data sets and uncertainty estimates to be used in the development of the new model. It also presents the application of uncertainty analysis to analytical models and the uncertainty analysis for the conservation of mass and energy balance relations is presented. A new methodology for the assessment of the uncertainty associated with linear regressions is presented.

17. Key Words (Suggested by Author(s))	18. Distribution Statement
Experimental Uncertainty Analysis Modeling Uncertainty Analysis Regression Uncertainty Analysis Space Shuttle Main Engine Testing Space Shuttle Main Engine Modeling	

19. Security Class. (of this report)	20. Security Class. (of this page)	21. No. of pages	22. Price
Unclassified	Unclassified		